AD NUMBER

ADB004737

LIMITATION CHANGES

TO:

Approved for public release; distribution is unlimited.

FROM:

Distribution authorized to U.S. Gov't. agencies only; Critical Technology; MAR 1975. Other requests shall be referred to Federal Aviation Administration, Supersonic Transport Office, 800 Independence Avenue, SW, Washington, DC 20590. This document contains export-controlled technical data.

AUTHORITY

FAA ltr, 26 Apr 1977

Report No. FAA-SS-73-11-10

SST Technology
Follow-On Program—Phase II
NOISE SUPPRESSOR/NOZZLE DEVELOPMENT
VOLUME X

ADVANCED SUPPRESSOR CONCEPTS AND FULL SCALE TESTS

R. S. Armstrong, J. Atvars, C. R. Fullerton,
C.P. Wright

Boeing Commercial Airplane Company
P.O. Box 3707
Seattle, Washington 98124

D6-42445

March 1975

FINAL REPORT

Task III

Prepared for
FEDERAL AVIATION ADMINISTRATION
Supersonic Transport Office
800 Independence Avenue, S.W.
Washington, D.C. 20590

The contents of this report reflect the views of the Boeing Commercial Airplane Company, which is responsible for the facts and the accuracy of the data presented herein. The contents do not necessarily reflect the official views or policy of the Department of Transportation. This report does not constitute a standard, specification, or regulation.

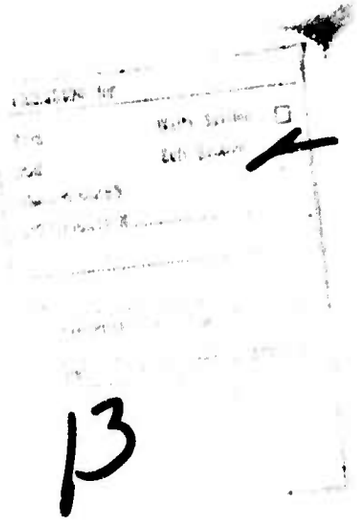

TECHNICAL REPORT STANDARD TITLE PAGE

1. Report No.	2. Government Accession No.	3. Recipient's Catalog No.
FAA-SS73-11-1		

4. Title and Subtitle: SST Technology Follow-On Program-Phase II
NOISE SUPPRESSOR/NOZZLE DEVELOPMENT
VOLUME X ADVANCED SUPPRESSOR CONCEPTS AND FULL SCALE TESTS

5. Report Date: 184 p.

6. Performing Organization Code

14 D6-42445

7. Author(s): R.S. ARMSTRONG, J. ATVARS, C.R. FULLERTON, C.F. WRIGHT

8. Performing Organization Report No.

9. Performing Organization Name and Address
BOEING COMMERCIAL AIRPLANE COMPANY
P.O. Box 3707
SEATTLE, WASHINGTON 98124

10. Work Unit No: Mar 75

11. Contract or Grant No.
15 DOT-FA-72WA-2893

13. Type of Report and Period Covered
FINAL REPORT TASK III

12. Sponsoring Agency Name and Address
FEDERAL AVIATION ADMINISTRATION
SUPERSONIC TRANSPORT OFFICE
800 INDEPENDENCE AVENUE, S.W.
WASHINGTON, D.C. 20590

14. Sponsoring Agency Code

15. Supplementary Notes

S. BLATT, DOT/SST Program Monitor

16. Abstract

The goal of this program was to develop and demonstrate an engine exhaust system suitable for use on a commercial supersonic transport which would allow the airplane to meet FAR Part 36 takeoff and sideline noise requirements. A series of model-scale jet noise suppressor test programs and a design feasibility study were conducted to identify the exhaust system design which would meet this goal. A model-scale test and a full-scale test of a "boilerplate" version of the final design were conducted statically to demonstrate thrust performance and noise suppression characteristics. Full-scale test results were limited to a jet velocity of 2300 fps due to engine operating limits, while model-scale results were extended beyond the design velocity of 2550 fps. The full-scale suppressor system test achieved 15.8 PNdB sideline jet noise reduction for 0.75% static gross thrust loss at V_j = 2300 fps. Model-scale tests of the same system show that the jet noise suppression should increase to 16.8 PNdB at V_j = 2550 fps. Forward flight effects during climb-out are predicted to degrade the suppressor performance to a value of 15 PNdB noise reduction for 7% net thrust loss. Consequently, it is shown that the application of such a suppressor system to the Boeing B2707-300 SST configuration would achieve FAR Part 36 sideline noise levels. Further, it is shown that such an installation would allow an approximately 7.5% increase in the airplane's maximum takeoff weight, thereby improving its economic and mission flexibility.

V sub J

17. Key Words	18. Distribution Statement
JET NOISE JET NOISE SUPPRESSION MULTITUBE JETS EJECTORS SUPPRESSOR THRUST PERFORMANCE	Approved for U.S. Government only. This document is exempted from public availability because of restrictions imposed by the Export Control Act. Transmittal of this document outside the U.S. Government must have prior approval of the Supersonic Transport Office.

19. Security Classif. (of this report)	20. Security Classif. (of this page)	21. No. of Pages	22. Price
UNCLASSIFIED	UNCLASSIFIED	173	

Form DOT F 1700.7 (8-69)

390 145

PREFACE

This is one of a series of final reports on noise and propulsion technology submitted by the Boeing Commercial Airplane Company, Seattle, Washington, 98124, in fulfillment of Task III of Department of Transportation Contract DOT-FA-72WA-2893, dated 1 February 1972.

To benefit utilization of technical data developed by the noise suppressor and nozzle development program, the final report is divided into 10 volumes covering key technology areas and a summary of total program results. The 10 volumes are issued under the master title, "Noise Suppressor/Nozzle Development." Detailed volume breakdown is as follows:

			Report No.
Volume I	–	Program Summary	FAA-SS-73-11-1
Volume II	–	Noise Technology	FAA-SS-73-11-2
Volume III	–	Noise Technology–Backup Data Report	FAA-SS-73-11-3
Volume IV	–	Performance Technology Summary	FAA-SS-73-11-4
Volume V	–	Performance Technology–The Effect of Initial Jet Conditions on a 2-D Constant Area Ejector	FAA-SS-73-11-5
Volume VI	–	Performance Technology–Thrust and Flow Characteristics of a Reference Multitube Nozzle With Ejector	FAA-SS-73-11-6
Volume VII	–	Performance Technology–A Guide to Multitube Suppressor Nozzle Static Performance: Trends and Trades	FAA-SS-73-11-7
Volume VIII	–	Performance Technology–Multitube Suppressor/ Ejector Interaction Effects on Static Performance (Ambient and 1150° F Jet Temperature)	FAA-SS-73-11-8
Volume IX	–	Performance Technology–Analysis of the Low-Speed Performance of Multitube Suppressor/ Ejector Nozzles (0-167 kn)	FAA-SS-73-11-9
Volume X	–	Advanced Suppressor Concepts and Full-Scale Tests	FAA-SS-73-11-10

ACKNOWLEDGEMENTS

The achievements of this program are the result of efforts of many individuals aside from the authors. The following contributions are gratefully acknowledged:

S. W. Krein - Model-Scale Thrust Performance Program
J. D. Nuhse - Model-Scale Acoustic Program

In order to verify the J-58 engine start capability, NASA successfully conducted three engine starts, with the Boeing round convergent (R/C) reference nozzle installed, at Edwards AFB prior to shipment of the engine to the Boardman test site. In addition to the engine, NASA furnished all required engine support equipment and personnel to operate the engine at Boardman. The excellent support and cooperation provided by NASA-FRC contributed greatly to the success of the full-scale test program.

CONTENTS

FIGURES

SUMMARY

The goal of this program was to develop and demonstrate an engine exhaust system suitable for use on a commercial supersonic transport which would allow the airplane to meet FAR Part 36 takeoff and sideline noise requirements. The static gross thrust penalty of such an exhaust system should not exceed 2% relative to a 10° half-angle conical nozzle. A series of model-scale jet noise suppressor test programs and a design feasability study were conducted to identify the exhaust system design which would meet this goal. A model-scale test and a full-scale test of a "boilerplate" version of the final design were conducted statically to demonstrate thrust performance and noise suppression characteristics. Full-scale test results were limited to a jet velocity of 2300 fps due to engine operating limits, while model-scale results were extended beyond the design velocity of 2550 fps.

Three model-scale multitube-nozzle noise suppressor concepts were designed, fabricated, and tested with acoustically lined ejectors. The suppressors were designated LNHP-2 (57 tubes, 3.1 area ratio), LNHP-3 (85 tubes, 3.7 area ratio), and LNHP-4 (31 tubes, 3.1 area ratio). These nozzles were one-eighth-scale SST models. A large-scale LNHP-2 nozzle was tested on a J-58 engine at the Boardman, Oregon test site.

The maximum 2128-ft sideline, jet noise suppression values attained by the LNHP series of suppressors were: 16.8 PNdB for 3.2% static gross thrust loss for the LNHP-2; 20.8 PNdB for 7.8% static gross thrust loss for the LNHP-3; and 15.2 PNdB for 1.2% static gross thrust loss for the LNHP-4 atmozzle pressure ratio of 3.0 and jet temperature of 1500°F. The full-scale version of the LNHP-2 suppressor achieved 15.8 PNdB noise suppression for 0.75% static gross thrust loss at the 2300 fps velocity condition. In terms of indoor noise using the AIR 1081 transmission loss standard for a typical family dwelling, the LNHP-2 suppressor would attain 19.6 PNdB jet noise reduction.

The predicted noise suppression and thrust performance values agreed with model-scale and full-scale test results within a measurement accuracy of ±1 PNdB and within 3/4% ΔC_{Fg} respectively. This places a high degree of confidence in the propulsion and noise technology applied and adds credibility to model-scale testing.

Forward flight effects during climbout are predicted to degrade the LNHP-2 suppressor performance to a value of 15 PNdB noise reduction for 7% net thrust loss. Consequently, it is shown that the application of such a suppressor system to the Boeing B2707-300 SST configuration would achieve FAR Part 36 sideline noise levels. Further, it is shown that such an installation would allow an approximately 7.5% increase in the airplane's maximum takeoff weight, thereby improving its economic and mission flexibility.

In addition to demonstrating the suppressor system's performance, the full-scale tests also verified the existence of the following noise components in the engine noise signature. Spiral-mode flow-instability noise was identified in the J-58 engine noise spectrum at high nozzle pressure ratios (>2.4) and it was dominant at angles of 80° and 90° from the engine inlet. Engine core noise was detected at the lowest power settings in the noise spectra at 120°. Core noise appeared to peak in the 400 Hz band. Neither of these noise sources affected the peak sideline noise suppression by the suppressor systems, however, they are potential noise floors for further jet noise reduction.

ABBREVIATIONS AND SYMBOLS

A	Area
A*	Nozzle throat area
alt	Altitude
AR	Area ratio = $\frac{\text{total cross-sectional area}}{\text{primary flow area}}$
a_o	Speed of sound in air
C_D	Discharge coefficient accounting for temperature-induced nozzle area growth
C_{Fg}	Gross thrust coefficient
dia	Diameter
D_E	Equivalent round convergent nozzle diameter
d	Nozzle diameter
dB	Decibel
F_{ID}	Ideal thrust
F_N	Net thrust
f	Frequency in Hz
fps	Feet per second
Hz	Hertz
kHz	Kilo Hertz
L	Ejector length
M_J	Jet Mach number
MTW	Maximum takeoff weight
NOY	Unit of noisiness
OBL	Octave band level
P_{amb}	Ambient pressure
P_S	Static pressure
P_T	Total pressure
PA	Polar arc
PNL	Perceived noise level
PNdB	Perceived noise units in dB
PR	Nozzle pressure ratio
PTN	Nozzle charging station average total pressure
PWL	Sound power level
R	Radius
r	Radius
R/C	Round convergent (nozzle)
SB	Setback distance
SL	Sideline
SPL	Sound pressure level
SST	Supersonic transport
T	Tubes
TOFL	Takeoff field length
TTN	Nozzle charging station average total temperature
TT5	Engine turbine exhaust average total temperature

$V_{A/C}$	Airplane velocity
V_J	Fully-expanded jet velocity
W_a	Airflow lb/sec
μ bar	Microbar (pressure)
ρ	Gas density

1.0 INTRODUCTION

The high-velocity jet noise suppression acoustic and performance technology has been described in great detail in volumes II through IX.

During the initial stages of this program, a parametric group of model-scale multitube nozzles and ejectors were examined in an attempt to further understand the fundamental acoustic and propulsive mechanisms present in multielement supersonic jet flow. Analysis of the results of this test series culminated in an improved design and prediction procedure for tubular nozzle/ejector systems.

Concurrently, a design feasibility study was conducted to determine how the advanced noise suppression exhaust systems being developed could be integrated into a suitable airplane nacelle configuration. The design study was based on the use of a nonaugmented GE4-J6H2 engine in place of the afterburning GE4 engine used earlier in the SST airplane program. The suppressor system's, overall size and position were selected to meet the requirements of space for stowing the nozzle elements within the nacelle contours.

Using the above guidelines, three model-scale nozzle/ejector suppressor systems were designed and tested to demonstrate this newly acquired acoustic and propulsive technology. The three low-noise, high-performance, proof-of-concept nozzles tested were designated LNHP-2, -3, and -4, and are pictured in figures 1, 2 and 3. The "best" overall nozzle, the LNHP-2, represents a balance between the usually conflicting requirements of being a good jet noise suppressor as well as an efficient thrust producer. Its design goal was 17 PNdB noise suppression with less than 2.5% static thrust loss, relative to an equivalent R/C nozzle. The LNHP-2/ejector is considered to be a viable design for installation on an SST.

The LNHP-3 nozzle was designed and tested to demonstrate the jet noise suppression state-of-the-art in multitube-nozzle technology, (predicted: 20 PNdB suppression for 5.5% thrust loss). For optimum acoustic performance, thrust and size constraints were necessarily relaxed. The design philosophy of the LNHP-3 was similar to that of the LNHP-2. The tube number was increased to aid reduction of premerged jet noise and the area ratio was increased to aid suppression of postmerged jet frequencies. However, the increased tube number caused increased internal flow losses and the enlarged area ratio increased base pressure losses.

The LNHP-4 nozzle was the thrust-performance demonstrator with noise suppression constraints relaxed, (predicted: 0% thrust loss and 14 PNdB suppression). A lower tube number has been used (31 tubes) to reduce internal flow losses and arranged on radial lines to aid base ventilation. The nozzle area ratio was confined to 2.7 to minimize base drag.

The full-scale suppressor demonstrator system to be tested on the J-58 engine was designed as a scaled-up version of the LNHP-2 model. Some detail differences existed as a result of fabrication and financial constraints; however, these differences were not expected to significantly alter noise or performance characteristics.

The design philosophy used in selecting the suppressor systems, the model-scale and full-scale test results, and analyses are presented in this report. A brief discussion is included about the expected flight effects on the static results as well as the impact on an SST if the LNHP-2 system were installed in a production airplane.

2.0 DESIGN CRITERIA

The exhaust system for a supersonic airplane requires a high jet velocity for efficient cruise performance, but this results in a high noise level during takeoff. To minimize takeoff jet noise levels, a suppressor is required for the primary jet flow. Provisions have to be made to retract and stow the suppressor after takeoff in order to avoid excessive performance losses. Consequently, the suppressor nozzle size or area ratio is limited by the available space within a set of nacelle contours to house the nozzle and the retraction mechanisms.

The design study was based on the use of the nonaugmented GE4-J6H2 turbojet engine and the Boeing B2707-300 SST airplane. The total exhaust system (including thrust reverser) was limited to a maximum diameter of 100 in. It would attach to the engine's aft-turbine flange, and extend aft approximately 15.5 ft. These ground rules resulted in a maximum nozzle area ratio of 2.9, ejector area ratio of 3.1 and ejector length approximately equivalent to two primary nozzle diameters. The engine gas conditions for the takeoff power setting were assumed to be 1500°F jet temperature and 3.0 nozzle pressure ratio.

The model-scale studies in volume II showed that for regular (close-packed) nozzle arrays the area ratio and the tube number are the major acoustic parameters. Tube number mainly affects the premerged jet noise, and area ratio, the postmerged jet noise. Making an allowance for premerged jet noise absorption with acoustical linings in an ejector, the trend curves in figure 4 were generated. These curves show the variation of the premerged jet noise contribution to the sideline perceived noise level (PNL) as a function of tube number. The test data has been extrapolated for tube numbers beyond 61. The premerged jet noise peak PNL generally occurs at 110° from the inlet. Similar trend curves were generated for the postmerged jet noise contribution to the sideline PNL as shown in figure 5. The postmerged jet noise varies with area ratio and generally peaks at 140° from the inlet.

In order to combine both the premerged and postmerged jet noise components of the sideline PNL's it is necessary to add them on the basis of their relative directivity patterns as shown for the design gas conditions in figure 6. The resulting maximum sideline PNL's as a function of tube number and suppressor area ratio are shown in figure 7. It can be seen that for a given area ratio there is some limiting tube number beyond which further noise reductions can not be achieved because of postmerged jet noise dominance. Therefore, for this particular design exercise, where the maximum practical suppressor area ratio was established as 3.1, a reasonable number of tubes appeared to be on the order of 60.

Starting with the above basic suppressor area ratio and tube number requirement, detailed tube array layouts led to a 57-tube configuration (LNHP-2, figure 8) with the following refinements to maximize acoustic and thrust performance characteristics. To further suppress postmerged jet noise frequencies, the LNHP-2 nozzle postmerged jet velocity profiles are favorably shaped (i.e., flattened) by distributing the initial mass flow radially, through the arrangements of tubes of varying diameters so that the mass flow per unit of annular area is nearly equal over the entire exhaust plane. LNHP-2 thrust performance losses are minimized by arranging the tubes on radial lines to aid base ventilation. A further ventilating aid is the elliptical shape of the outer row of tubes that are located in such a way that the major axis of each ellipse is directed towards the nozzle center (i.e., maximum entrainment flow area is created). Internal flow losses are minimized by making the round tubes

convergent at the ends. The outer row tubes were left nonconvergent as a trade for an increased ambient entrainment area. The predicted static performance of the LNHP-2 suppressor system was 17 PNdB for 2.5% gross thrust loss. This configuration was considered as the best design to meet the mutual acoustic and performance goals of the jet noise-suppression technology demonstrator program.

It was also clear from these studies that higher jet noise suppression was achievable if some of the design constraints of area ratio (nacelle diameter) and performance goals were relaxed. Similarily better thrust performance could be demonstrated if lower noise suppression goals could be accepted. To demonstrate the above claims, two additional suppressor systems (LNHP-3 and LNHP-4) were built for model-scale evaluation. To demonstrate higher jet noise suppression, figure 7 shows that the area ratio has to be increased with a corresponding increase in tube number. The LNHP-3 suppressor system hence was chosen to have 85 tubes and an area ratio of 3.7 as shown in figure 9; It was predicted to be capable of 20 PNdB jet noise suppression for 5.5% static gross thrust loss. Thrust performance losses can be minimized in general by reducing internal losses and by increasing base ventilation. This leads to fewer tubes as shown by the LNHP-4 suppressor system (figure 10) which has 31 tubes in a radial array with a 3.1 AR ejector. This system was predicted to be capable of 14 PNdB jet noise suppression for *zero* static gross thrust loss.

3.0 MODEL-SCALE DEMONSTRATOR PROGRAM

The three jet noise suppression demonstrator systems, discussed in section 2.0, were built and tested on a model scale. The scale chosen was approximately 1/8 of the GE4-J6H2 engine or equivalent to the flow area from a 6-in. R/C nozzle.

3.1 TEST PROGRAM DESCRIPTION

3.1.1 TEST FACILITIES

The model-scale tests of the advanced technology multitube-nozzles were conducted at the Hot Nozzle Test Facility (HNTF) at North Boeing Field, Seattle, Washington. This facility is used for the determination of exhaust nozzle thrust performance and jet noise levels. It is a single axis thrust rig with an air supply capable of providing a maximum flow of 45 lb/sec. Airflow rates are measured using a critical-flow venturi. An in-line kerosene-type burner is mounted on the rig to provide combustion products to the test nozzle at temperature up to 1500°F and nozzle pressure ratios of 4.0. Figure 11 shows the test installation. The nozzle centerline is 5 ft 8 in. above ground level.

Thrust is measured using a 2000 lb capacity Baldwin load cell. Thrust measurement accuracy is ± 1/4% of full scale, with ± 1/4% repeatability of measured value. Airflow measurement repeatability is ± 1/4%. A 10.25-in.-diameter instrumentation section was used to measure the nozzle charging station's total temperature and total pressure. Probe arrangement is shown in figure 12. The facility includes a digital-type data system for recording all measured performance parameters.

The arena for acoustic measurements consists of a smooth, flat concrete surface as shown in figure 13. The arena is large enough to allow acoustic far-field measurements to be made on a 50 ft radius centered on the test nozzle exit. Noise measurements are limited, however, to the quadrant of 90° to 180° from the nozzle inlet axis. Building surfaces in the vicinity of the test stand are covered with a 4-in.-thick acoustically absorptive material to minimize sound reflections into the acoustic arena.

3.1.2 INSTRUMENTATION

All acoustic data were recorded on magnetic tape. Microphone arrays were placed in the far-field. The far-field array consisted of two sets of microphones, one set at the ground plane and the second at the horizontal plane containing the jet axis. Microphones were located at 10° increments from 90° to 150° with the addition of a microphone at 155°(angle relative to the nozzle inlet axis). Both arrays were at a 50-ft polar radius.

The ground plane microphones were mounted flush with the test arena surface so that direct and reflected sound waves were in-phase over the frequency range of interest. This technique allows spectra to be measured which are free-field in shape but 6 dB above free-field in level. Data are then easily corrected to free-field levels for analysis.

The acoustic far-field pressure was monitored by 1/4-inch Bruel and Kjaer condenser-type microphones having a flat frequency response (after correction) from 50 Hz to 80 kHz. Microphones at ground level were oriented for near 90°(grazing) incidence. Microphones at nozzle centerline height were oriented for 0°(normal incidence).

The analog data from each microphone were recorded simultaneously on a fourteen-channel Ampex Type 1800L tape recorder. The taped data were reduced later by the Acoustic Laboratory using a General Radio Model 1925-26 analyzer. The data were presented in 1/3-octave bands from 200 Hz to 80 kHz and stored on digital magnetic tape for subsequent analysis.

Static pressure measurements were taken with pressure taps located on the baseplate and ramp of each suppressor nozzle to allow calculation of base drag and ramp drag. The locations of the base pressure taps and ramp pressure taps for the three nozzles are shown in figures 14 through 16. Ejector lip static pressures were measured for the calculation of the thrust augmenting ejector lip force. The locations of static pressure taps on the ejector lips are shown in figure 17.

3.1.3 TEST HARDWARE

6 in. R/C Nozzle.—The R/C nozzle employed in these tests was a round, convergent nozzle of 10° half-angle (shown installed in figure 18). The measured geometric flow exit area was 28.17 sq in.

LNHP-2.—The LNHP-2 suppressor is a 57-tube nozzle (56 tubes and a center hole) having a geometric-flow exit area of 25.4 sq in. The nozzle AR is 2.9, where, the nozzle area ratio is defined as the base area enclosed by the upstream periphery of the outer-tube row divided by the geometric flow area. As shown in figure 8, the outer row consists of small, constant cross-section tubes. The remaining tubes are round with round convergent exits, providing maximum internal performance. The baseplate design incorporates a 9.77-in. spherical radius, terminating in the circular central hole. The tube exits are noncoplanar to conform to stowage requirements of an SST suppressor nozzle installation.

The hardwall ejector used with the LNHP-2 nozzle is cylindrical and has an ejector AR of 3.1 (where the ejector area ratio is defined as the cross-sectional area at the ejector throat divided by the primary nozzle exit area). The ejector length is 10.9 in., and the throat diameter is 9.81 in. As shown in figure 19, the ejector is mounted aft of the nozzle by means of four struts placed at 90° increments around the nozzle body, and located 45° from the nozzle vertical centerline.

The LNHP-2 hardwall ejector lip consists of a 1.20/.60 in. inner ellipse extending from the throat to the highlight, and a .60/.30 in. outer ellipse from the highlight outward. The mounting struts attach to this outer portion of the ejector lip.

A 24-sided acoustically lined ejector used with the LNHP-2 nozzle (figure 20), has a flat-to-flat dimension across the lined ejector of 9.782 in., providing the same value of cross-sectional area as in the hardwall ejector. The lined ejector has a length of 10.9 in., the same as that of the hardwall ejector.

This lined ejector shares a common mounting assembly with the hardwall thus having an identical outer lip. The inner lip has the same elliptical shape described above, but is faired to match the 24-sided throat geometry. A schematic of the nozzle/ejector installation is shown in figure 21.

A second lined ejector (16-sided), 12 in. long, and primarily designed for the LNHP-3 and LNHP-4 nozzles, was also used with the LNHP-2 nozzle. This ejector is described in the following LNHP-3 section.

LNHP-3. – The LNHP-3 suppressor is an 85-tube nozzle (84 tubes and a center hole) having a geometric flow exit area of 22.6 sq in. and a nozzle AR of 3.4. The outer row consists of smaller diameter tubes, (figure 9). The remainder of the tubes have elliptical upstream portions in order to improve base ventilation and therefore decrease the base drag. All tubes have round convergent ends. The baseplate design incorporates a 10.43-in. spherical radius, terminating in the circular central hole. The nozzle is designed for balanced flow. The tubes are uniformly spaced and all tube ends are coplanar except the center hold.

Three 16-sided, AR 3.7 ejectors were used with the LNHP-3 nozzle (figure 22). The hardwall ejector has a length of 12 in. and a flat-to-flat dimension of 10.12 in. The two acoustically-lined ejectors have the same flat-to-flat dimension of 10.12 in., one having a length of 12 in. and the other a length of 17 in. The ejector lip used with these three ejectors is a flight lip design. The mounting struts which hold the ejector in position attach to this ejector lip.

LNHP-4. – The LNHP-4 suppressor is a 31-tube nozzle (30 tubes and a center hole) having a geometric flow exit area of 26.9 sq in. and a nozzle AR of 2.7. The tubes are elliptical with round convergent ends to maximize internal performance while allowing maximum base ventilation.

The baseplate design uses a 10.14-in. spherical radius terminating in the circular central hole, and the nozzle is designed for balanced flow. The tubes are arranged in a radial array (six 60° wedge-shaped segments), with all tube ends coplanar except the center hole (figure 10).

The two 12-in. long ejectors (hardwall and acoustically lined) described in the previous section are also used with the LNHP-4 nozzle. The ejector lip described in the previous section is also used for the LNHP-4 tests.

Acoustic Linings. – Two sets of double-layer perforated-plate acoustic linings were developed and tested in conjunction with the multitube-nozzle ejectors. The two layers in each lining were designed to be tuned at separate frequencies in order to broaden the overall absorption characteristics.

Lining No. 1 has a 30% open-area face sheet with a 0.21-in. honeycomb backing followed by a 6.5% open-area inner sheet with a 0.15 in. honeycomb backing and closing out with a solid backing plate. The lining was tuned to have a flat frequency response between 8 kHz and 16 kHz. This lining was used in ejectors with a $L/D_E = 2$ (12 in. long) and $L/D_E = 3$ (17 in. long).

Lining No. 2 has a 25% open-area face sheet with a 0.35-in. honeycomb backing followed by an 8% open-area inner sheet with a 0.15 in. honeycomb backing and closing out with a solid backing plate. The lining was tuned to have a flat frequency response between 6.3 kHz and 12.5 kHz. This lining was used in an ejector with a $L/D_E = 2$ (10.9 in. long).

3.1.4 TEST CONDITIONS

The various nozzle and ejector combinations described in the previous section were tested by varying the gas conditions at the nozzle charging station. The nozzle exit conditions were varied over a temperature fange from T_T = 800°F to 1500°F and pressure ratios from PR = 1.6 to 4.0.

3.1.5 ACOUSTIC DATA HANDLING

The acoustic data acquisition, reduction and management was the same as that described in detail in volume II of this report.

3.2 ACOUSTIC RESULTS

The jet noise results for the LNHP-2, -3 and -4 suppressor systems are first analyzed from the sound power level (PWL) point of view followed by sound pressure level (SPL) and directivity effects. Finally a detailed examination is made of the suppressor system's effectiveness in terms of perceived noise levels scaled to full-scale and extrapolated to a 2128 ft sideline.

3.2.1 JET NOISE POWER LEVELS

Total noise power (premerged jet plus postmerged jet noise) is shown in figure 23 for the LNHP-2, LNHP-3, LNHP-4 and RC nozzles. The noise power levels have been normalized by $-10 \log \rho^2$ A. The noise power suppression values are shown in figure 24. The peak noise power suppression attained by the nozzles without ejectors was 11 dB for the LNHP-2 nozzle, 11.5 dB for the LNHP-3 nozzle, and 7.4 dB for the LNHP-4 nozzle. For jet velocities above 2200 fps, the noise power suppression decreases, because postmerged jet noise becomes increasingly dominant.

The effect of various lined and unlined ejector configurations on LNHP-2 nozzle (57-T, 2.9 AR) noise power suppression is shown in figure 24. The unlined ejector provides about 1 dB more suppression, probably as a result of the relative velocity effect on the premerged jet noise within the confines of the ejector. The lined-ejector configurations provide 2.5 to 4 dB suppression over the unlined ejector case at the lower jet velocities. This is due to lining absorption of premerged jet noise. At very high jet velocities (PR = 4.0) all ejectors approach the bare nozzle in suppression, because postmerged jet noise is the dominant source of noise.

3.2.2 LINED-EJECTOR SOUND POWER INSERTION LOSS

Effectiveness of ejector linings may be determined by comparing nozzle/ejector radiated noise power levels between the unlined (hardwall) ejector case and the lined ejector case. In this way the relative velocity effect and acoustic reflection/refraction effects due to the presence of an ejector do not confuse the results. The difference in premerged jet noise power levels between the unlined ejector and lined ejector is identified as the lining sound power insertion loss. At high nozzle pressure ratios when postmerged jet noise levels are dominant, the true lining sound power insertion loss cannot be determined since premerged jet noise is being masked by the postmerged jet noise floor. Measured lining sound power insertion loss values tend to become more accurate at the lower pressure ratio conditions.

Figures 25 through 32 show measured noise power insertion losses for the model-scale LNHP-2, LNHP-3 and LNHP-4 together with the lined ejectors. The sound power insertion loss is given in terms of one-third-octave band levels (OBL) to show the region of the noise spectrum affected by lining absorption.

The ejector lining insertion loss for the LNHP-2 nozzle with a 12-in.-long lined ejector is shown in figures 25 and 26 for T_T = 1150°F and 1500°F.

The peak loss in the design frequency region occurs at 10 kHz with 7.5 dB-to-9 dB loss achieved (PR = 2.0). The minimum which occurs at 25 kHz is due to a condition where both lining layers are resonant with little absorption evident. The second absorption peak at 50 kHz to 60 kHz has not been determined conclusively. This high-frequency portion of the premerged jet noise spectrum is generated relatively close to the nozzle exit plane. It is possible that these high frequencies are undergoing multiple reflections within the ejector before the residue noise is radiated to the far-field. Multiple reflections increase lining effectiveness in absorbing noise power.

Similar power insertion loss characteristics are shown for the LNHP-2 suppressor system with lining No. 2 in figures 27 and 28. A closer comparison in figure 29 shows that lining No. 1 attained slightly higher insertion loss levels. This difference in the lining performance could be due to the impedance characteristics of lining No. 1 being closer to optimum for the ejector flow and noise environment.

The LNHP-3 suppressor system was tested with two lined-ejector lengths because the larger area ratio of this design demands a longer ejector length for complete mixing than do the other two nozzles. The resultant comparison between the two ejector lengths is shown in figure 30. Noise power insertion loss for the longer ejector is about 1 to 2 dB greater at the design frequency. The noise loss at 50 kHz to 60 kHz is about 4 to 8 dB greater for the longer ejector. The longer ejector offers more acoustic absorption area and more possibility for multiple reflection effects for improved acoustic performance.

The LNHP-4 suppressor system achieved the sound power insertion loss levels shown in figure 31. Since the same lined ejector was tested with three different jet noise sources (nozzles) a comparison of lining effectiveness could be made as shown in figure 32. Contrary to expectations the lined ejector appears to perform best as the number of tubes decrease. The lined ejector achieved 3 dB more noise power absorption with the LNHP-4 nozzle (31 tubes) than with the LNHP-3 nozzle (85 tubes) for PR = 2.0. The lining effectiveness is dependent on flow temperature at the ejector wall, flow velocity at the wall, and the noise environment inside the ejector as well as the jet noise-source locations, making it difficult to optimize the lining impedance for all cases. Secondly the LNHP-4 nozzle had tubes distributed in a radial arrangement pattern which resulted in a higher spacing ratio between tubes in the outer row of the array compared to the LNHP-3 nozzle, close-packed arrangement. This could have resulted in lower ejector wall grazing velocity between tube elements in the outer row, improving the lining absorption.

3.2.3 JET NOISE DIRECTIVITY

Jet noise levels radiated to the far field exhibit strong directivity characteristics. These are especially important in sideline PNL analyses. It was shown in volume II that sideline noise

levels are sensitive to premerged jet noise directivity at low jet velocities and to postmerged jet noise directivity at high velocities. The peak premerged and postmerged jet noise-directivity characteristics are examined in this section.

3.2.3.1 Premerged Jet Noise

Figures 33 and 34 show the model-scale LNHP-2/ejector's peak premerged jet noise beam patterns. It is evident that pronounced ejector-related refraction effects are occurring and that the critical refraction angle (110°) is of primary concern. The peak premerged jet noise levels at the 110° angle for the LNHP-2 nozzle/ejector configurations are plotted in figure 35. Note that for the LNHP-2 nozzle with unlined ejector the premerged jet noise levels are higher at PR $<$ 2.8 when compared to the LNHP-2 with no ejector installed.

The amount of peak premerged jet noise suppression attained with the various ejector configurations as a function of pressure ratio is shown in figure 36 for T_T = 1150°F and 1500°F at the 110° angle. The best peak premerged jet noise suppression occurs with the larger and longer lined ejector.

Irregularities occur in the noise suppression which may be related to ejector wall reflections which can effect the radiation efficiency of the jet turbulence noise source. This hypothesis is discussed in volume II regarding noise suppression by hardwall (unlined) ejectors.

Figure 37 shows the LNHP-3 nozzle/ejector's peak premerged jet noise directivity. The results are substantially the same as those for the LNHP-2 nozzle/ejectors.

Figure 38 shows the LNHP-4 nozzle/ejector's peak premerged jet noise directivity. Again, the results are similar to the LNHP-2 and LNHP-3 nozzle/ejectors. In all cases the nozzles with ejectors have the premerged jet noise peaking at approximately 110° where the sideline maximum PNL tends to peak. This sharp peaking of premerged jet noise is believed to be due to an acoustic refraction phenomenon associated with the ejector. A better understanding of this phenomenon is essential to provide the controls necessary to reduce this sharp peaking of premerged jet noise and improve maximum PNL suppression values.

3.2.3.2 Postmerged Jet Noise

The peak postmerged jet noise beam patterns for the LNHP-2, LNHP-3 and LNHP-4 nozzles without ejectors are shown in figure 39. Postmerged jet noise tends to dominate sideline perceived noise levels at PR $\geq$3.0 and at the 130° angle. As expected the nozzle with the smallest area ratio, i.e., LNHI -4 nozzle, has the highest postmerged jet noise levels. It was shown in volume II that the postmerged jet noise level is inversely related to multitube-nozzle flow area ratio.

The LNHP-2 nozzle (57-T, 2.9 AR) was designed to increase the diameter of the postmerged jet core by placing larger diameter jets in the outer part of the array (2nd row of tubes). Since the secondary cross-flow increases the mixing rate of the outer row of jets, it was considered advisable to increase elemental jet size to compensate for this high mixing rate. This was a method which offered potential for lowering postmerged jet noise without increasing nozzle area ratio. A comparison of LNHP-2 (57-T, 2.9 AR) and LNHP-3 (85-T, 3.4 AR)

shows that peak postmerged jet noise levels at 130° are very close to being the same even though there is a substantial difference in nozzle area ratios, i.e., 2.9 versus 3.4.

Figure 40 shows the effect of lined and unlined ejector installation on the LNHP-4 nozzle (31-T, 2.7 AR) peak postmerged jet noise levels. The ejectors provide about 2 dB attenuation of postmerged jet noise at the 130° angle. Since the postmerged jet noise is generated beyond the exit one must assume that the presence of an ejector must promote higher mixing rates of the elemental jets. This results in a lower postmerged jet core velocity. The ejector installation does not appear to change the postmerged noise directivity characteristics.

The peak postmerged jet noise frequency, when adjusted to full scale occurs at the very low-frequency portion of the jet noise spectrum where annoyance is not heavily weighted. The 1600 Hz (model-scale) frequency is near the peak NOY level at high pressure ratios in the 110° to 130° sector. The 1600 Hz directivity characteristics for the three nozzles at PR = 3.5 are shown in figure 41. The LNHP-4 nozzle without ejector shows the 1600 Hz noise peaking at 130° - 140°. The LNHP-2 nozzle 1600 Hz noise peaks at 150° - 155°, while the LNHP-3 nozzle peaks at 140°. At 130° the LNHP-4 nozzle is 5.5 dB noisier than the LNHP-2 nozzle and 8.3 dB noisier than the LNHP-3 nozzle. The explanation for the high postmerged jet (1600 Hz) noise levels common with the LNHP-4 nozzle lies with the tube arrangement. The tubes are arranged along nozzle radii which results in increasing peripheral tube spacing ratios in the outer rows of tubes. The postmerged jet core for a radial arrangement of tubes has a high-velocity gradient which directs postmerged jet mixing noise away from the jet axis (see vol. II). Radial tube arrays provide good noise suppression when premerged jet noise is dominant (low pressure ratios) and good thrust performance. But they do not have good noise suppression characteristics when postmerged jet noise is dominant (high pressure ratios).

3.2.4 PERCEIVED NOISE LEVEL SUPPRESSION

For high-speed aircraft, jet noise is a problem mainly during the full takeoff phase of flight and for noise certification purposes this translates to a sideline noise case. In this section the jet noise suppression characteristics are examined in light of the annoyance weighted PNL scale. The changes in jet noise spectra due to atmospheric absorption over long distances (i.e., sideline noise) are also taken into account.

The model-scale suppressor nozzle data recorded on a 50 ft polar arc in the Hot Nozzle Test Facility were scaled up and then extrapolated to 2128-ft sideline and converted to PNL's. In an attempt to generate realistic PNL values the following standard set of aircraft/flight parameters were used in the PNL computation program:

(1)	Number of engines:	4
(2)	Airplane altitude for max. noise	1000 feet
(3)	Engine attitude (angle of incidence + climb angle)	20°
(4)	Ambient temperature	77°F
(5)	Relative humidity:	70%
(6)	Observer location:	2128-ft sideline
(7)	Scale factor:	1 to 8

The computed PNL values were derived from free-field noise levels. Presented PNL values include a +3 PNdB correction to represent nominal ground reflection interference adjustments as required for noise certification purposes.

Reference Nozzle.—The 6-in.-diameter R/C nozzle was tested to provide unsuppressed jet noise data. It is equivalent to a jet engine nozzle of 12.57 sq ft exit area, full scale. The peak PNL values calculated from the test data were normalized by 10 log $\rho^2 A$ and are shown compared to the SAE predicted levels in figure 42. The reference nozzle PNL levels are within ±2 PNdB of the SAE curve. The SAE predicted PNL curve is used in this report, to determine multitube-nozzle PNL suppression values.

LNHP-2 Jet Noise Suppressor System.—The LNHP-2 nozzle was tested without an ejector, with a hardwall ejector at a setback of 0.8 in., and with two acoustically lined ejectors at setbacks of 0.8 and 1.5 in.

Extrapolated and normalized peak PNL values for the LNHP-2 nozzle and ejector configurations were used to derive PNL suppression values shown in figure 43 for T_T = 1150°F and figure 44 for T_T = 1500°F. The LNHP-2/12-in. lined ejector suppressor system is seen to exhibit the best PNL suppression characteristics over most of the jet velocity range, reaching a peak suppression value of 18 PNdB at 1150°F and 16.8 PNdB at 1500°F. Its suppression performance relative to the bare LNHP-2 and LNHP-2/hardwall ejector is due to the ejector's acoustic lining which absorbs the premerged jet high frequencies, occurring within the ejector.

The increased suppression values for the 12-in. lined ejector case versus the 10.9-in. lined ejector, are most probably attributable to the 1.1-in. longer acoustic lining and slightly larger area ratio of the 12-in. lined ejector. Figures 43 and 44 also show the convergence of the PNL suppression values at the higher jet velocities. This similarity in PNL suppression at high jet velocity occurs because of postmerged jet noise domination which is not controlled effectively by the ejector. The postmerged jet noise is generated beyond the ejector exit plane.

When pressure ratio increases in the supersonic flow regime, the fully-expanded flow area ratio decreases, resulting in a high postmerged jet core velocity. This increase in postmerged jet core velocity causes a rapid increase in the low-frequency portion of the jet noise spectrum which soon dominates the PNL. The most effective way to reduce the postmerged jet noise is to increase the suppressor nozzle area ratio.

LNHP-2/ejector suppressor PNL beam patterns are shown in figure 45 for PR = 2.0 and 3.0 (T_T = 1500°F). It can be seen that the sharp directivity occurring at the 110° angle for the nozzle with an ejector installed affects peak PNL suppression significantly. It may be possible to reduce this peak if acoustic refraction/reflection phenomena inherent with the fluid flow within the ejector can be better understood and controlled.

LNHP-3 Jet Noise Suppressor System.—The LNHP-3 (85-tube) nozzle and ejector system, was tested to demonstrate supersonic jet noise-suppression technology to obtain over 20 PNdB suppression using a multitube-nozzle concept.

The normalized peak PNL's were used to derive PNL suppression values of the various nozzle/ejector combinations of the LNHP-3 series. The results are given in figures 46 and 47. The 17-in.-long lined ejector is seen to attain a peak PNL suppression value of 21.4 PNdB at V_J = 2450 fps (T_T = 1500°F) and suppression values roll off steeply as jet velocity increases. The sharp suppression peak versus that of the shorter lined ejector data emphasizes the effectiveness of the extra 5 in. of acoustic lining, in the V_J range where PNL's are still dominated by the premerged jet noise high frequencies. The convergence of the data at high V_J's is the result of NOY spectrum domination by the postmerged jet noise.

Typical PNL beam patterns for the LNHP-3 nozzle/ejector configurations are shown in figure 48. It is of interest to note that the longer (17-in.) lined ejector appears to dampen the sharp directivity peak which tends to occur at 110°.

LNHP-4 Jet Noise-Suppressor System. –This 31-tube nozzle/ejector system was designed and tested to demonstrate low static thrust loss while achieving reasonable noise suppression values.

The PNL suppression results for the LNHP-4/ejector are given in figures 49 and 50. Significant premerging noise suppression at the lower jet velocities by the lined ejector is again evident. Peak suppression of 16 PNdB at 1150°F and 15.2 PNdB at 1500°F is achieved after which the suppression falls off and the lined ejector data rapidly approaches that of the bare suppressor nozzle data, as the PNL spectra of both configurations become postmerged jet noise dominated.

PNL beam patterns are shown in figure 51 for the LNHP-4/ejector configurations. The LNHP-4 nozzle peak PNL occurs at 130° for PR = 3.0 indicating postmerged jet noise has become dominant. The LNHP-4 nozzle has a radial arrangement of tubes. In volume II it was shown that a radial array of tubes tends to result in a postmerged jet core having a large velocity gradient. This results in postmerged jet noise being directed away from the jet axis which adversely affects sideline PNL values. A radial arrangement of tubes is beneficial to thrust performance but suffers a degradation of noise suppression characteristics for high nozzle pressure ratios.

PNL Suppression Versus Static Thrust Loss. –A summary of the composite multitube nozzles suppression characteristics and static thrust loss values are shown in figures 52 through 54. The maximum PNL suppression values attained with the accompanying static thrust losses for the various nozzle configurations are as follows:

Configuration	PR	T_T	PNdB	C_{Fg}%
LNHP-2 (no ejector)	3.0	1500°F	14.7	4.8
LNHP-3 (no ejector)	3.5	1500°F	16.4	9.2
LNHP-4 (no ejector)	2.7	1500°F	11.6	3.8
LNHP-2 (Unlined ejector)	3.0	1500°F	15.3	2.1
LNHP-3 (Unlined ejector)	3.5	1500°F	18.0	7.3
LNHP-4 (Unlined ejector)	3.0	1500°F	12.9	-0.4

Configuration	PR	T_T	PNdB	C_{Fg}%
LNHP-2 (12-in. Lined ejector)	2.7	1500°F	16.6	3.5
LNHP-3 (12-in. Lined ejector)	3.5	1500°F	19.0	8.5
LNHP-3 (17-in. Lined ejector)	2.7	1500°F	21.5	8.2
LNHP-4 (12-in. Lined ejector)	2.7	1500°F	15.2	1.1

To achieve very high multitube nozzle noise-suppression values at typical SST takeoff engine conditions, it is necessary to resort to a larger number of tubes, larger area ratios, and the use of a lined ejector. Unfortunately, these methods to improve suppression tend to result in large thrust penalties.

The LNHP-2 jet noise-suppressor system was chosen to be tested full-scale on a J-58 engine. In order to facilitate model-to-full-scale acoustic data comparisons, the model-scale data was also recorded at power settings approximating the J-58 engine operating line (both nozzle PR and T varying simultaneously). The results were then scaled to the J-58 engine size (5 times model scale) and extrapolated to the 2128-ft sideline. The resultant predicted sideline noise reduction values are shown in figure 55.

3.3 PERFORMANCE RESULTS

Thrust and mass flow rate were measured for all model configurations. Nozzle discharge coefficients and gross thrust coefficients are presented as functions of nozzle pressure ratio and nozzle total temperature. Data shown represent an average of at least two runs for each configuration. Included on each plot of LNHP-2 data is a curve which is an estimate of what the performance would be if that particular model configuration were tested with the same pressure-temperature relationship encountered with the engine used in the full-scale test. For the calculation of discharge coefficient for elevated temperature runs the nozzle exit area was adjusted to account for thermal expansion.

3.3.1 6-INCH DIAMETER R/C NOZZLE

The performance baseline data is provided by the 6-in. diameter R/C nozzle. Measured discharge coefficients and gross thrust coefficients for the reference nozzle are shown in figure 56. Results are as expected for a 10° half-angle R/C nozzle.

3.3.2 LNHP-2 JET NOISE-SUPPRESSOR SYSTEM

The LNHP-2, 57-tube suppressor was tested in the nozzle-only configuration, with a hard-wall ejector at a setback (distance between the exit plane of the iongest tubes and the plane of the ejector lip highlight) of 0.8 in. and with an acoustically-lined ejector at setbacks of 0.8 and 1.5 in. Performance plots of discharge coefficient and gross thrust coefficient for the LNHP-2 are presented in figures 57 through 60.

Figure 57 shows flow discharge coefficients for the bare suppressor for cold and hot flow conditions. The cold-flow discharge coefficient approaches a value of 0.974 for pressure ratios of 3.0 and above. Slightly lower values are observed for hot jet conditions. This decrease is believed to be due to Reynolds number effects caused by the increased total temperature of the nozzle flow. As shown in figure 57, the maximum cold-flow gross thrust coefficient

for the LNHP-2 bare suppressor has a value of 0.948 at a pressure ratio of 3.0. This figure also shows the effect of hot flow on the nozzle gross thrust coefficient. Again, a slight decrease can be seen with higher temperatures.

When a hardwall ejector is installed at a setback of 0.8 in., the value of gross thrust coefficient increases by 4% to 0.988 at a pressure ratio of 3.0 as shown in figure 58. The gross thrust coefficient can be seen to fall off sharply at pressure ratios above 3.0, due to insufficient secondary air entering the restricted ejector inlet of the short setback configuration. Figure 58 also shows that increased nozzle flow total temperature has a much more pronounced effect on the thrust performance with the ejector installed than is seen with the bare suppressor. At a nozzle total temperature of 1500 F, the increase in gross thrust coefficient resulting from the addition of the ejector is only 2.7% at a pressure ratio of 3.0. The trend in gross thrust coefficient with pressure ratio is, however, similar to that exhibited in the cold-flow data.

The addition of acoustic lining to the ejector causes a reduction in gross thrust coefficient. Figure 59 shows a gross thrust coefficient of 0.972 for the suppressor with lined ejector at a setback of 0.8 in. for cold flow at a pressure ratio of 3.0. This reduction of 1.6% is due to the addition of acoustic lining. The presence of the lining panels results in an increase in skin friction which causes an increase in boundary layer thickness on the ejector walls. The effective ejector area is thus decreased, resulting in reduced secondary air handling capability and an attendant decrease in thrust augmentation. The reduction in gross thrust coefficient of 1.6% due to the addition of acoustic lining is typical for hot nozzle flows as well as in the cold flow case. The trends of gross thrust coefficient with pressure ratio are similar for the lined and hardwall ejector configurations. The performance is increased by approximately one-half percent at a pressure ratio of 3.0 for both cold and hot nozzle flows when the ejector is setback 1.5 in. The increased setback provides a larger ejector inlet area which results in a decrease in inlet losses and an attendant increase in thrust performance (fig 60).

The nozzle base and ramp pressure forces act as external drags, and are combined in a term known as afterbody drag; pressure forces on the ejector lip act to augment thrust. These forces and the nozzle and ejector internal skin friction constitute the principle elements of suppressor/ejector performance. Nominal values of afterbody drag and ejector lip forces are calculated from measured static pressures and areas upon which they act. These values are then nondimensionalized by dividing by the ideal thrust. Figures 61, 62 and 63 show values of nondimensionalized afterbody drag and lip forces as a function of nozzle pressure ratio for the LNHP-2 bare suppressor and with the hardwall and lined ejectors installed. Included on these plots are values for the corresponding full-scale configuration which will be discussed in section 5.3. Changes in nozzle/ejector configuration cause variations in the static pressure distribution and thus body forces on the nozzle afterbody and ejector lip. Ejector addition restricts ventilation of the nozzle base, thereby increasing the value of base drag. As an example, addition of the hardwall ejector increases the nominal value of afterbody drag coefficient from 3.4% to 8.5% for 1500 F nozzle flow at a pressure ratio of 3.0. The addition of acoustic lining panels modifies the flow field so as to decrease both the afterbody drag and the ejector-lip suction. This effect is due to the reduced amount of air that is entrained into the lined ejector inlet as a result of the increased skin friction and boundary layer thickness inside the ejector. The lip suction coefficient suffers a larger decrease than the afterbody drag coefficient, resulting in a decreased value of gross thrust coefficient.

3.3.3 LNHP-3 JET NOISE-SUPPRESSOR SYSTEM

The LNHP-3 85-tube suppressor was tested in the nozzle-only configuration and with three AR 3.7 ejectors including a 12-in.-long hardwall ejector, a 12-in.-long acoustically-lined ejector, and a 17-in.-long lined ejector. Each ejector configuration was tested at a setback of 0.74 in. and 1.44 in. Performance plots of discharge coefficient and gross thrust coefficient for the LNHP-3 are presented in figures 64 through 69.

The bare suppressor performance is shown in figure 64. The discharge coefficient approaches a value of 0.972 for pressure ratios of 3.0 and above, independent of jet temperature. The peak cold-flow gross thrust coefficient occurs at a pressure ratio of 3.0 and has a value of 0.902. Hot flow results in a slight decrease in gross thrust coefficient, as with the LNHP-2 bare suppressor.

With the addition of the 12-in.-long hardwall ejector at a setback of 0.74 in., the gross thrust coefficient increases 3.3% to a value of 0.935 at a pressure ratio of 3.0 for cold flow. Nozzle discharge coefficient was unaffected by the ejector. The adverse effect of hot nozzle flow on the thrust performance of the LNHP-3 shrouded configuration, shown in figures 65 and 66 is similar in magnitude to that observed for the LNHP-2.

Figure 67 shows values of the gross thrust coefficient for the LNHP-3 with the 12-in.-long acoustically-lined ejector installed at a setback of 0.74 in. The amount of gross thrust coefficient decrease due to the addition of lining is approximately 1% at a pressure ratio of 3.0 and is independent of nozzle-flow total temperature. Increasing the ejector setback to 1.44 in. causes an increase in gross thrust coefficient for both cold and hot nozzle flows at a pressure ratio of 3.0. This increase amounts to approximately 1% for cold flow and 0.4% for hot flow. Figure 68 shows values of gross thrust coefficient for the LNHP-3 with the 12-in.-long lined ejector installed at a setback of 1.44 in. Increasing the lined ejector length to 17 in. results in a slight decrease in gross thrust coefficient relative to that of the 12-in.-long lined ejector. The additional mixing length seems to have merely resulted in increased skin friction drag rather than providing improved ejector performance indicating that the 17-in.-long ejector is longer than required to achieve optimum mixing. Results for the LNHP-3 with the 17-in.-long lined ejector installed at a setback of 1.44 in. are shown in figure 69.

3.3.4 LNHP-4 JET NOISE-SUPPRESSOR SYSTEM

The LNHP-4 31-tube suppressor was tested in the nozzle-only configuration, with a 12-in.-long hardwall ejector and with a 12-in.-long acoustically-lined ejector. Both ejectors were tested at setbacks of 0.74 and 1.44 in. Performance plots of discharge coefficient and gross thrust coefficient for the LNHP-4 are presented in figures 70 through 74.

The bare suppressor performance is shown in figure 70. The cold-flow discharge coefficient approaches a value of 0.976 for pressure ratios of 3.0 and above. A slight decrease in discharge coefficient is seen with increasing nozzle-flow total temperature with a value of 0.972 occurring at a nozzle total temperature of 1500°F and a pressure ratio of 3.0. At a pressure ratio of 3.0 the cold flow gross thrust coefficient has a value of 0.959. Hot flow is seen to cause a decrease of approximately one-half percent.

The addition of the hardwall ejector at a setback of 0.74 in. increases the gross thrust coefficient by 5.1% to a value of 1.000 at a pressure ratio of 3.0 for cold flow. Figure 71 shows the adverse effect of hot nozzle flow on the gross thrust coefficient for the LNHP-4 with hardwall ejector. This effect is similar to that observed for the LNHP-2 and LNHP-3. Figure 72 shows values of gross thrust coefficient for the LNHP-4 with the hardwall ejector installed at a setback of 1.44 in. No increase in thrust performance is observed due to the increase in ejector setback.

The addition of lining to the ejector results in a decrease in the value of gross thrust coefficient for both cold and hot flows as was previously observed for the LNHP-2 and LNHP-3. Figure 73 shows values of gross thrust coefficient for the LNHP-4 with the lined ejector installed at a setback of 0.74 in. Figure 74 shows performance with ejector setback increased to 1.44 in. Again, no significant change in thrust performance is noted as a result of the increased ejector setback.

4.0 DESIGN FEASIBILITY STUDY

The previously discussed model-scale test results showed that the 57-tube LNHP-2 jet noise suppressor system represents the latest state-of-the-art design to meet both acoustic and thrust performance requirements. Before such a suppressor system can be considered as a serious contender for an actual airplane installation, design feasibility studies have to be conducted to determine how it could be transformed into flightworthy hardware. This section presents the results of a design effort which shows an optimum exhaust configuration for the Boeing B2707-300 SST airplane with provisions for deploying the jet noise suppressor for takeoff and stowing it during all other flight regimes. This design is a development of the exhaust system previously considered for the original SST airplane. The new design encompasses improvements in noise reduction, lower thrust losses, smaller space for stowage of suppressor components and a reduced temperature environment as a result of the use of a dry-turbojet engine.

4.1 DESIGN CONSIDERATIONS

The design study was based on the useof the nonaugmented GE4-J6H2 engine in place of the afterburning GE4 engine used in the SST airplane program. Selection of this new engine reduced exhaust gas temperatures to 1500°F, but increased the flow sizing from 633 lb/sec to 815 lb/sec. The suppressor has to be designed to be stowed into the nacelle wall upstream of the variable convergent-divergent ejector nozzle. In the suppressed mode the ejector would serve as a means to ventilate the suppressor, to provide space for absorptive acoustic linings and to provide thrust augmentation to offset suppressor nozzle flow losses.

4.2 DESIGN DESCRIPTION

The exhaust system for the supersonic airplane was configured to include a clamshell thrust reverser with cascade exits, a variable-area primary nozzle, a tube-type suppressor capable of being stowed, a convergent-divergent ejector nozzle with a variable throat, and closure doors for the ejector inlet.

Figure 75 is a schematic showing this system as configured to match the GE4-J6H2 engine. The exhaust system having a maximum diameter of 100.0 in. will attach to the engine aft turbine flange, and extend aft approximately 15.5 ft. Four longerons will form the backbone of the exhaust system and transmit all loads from the thrust reverser, jet suppressor, and cruise nozzles to the main engine structure. It is anticipated that the exhaust system will be fabricated of titanium and inconel.

4.2.1 THRUST REVERSER

A conventional type clamshell thrust reverser, upstream of the primary nozzle, diverts the exhaust flow through cascade units in the upper and lower quadrants. This type of reverser can be integrated with engine and nozzle to provide an efficient and reliable system. Because of its application on current Boeing airplanes, the development and manufacturing aspects are well known. The side quadrants will house the hydraulic actuation system for the reverser, and will contain ducts carrying secondary (inlet) air through to the primary nozzle area.

4.2.2 PRIMARY NOZZLE

The 16-segment variable-area primary nozzle controls the engine flow area during all cruise regimes (subsonic and supersonic). During noise suppression operation the nozzle segments open wide to seal against the outer lip of the suppressor and thereby complete the exhaust passage to the suppressor. Considerable segment overlap is required to permit the segments to adjust to the range of areas required. Seals on the segments are required, as well as a seal between the extremities of the segments and the suppressor. Individual nozzle segments are interconnected through links to a unison ring which is moved by hydraulic actuators in a track supported under the longerons. The primary nozzle assembly is mounted on a bulkhead ring which is supported by the main longerons of the exhaust system. The bulkhead ring also serves as the aft portion of the thrust reverser.

4.2.3 VENTILATION AIR SYSTEM (EJECTOR)

The convergent-divergent ejector nozzle system requires control of its air inlet so that it is open during takeoff and approach and closed during cruise. This is accomplished by hinged doors in the front portion and a translating-cowl ring in the aft portion. Each of the four quadrants between longerons of the nacelle contains four hinged doors of the overlapping-segment type. These doors are supported from a frame between longerons and are operated by individual hydraulic actuators. The translating-cowl ring is retained in tracks attached to the longerons and operated by ballscrew jacks driven by the suppressor segment actuators discussed below. When the system is closed for cruise, the hinged doors are secured against the lip of the translating cowl. Suitable seals are required between doors, between doors and translating cowl, and between translating cowl and ejector leading edge, when the system is closed for cruise.

4.2.4 SUPPRESSOR SYSTEM

The suppressor is a radial-tube array with an AR of 2.9; 56 tubes plus a center hole make up the exhaust flow passages. To enable the suppressor to be stowed during cruise it is divided into four hinged, pie-shaped segments, each of which contains 14 tubes. The tube array has elliptical tubes on the outer row and circular tubes of two sizes on the inner rows. Tube lengths vary from 13.5 to 7 in. with the longest on the outer row. The elliptical tubes are of a constant section while the circular ones have conical nozzles at their ends.

Each segment is structurally designed to carry the nozzle loads across the forward face of the tube array to the pivot bearings supported at each side through hinged links attached to the longerons of the exhaust system.

4.2.5 SECONDARY NOZZLE AND SHROUD

The convergent/divergent secondary nozzle and 3.1 AR shroud has 24 segments, the inner and outer surfaces of which are capable of independent motion, to provide the throat and exit configurations required during takeoff and landing, subsonic and supersonic cruise. Acoustic treatment is provided on the internal surfaces of alternate inner segments only, as considerable segment overlap is required to accomodate the diameter change between cruise and suppression positions. This treatment provides 45 sq ft of lining with depths varying from 2-1/2 to 1 in.

5.0 FULL-SCALE DEMONSTRATION PROGRAM

The final evaluation of a jet noise suppressor system has to be performed full-scale or at least on a large scale, using a turbojet engine. This has to be done to overcome some deficiencies of model-scale testing. The main reasons are that engines have their own peculiar nozzle exhaust temperature profiles that can affect the suppressor performance, and that full-scale hardware will have different Reynolds number effects on skin friction and ejector air handling. The acoustic lining surfaces full-scale can also be made smoother by choice of smaller perforations to further reduce thrust losses.

Because the GE4-J612 turbojet engines were never built, the only available engine today that comes anywhere near in performance characteristics is the J-58 (or JT11D). Therefore the LNHP-2 57 tube suppressor system was scaled to the J-58 engine size and tested at the maximum jet velocity of 2280 fps which is somewhat short of the suppressor design goal of 2550 fps.

5.1 TEST PROGRAM DESCRIPTION

5.1.1 TEST FACILITY

The full-scale test was conducted on test stand B-2 located at the Boeing Boardman Test Site, Boardman, Oregon. The test stand is a single-axis engine thrust rig with a thrust-measuring capability of 25,000 lb. The engine's fuel supply system includes a 20,000 gallon tank, a boost pump, fuel filters and turbine-type flow meters for flow measurement. Figure 76 shows the test stand with the engine installed. The engine centerline is approximately 12 ft above the concrete base pad. The engine's operating console and parts of the data acquisition system were housed in a small block house to the side of the test stand. The main data acquisition and quick-look data reduction systems were located in another building, a long distance away, so that acoustic reflection effects were minimized in the test arena.

A flat concrete test pad with a 250-ft radius, centered on the engine nozzle exhaust, composed the acoustic arena ground plane. Microphones were situated on a 200 ft polar arc from 80° to 150°. Figure 77 shows the LNHP-2 nozzle/ejector installed on the J-58 engine. The 16-ft-high acoustic baffle to one side of the engine was used to shield the microphones from engine inlet noise.

5.1.2 INSTRUMENTATION

A three-ft-long instrumentation section was installed between the engine and the test nozzle. Contained in this section was a total pressure-total temperature rake for the determination of nozzle charging station conditions. The rake, containing 18 area-weighted total pressure probes and 18 area weighted-total temperature probes, was located at the 0° position. One total pressure probe and one total temperature probe were also located at 90°, 180° and 270° to evaluate circumferential distortion. Figure 78 shows nozzle charging station probe locations. Twenty-two static pressure taps were located on the suppressor nozzle baseplate and ramp to allow calculation of base and ramp-drag forces. Figure 79 shows the location of these pressure taps. Ejector-lip static pressures were measured to allow calculation of the thrust-augmenting lip-suction force. Locations of the 17 lip-static-pressure taps are shown in figure 80.

Microphone arrays were placed in the far-field. The arrays consisted of two sets of microphones, one set at the ground plane and the second set in the norizontal plane containing the jet axis. Ground level microphones were situated on a 200-ft polar arc, centered at the nozzle exit, at 80°, 90°, 100°, 110°, 115°, 120°, 125°, 130°, 135°, 140° and 150°. The microphones at engine centerline height were situated at 100°, 110°, 120°, 130°, and 140° referenced to the engine inlet axis.

The acoustic far-field pressure was monitored by 1/2-in. Bruel and Kjaer condensor-type microphones with wind screens installed. Microphones at ground level were oriented for near 90° (grazing) incidence. The microphone diaphragm was placed about 1/2 in. above the concrete with the major axis directed downwards. This resulted in spectra to be measured which are free-field in shape but 6 dB higher than free-field levels due to pressure doubling in the frequency range of interest (50 Hz to 10 kHz). Data was easily corrected to free-field levels by subtracting 6 dB. The microphones at nozzle centerline height were oriented for 90° (grazing) incidence. The major axis of these microphones were directed upwards. Wind screens were installed.

The analog data from each microphone were recorded simultaniously on a fourteen-channel, Ampex Type FR1300 tape recorder at a tape speed of 30 in./s. Because of the number of microphones which had to be monitored, two sets of recordings were made. The first set recorded the ground-level microphones data at 100°, 110°, 120°, 130°, 140° and the nozzle centerline-height microphones at the same angles. The second set of recordings recorded data from the ground-level microphones at 80°, 90°, 115°, 125°, 135° and 150°. Twenty seconds of data were recorded each time.

The taped data were reduced the same day at the test site using a General Radio, Model 1925-26 analyzer. The data were presented in 1/3-octave-band levels from 50 Hz to 10 kHz and transmitted to the CDC 6600 computer at Renton, Washington by telephone line for storage on digital magnetic tapes for further reduction.

An "on-line" acoustic monitoring system was utilized during the tests to assure that acoustic shadowing, due to atmospheric refraction was not occurring at the ground-level microphones. This was accomplished by comparing ground-level microphone data with centerline-height microphone data. Under normal conditions the high-frequency portion of the spectrum should be 3 dB higher for the ground level microphones relative to the centerline microphones, because of the ground reflection effects.

5.1.3 TEST HARDWARE

The R/C nozzle fabricated for this test is a 10° half-angle R/C nozzle. The nozzle was originally fabricated with an exit area of 706.15 $in.^2$. During the test the nozzle was trimmed back to match the effective area of the suppressor nozzle based on measured mass flow. The trimmed area of the R/C nozzle is 712.9 $in.^2$.

57-Tube Suppressor Nozzle.—The full-scale suppressor has 57-tubes (56 tubes and a center hole) with a geometric exit-flow area of 734.9 $in.^2$ (fig. 81). The nozzle was designed as a scaled-up version of the LNHP-2 model suppressor. The nozzle area ratio is 2.9. The outer row of tubes consists of 24 constant, elliptical cross-section tubes. The remaining tubes are

circular in cross section with a 3° to 4° half-angle convergence. This is different from the model in that the model-scale tubes are straight with 10° half-angle convergent ends. The full-scale baseplate is of standard ASME pressure vessel head design with a spherical radius of 54 in., an outside diameter of 58 in. and a wall thickness of 0.5 in. The tubes are installed through holes in the baseplate from the upstream side. The upstream ends of the tubes are rolled over to retain the tubes in case of weld failure and to provide low-loss tube-entry radii. The entry radius of the model-scale tubes is large compared to the full-scale suppressor, and since the upstream face of the model baseplate is flat, the tube length is relatively greater than the full-scale version. Full-scale tube exits are noncoplanar, as are those of the model, to conform to stowage requirements of an SST suppressor/ejector installation. The nozzle assembly includes an 8° half-angle diffuser connecting the downstream end of the instrumentation section to the suppressor baseplate (fig. 82). This diffuser, which is not included in the model assembly, is to simulate the primary nozzle contour in the takeoff mode for an SST installation (fig. 75).

Ejector Assembly. – The ejector used with the 57-tube suppressor is 24-sided with a constant cross section and an AR of 3.1 (fig. 83). The distance across the ejector is 53.2 inches from flat-to-flat and the overall length is 60 in. The forward 7 in. is the inlet lip which has a 2:1 ellipse contour with the lip highlight 3.5 in. radially outward from the ejector inner wall. The aft 7 in. is of hardwall construction to simulate the airplane installation where the ejector trailing edge would contain secondary nozzle hinges and could not be lined. The remaining 46-in. of ejector wall length is comprised of 2-layer lining panels. These panels are a furnace-brazed assembly with two layers of metal honeycomb separated by a perforated sheet with a perforated sheet on one face and a solid sheet on the other face (fig. 84).

The panels are supported by longitudinal rails in the 24 corners of the ejector and can be turned over to present either the lined face or the hardwall face to the inside of the ejector. This type of ejector structure was designed for use in the full-scale test only and would not be typical for an airplane installation. The ejector is mounted to the suppressor nozzle with four struts, located 90° apart, 45° off the nozzle vertical centerline. The inner surfaces of the struts are at a radius equal to that of the ejector inlet-lip highlight. The cross section of the struts is of a size and shape to contain the mechanism required for stowage and deployment of the components in an SST suppressor/ejector installation.

Provisions for installing the ejector with a setback of either 4.5 or 8.25 in. are incorporated into the strut design.

5.1.4 TEST CONDITIONS

The J-58 engine cycle permitted the tests to be conducted over a nozzle pressure ratio range of 1.6 to 2.5 and corresponding jet total temperature between 900°F and 1430°F.

5.2 ACOUSTIC RESULTS

Acoustic data recorded at the Boardman engine test facility with the J-58 engine was analyzed both from the physical and subjective points of view. The nozzle configuration tested full scale were:

(1) R/C baseline nozzle $A^* = 4.9038\ ft^2$ (untrimmed)
$A^* = 4.9507\ ft^2$ (trimmed)
(2) LNHP-2 (no ejector) $A^* = 5.1035\ ft^2$
(3) LNHP-2 with unlined (hardwall) ejector, 4 in. set back
(4) LNHP-2 with half-lined ejector, 4 in. set back
(5) LNHP-2 with fully-lined ejector, 4 in. set back

5.2.1 JET NOISE POWER LEVELS

Total noise power radiated by the LNHP-2 nozzle/ejector configurations is shown in figure 85 as a function of V_J(ideal). These values expressed in terms of noise power suppression are shown in figure 86 relative to the R/C baseline nozzle noise power output. The full-scale LNHP-2 nozzle (no ejector) achieved 11 dB reduction in total noise power output (V_J = 2100 fps). The LNHP-2 nozzle with unlined ejector installed achieved 1.5 to 2.5 dB additional suppression of noise power, probably due to relative velocity reduction of jet turbulence within the confines of the ejector. The fully-lined ejector case achieved a peak suppression of noise power of 15 dB (V_J = 2000 fps). The lining is evidently absorbing 1.2 dB to 3.5 dB of the total noise output when compared with the unlined ejector case.

The noise power spectrum can be separated into postmerged jet noise (low-frequency peak) and premerged jet noise (high-frequency peak). This permits the investigation of the noise characteristics of the two major sources of noise radiating from a multitube-nozzle jet. Figures 87 through 90 show the postmerged and premerged jet components of noise power for the LNHP-2 configurations.

The premerged jet noise is dominant at low jet velocities increasing at the rate of V_J^4 to V_J^6. The postmerged jet has characteristics similar to a low-velocity simple jet increasing at the rate of V_J^9 (no ejector). Premerged and postmerged jet noise power suppression with the ejectors, relative to the LNHP-2 (no ejector) case is shown in figure 91. The unlined ejector provides 1.6 dB to 2.6 dB suppression of premerged jet noise. This is considered to be largely associated with the relative velocity effect of turbulence noise generated within the confines of the ejector. The half-lined ejector provides about 3 dB suppression of premerged jet noise relative to the unlined ejector. The fully-lined ejector provides 5.2 dB to 6.5 dB suppression of premerged jet noise relative to the unlined ejector case. This indicates that suppression of premerged jet noise is approximately proportional to the treated area (acoustical lining) within the ejector.

The postmerged jet noise power suppression at V_J(ideal) $\geq$ 1900 fps is about 0.5 dB for all ejectors indicating that lining had no affect on this region of noise generation which exists beyond the ejector exit. The 0.5 dB suppression is assumed to be due to improved mixing within the ejector resulting in a lower postmerged jet velocity. This effect is discussed in volume II. At low jet velocities V_J < 1700 fps there is evidence of a possible increase in postmerged jet noise as shown by the half-lined and fully-lined ejector cases. This may be due to engine core noise and bears further investigation, however, postmerged jet noise contributed very little to the total noise at low velocities.

5.2.2 LINED EJECTOR SOUND POWER INSERTION LOSS

The full-scale ejector was tested with no lining (hardwall), 50% lined and 100% lined in conjunction with the LNHP-2 nozzle. By comparing the lined ejector cases to the unlined ejector an estimate of lining effectiveness can be derived. Figure 92 shows sound power insertion loss (1/3-octave-band levels) attained by the lined ejector configurations. The 100% lined ejector attenuated the 2 to 2.5 kHz frequencies most with about 7 dB loss at the lower pressure ratios. The 50% lined ejector had power insertion loss characteristics similar to the 100% lined ejector for the frequency range of 400 Hz to 1 kHz. At frequencies above 1 kHz the 50% lined ejector insertion loss degraded significantly.

Figure 93 compares the full-scale and model-scale lined ejector's sound power insertion loss characteristics after the model-scale frequencies have been adjusted to full-scale. Good agreement occurs from 500 Hz to 4 kHz. However, the model-scale ejector has higher sound power insertion loss at 10 kHz

The amount of suppression of premerged jet noise attained by the full-scale lined ejectors relative to the unlined ejector is shown in figure 94. The 100%-lined ejector's sound power insertion loss was about 5.3 dB for V_J from 1700 fps to 2300 fps. The 50% lined ejector achieved about 2.7 dB over the same range of jet velocity. These results indicate that acoustic lining effectiveness is directly related to the amount of ejector wall area treated.

5.2.3 JET NOISE DIRECTIVITY

The microphone layout for the full-scale tests covered the aft quadrant at 10° intervals between 80° and 150° from the engine inlet. To increase directivity resolution, additional microphones were located at 5° intervals between 110° and 140°. This provided a more detailed look at the refraction phenomena associated with the ejector configurations.

The peak premerged jet noise beam patterns (2 kHz band) for the LNHP-2 nozzle without ejector are shown in figure 95. At the lowest engine power setting, a noise peak occurs at 115°. This angle is apparently the cutoff angle where noise generated by the inner array of jets becomes reflected by the outer-row jet flow. At angles of 80° to 115°, premerged jet noise generated by the inner array of jets is transmitted through the outer-row fluid layer suffering a nominal amount of transmission loss at this relatively low jet velocity. This hypothesis is discussed in volume II. The irregularities in the 2 kHz beam patterns in the mid-power settings (V_J = 1578 to 2132 fps) is of some interest, since they showed up repeatedly in the multitube-nozzle data. The wind conditions during these tests were less than 5 knots so it was unlikely that this could cause the erratic behavior of the beam patterns. Figure 96 shows the 2 kHz beam patterns measured with the R/C nozzle installed. The erratic behavior in the beam patterns is not apparent in this case. One may conclude that this characteristic in the premerged jet noise beam patterns is due to phasing effects between sound sources in the elemental jets.

Figure 97 shows the peak premerged jet noise beam pattern for the LNHP-2 nozzle with the unlined ejector installed. The beam patterns show a definite refraction type shape discussed in volume II. The critical angle for refraction is 120° at the low power setting, changing to 115° at the highest power setting. Refraction provides considerable attenuation at angles

beyond the critical angle, however emphasis of premerged jet noise is apparent at the critical angle, amounting to 1 or 2 dB, a phenomanon discussed by Lu (ref. 1). The amplification peak at the critical refraction angle results in a decrease in peak PNL sideline suppression values.

The LNHP-2 nozzle with fully-lined ejector installed also shows the presence of noise refraction effects in the peak premerged jet noise beam pattern (fig. 98). The lining provides up to 6 dB or suppression of premerged jet noise relative to the unlined ejector case.

Figures 99 and 100 provide a comparison of peak premerged jet noise beam patterns for the various LNHP-2/ejector configurations at V_J(ideal) of approximately 1910 and 2250 fps. It is apparent that noise amplification at the critical angle of refraction (110°- 120°) might be exacting a 1 to 3 dB penalty on premerged jet noise levels. Peak sideline PNL values tend to occur at this angle, also, except when postmerged jet noise is dominant. Control over noise amplification at the critical refraction angle has the potential of providing significant improvements in multitube nozzle/ejector peak PNL values. This necessitates an understanding of the mechanisms of the refraction phenomenon due to the flow field within the ejector.

A comparison of the LNHP-2 nozzles peak premerged jet noise beam patterns can be made from figures 101 to 103 between full-scale and model-scale results. The premerged jet noise levels are within ±2 dB between 90° to 120°. Beyond 120° the differences can be as much as 4 dB for the no-ejector case. The ejector cases show about the same trend. During full-scale testing, the jet temperature and velocity were found to be lower in the center of the multitube array than in the outer two rows of tubes. Since the outer row of jets dominates the far-field premerged jet radiated noise the higher velocities common to the full-scale tests understandably yielded higher noise levels.

Full-scale LNHP-2/ejector peak postmerged jet noise beam patterns are shown in figure 104 at the maximum dry power setting. The beam patterns are similar except the no-ejector case is about 1 dB noisier in the 80° to 130° sector. This is believed due to improved mixing when an ejector is installed resulting in a lower velocity postmerged jet core.

Good agreement between 1/5th-scale and full-scale LNHP-2 nozzle peak postmerged jet noise beam patterns occurred in the 90° to 130° sector, see figure 105. The full-scale data did show about a 5 dB higher level at 150°, however.

5.2.4 SPIRAL-MODE FLOW-INSTABILITY NOISE

A noise phenomenon associated with supersonic jet noise called spiral mode-flow-instability noise was evident from the J-58 engine tests when the R/C nozzle was installed. The theoretical relationships regarding spiral-mode flow-instability noise have been published by Tam (ref 2) and also discussed in volume II of this report. The mechanism for spiral-mode flow instability is the selective amplification of flow disturbances by shock cells in the jet which results in large-scale flow instabilities downstream. These large-scale flow-inabilities are believed responsible for transferring jet kinetic energy into noise radiation.

Figure 106 shows jet noise spectra from this test program where spiral-mode flow-instability noise has been identified. This source of acoustic interference peaked in the 630 and 800 Hz bands at 80° and 90° respectively, relative to the engine inlet, during the maximum dry engine power condition.

The spiral-mode flow-instability peak frequency can be estimated by using an abbreviated form of Tam's equation. This form was found to relate well with model-scale nozzle data (see vol. II).

$$f = \frac{1.202\, a_o}{\pi d}\left(\frac{M_J + 1}{M_J - 1}\right)^{0.5}\left(1.436\text{-}0.361\,\frac{V_J}{a_o}\right)^{-1}$$

a_o is the speed of sound in air
d is the nozzle diameter
M_J is the jet Mach number
V_J is the fully expanded jet velocity

The predicted spiral-mode-flow-instability peak frequency is 700 Hz which is in good agreement with the test data. The presence of this noise component in the jet noise spectrum (fig. 106) has the potential of an additional noise in an unsuppressed SST type engine during maximum power takeoff.

5.2.5 J-58 ENGINE CORE NOISE

A multitube nozzle provides significant noise suppression in the low frequency portion of the spectrum. This means that engine core noise can mask the multitube-nozzle effectiveness, since core noise generally peaks at the low frequencies, i.e., 320 to 400 Hz.

Engine core noise is quite directive, peaking at 120° relative to the engine inlet axis (ref. 3). Full-scale test data were examined to identify the presence of engine core noise. The indication of core noise was subtle, however by concentrating attention on the 320 to 400 Hz frequency bands and 120° angle this source of interference may be recognized.

Figure 107 shows the LNHP-2 nozzle/lined ejector's noise spectra at the 120° angle. The core noise spectrum predicted by the method from reference 3 has been added to show the fit to the peak which is present in the low frequency region of the measured noise spectrum. This is one indication that J-58 engine core noise may be present.

Figures 108 to 110 are plots of 250 Hz, 320 Hz, and 400 Hz band levels as a function of jet velocity. R/C nozzles and various LNHP-2/ejector configurations are represented. The R/C nozzle data shows a constant slope for noise as a function of velocity indicating that jet noise is masking core noise. The LNHP-2 nozzle/ejector noise data shows a decreasing noise slope as jet velocity decreases. This is an indication of the presence of another source of noise, such as core noise. An estimate of LNHP-2 nozzle jet noise and J-58 engine core noise deduced from the test data is shown. From these results core noise doesn't seem to have any influence on LNHP-2 perceived noise level suppression values at V_J(ideal) $\geq$2000 fps.

5.2.6 PERCEIVED NOISE LEVEL SUPPRESSION

The full-scale LNHP-2 suppressor system was evaluated on the subjective perceived noise level scale, similar to the model-scale studies described in section 3.2.4. The extrapolated sideline PNL beam patterns are shown in figures 111 through 113 for the major configurations tested. The beam patterns for the suppressor without an ejector are relatively broad and peak at 115° to 120° from the engine inlet axis as shown in figure 111. When the hard-wall ejector was installed the PNL values at angles beyond 120° were considerably reduced (figure 112) in the same way as shown earlier for the premerged jet noise. This is believed to be due to acoustic refraction effects caused by flow gradients across the ejector exit. Similar directivity characteristics are also shown for the fully-lined ejector configuration in figure 113. It is believed the LNHP-2 lined-ejector's peak PNL suppression values could be improved potentially by up to 2 PNdB if the ejector refraction effects could be controlled.

The peak PNL suppression values achieved with the LNHP-2 nozzle/ejector configurations are summarized in figure 114. The LNHP-2 nozzle without an ejector attained 12.5 PNdB at V_J = 2200 fps. The LNHP-2 nozzle with a fully-lined ejector installed reached 15.8 PNdB suppression at V_J = 2300 fps. This is quite close to the 16-17 PNdB peak suppression value originally predicted from model-scale results.

The LNHP-2 nozzle tested at the HNTF was approximately a 1/5-scale model of the nozzle tested on the J-58 engine at Boardman. The HNTF test conditions included those simulating J-58 engine power settings. The model test data scaled to the J-58 engine size predicted the suppression levels shown in figure 55. A comparison between the model-scale predicted results and actual measured data is shown in figures 115 through 117. Although there were differences in the radial temperature and velocity profiles across the nozzle exhaust plane between the model test rig and the J-58 engine, there is good agreement between the peak PNL suppression levels.

An attempt was made to subjectively evaluate the LNHP-2/ejector noise suppression during the test period at Boardman. At a distance of about 750 ft from the engine and 120° relative to the engine inlet the radiated jet noise was observed at the highest power setting for each configuration. It was impossible to remove the ear protectors when the R/C nozzle was running without experiencing severe discomfort bordering on the sensation of pain. When the LNHP-2 nozzle with lined ejector was installed and running at the same power setting, the need for ear protection was unnecessary and a normal conversation was conducted between two persons, standing 2 ft apart. At angles beyond 130° the R/C nozzle jet noise was modulated by a crackling-type noise which was not evident when the LNHP-2 nozzle was installed.

In jet noise suppressor studies, the acoustic filtering characteristics of atmospheric absorption of sound over long distance (e.g., sideline noise) usually serves to the advantage of multielement-nozzle noise suppression values. This is particularly the case if the suppressor design is premerged jet noise dominated. In the preceeding discussion the jet noise suppressor results have been analyzed from the point of view of an observer out of doors. It is very interesting and pertinent to see what the impact would be on people indoors, such as in an average family dwelling with windows and doors closed. The sound transmission loss characteristics of typical American family dwellings according to the SAE AIR 1081 standard is shown in figure 118. These transmission loss values were applied to the extrapolated sideline noise

levels for the unsuppressed and suppressed configurations. The resultant PNL suppression values as they would be observed indoors are shown in figure 119. The fully-lined ejector/suppressor configuration achieves a maximum of 19.6 PNdB jet noise reduction indoors which is about 3 PNdB better than for the outdoor observer.

The design, development and testing of the composite multitube nozzles was to demonstrate that the technology gained by this program could be put to practical use. The multitube nozzle designs were formulated to provide viable noise suppressor concepts. This required applying the principles of noise suppression, being able to predict the results, and demonstrating that the results met the predictions.

The LNHP-2, LNHP-3, and LNHP-4 nozzles were designed for gas conditions of PR = 3.0 and T_T = 1500°F. This is approximately the static engine condition for a typical SST engine at takeoff and close to the maximum capability of a modified J-58 engine. The predicted values of 2128-ft sideline suppression compared with model-scale and full-scale test results are shown below.

	Noise Suppression Values		
Nozzle/Ejector	Prediction	Model-Scale Results	Full-Scale Results
LNHP-2	17 PNdB	16.8 PNdB	(1) 15.8 PNdB
LNHP-3	20	20.8	
LNHP-4	14	15.2	

(1) Extrapolated from PR = 2.6, T_T = 1380°F data.

The predicted values of suppression were within ±1 PNdB of those attained by model-scale and full-scale testing.

5.3 PERFORMANCE RESULTS

During the full-scale engine tests, thrust, mean flow, nozzle changing station total pressure and total temperature, wind direction and velocity and all normal engine operating parameters were measured and recorded. In addition, the suppressor nozzle's base and ramp static pressures and ejector-lip static pressures were recorded as appropriate. Nozzle discharge coefficients and gross thrust coefficients are presented as functions of nozzle pressure ratio. Calculation of the nozzle discharge coefficient included an adjustment to the nozzle exit area to account for thermal expansion. With the exception of the suppressor nozzle with half-lined ejector and suppressor nozzle with hardwall ejector set back 8.25 in., all plots reflect an average of data from at least two runs.

Post-test data analysis revealed that a problem existed with the nozzle charging station's temperature-measuring instrumentation through most of the test. This was evidenced by the fact that the relationship of the average nozzle charging-station total temperature (TTN) to the average engine turbine exit temperature (TT5) changed from run to run during the test. A complete post-test checkout of the engine TT5 probes verified the integrity of the TT5 system therefore indicating that a deterioration of the TTN probes was occurring.

Early test results indicated that TTN should equal 0.953 times TT5 for all engine power settings. This relationship was used in the calculation of discharge coefficient and gross thrust coefficient for all test conditions, with the measured value of TTN being ignored.

5.3.1 BASELINE R/C NOZZLE

Performance plots of discharge coefficient and gross thrust coefficient for the baseline R/C nozzle are presented in figure 120. The values of these coefficients at PR 2.5 are as expected for a 10° half-angle R/C nozzle; however, the nozzle discharge coefficient is higher than would be expected at lower pressure ratios and this discrepancy is discussed in section 5.3.3. These plots include data from one run with the nozzle "as built" and three runs after the exit area was increased.

5.3.2 LNHP-2 JET NOISE SUPPRESSOR SYSTEM

5.3.2.1 LNHP-2 Nozzle Without Ejector

Plots of discharge coefficient and gross thrust coefficient for the 57-tube bare nozzle are presented in figure 121. At a pressure ratio of 2.5, the gross thrust coefficient is 0.950 or 4.1% lower than that of the R/C nozzle at the same pressure ratio.

The discharge coefficient of the suppressor becomes a constant with a value of 0.976 at a pressure ratio of 2.5. At lower pressure ratios the value of the discharge coefficient is greater, with the curve having a shape characteristic of a convergent-divergent nozzle. The suppressor nozzle is made up partly of straight tubes and partly of tubes with a small convergence angle with all tubes having a relatively small inlet radius. It is believed that at lower pressur ratios the flow separates at the tube inlets, especially in the outer row (straight tubes), forming effective throats just inside the tubes. Each tube then behaves as a convergent-divergent nozzle. Another factor which can contribute to a high discharge coefficient below the critical pressure ratio is the fact that in a multitube nozzle the individual tubes exhaust to a pressure less than that of ambient; this is especially true of tubes that are near the center of the array. The actual tube pressure ratio then is greater than that used for calculation of the ideal mass flow rate. As a result, the calculated discharge coefficient is higher than would be expected for a single exit nozzle.

When an ejector is installed on the multitube nozzle the tube exit pressure is further reduced. This results in an even higher calculated discharge coefficient. Figure 122 shows a comparison of the discharge coefficient of the 57-tube bare suppressor and with the lined ejector installed.

5.3.2.2 LNHP-2 Nozzle With Hardwall Ejector

Plots of discharge coefficient and gross thrust coefficient for the suppressor nozzle with the hardwall ejector installed at a setback of 4.5 in. are presented in figure 123. As with all other configurations which included the suppressor nozzle, the discharge coefficient with the hardwall ejector installed had a value of 0.976 at a pressure ratio of 2.5. The measured gross thrust coefficient is 0.991 at a pressure ratio of 2.5. This performance equals that measured for the R/C nozzle and represents a gain of 4.1% over the bare suppressor nozzle at similar conditions.

When the hardwall ejector setback is changed to 8.25 in., the gross thrust coefficient is still 0.991 at a pressure ratio of 2.5. However, at lower pressure ratios performance is less than for a setback of 4.5 in. It also appears, as can be seen in figure 124, that at pressure ratios above 2.5, some increase in thrust performance for the 8.25-in. setback might occur, while further increase in the thrust performance of the 4.5-in. setback installation would not be expected as seen in figure 123. Unfortunately, engine operating limits did not allow investigation in this area.

5.3.2.3 LNHP-2 Nozzle With Fully-Lined Ejector

Performance of the suppressor nozzle with lined ejector installed at a setback of 4.5 inches is shown in figure 125. The addition of acoustic lining caused the gross thrust coefficient to decrease by 0.7% to 0.984 at a pressure ratio of 2.5. This decrease is less than that associated with the addition of lining in the model case and is discussed in section 5.3.3.

5.3.2.4 LNHP-2 Nozzle With Half-Lined Ejector

To obtain the best simulation of an ejector for use in an SST installation a half-lined ejector configuration was also tested. In this configuration the lining panels were installed with the perforated side and the solid side alternately facing inward around the circumference of the ejector.

In the takeoff mode of an SST installation the ejector lining configuration would be similar to the half-lined ejector tested in the full-scale test program. Figure 126 shows discharge coefficient and gross thrust coefficient for the suppressor nozzle with half-lined ejector installed at a setback of 4.5 in. Although it is reasonable to assume that the gross thrust coefficient for the half-lined configuration should fall somewhere between the hardwall and fully-lined gross thrust coefficients the measured performance is shown to be slightly lower than for the fully-lined configuration. Since the measured engine mass flow produced a nozzle discharge coefficient similar to that in the remaining tests with the suppressor it is believed that measured thrust is in error on the run with the half-lined ejector. A detailed analysis of suppressor and ejector body forces derived from static pressure measurements was undertaken to confirm this belief. Thrust is a function of internal nozzle performance, nozzle base drag and ejector lip suction. Analysis of these data revealed that the base drag and lip suction forces for the half-lined configuration did, in fact, fall between those of the hardwall and fully-lined configurations. Since internal nozzle performance must be identical for the three lining configurations, measured thrust must follow the same order as base drag and lip suction forces.

Figures 127 and 128 are plots of measured baseplate and ejector-lip radial static-pressure distribution for the three different ejector lining configurations tested at a pressure ratio of 2.16. Included in figure 126 is a plot of estimated gross thrust coefficient which is based on analysis of body forces from these pressure measurements. The plot of estimated gross thrust coefficient gives a value of 0.987 at a pressure ratio of 2.5, or 0.4% less than for the hardwall ejector configuration at the same pressure ratio.

5.3.3 COMPARISON WITH MODEL-SCALE RESULTS

A summary plot of gross thrust coefficient for the various full-scale configurations is presented in figure 129 along with gross thrust coefficient plots for the corresponding model configurations. It can be seen that gross thrust coefficients of the full-scale and model-scale R/C nozzles agree closely at a pressure ratio of 2.5. At lower pressure ratios the full scale gross thrust coefficient is less than for the model scale R/C nozzle. Reynolds number effects associated with scaling would indicate that the full-scale gross thrust coefficient should be slightly greater (0.1% - 0.2%) than for the model R/C nozzle.

The fact that the full-scale gross thrust coefficient is lower than the model gross thrust coefficient at low pressure ratios leads to suspicion of an error in full-scale airflow measurements at low engine flow rates. It is believed that the model-scale measured airflows are correct, based on previous model-test data and the measurement methods used (refs. 4 and 5). Figure 130 compares full-scale and model-scale nozzle discharge coefficients and indicates a higher than expected full-scale mass flow rate with the R/C nozzle at low pressure ratios. The difference between model- and full-scale R/C nozzle discharge coefficients at low pressure ratios cannot be explained by geometry differences or scaling effects. Again, this difference leads to suspicion of an error in full-scale airflow measurements at low engine-flow rates.

Since no basis for adjustment of full-scale mass flow rate at low nozzle pressure ratios has been verified, data are presented as calculated and all full-scale and model performance data are compared at a pressure ratio of 2.5 only.

As shown in figure 129, the gross thrust coefficient of the full-scale bare suppressor is 0.950 at a pressure ratio of 2.5. This value is 0.9% higher than for the LNHP-2 model suppressor at the same pressure ratio. Three factors contribute to the difference between model- and full-scale suppressor thrust performance. One is the fact that the full-scale individual nozzle tubes are relatively shorter than the model tubes. Externally the tube lengths are to scale, but internally the tube entrances are at different stations. This is the result of the model baseplate being a solid piece of material with the tube entries flush with the upstream flat face, while in the full-scale case the baseplate is a constant thickness with the upstream face contour similar to the downstream face.

The tube-length differences between model- and full-scale are more pronounced in the row of tubes nearest the center of the nozzle than in the outer tube row. A difference of approximately 0.4% in gross thrust coefficient could be expected because of the difference in relative tube length with the full-scale value being the higher. The second factor contributing to a difference in model- and full-scale gross thrust coefficient is the effect of the difference in tube convergence angle. This is a minor effect and would be expected to lower the full-scale gross thrust coefficient relative to that of the model on the order of 0.1% - 0.2%.

The other factor, which contributes to the higher value of full-scale gross thrust coefficient, is the Reynolds number effect associated with scaling and explains the remaining difference between model- and full-scale performance.

The fact that the full-scale suppressor nozzle assembly includes an 8° half-angle diffuser, while the model does not, makes no measurable contribution to the difference in gross thrust coefficient. Considering the Mach number at the diffuser entrance (≤ 0.25) and the diffuser area ratio (1.48), the diffuser loss has less than 0.15% effect on the full-scale gross thrust coefficient and is therefore not included in the model- versus full-scale suppressor nozzle performance comparison.

The suppressor tube's exit convergence angle difference between the model- and full-scale suppressor has an appreciable effect on nozzle discharge coefficient. The difference between the model- and full-scale suppressor nozzle discharge coefficient at pressure ratio of 2.5 is 1% and is due to this difference in tube convergence angle. Differences in model- and full-scale suppressors can be seen by comparing figures 21 and 82.

The addition of a hardwall ejector to the suppressor nozzle results in an increase in gross thrust coefficient of 4.1% on full-scale and 3.3% in the Model-scale case at a pressure ratio of 2.5. The difference in performance increase due to addition of the ejector between model- and full-scale is attributed to Reynolds number scaling effects.

When a full acoustic lining is added to the ejector, the gross thrust coefficient is decreased by 1.3% for the model case and only 0.7% in the full-scale case at a pressure ratio of 2.5. This difference is believed to be due to the greater relative roughness of the model-scale acoustic lining. The perforated face sheets of the acoustic lining panels were not scaled geometrically. The hole diameters in the model lining were 0.028 in. while the holes in the full-scale lining face were 0.0625 in. The model-scale hole size should be approximately 0.012-in. in diameter for geometrically-scaled lining, however, suitable material for the operating environment was not commercially available with this hole size and required percent of open area so an alternate was chosen which was suitable from an acoustic standpoint.

The greater relative roughness of the model-scale lining results in a relatively thicker boundary layer build-up and larger reduction in ejector flow area which in turn reduces the secondary air handling capability of the ejector. Lip suction force is a strong indicator of ejector air handling capability. Figure 63 shows a comparison of model and full- scale lined ejector nondimensionalized lip suction force. At a pressure ratio of 2.5 it can be seen that the full-scale lip suction is 0.9% greater than that of the model. This is essentially the performance difference between the model- and full-scale lined ejector configuration and is attributed to the greater air handling capability of the full-scale line ejector. The effects of ejector setback variation cannot be directly compared since the increased setback was only tested with the lined ejector on model-scale and with the hardwall ejector in full-scale testing. The trends, however, are very similar. Figure 131 shows gross thrust coefficient for the model scale with the lined ejector at setbacks of 0.8 and 1.5 in. and for full-scale with the hardwall ejector at comparable setbacks of 4.5 and 8.25 inches. In both cases the shorter setback results in higher thrust performance at the lower pressure ratios with greater setback showing higher performance at higher pressure ratios. The cross-over point occurs at a pressure ratio of approximately 2.4 in the model case and 2.5 with the full-scale configuration.

Body force data from full-scale and model-scale testing agrees very well. Plots of full-scale and model-scale afterbody drag and ejector lip suction forces, both nondimensionalized by dividing by ideal thrust, are shown in figures 61, 62, and 63 for the bare suppressor, suppressor

with hardwall ejector and suppressor with fully-lined ejector. There were no static pressure taps located outside the ejector-lip highlight on the full-scale test hardware; however, pressure taps were provided outside the lip highlight on the model ejector. The full-scale lip suction force was adjusted on the basis of model static pressure measurements. Figures 132 and 133 show model- and full-scale ejector-lip radial static pressure distributions for the hardwall and lined ejector configurations. The data were chosen from test runs where the model and full-scale configurations were operating at very nearly the same nozzle charging station conditions. As can be seen, the ejector-lip static pressure distribution is very similar from the ejector throat radius out to the lip highlight. The full-scale pressure distribution from the ejector-lip highlight to the lip outside diameter was estimated from model scale measurements in the same area. The nondimensionalized lip suction force for full-scale configurations in figures 62 and 63 has been corrected on this basis.

Figure 134 shows a typical suppressor nozzle baseplate and ramp radial static pressure distribution for model- and full-scale. Both configurations included hardwall ejectors and were operating at a pressure ratio of 2.2 with a TTN of 1150 F. Again good agreement between model- and full-scale static pressure distribution is found.

6.0 PREDICTED FLIGHT PERFORMANCE

An acoustic and performance test program was conducted in a low-speed wind tunnel to determine forward flight effects on jet noise suppression and performance at velocities typical of aircraft takeoffs. The acoustic and performance flight effects were discussed in detail in volumes II and IX respectively. It was shown that forward flight reduced jet noise levels because of the relative velocity effect on jet mixing. Performance losses with flight speed were shown to be a function of ejector air handling. It was not possible in this program to test the LNHP series of suppressor systems in the wind tunnel to actually measure the flight impact on noise suppression and performance. Therefore, estimates of the flight effects were made, using the technology from volumes II and IX, to provide an indication of the flight performance of these systems.

The LNHP-2 suppressor system achieved 16.8 PNdB suppression with a performance penalty of 3.2% of gross thrust statically ($V_{A/C}$ = 0 knots) at PR = 3.0 and T_T = 1500°F. Assuming a takeoff velocity of $V_{A/C}$ = 230 knots (389 fps) the LNHP-2 suppressor noise is expected to be affected in the following way:

(1) Postmerged Jet Noise: The postmerged jet velocity is estimated to be 1505 fps. This noise will be affected by relative velocity the same as for a simple jet. The low-frequency portion of the LNHP-2/ejector noise spectrum will change by 80 $\text{Log}\left(\frac{1505\text{-}389}{1505}\right)$ or -10.4 dB.

(2) Premerged Jet Noise: The premerged jet noise (high-frequency part of the spectrum) will not be affected significantly by forward flight, since secondary ambient flow velocity within the ejector does not change proportionally. About 1 dB decrease in premerged jet noise may be expected with an ejector installation from dynamic testing conducted in the 9- by 9-ft wind tunnel.

The resultant effect of forward flight on LNHP-2/ejector noise spectrum is shown in figure 135. The 2128-ft sideline perceived noise level peaked at 110° from static test data, therefore this angle was used to determine the effect of forward flight on PNL suppression. A takeoff velocity of 230 knots (389 fps) was estimated to reduce postmerged jet noise by 10.4 dB and premerged jet noise by 1 dB. The overall change in LNHP-2/ejector noise due to forward flight is -3.6 PNdB. The baseline (RC) nozzle will experience a change of -5.4 PNdB. Therefore the net change is 1.8 PNdB or the LNHP-2/ejector PNL suppression is estimated to change from 16.8 PNdB to 15 PNdB because of takeoff forward flight velocity.

Based upon the data of volume IX for similar ejector/suppressors, it is estimated that forward flight effects would degrade performance of the LNHP-2 by 6% in gross thrust at 230 knots relative to static performance. The flight effect on the baseline R/C nozzle is a performance loss of 2%. This results in a penalty for the LNHP-2 suppressor relative to the R/C nozzle at 230 knots of ΔC_{Fg} = 6.2% or 7.2% in terms of net thrust.

Similar estimates were made for the LNHP-3 and -4 suppressor systems and the resultant changes in noise suppression and thrust performance are shown in figure 136 referenced to the model-scale static data. The full-scale static performance value for the LNHP-2 system is also included for comparison to point out the fact that the absolute thrust performance

values would be different under full-scale test conditions for the other suppressor systems as well. However, the incremental changes shown in figure 136 are expected to hold true.

7.0 SST APPLICATION

The LNHP-2, jet noise suppressor system has been demonstrated through model- and full-scale tests, as well as, design feasibility studies, to be a realistic candidate for SST applications. If this suppressor systems were incorporated in the Boeing B2707-300 SST configuration then the expected static sideline noise reduction would be 16.8 PNdB for 0.75% gross thrust loss. Current estimates of flight effects would change the suppressor system performance to 15 PNdB sideline noise suppression for 7% net thrust loss at 230 kn climbout velocity. Figure 137 shows the sideline noise status at the termination of the SST program in 1971.

An 800,000 lb MTW airplane, with 815 lb/sec airflow, GE4/J6H2 turbojet engines could have achieved 110 EPNdB sideline noise levels through the use of a "chute" suppressor and with the engines throttled back. The LNHP-2 suppressor system on the same airplane would achieve FAR Part 36 sideline noise level of 108 EPNdB and still leave it with excess thrust. This thrust could be used to increase the airplane MTW to 860,000 lb which would improve the airplane's economics either through increased payload or range or a combination of both.

8.0 CONCLUSIONS

A high degree of confidence has been established in the multitube-nozzle jet noise suppression and performance technologies as demonstrated by the test results for the LNHP-2, LNHP-3 and LNHP-4 suppressor systems. Measured jet noise suppression values were within ± 1 PNdB and performance within ± 3/4% of the predicted numbers. Model-scale test results agreed well with full-scale test results adding to the credibility of the prediction techniques.

During full-scale tests on the J-58 engine, the LNHP-2 nozzle with a lined ejector achieved 15.8 PNdB suppression with 0.75% gross thrust loss relative to the R/C baseline nozzle. This compares with 16.8 PNdB and 3.2% gross thrust loss (1/5th-scale). By applying typical family dwelling noise-transmission loss values to the measured data, the LNHP-2 system achieved 19.6 PNdB jet noise suppression indoors relative to the baseline round convergent nozzle.

The results from this jet noise suppressor demonstrator program show that the application of the LNHP-2 suppressor system on the Boeing B2707-300 SST configuration would achieve FAR Part 36 sideline noise levels. Further, it was shown that such an installation would allow a substantial increase (7.5%) in the airplane's maximum takeoff weight because of suppressor improvements over earlier designs, thereby improving its economic flexibility.

Demonstration of flightworthy operational hardware is required to confirm the mechanical feasibility study results presented herein for the variable geometry concepts.

The LNHP-3 nozzle (85-tube, AR 3.4) shows the best noise suppression at the high pressure ratios, e.g., PR = 3.0 but at the expense of a large performance penalty. The high noise suppression and high performance penalty are both due to the increased area ratio and large number of small tubes. The LNHP-4 nozzle (31 tubes, 2.7 AR) has the best performance but at the expense of decreased noise suppression characteristics at the high pressure ratios. High nozzle pressure ratios generally result in postmerged jet noise domination which can only be reduced by increasing the multitube-nozzle area ratio and by arranging the elemental jets so they can expand to the maximum extent before they merge.

The LNHP-4 nozzle with lined ejector showed that a radial arrangement of tubes can offer excellent noise suppression and thrust propulsion characteristics providing that nozzle pressure ratios are not high, e.g., PR < 3.0. The LNHP-4 nozzle attained 15.2 PNdB suppression with 1.1% thrust loss (static) with a lined ejector installed.

Placing a row of larger tubes in one of the outer rows of tubes improves the postmerged jet characteristics of a multitube nozzle. The LNHP-2 nozzle had larger tubes in the 2nd row of tubes to offset the effect of potential core shortening due to entrained cross flow. This resulted in a larger diameter postmerged jet core with lower velocity than would be expected with equal-sized tubes. In fact the 2.9 AR LNHP-2 nozzle had postmerged jet noise characteristics approaching the 3.4 AR LNHP-3 nozzle.

Installation of an ejector tends to reduce postmerged jet noise levels by 1 to 2 dB at the 130° angle. This reduces the postmerged jet noise influence on PNL. The reduction in postmerged

jet noise level seems to be associated with higher mixing rates within the confines of the ejector resulting in lower energy in the postmerged jet.

The presence of an ejector, unlined or lined, resulted in a sharp PNL beam pattern causing sideline noise to peak at about 110°. This is believed due to acoustic refraction phenomena within the ejector. It is believed that higher PNL suppression values could be attained by further study of the flow fields within ejectors and determining methods to control this phenomenon.

The full-scale ejector completely lined with a double-layer acoustic lining achieved a 5.2 dB to 6.4 dB reduction of broadband, premerged jet noise power at the expense of 3/4% additional loss in gross thrust performance. A 50% lined ejector provided 2.8 dB to 3.2 dB reduction of broadband, premerged jet noise power with slightly under 1/2% performance penalty indicating that lining effectiveness and performance loss is directly proportioned to the treated area within the ejector.

Forward flight effects ($V_{A/C}$ = 230 kn) are expected to reduce LNHP-2 nozzle/lined ejector noise suppression from 16.8 PNdB to 15 PNdB and ΔC_{F_g} by 6.2%. These predictions are based on a nozzle PR = 3.0 and T_T = 1500°F (V_J = 2550 fps). Under these conditions the low velocity postmerged jet noise is predicted to decrease by −10.4 dB and the premerged jet by −1.0 dB.

Spiral-mode flow-instability noise was noted in the full-scale tests with the R/C nozzle installed. This source of supersonic flow related noise was maximum at 80° and 90° and occurred at PR $\geq$2.4. The spiral-mode flow-instability noise frequency in the full-scale tests coincided very nearly with the peak frequency of the jet mixing noise emphasizing PNL's by 2 to 3 PNdB at 80° to 90°. Full-scale nozzle spiral-mode flow-instability noise levels scaled with model-scale nozzle levels.

J-58 engine core noise was identified only for the lowest power settings when the LNHP-2 nozzle was installed. The core noise had a peak frequency of about 400 Hz with peak level occurring at 120°. The core noise interference was not considered to be affecting PNL noise suppression values.

9.0 RECOMMENDATIONS

It is recommended that the LNHP-2 suppressor system be tested for relative velocity effects to substantiate methods of predicting the suppressor nozzle's forward flight noise and performance levels. The state-of-the-art in adjusting static test data to predict relative velocity effects for ejectors is not well established in either acoustic or performance technologies as evidenced in particular by the conflicting claims in current literature for noise effects. This area of investigation should be emphasized in future research activities.

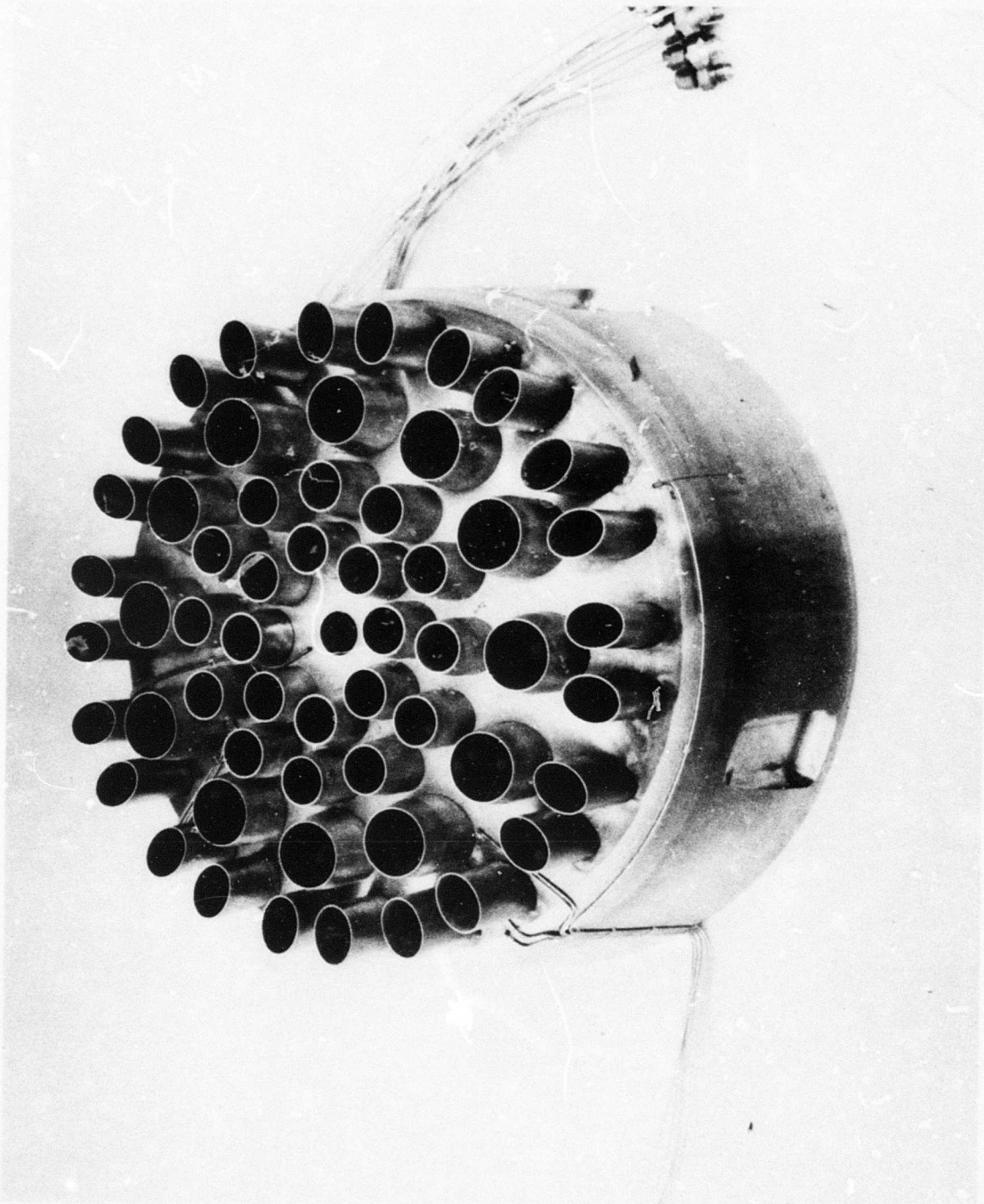

Figure 1. – LNHP – 2 Nozzle (57 – Tubes)

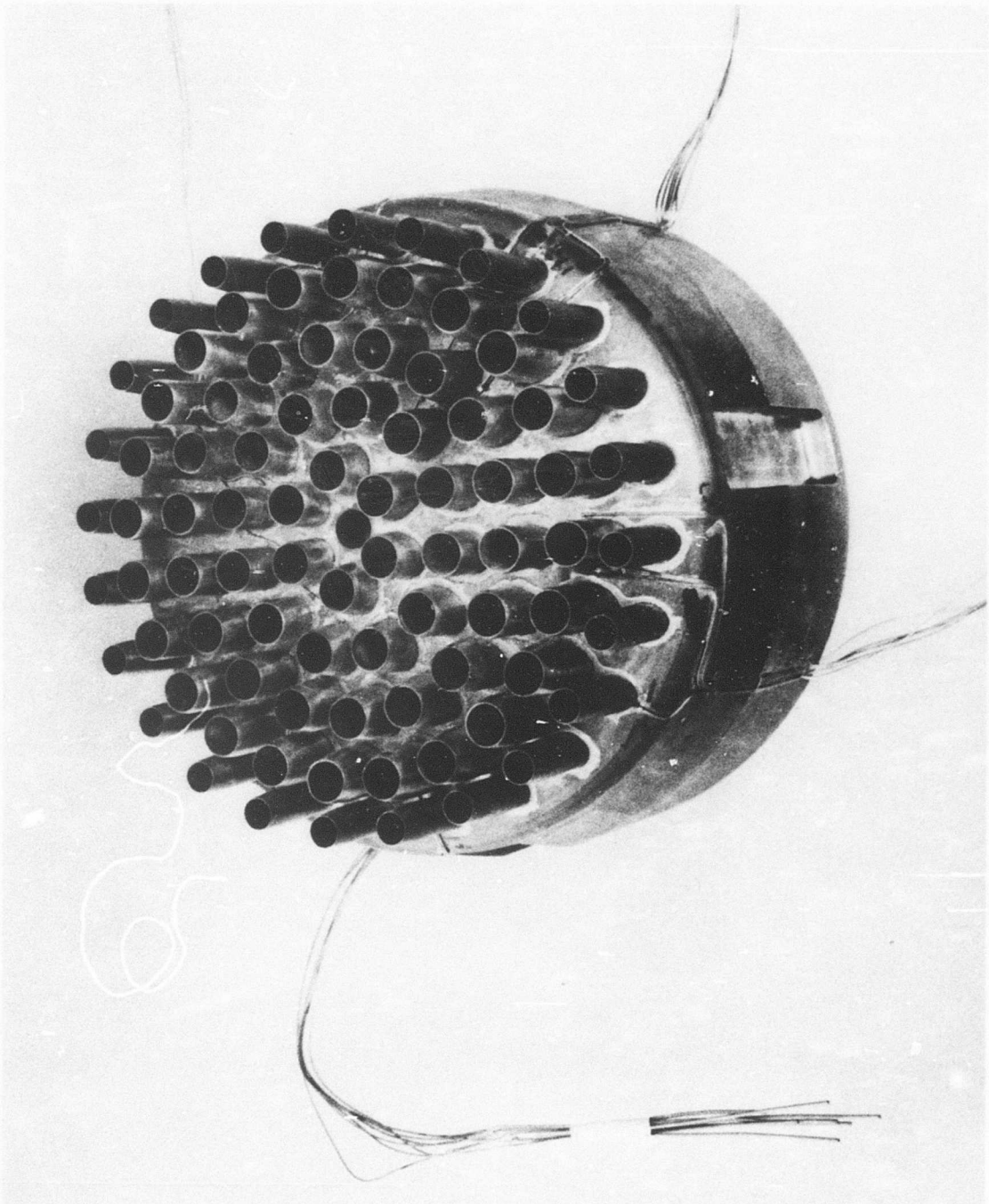

Figure 2. – LNHP – 3 Nozzle (85 – Tubes)

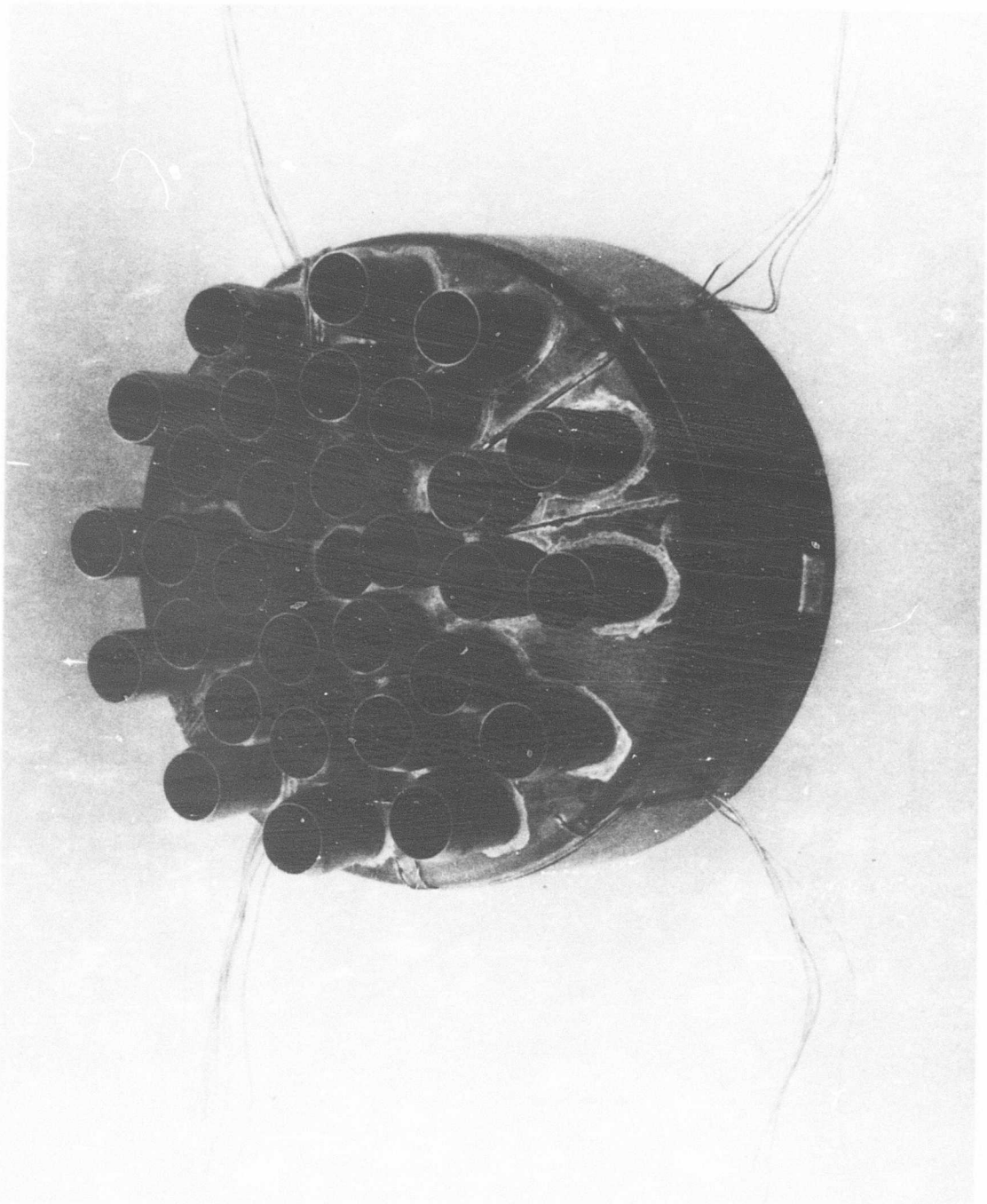

Figure 3. – LNHP – 4 Nozzle (31 – Tubes)

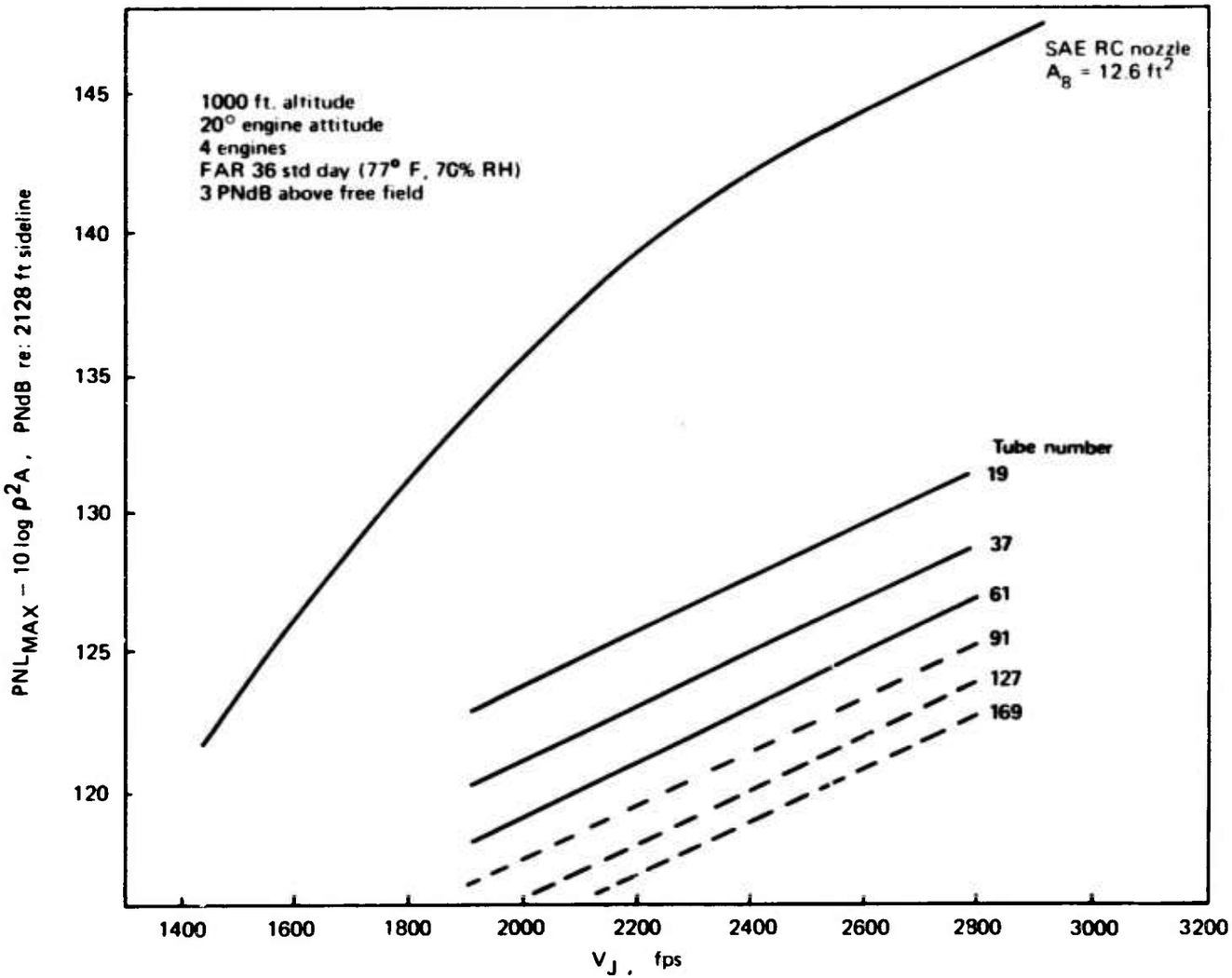

Figure 4. — Close-Packed Array, Jet Premerged Noise With L/D_E = 2 Lined Ejector, T_T = 1500° F

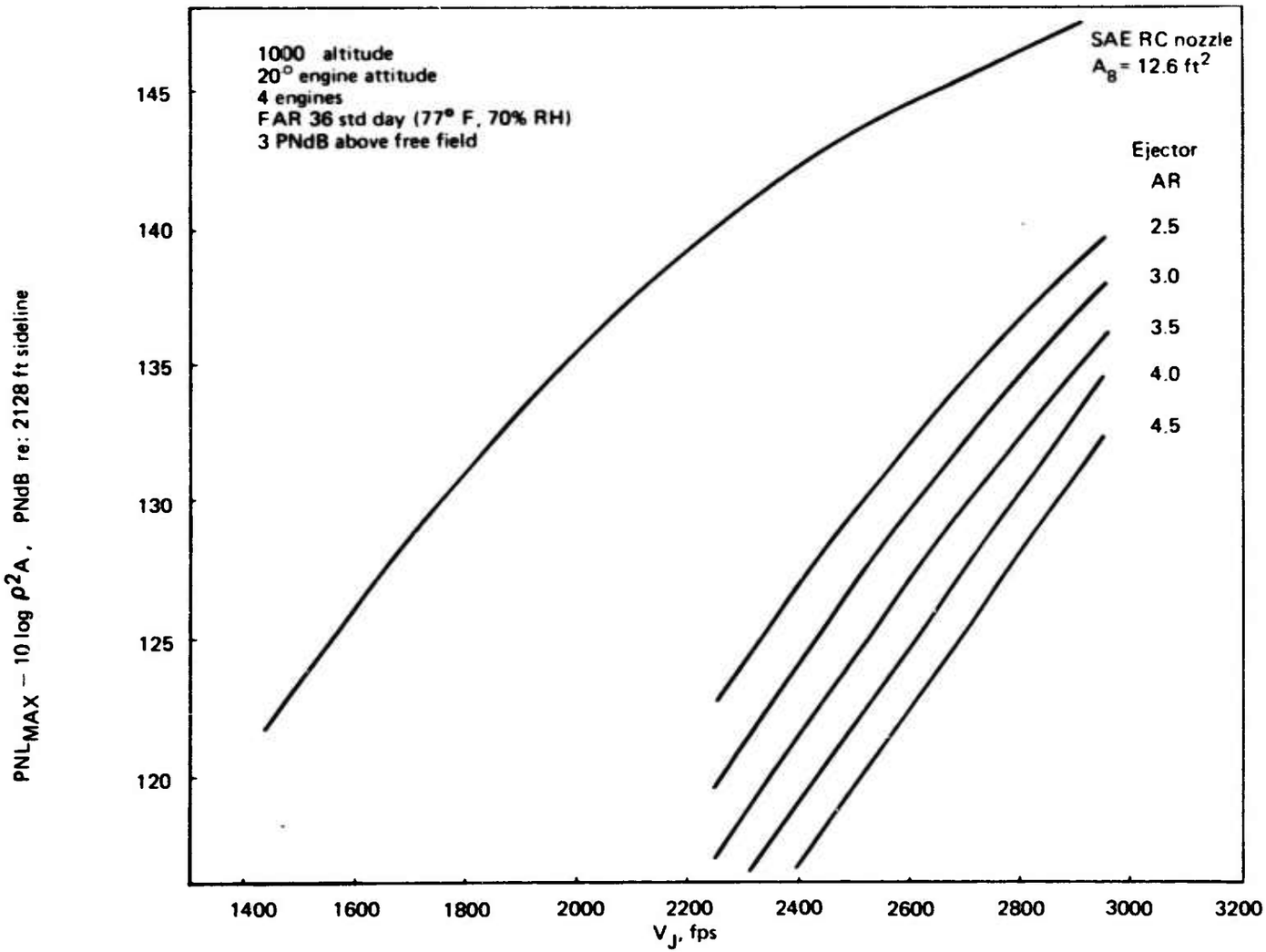

Figure 5. — Close-Packed Array, Jet Postmerged Noise at T_T = 1500° F

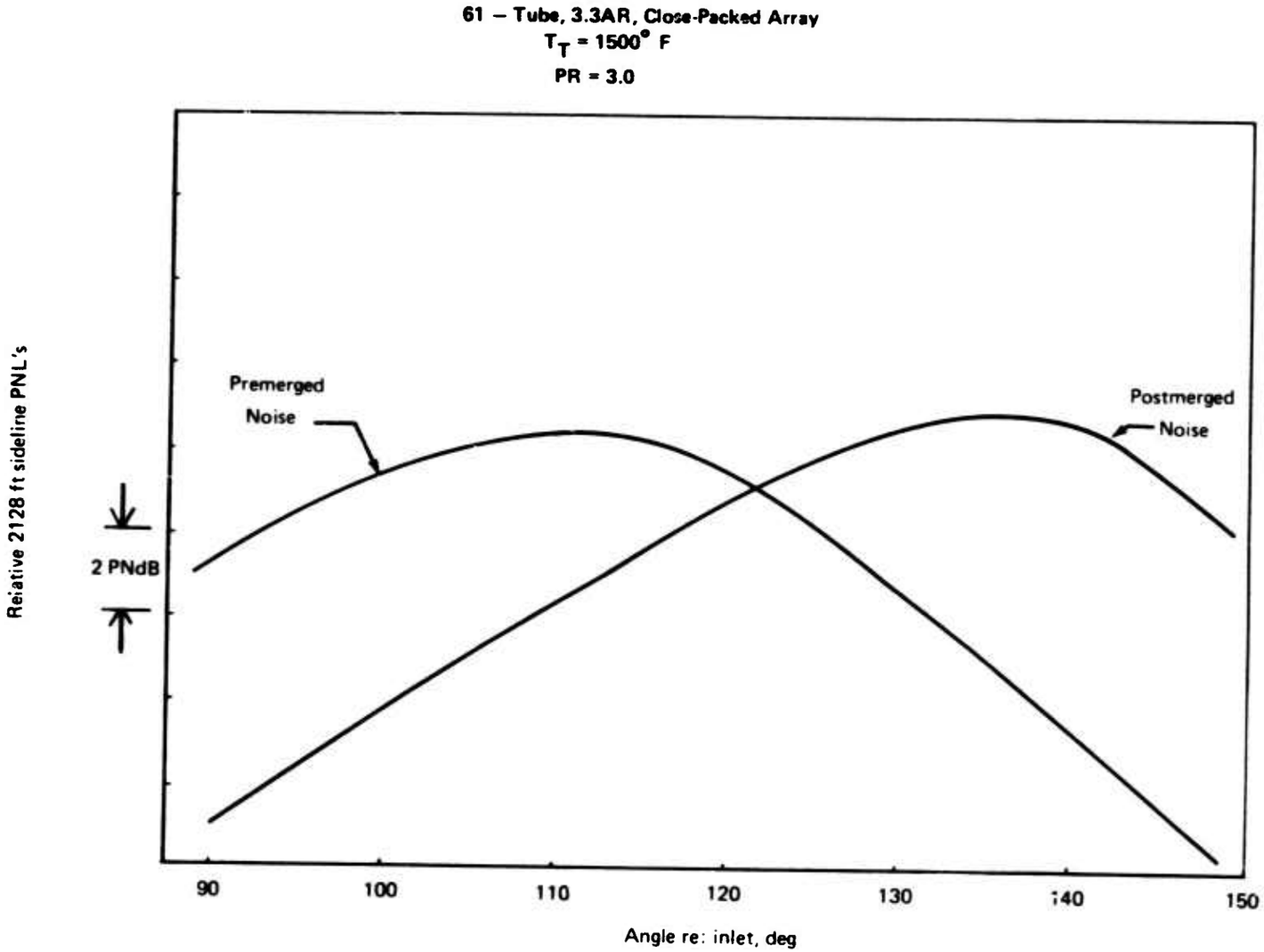

Figure 6. – Multitube Nozzle Suppressor System. Sideline Noise Directivity

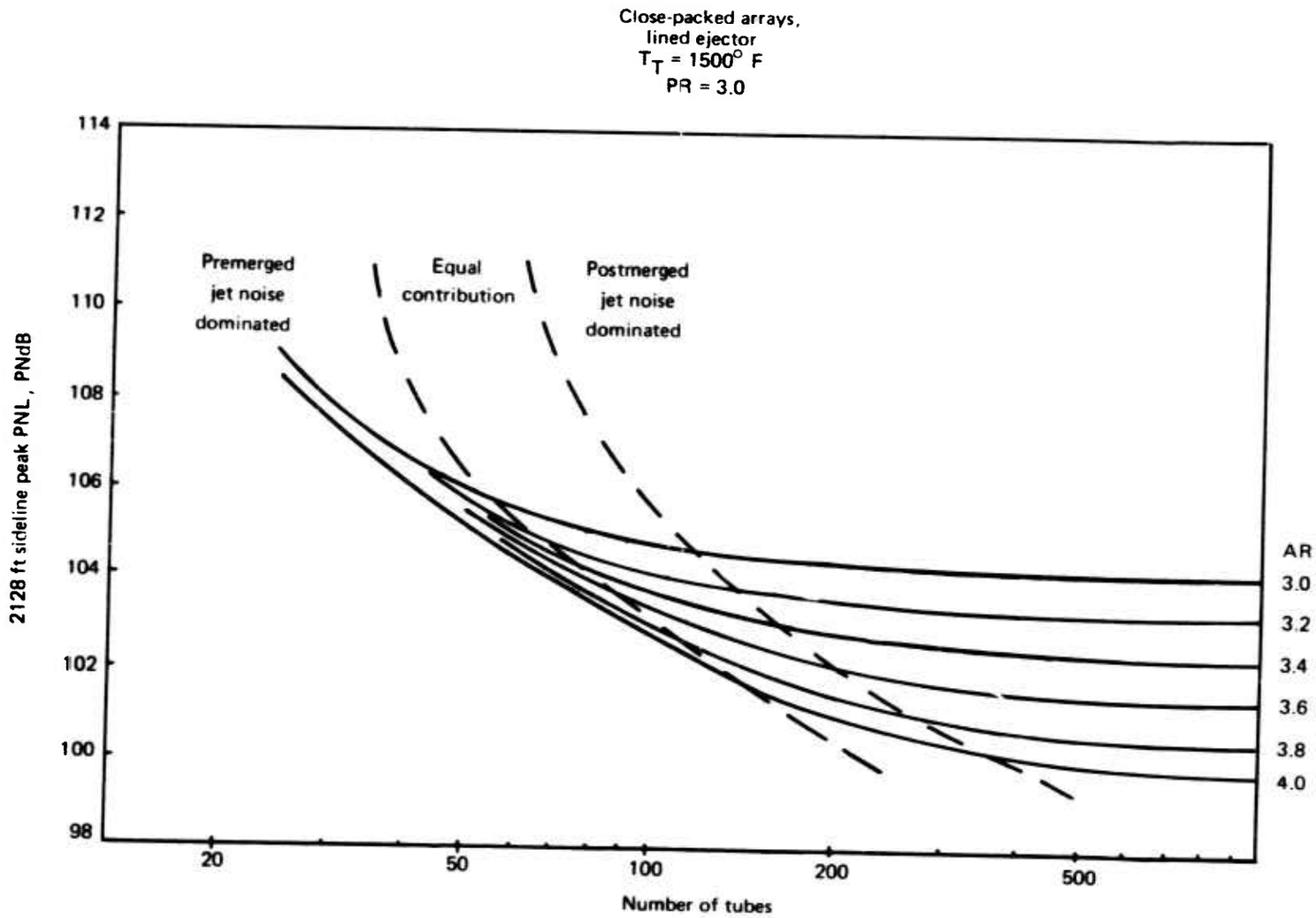

Figure 7. — Multitube Nozzle Suppressor System, Peak Sideline Perceived Noise Levels

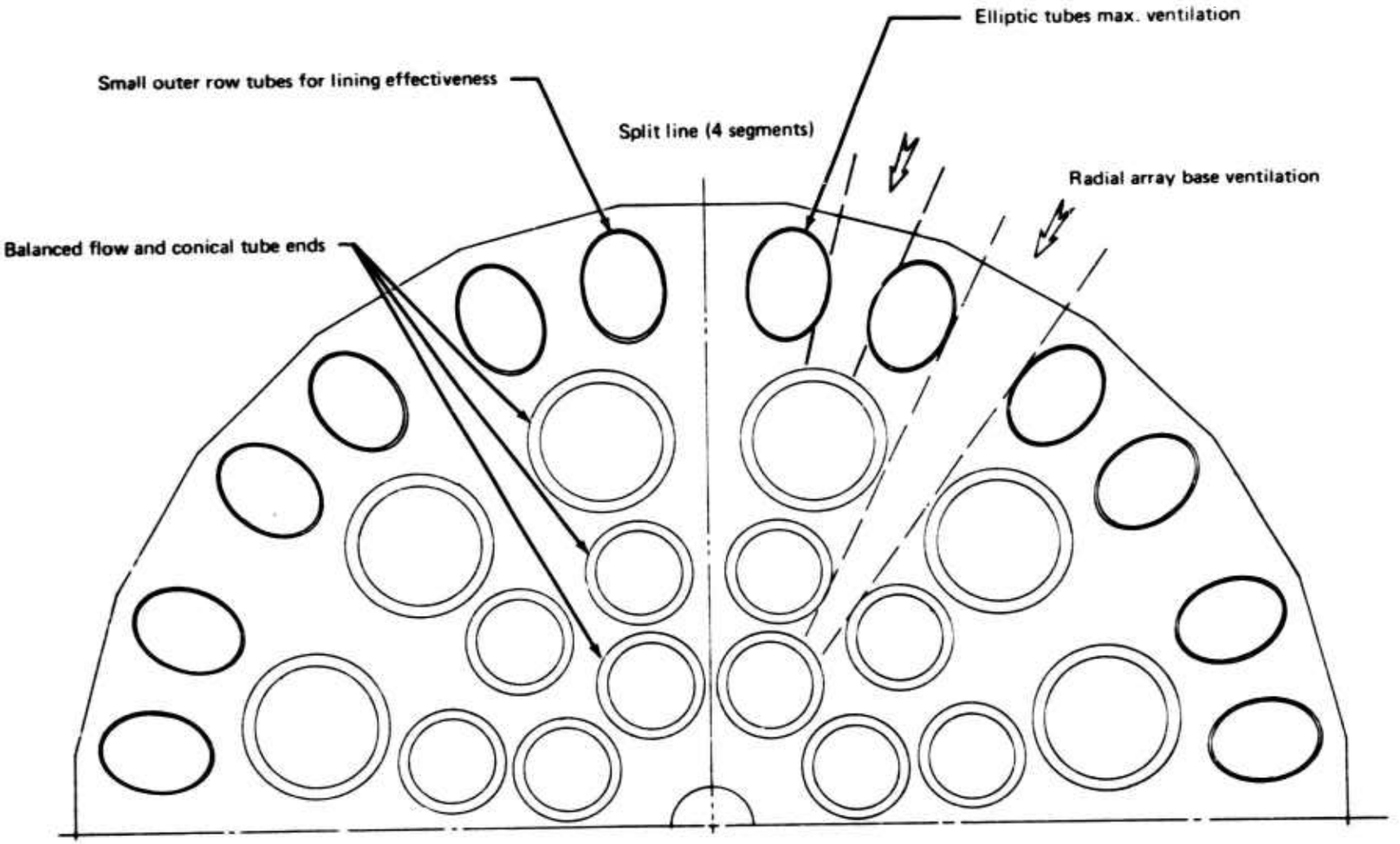

Figure 8.—LNHP-2 Jet Noise Suppressor System, 57-Tube Nozzle with 3.1 Area Ratio Ejector

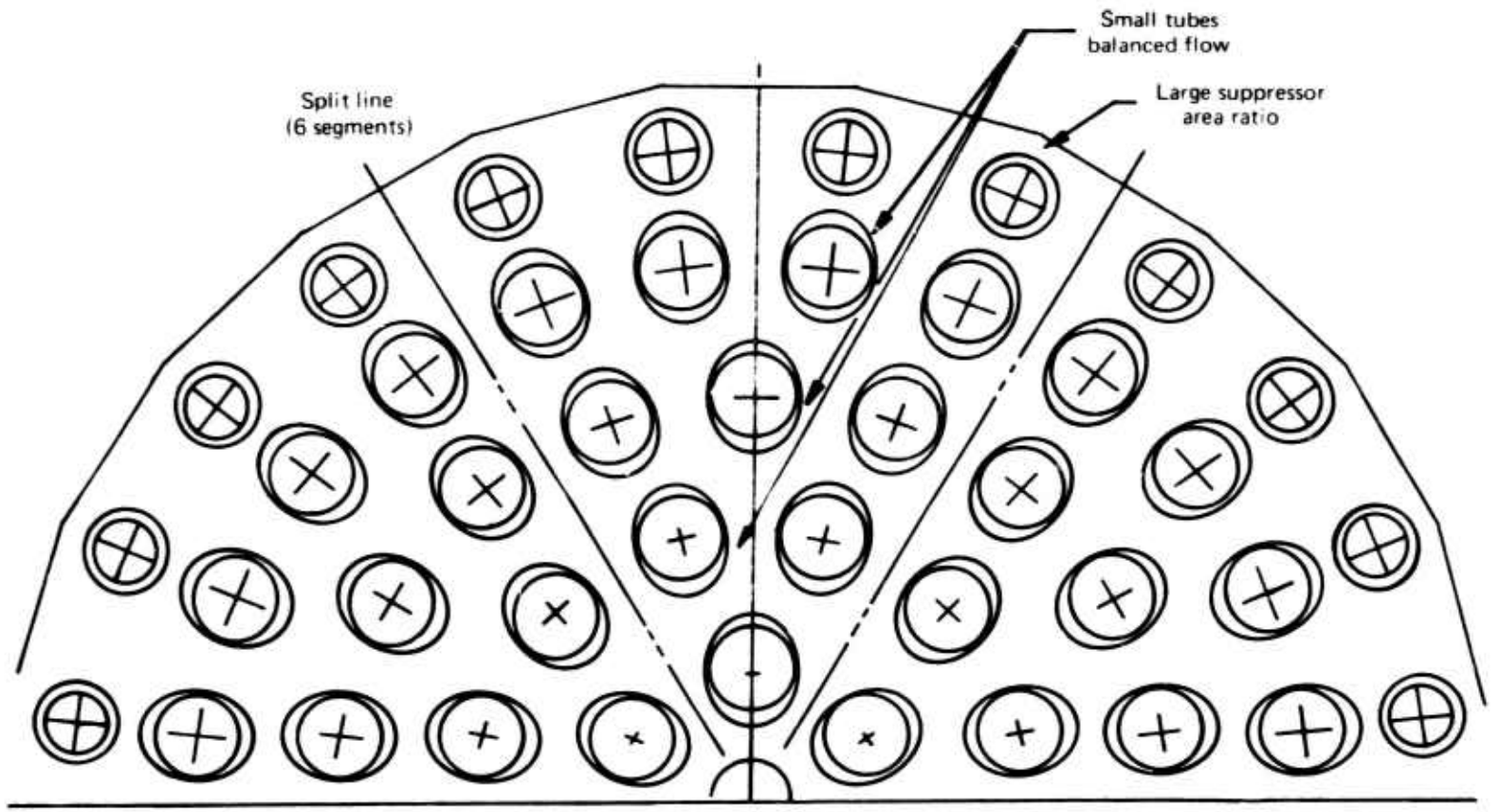

Figure 9.—LNHP-3 Jet Noise Suppressor System, 85-Tube Nozzle with 3.7 Area Ratio Ejector

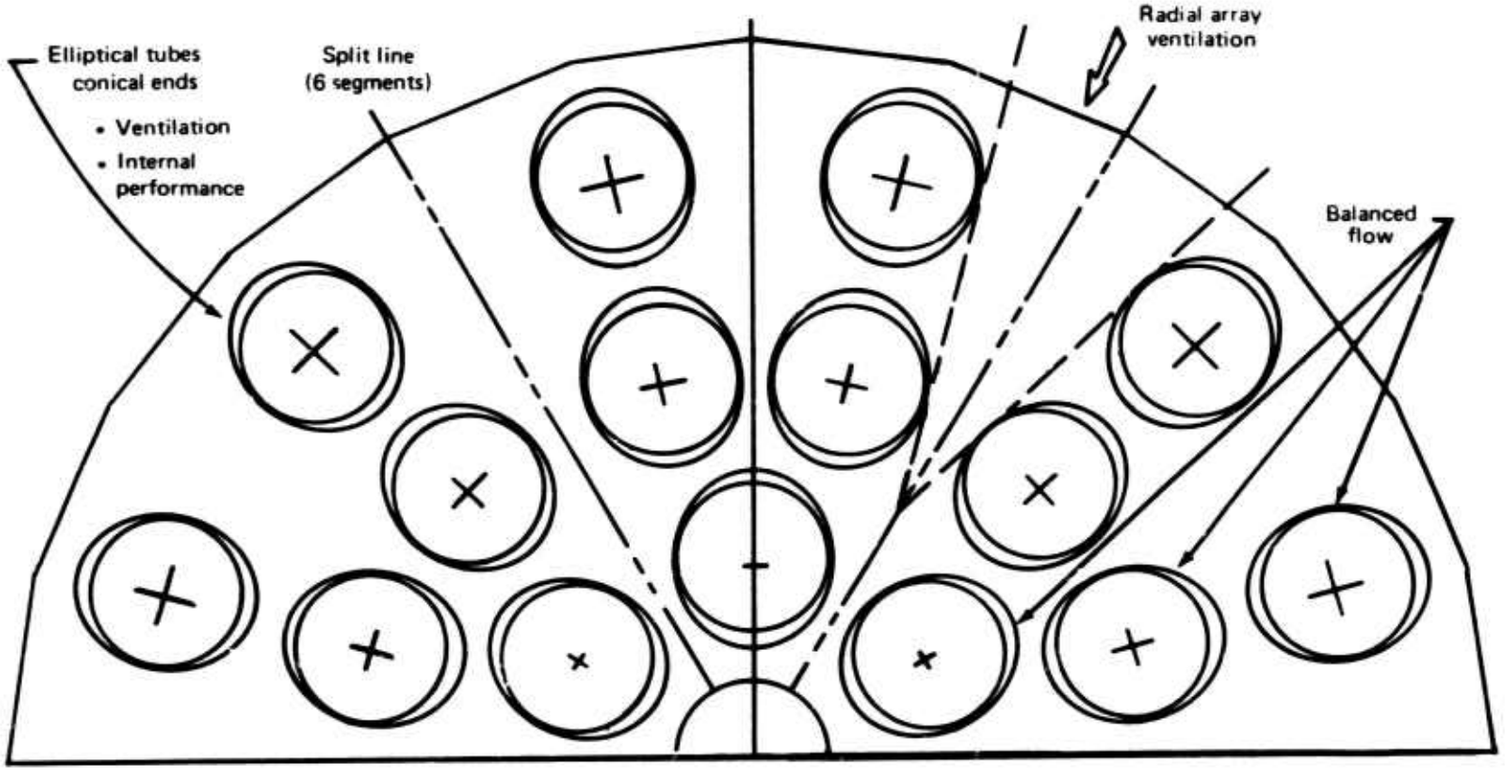

Figure 10.—LNHP-4 Jet Noise Suppressor System, 31-Tube Nozzle with 3.1 Area Ratio Ejector

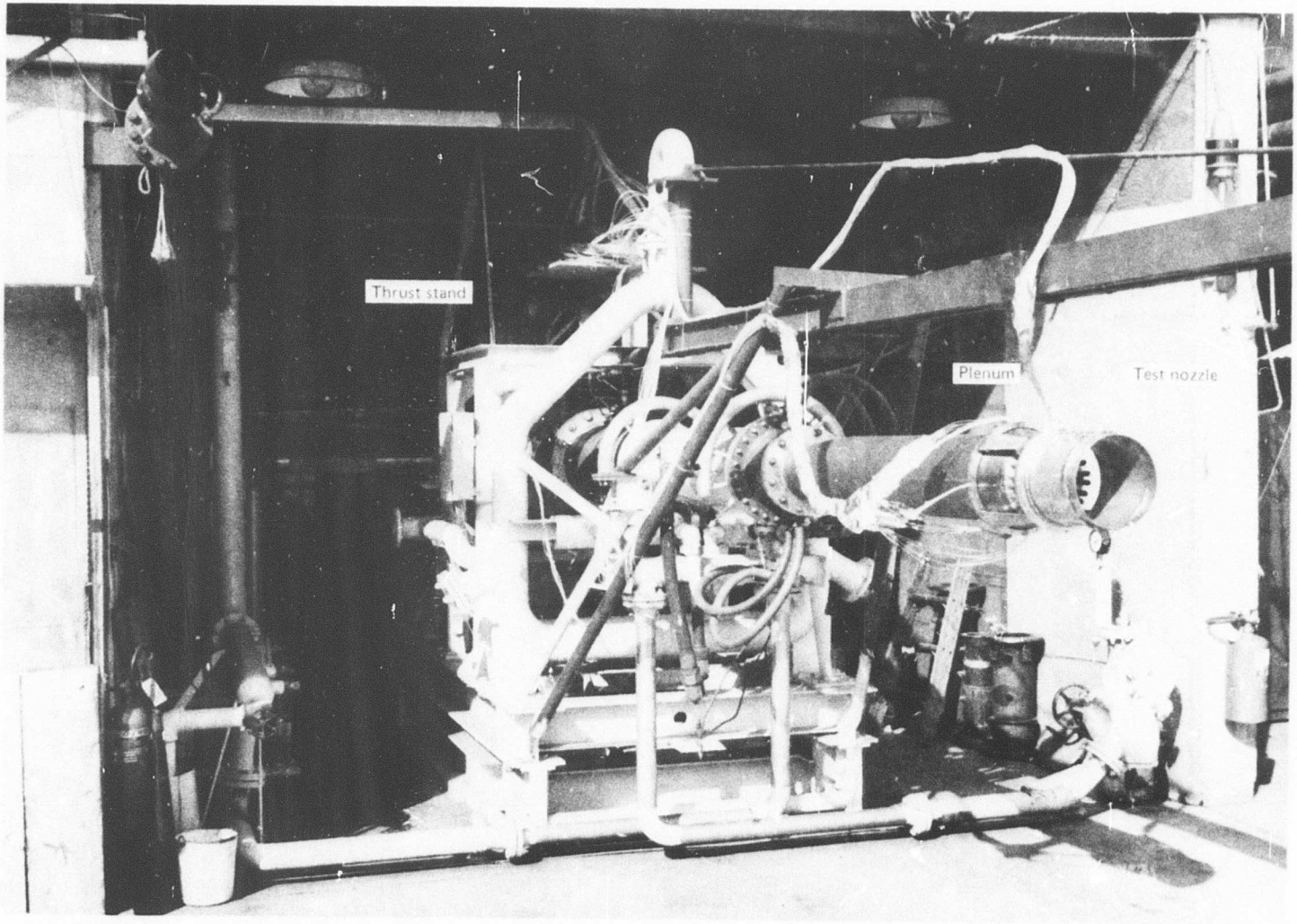

Figure 11. – Test Installation on the Hot Nozzle Rig

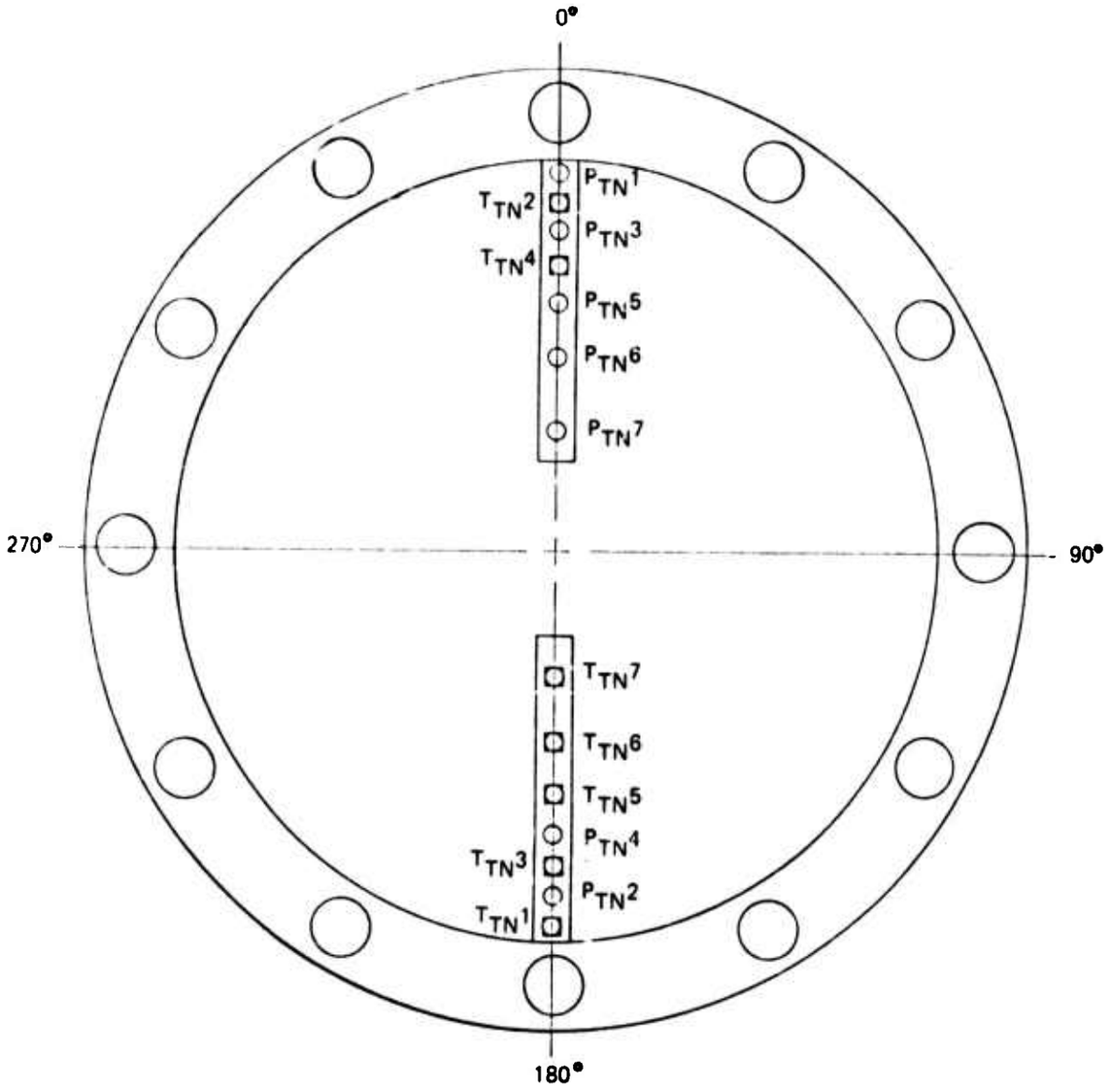

Figure 12. — Nozzle Charging Station, Total Pressure and Temperature Instrumentation

Figure 13. – Hot Nozzle Test Facility

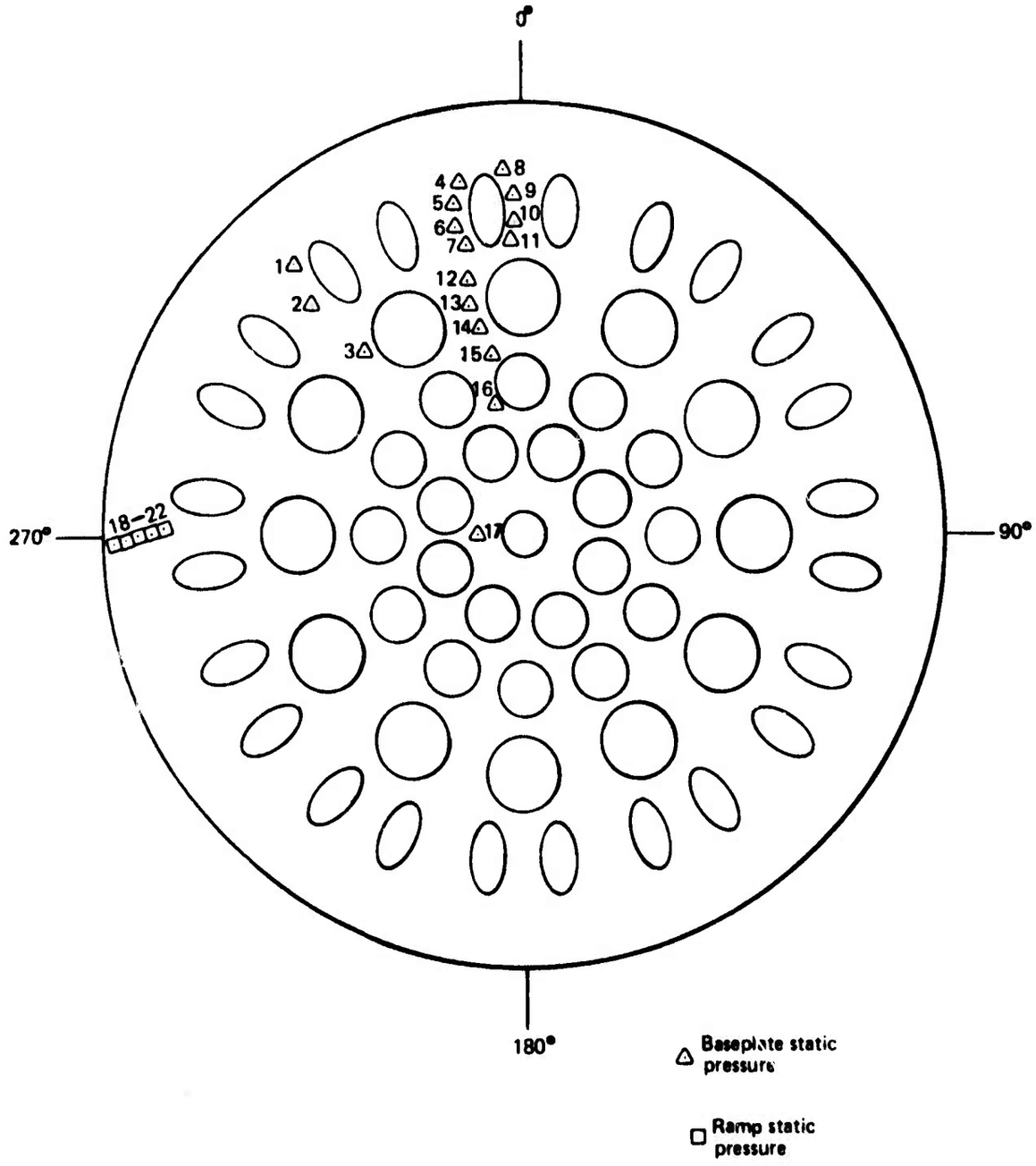

Figure 14. – LNHP – 2 Nozzle Static Pressure Instrumentation

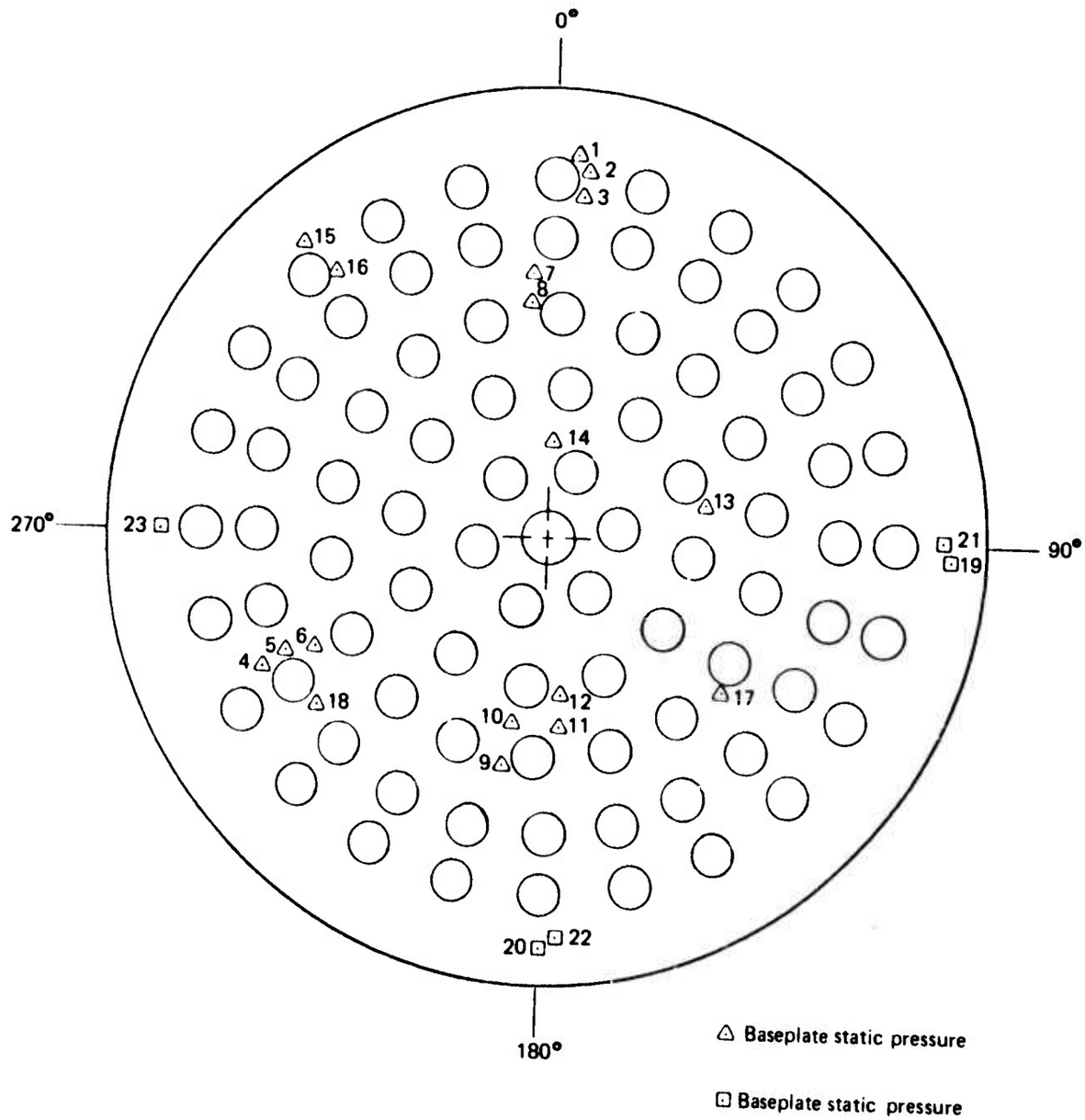

Figure 15. – LNHP – 3 Nozzle Static Pressure Instrumentation

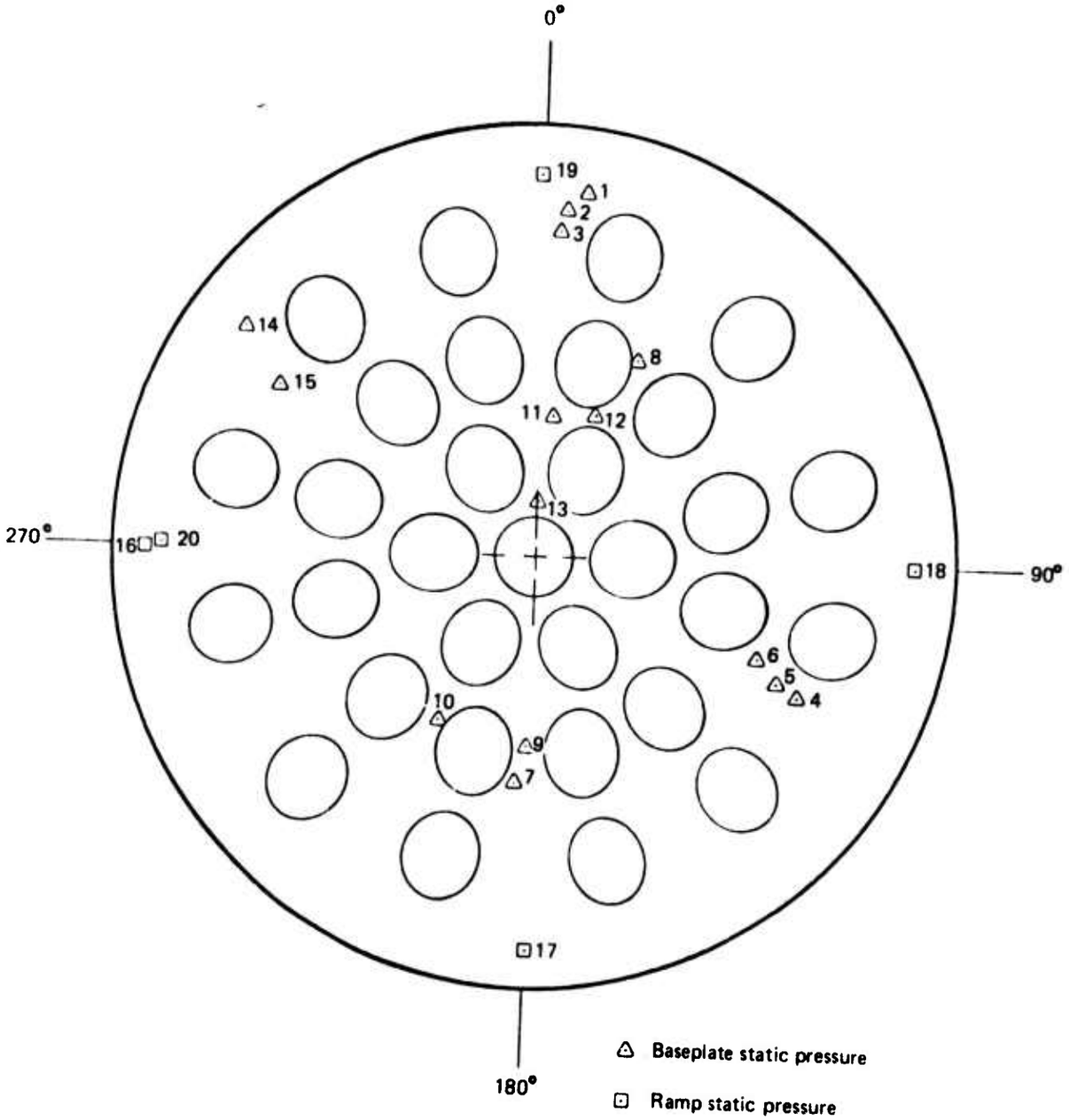

Figure 16. – LNHP – 4 Nozzle, Static Pressure Instrumentation

LNHP-2 Lip

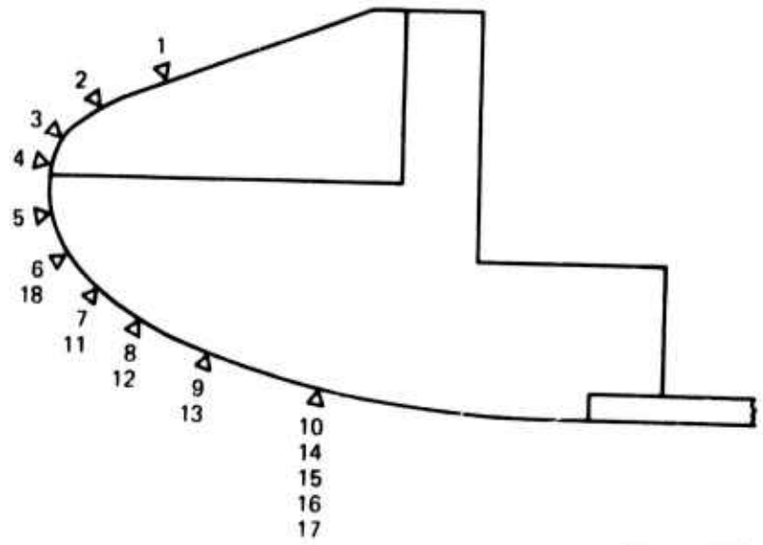

Taps 1-10 @ 0 °
Taps 11-14 @ 45°
Taps 15 @ 90°
Taps 16 @ 180°
Taps 17 @ 270°
Taps 18 @ 7.5°

LNHP-3 and LNHP-4 Lip

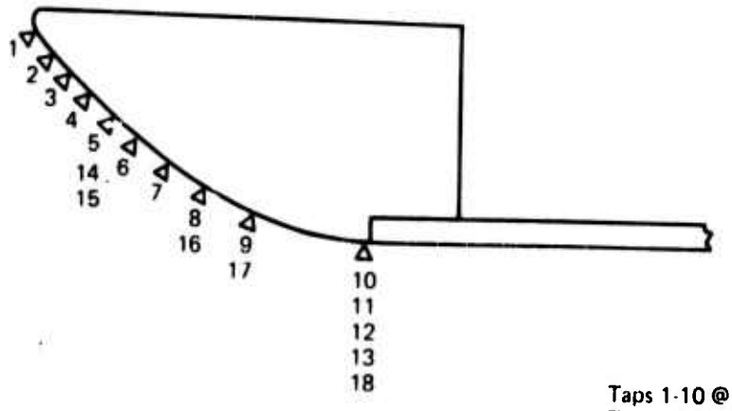

Taps 1-10 @ 0 °
Taps 11 @ 90°
Taps 12 @ 180°
Taps 13 @ 270°
Taps 14 @ 7.5°
Taps 15 @ 15°
Taps 16-18 @ 45°

Figure 17.—Ejector Lip Static Pressure Instrumentation

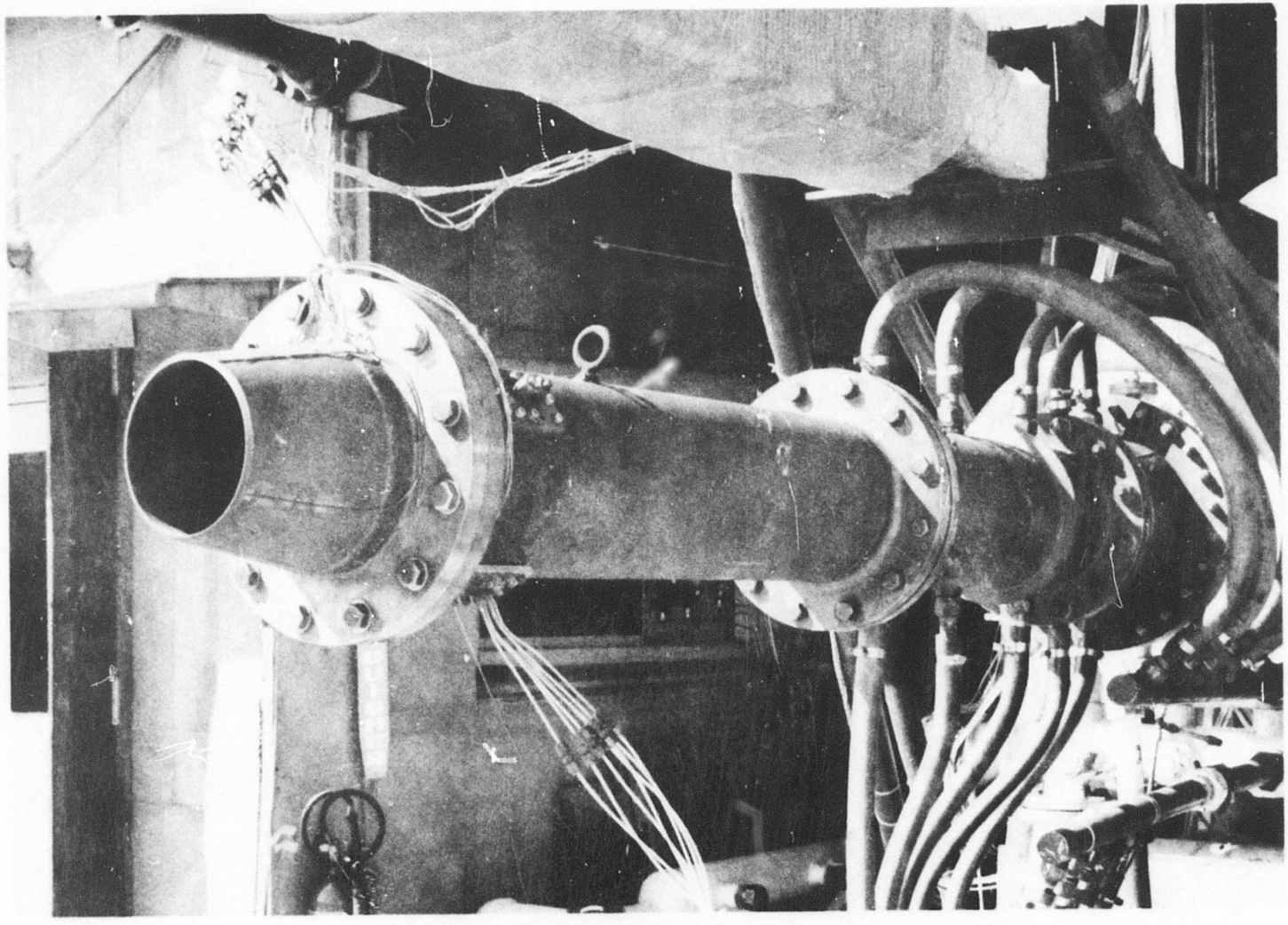

Figure 18. – 6-Inch Round Convergent Reference Nozzle

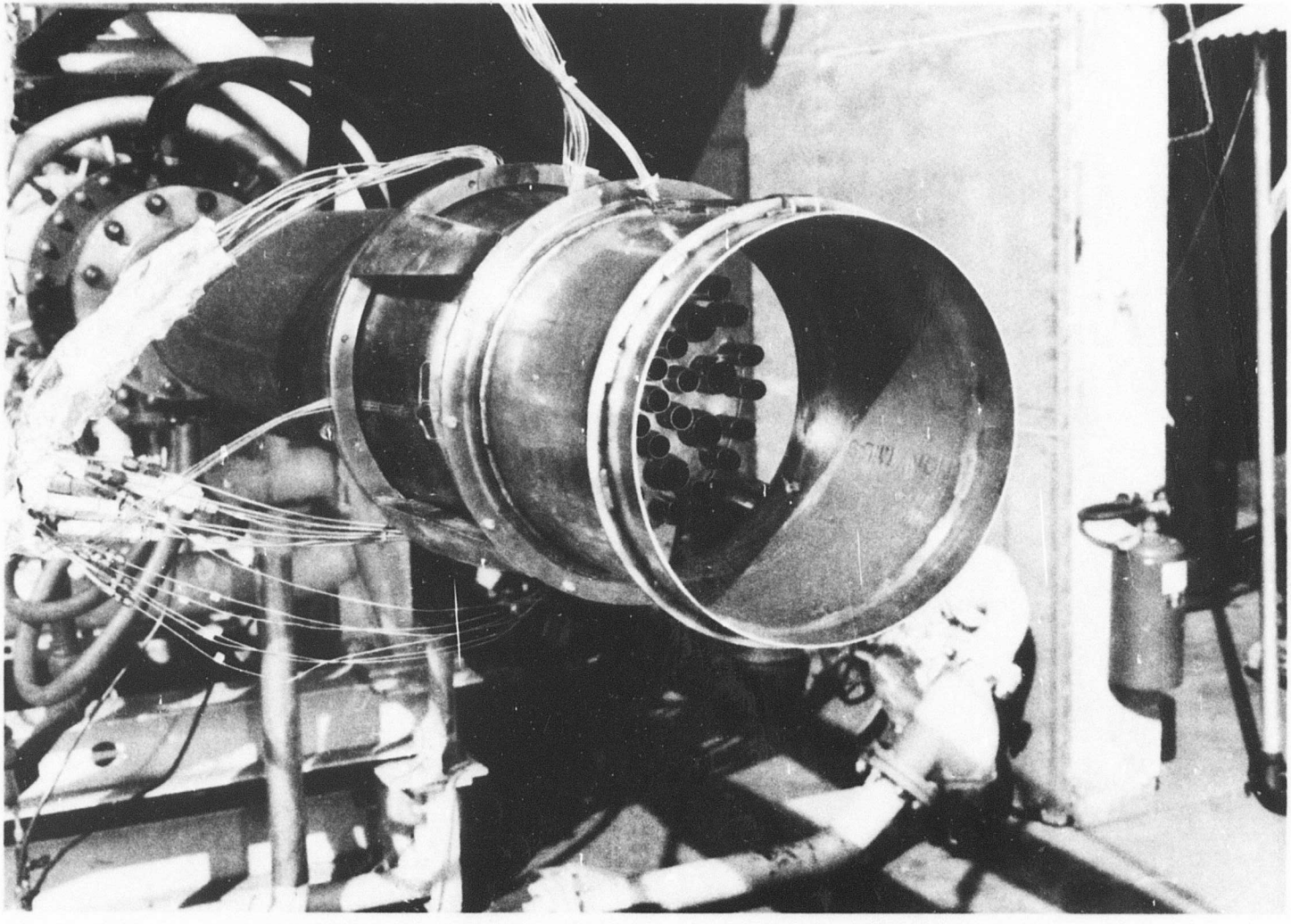

Figure 19. – LNHP – 2 Nozzle Hardwall Ejector Configuration

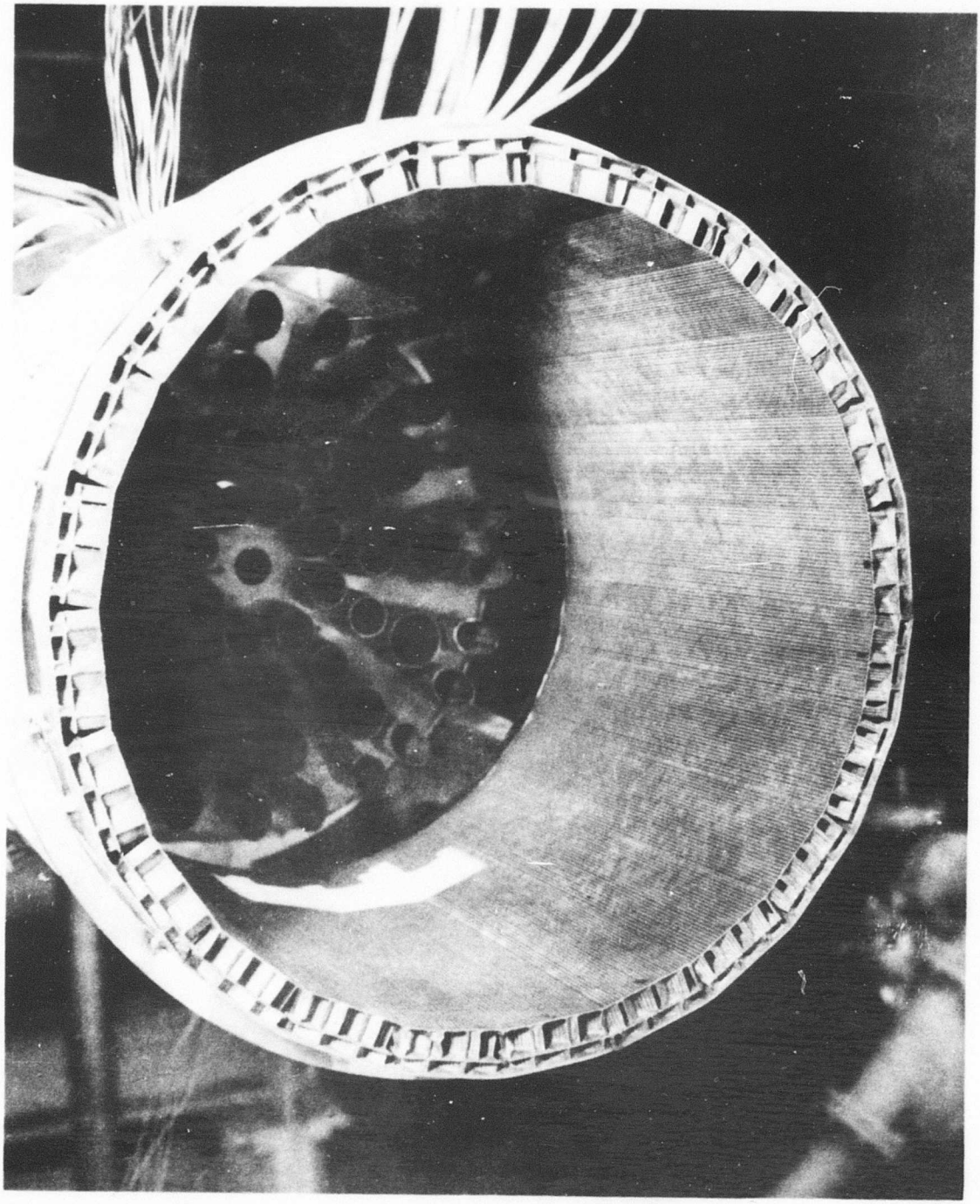

Figure 20. — LNHP — 2 Nozzle Lined Ejector Configuration

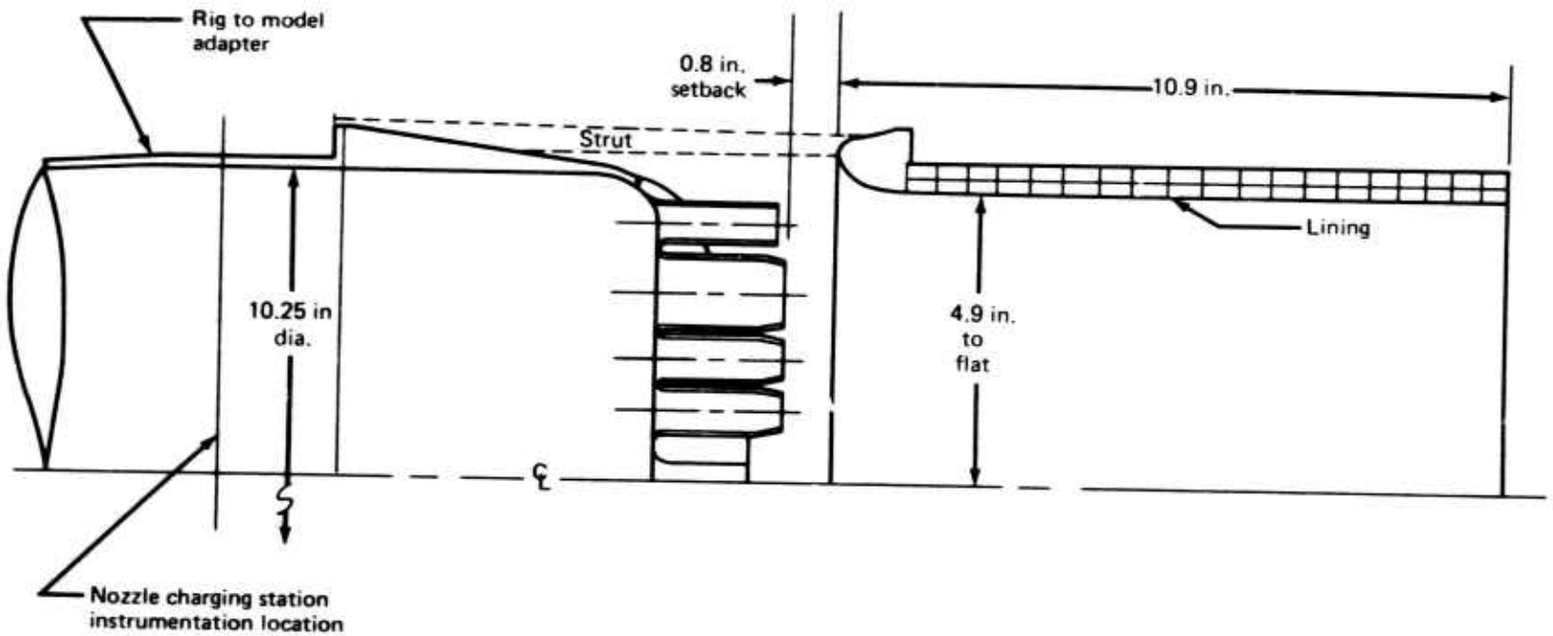

Figure 21. – LNHP – 2 Model Installation

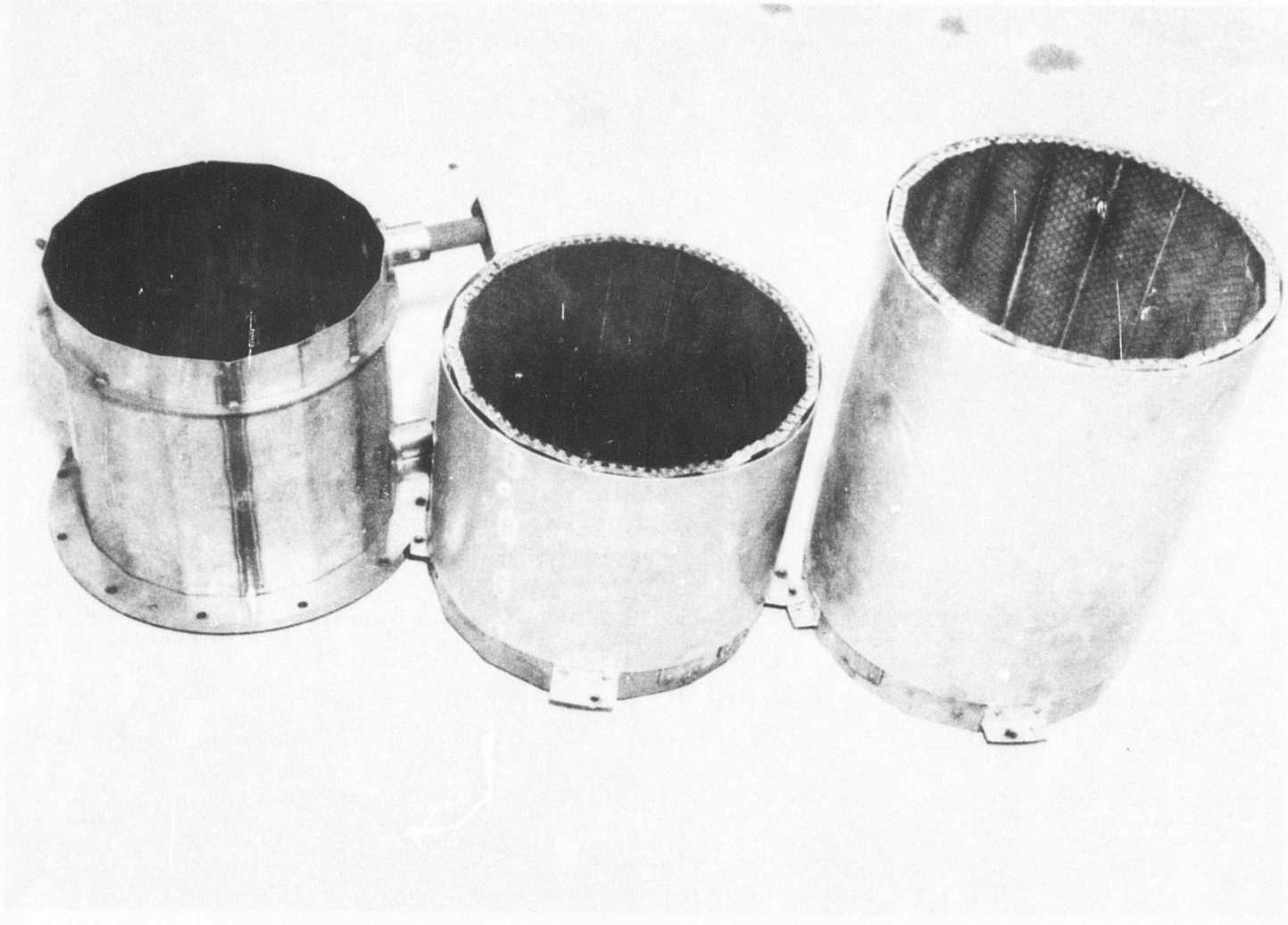

Figure 22. – LNHP – 3 and LNHP – 4 Ejectors

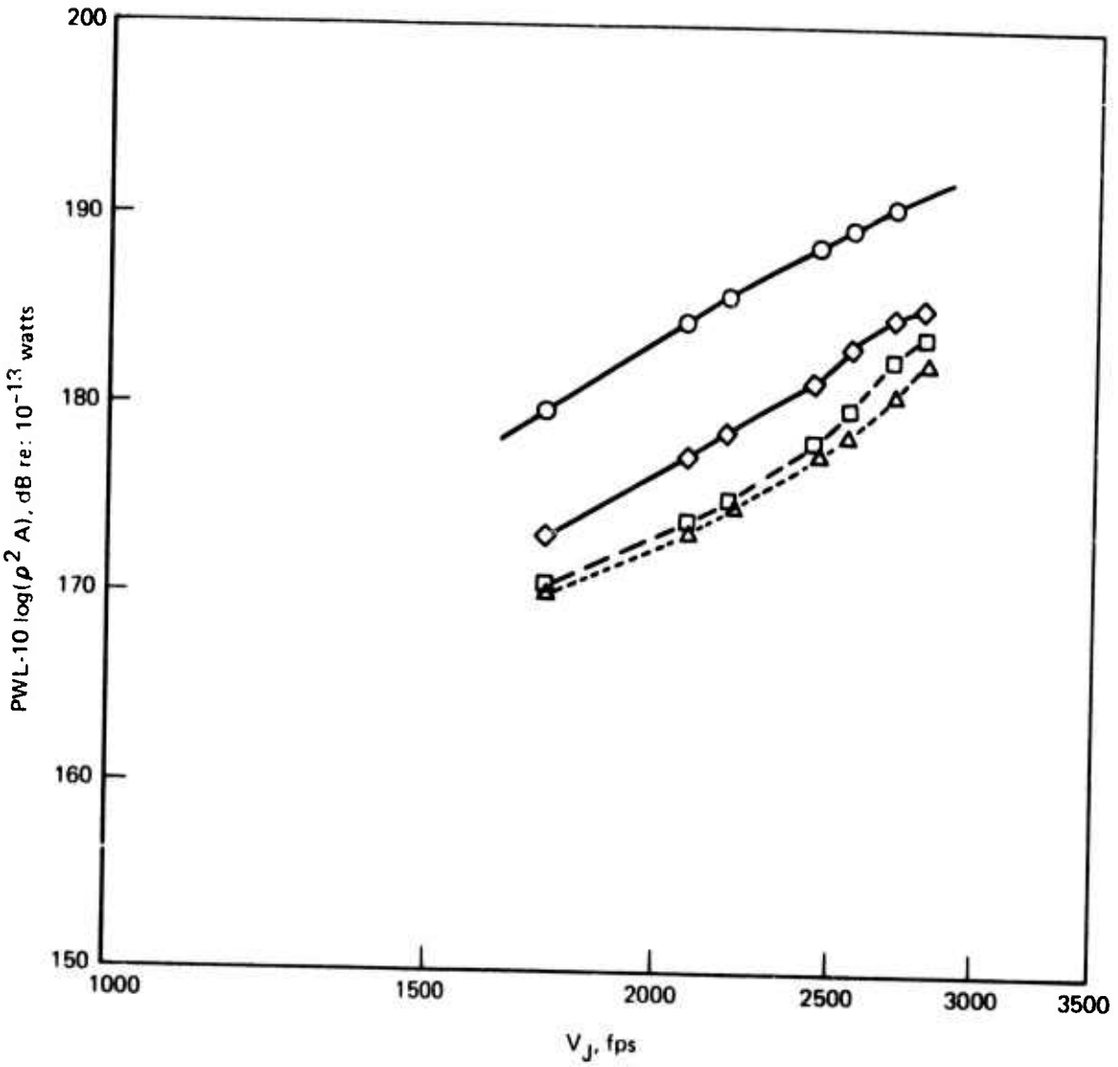

Figure 23.–Multitube Nozzle Total Noise Power (Without Ejector)

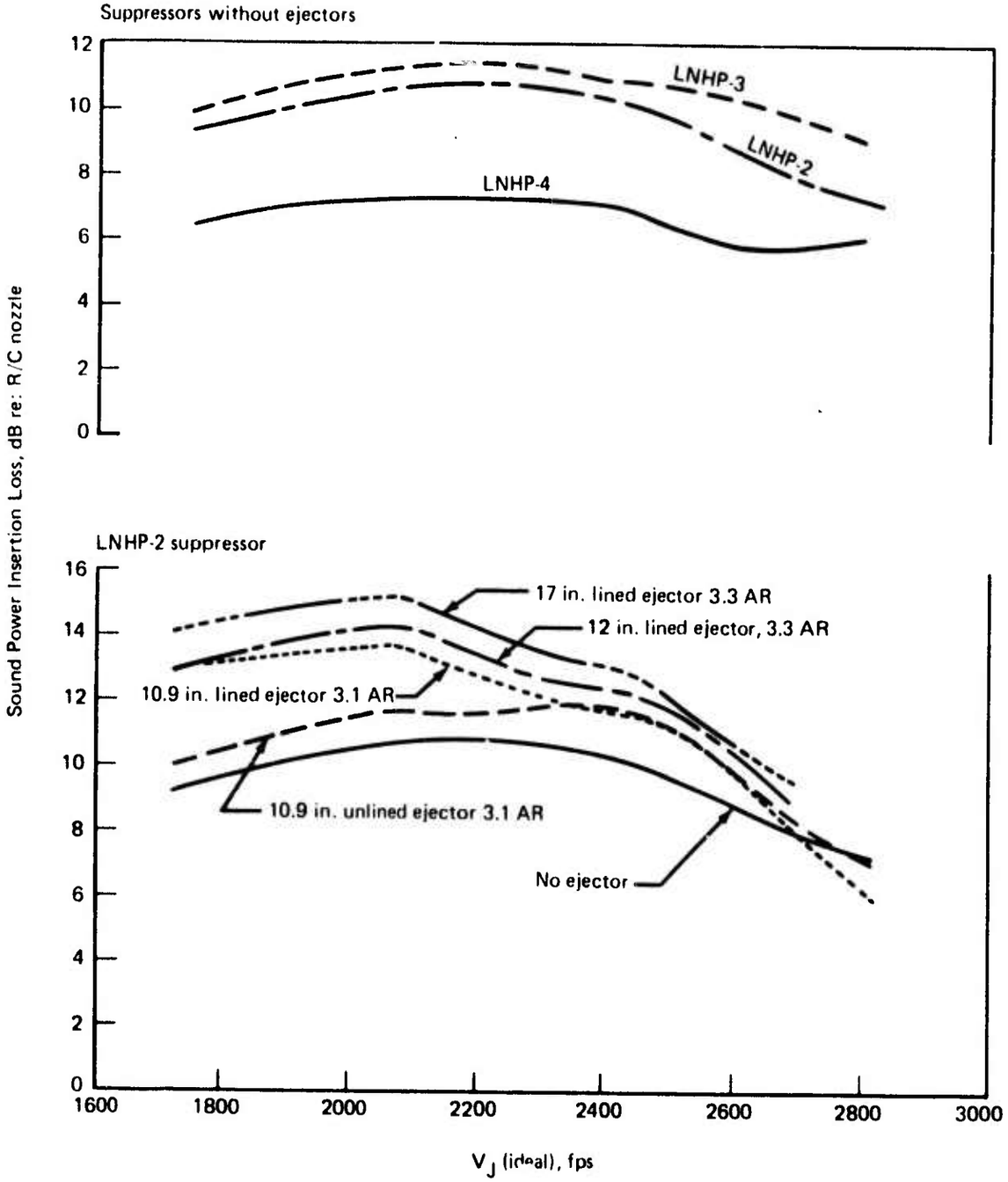

Figure 24.–Multitube Nozzle/Ejector, Total Noise Power Suppression at T_T = 1500°F

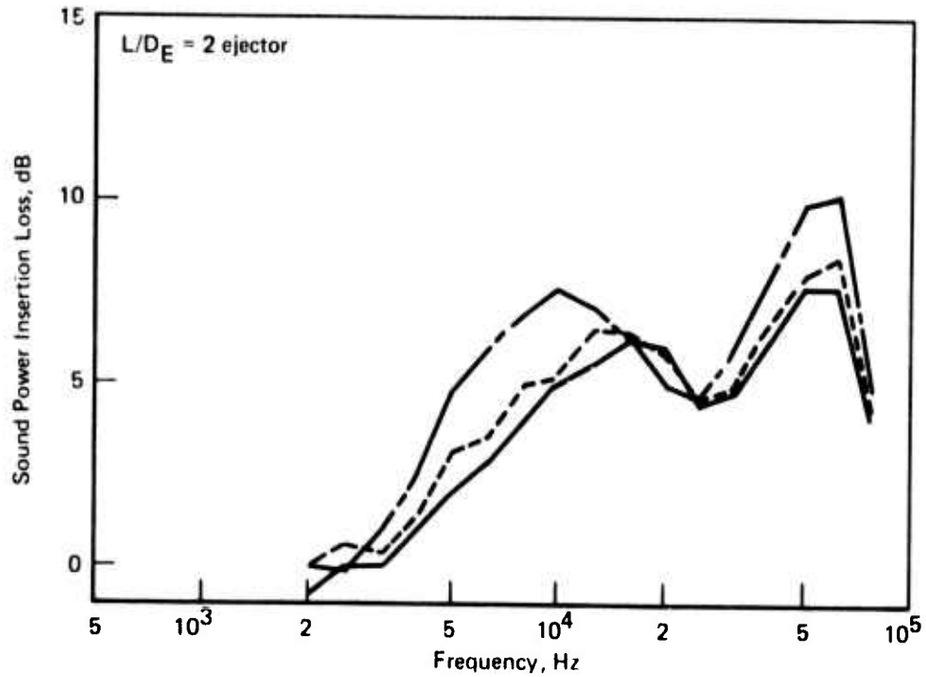

Figure 25.—LNHP-2 Suppressor System With Lining No. 1 at T_T = 1150°F

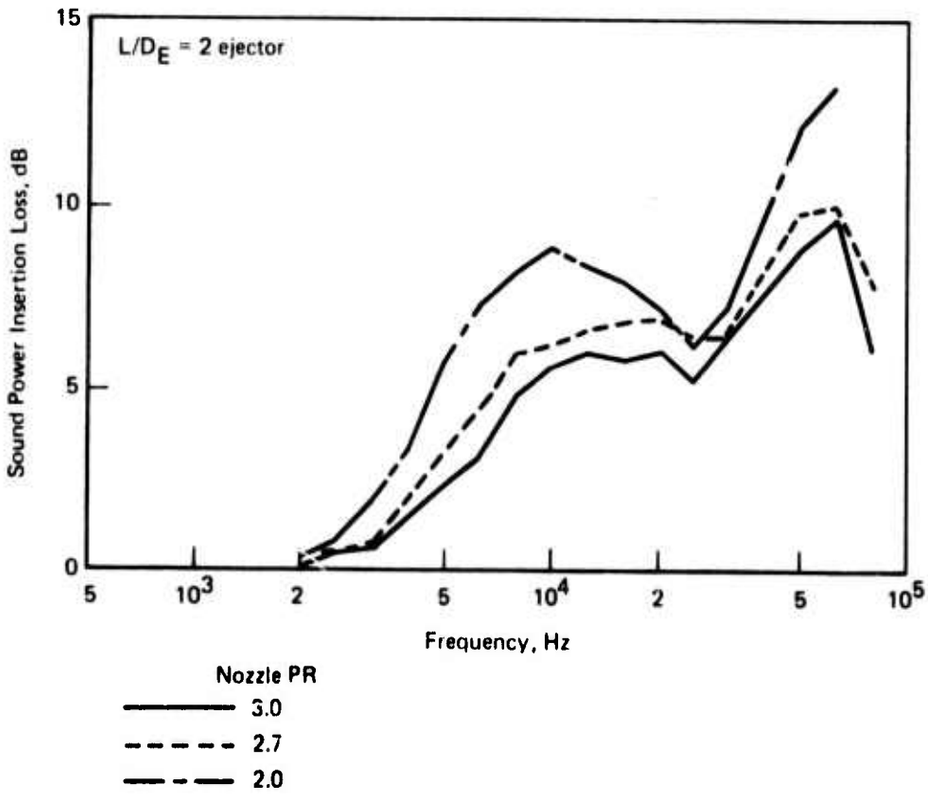

Figure 26.—LNHP-2 Suppressor System With Lining No. 1 at T_T = 1500°F

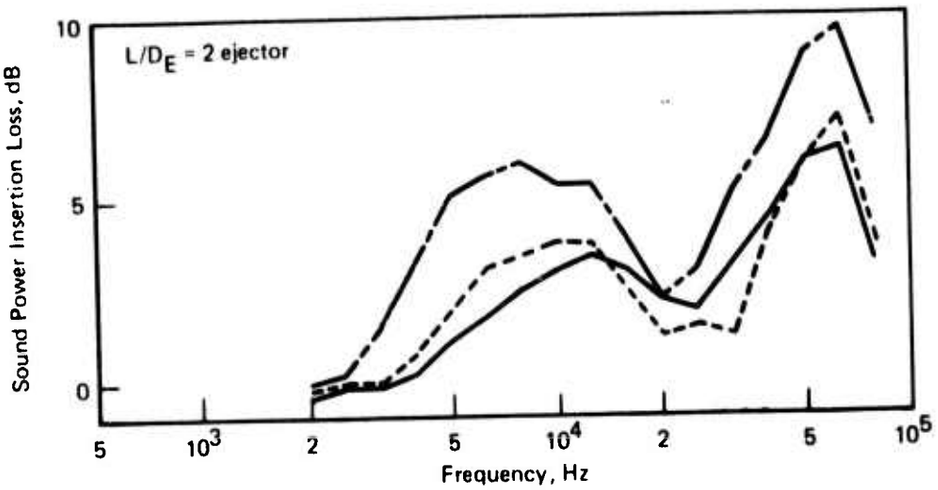

Figure 27.–LNHP-2 Suppressor System With Lining No. 2 at T_T = 1150°F

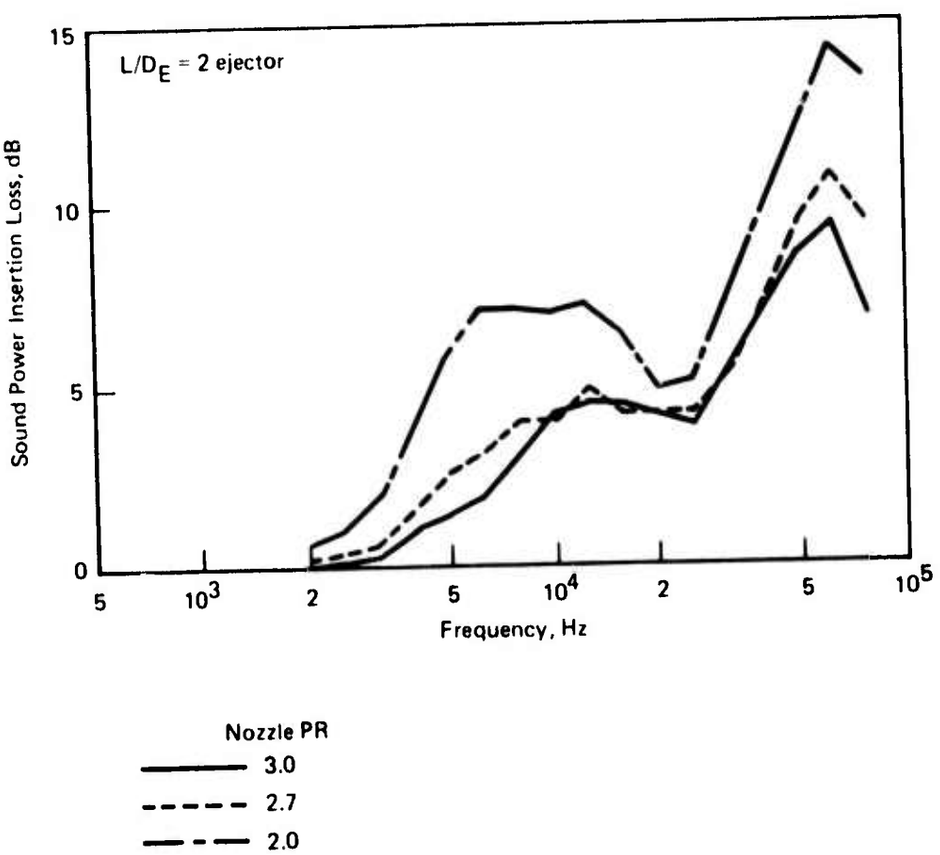

Figure 28.–LNHP-2 Suppressor System With Lining No. 2 at T_T = 1500° F

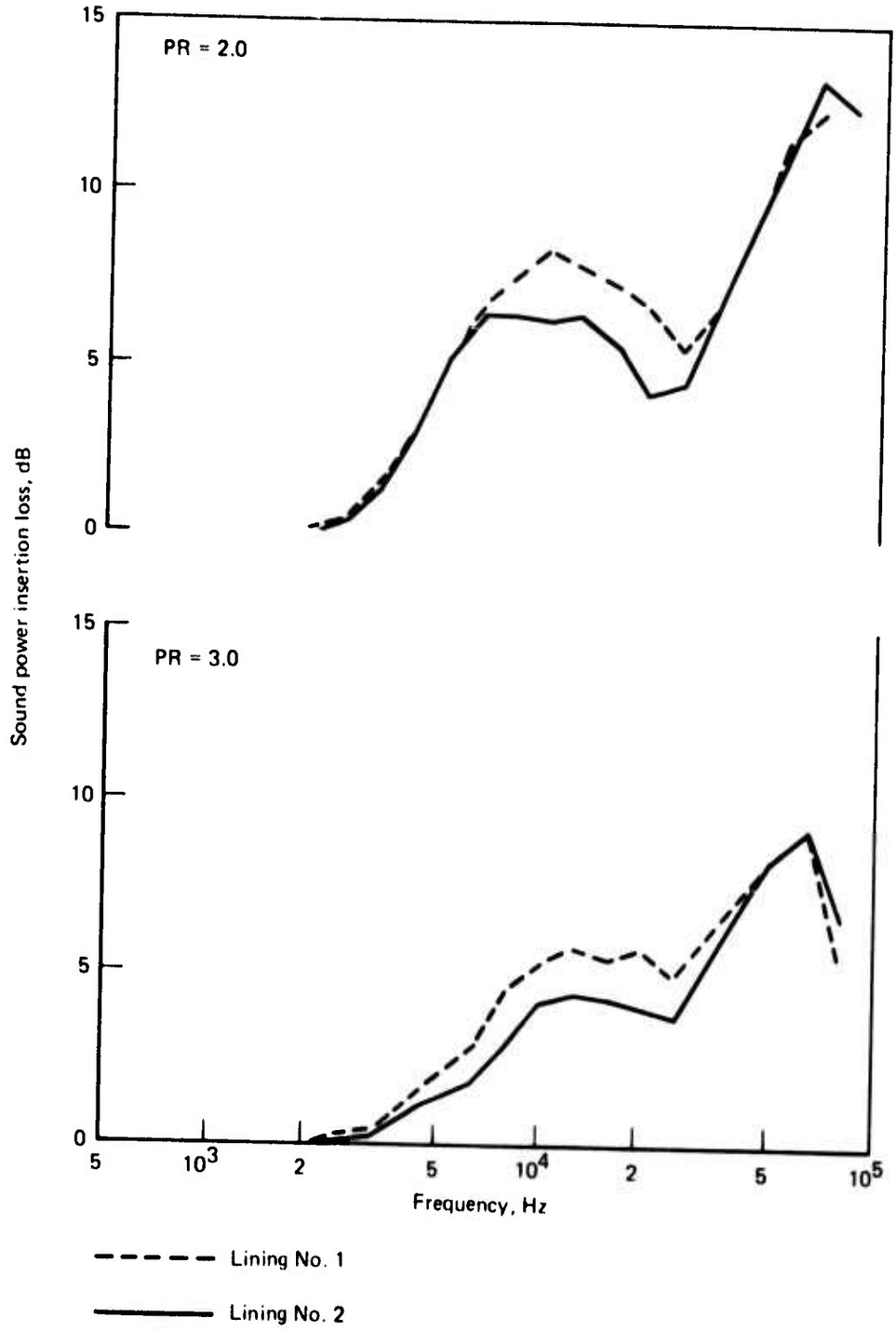

Figure 29.—LNHP-2 Suppressor System at T_T = 1500°F

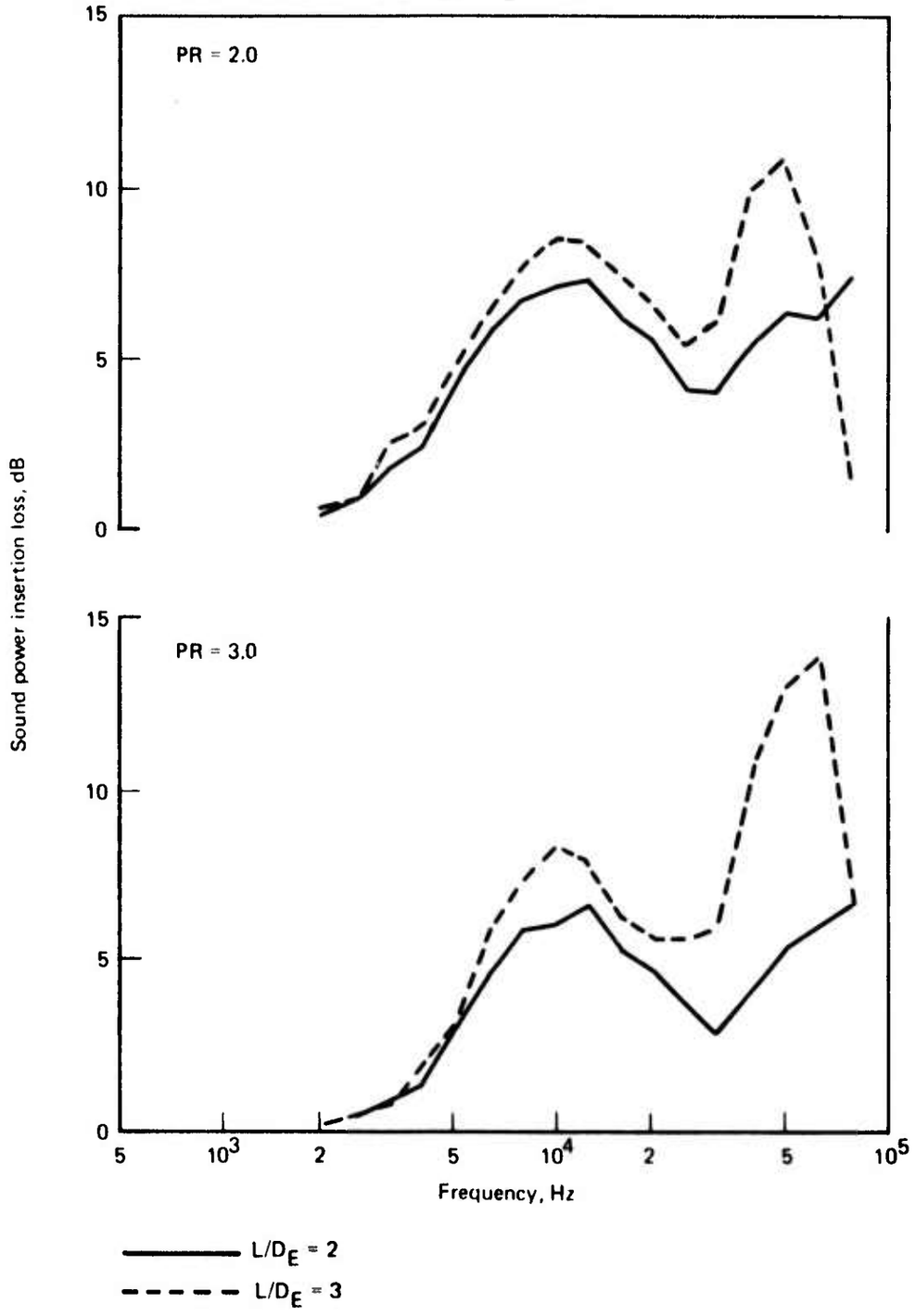

Figure 30.–LNHP-3 Suppressor System With Lining No. 1 at T_T = 1500°F

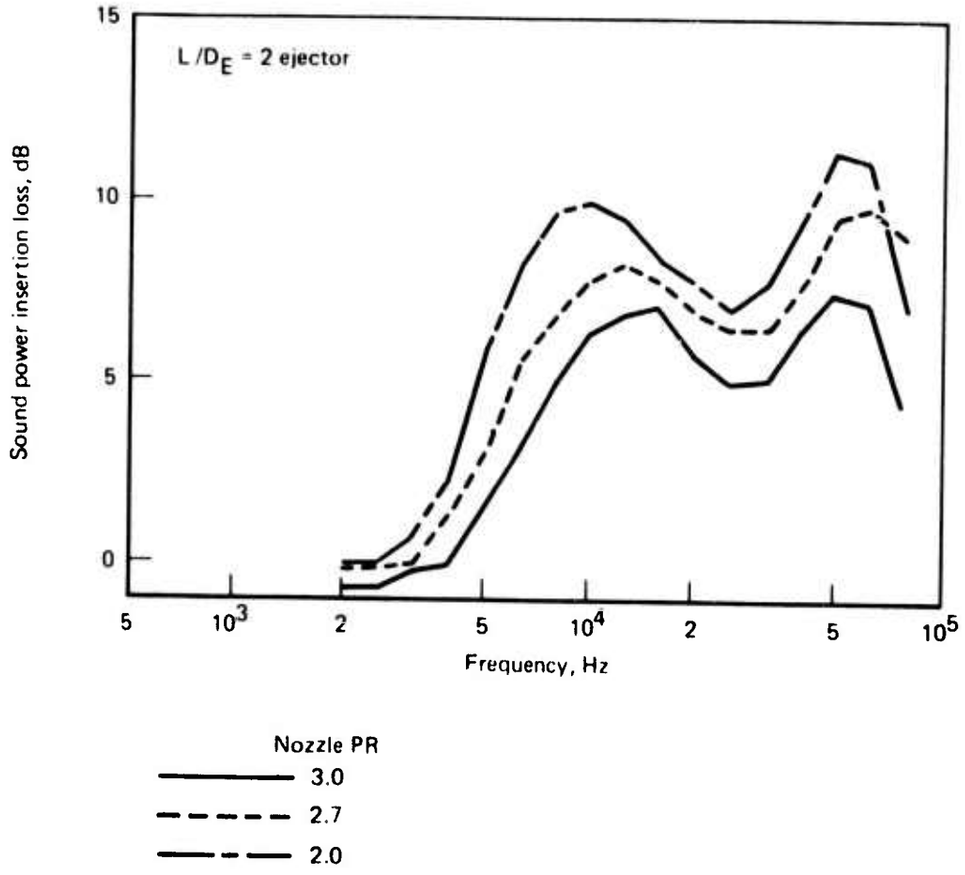

Figure 31.—LNHP-4 Suppressor System With Lining No. 1 at T_T = 1500°F

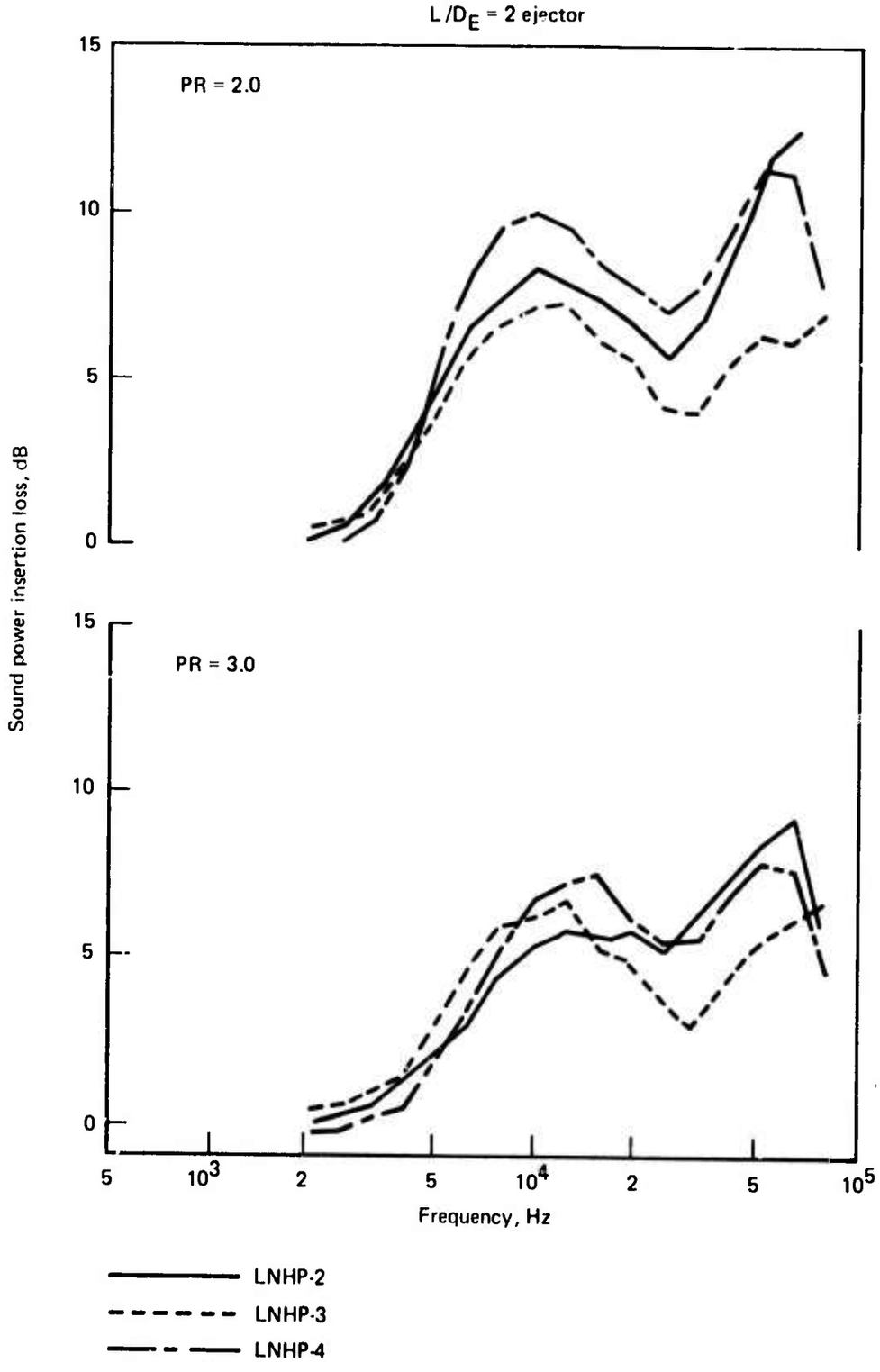

Figure 32.—Lining No. 1 in Combination With Various Noise Sources at T_T = 1500°F

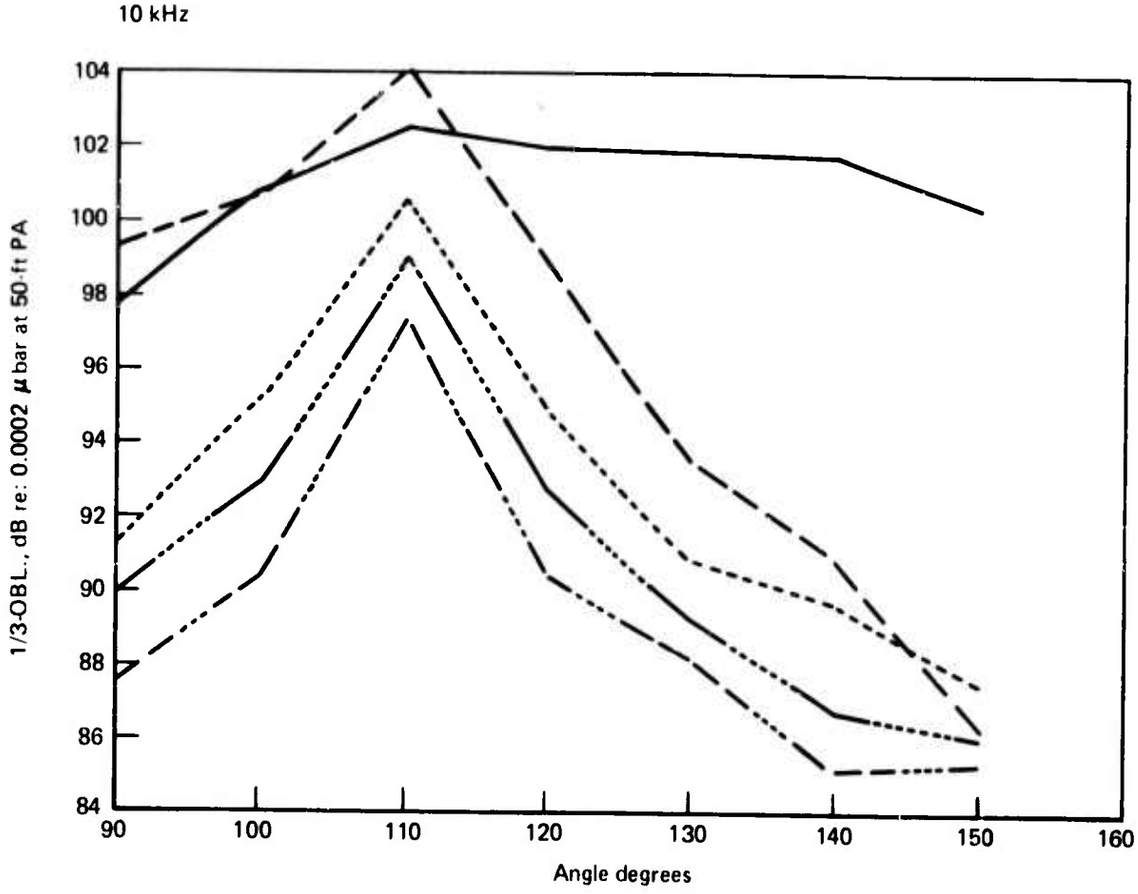

Figure 33.—LNHP-2 Suppressor Peak Premerged Jet Noise Beam Patterns, PR = 2.2 T_T = 1500°F

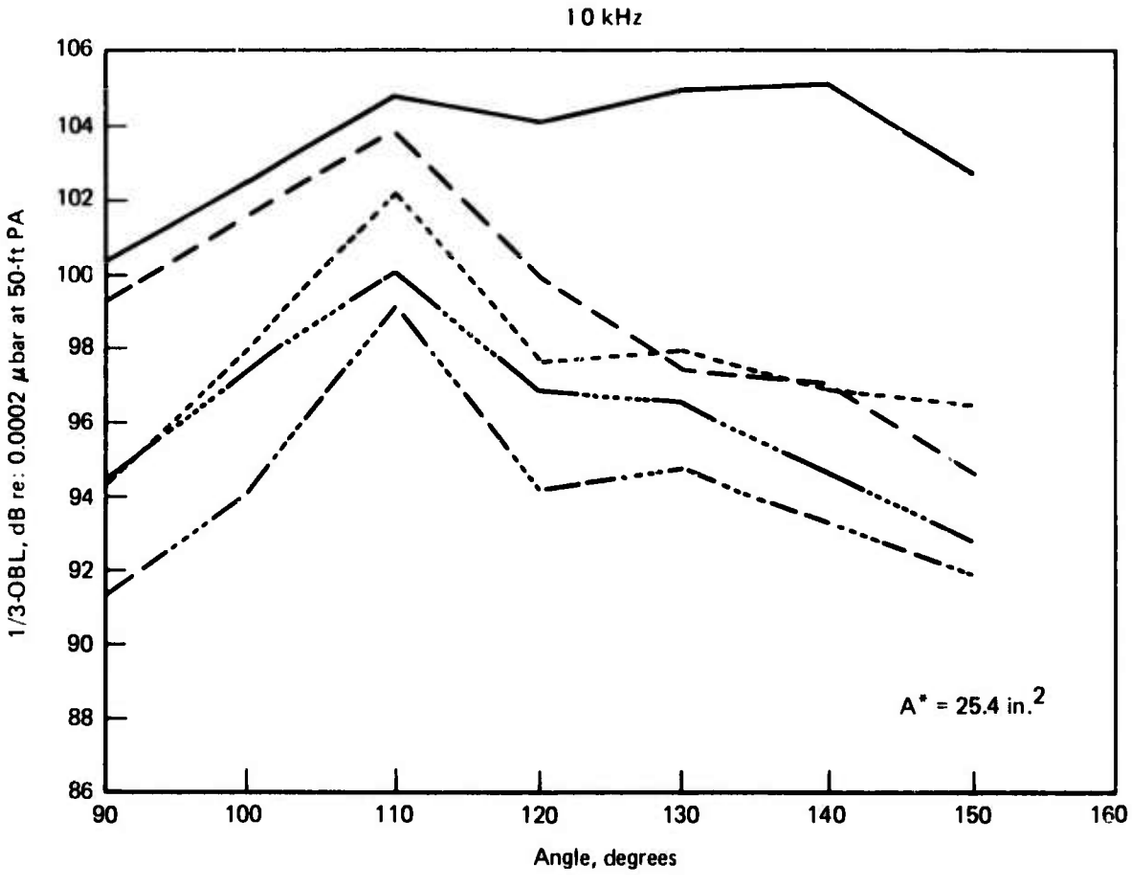

Figure 34.—LNHP-2 Suppressor, Peak Premerged Jet Noise Beam Patterns, PR = 3.0 T_T = 1500°F

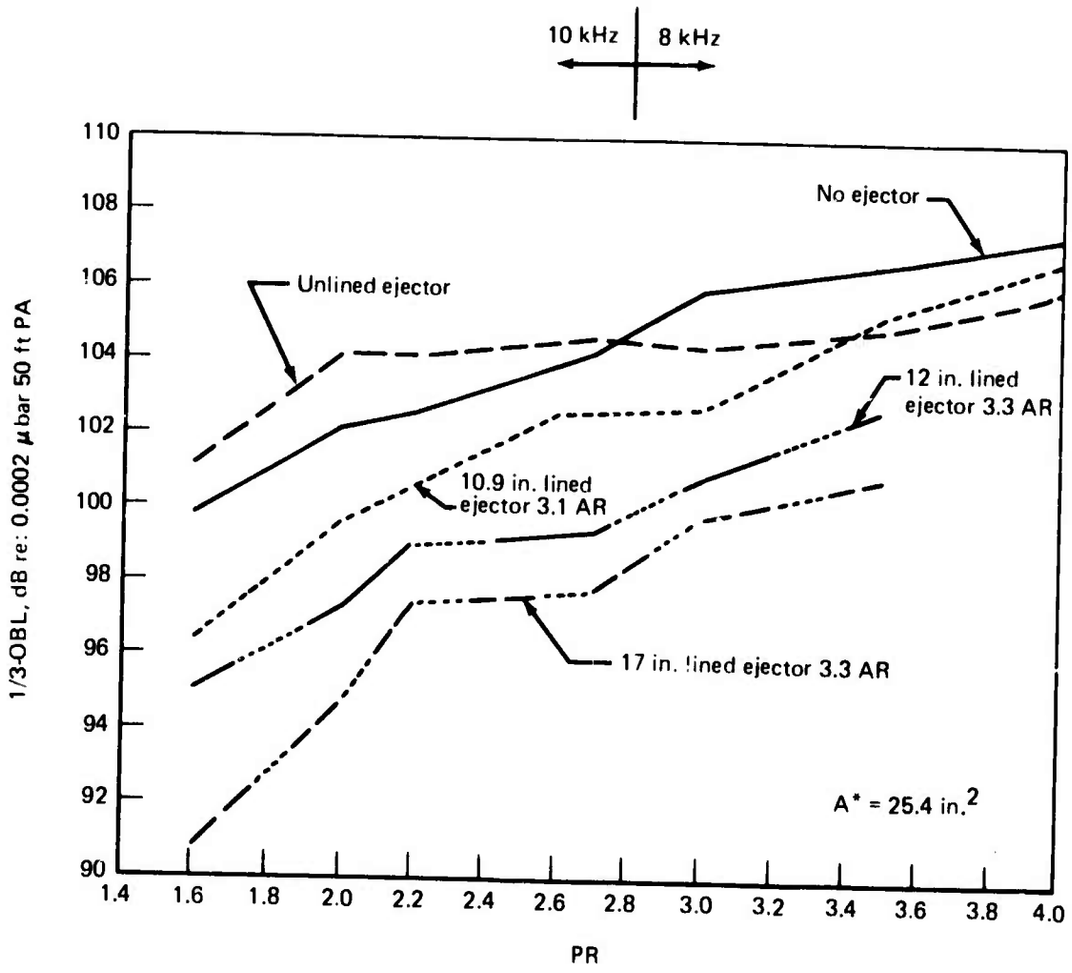

Figure 35.—LNHP-2 Suppressor, Configuration Peak Premerged Jet Noise, 110°, T_T = 1500°F

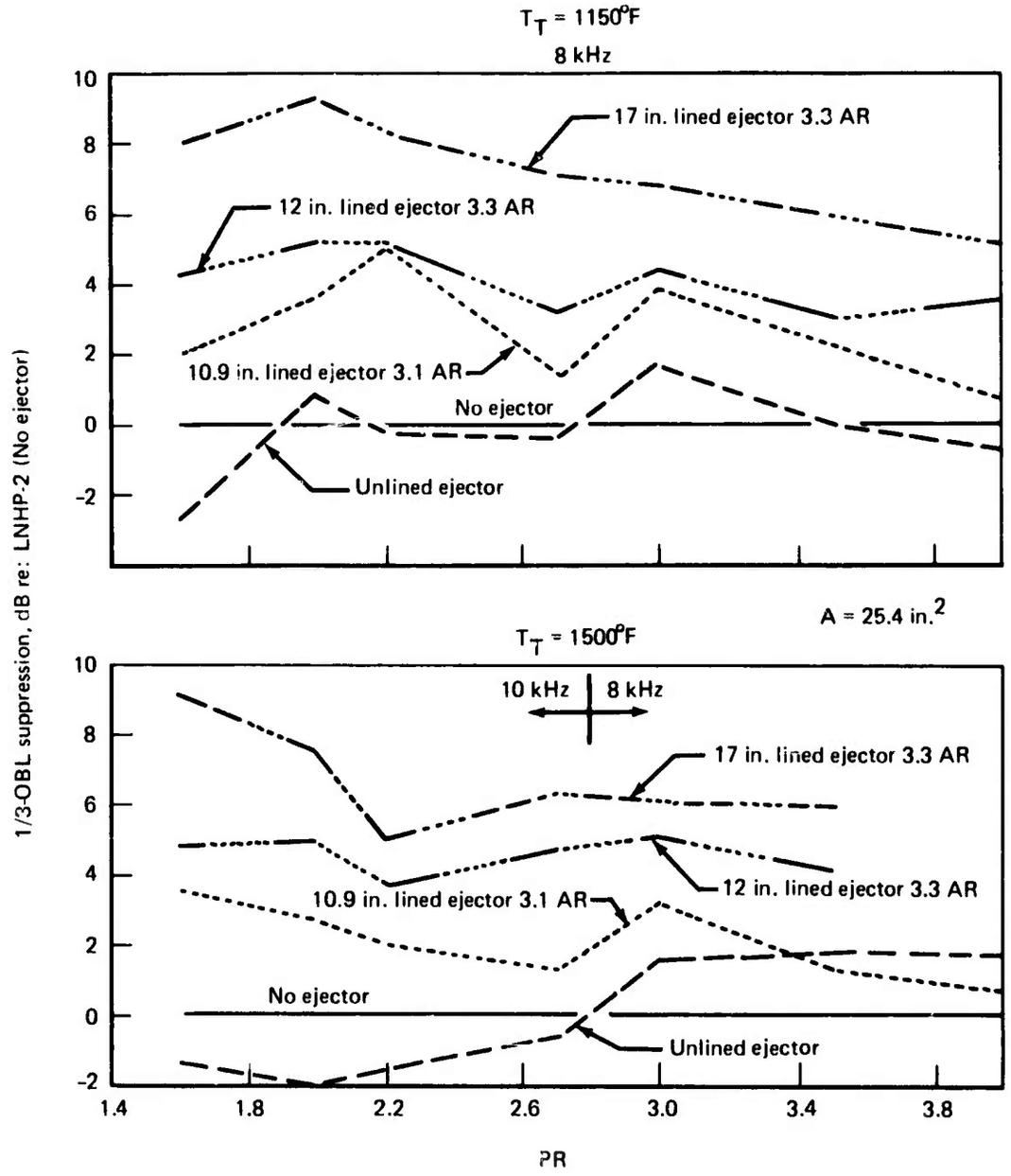

Figure 36.—LNHP-2 Suppressor, Peak Premerged Jet Noise Suppression at 110° re: inlet axis

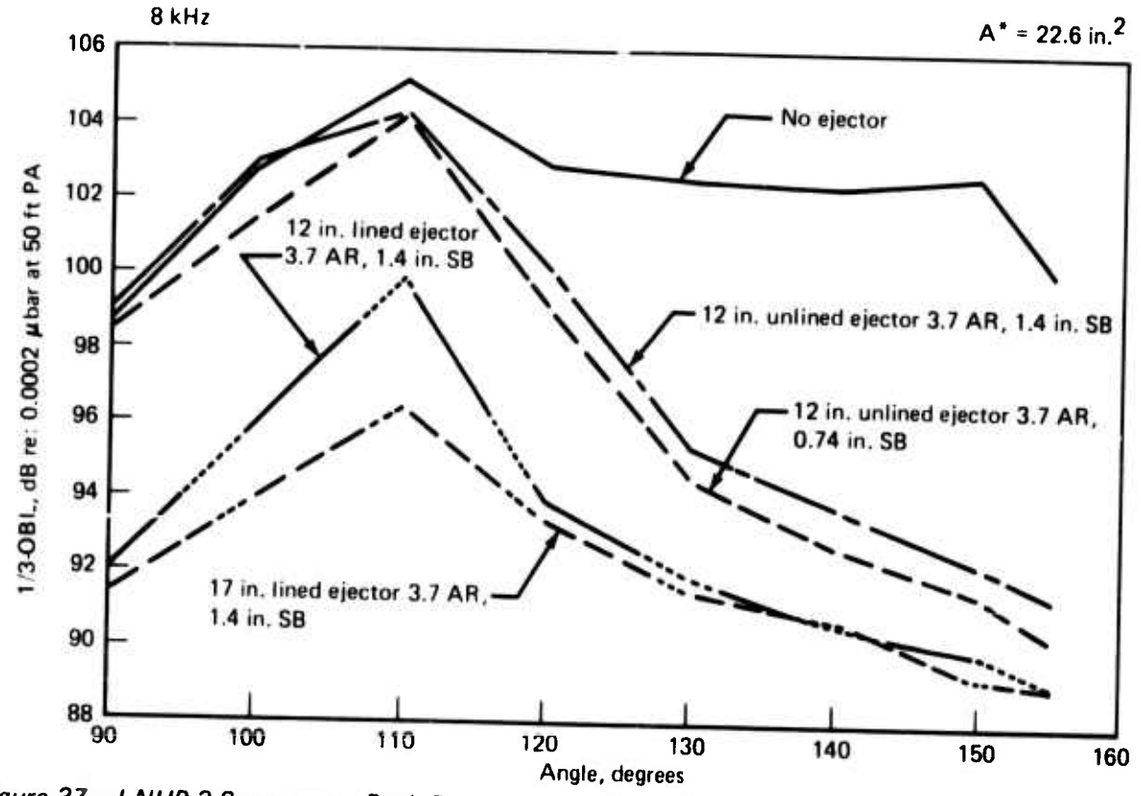

Figure 37.—LNHP-3 Suppressor, Peak Premerged Jet Noise Beam Patterns at PR = 3.0 T_T = 1500°F

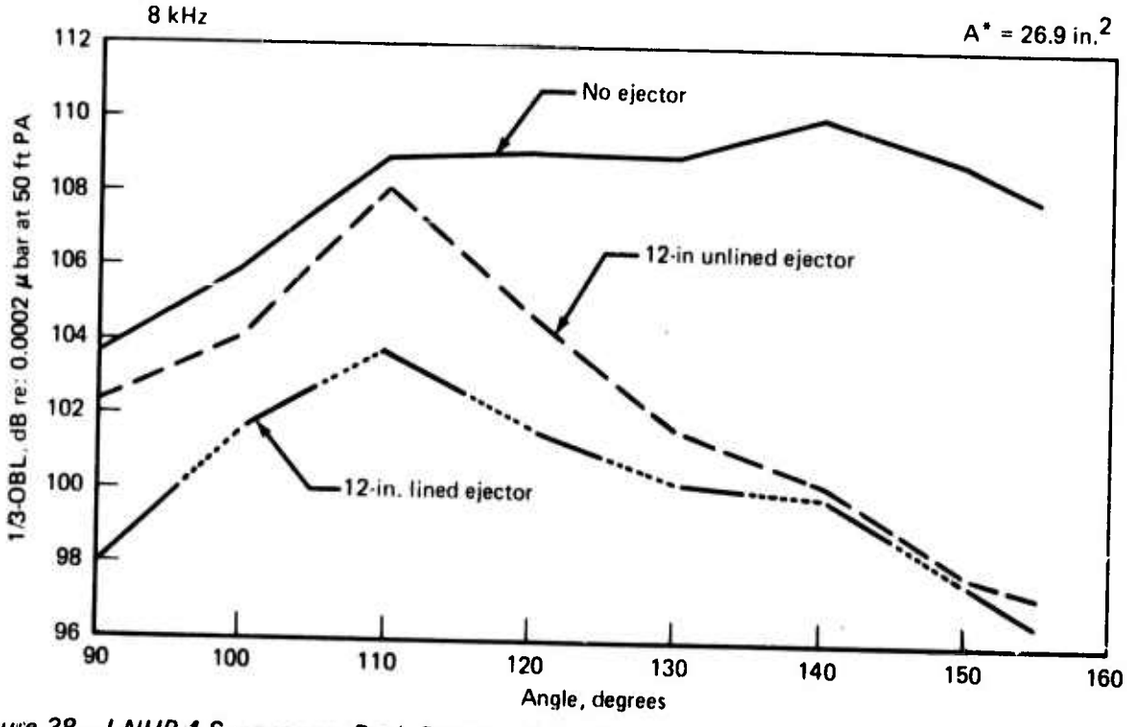

Figure 38.—LNHP-4 Suppressor, Peak Premerged Jet Noise Beam Patterns at PR = 3.0 T_T = 1500°F

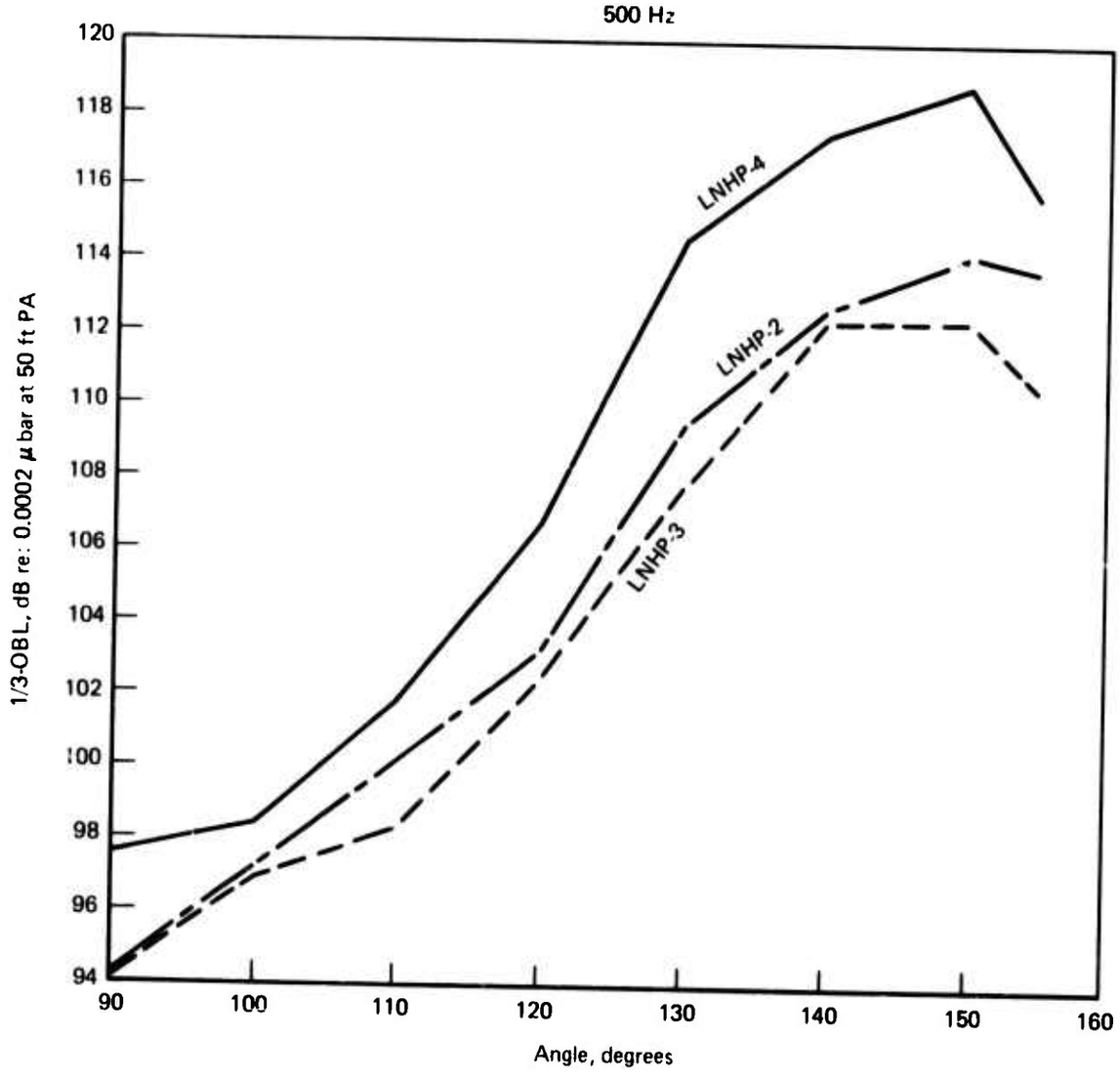

Figure 39.–Multitube Nozzle, Peak Postmerged Jet Noise Beam Patterns PR = 3.0 T_T = 1500°F

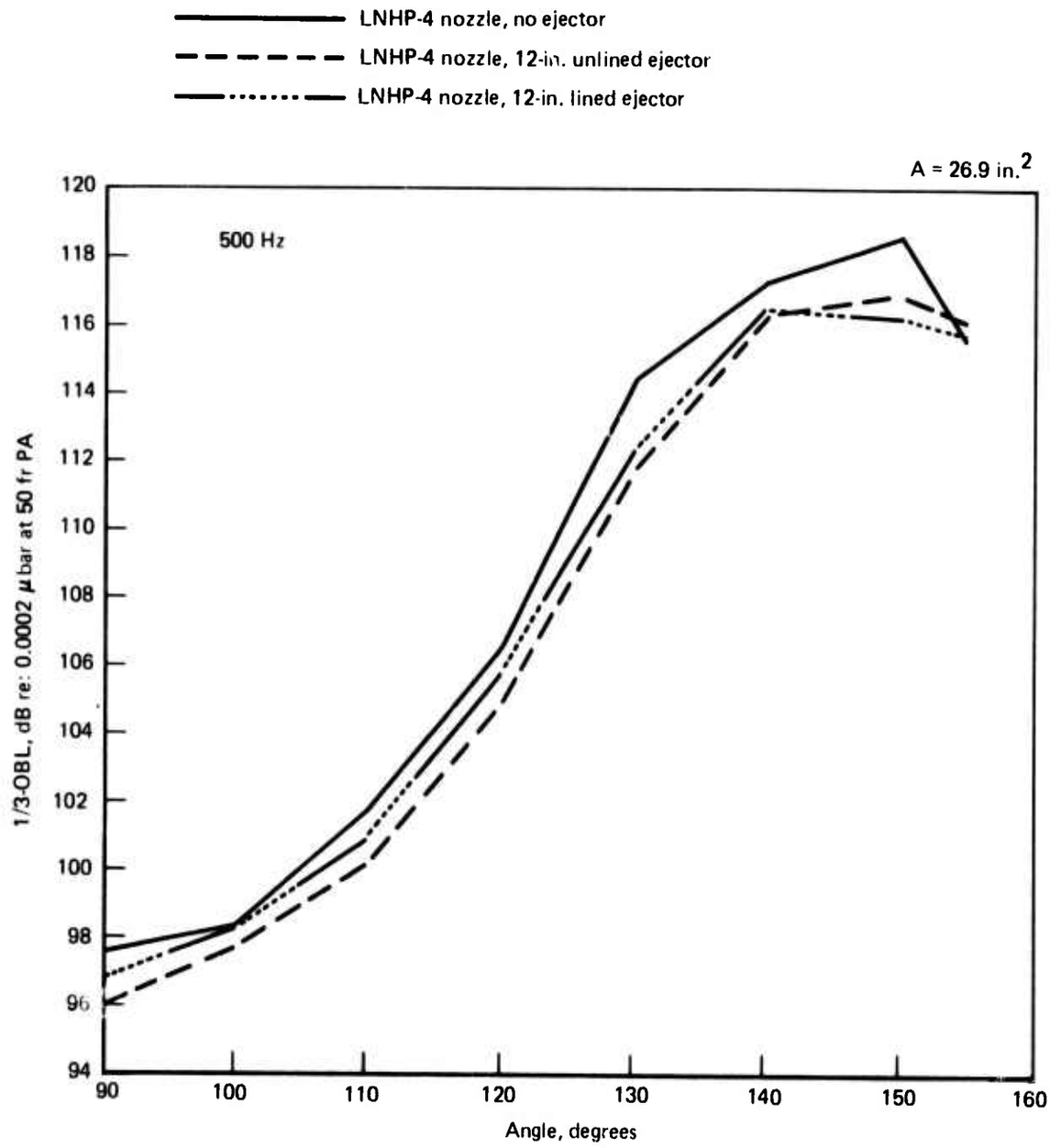

Figure 40.—LNHP-4 Suppressor, Peak Postmerged Jet Noise Beam Patterns, PR = 3.0 T_T = 1500°F

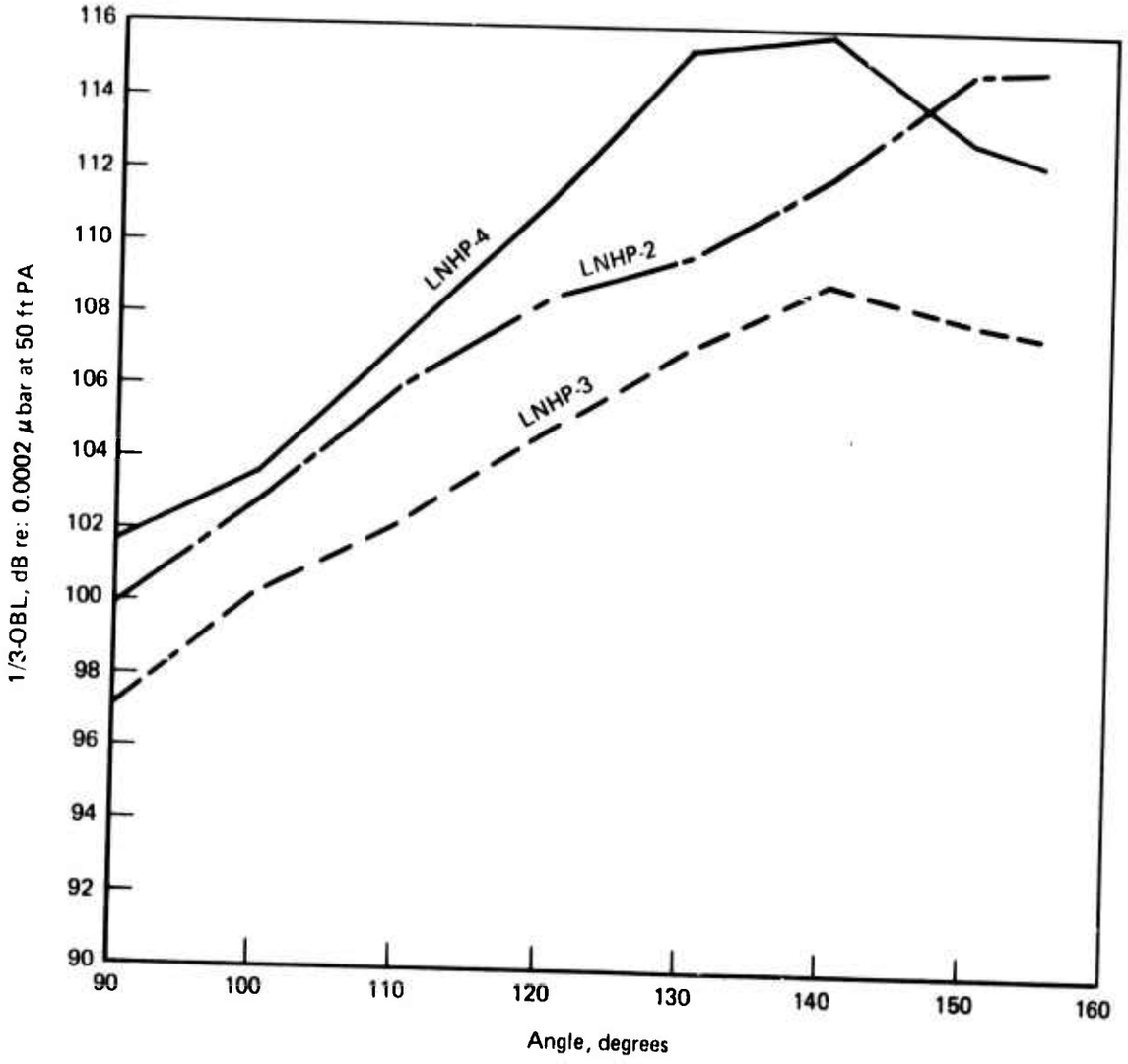

Figure 41.—Multitube Nozzle, Postmerged Jet Noise (1600 Hz) Beam Patterns PR = 3.5 T_T = 1500°F

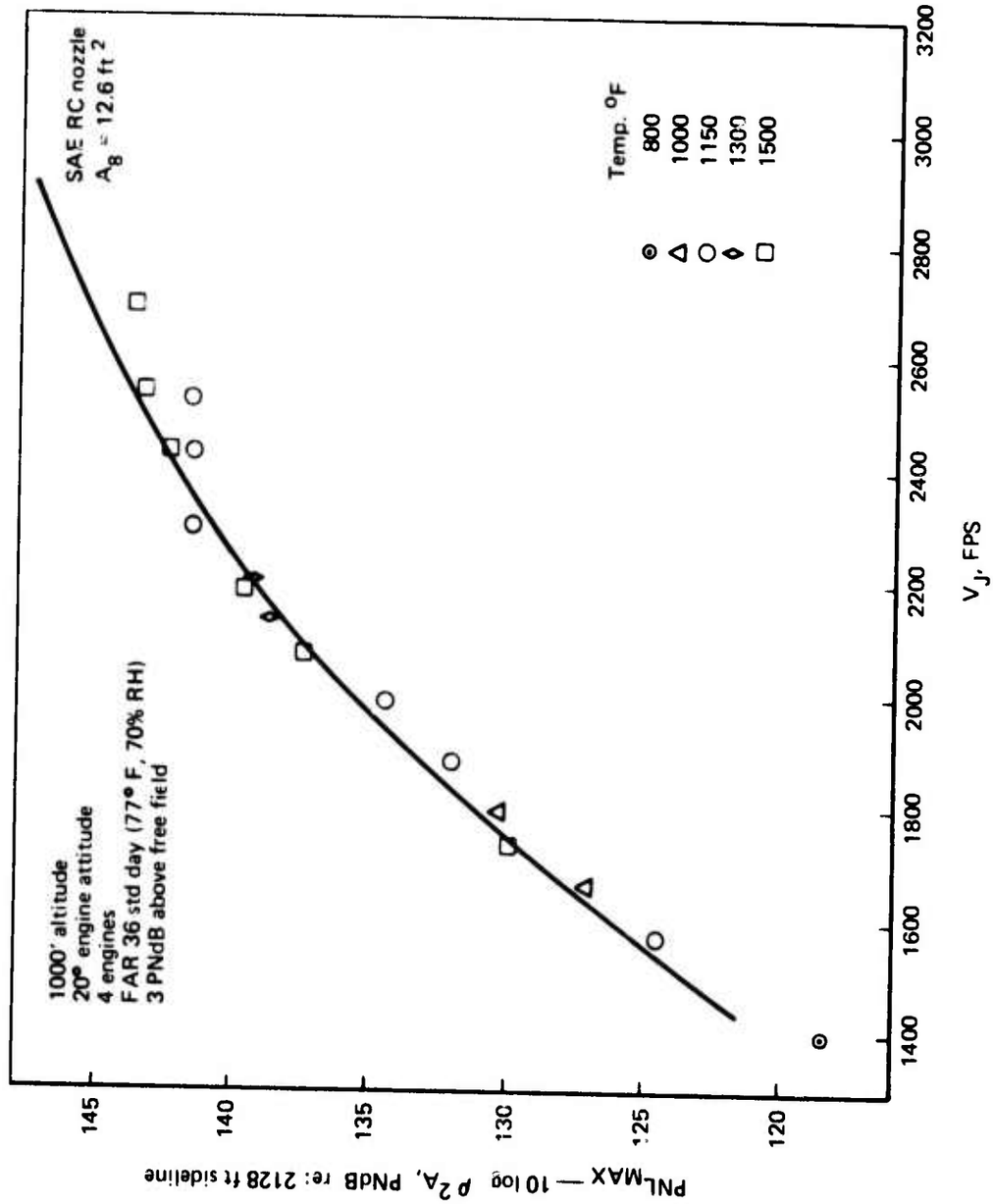

Figure 42. – Baseline Nozzle Normalized Peak Perceived Noise Levels

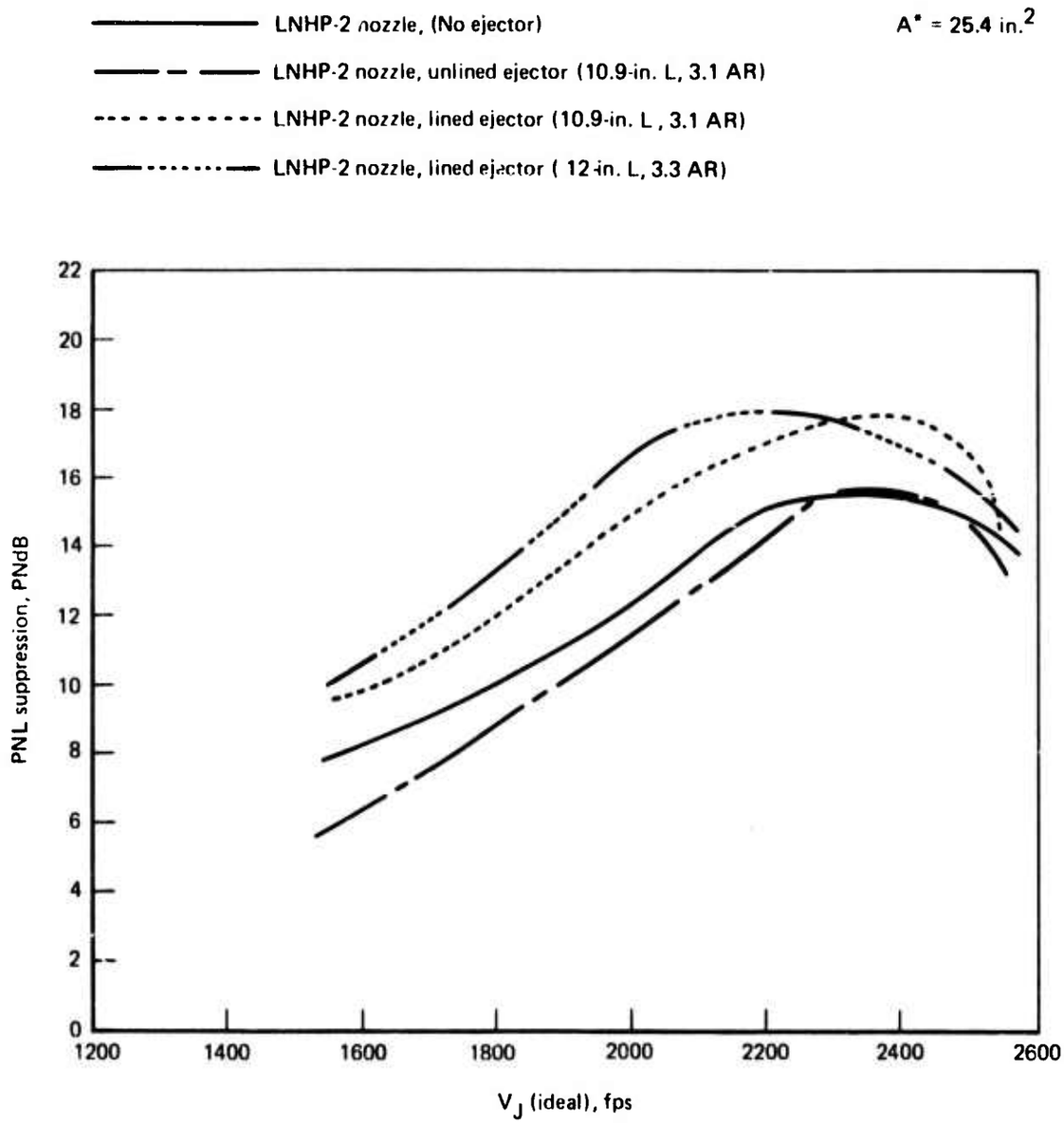

Figure 43.–LNHP-2 Suppressor, 2128-ft SL PNL Suppression, T_T = 1150°F

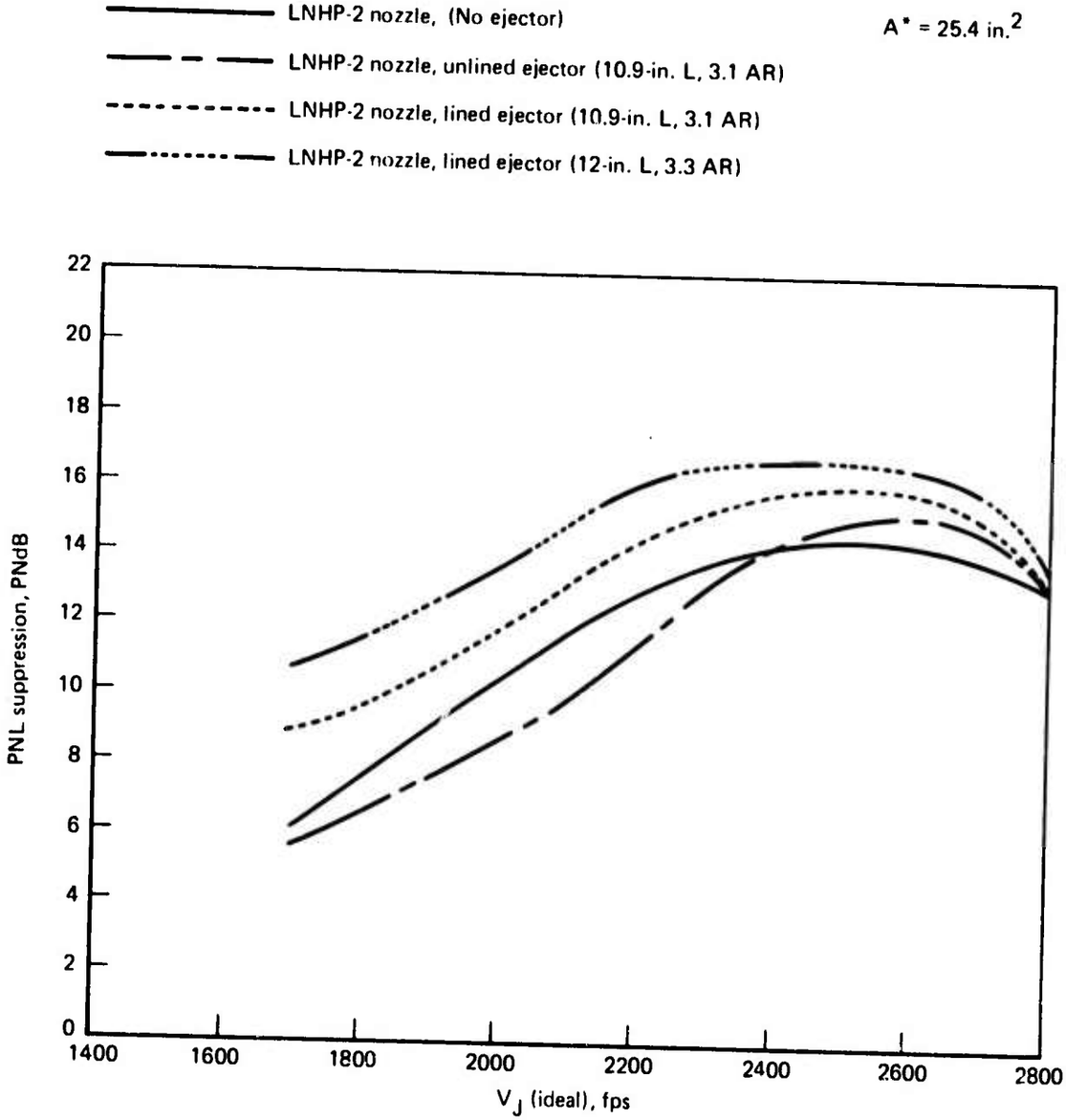

Figure 44.—LNHP-2 Suppressor, 2128-ft. SL PNL Suppression, T_T = 1500°F

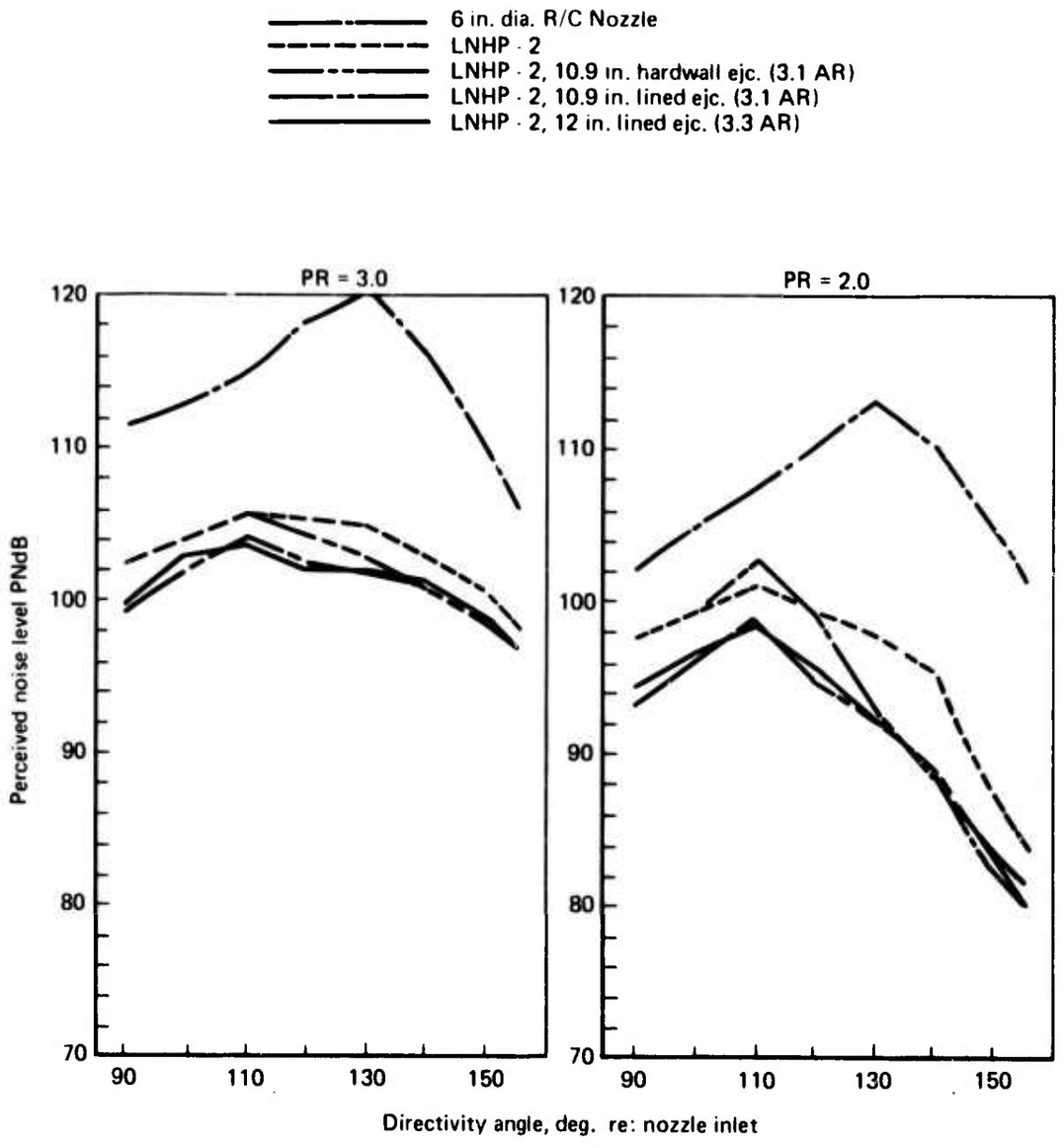

Figure 45. – LNHP – 2 Suppressor, 2128-ft. Sideline Directivity, T_T = 1500° F

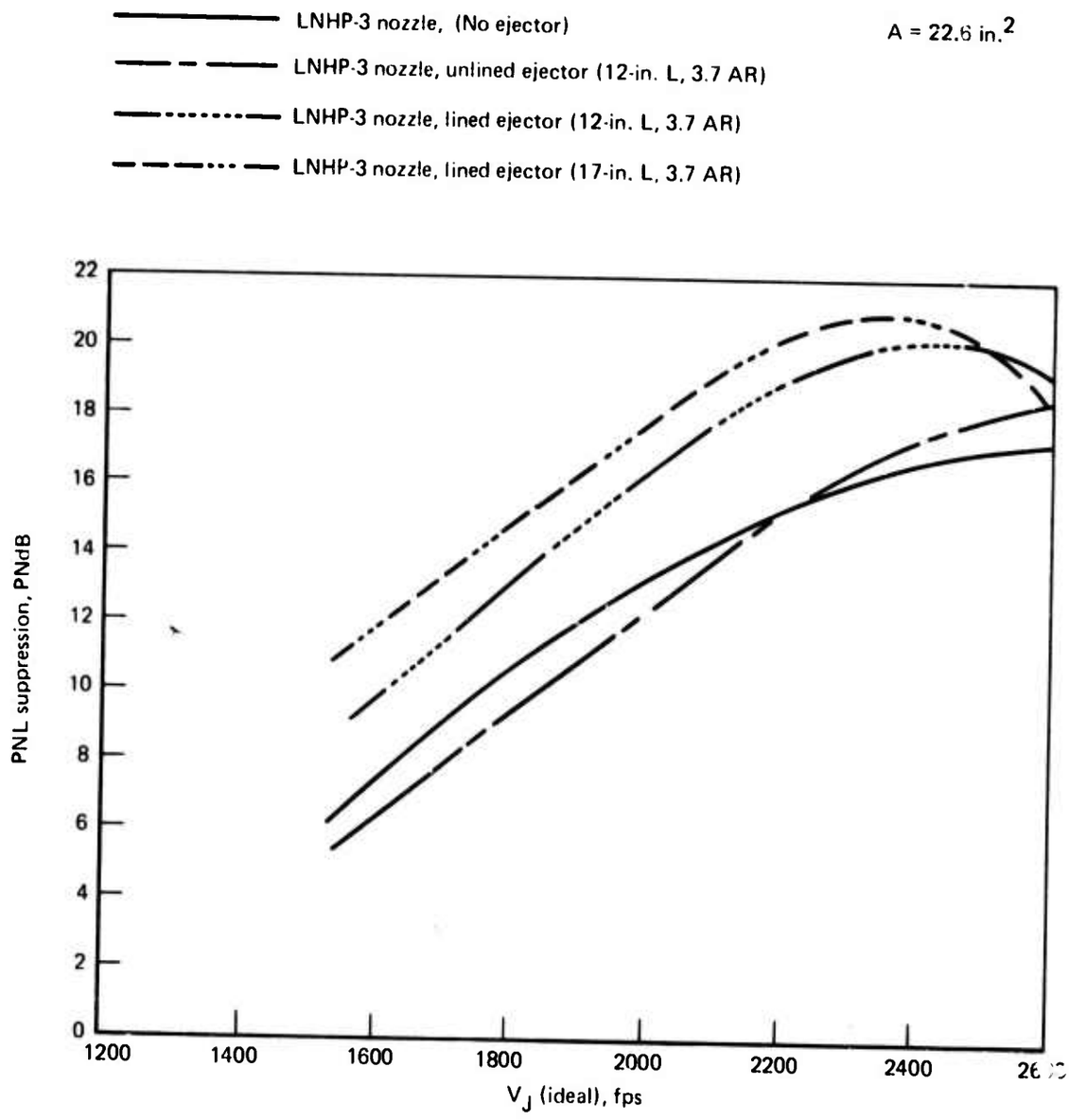

Figure 46.–LNHP-3 Suppressor, 2128-ft SL PNL Suppression T_T = 1150°F

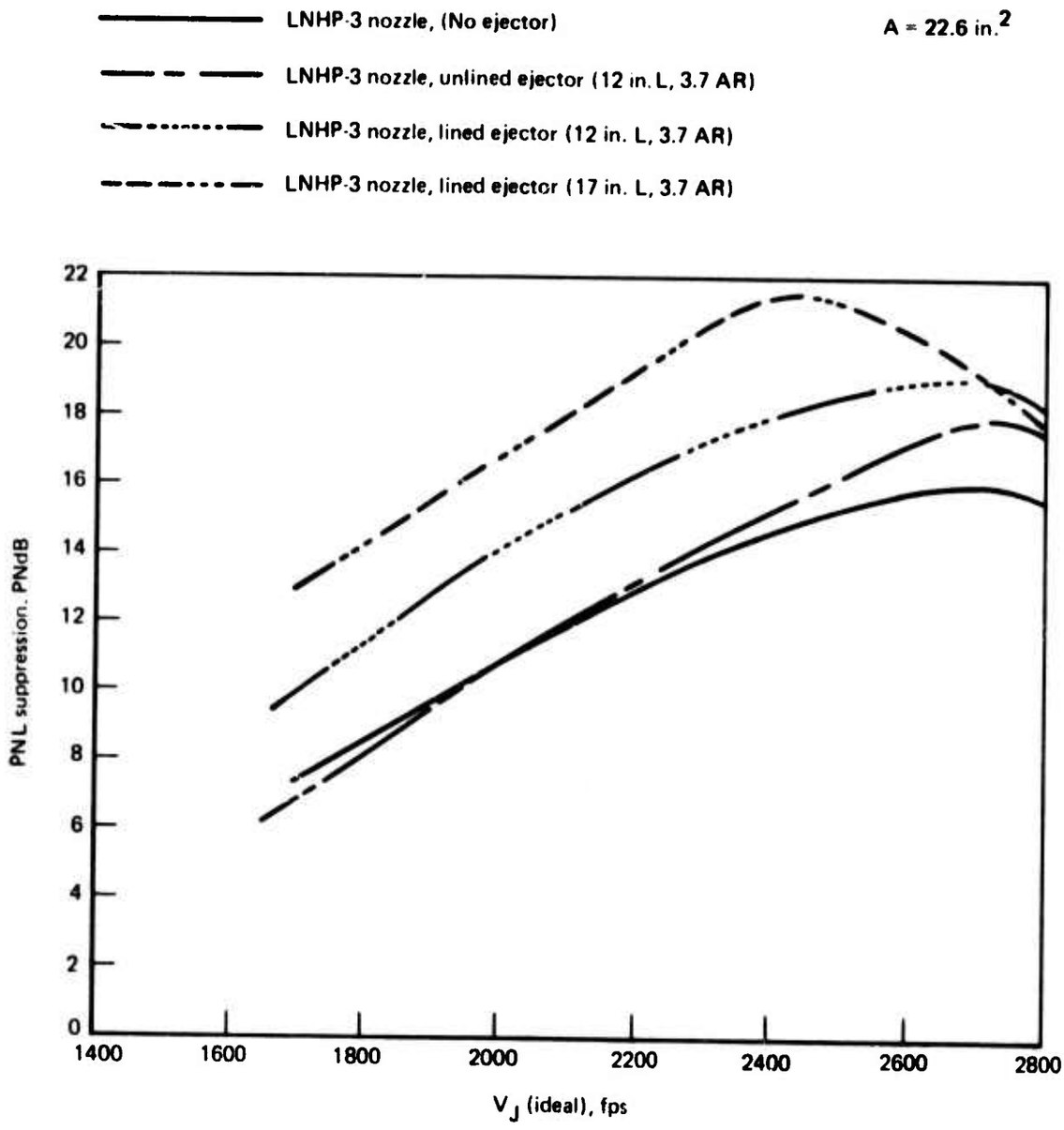

Figure 47.--LNHP-3 Suppressor, 2128-ft SL PNL Suppression T_T = 1500°F

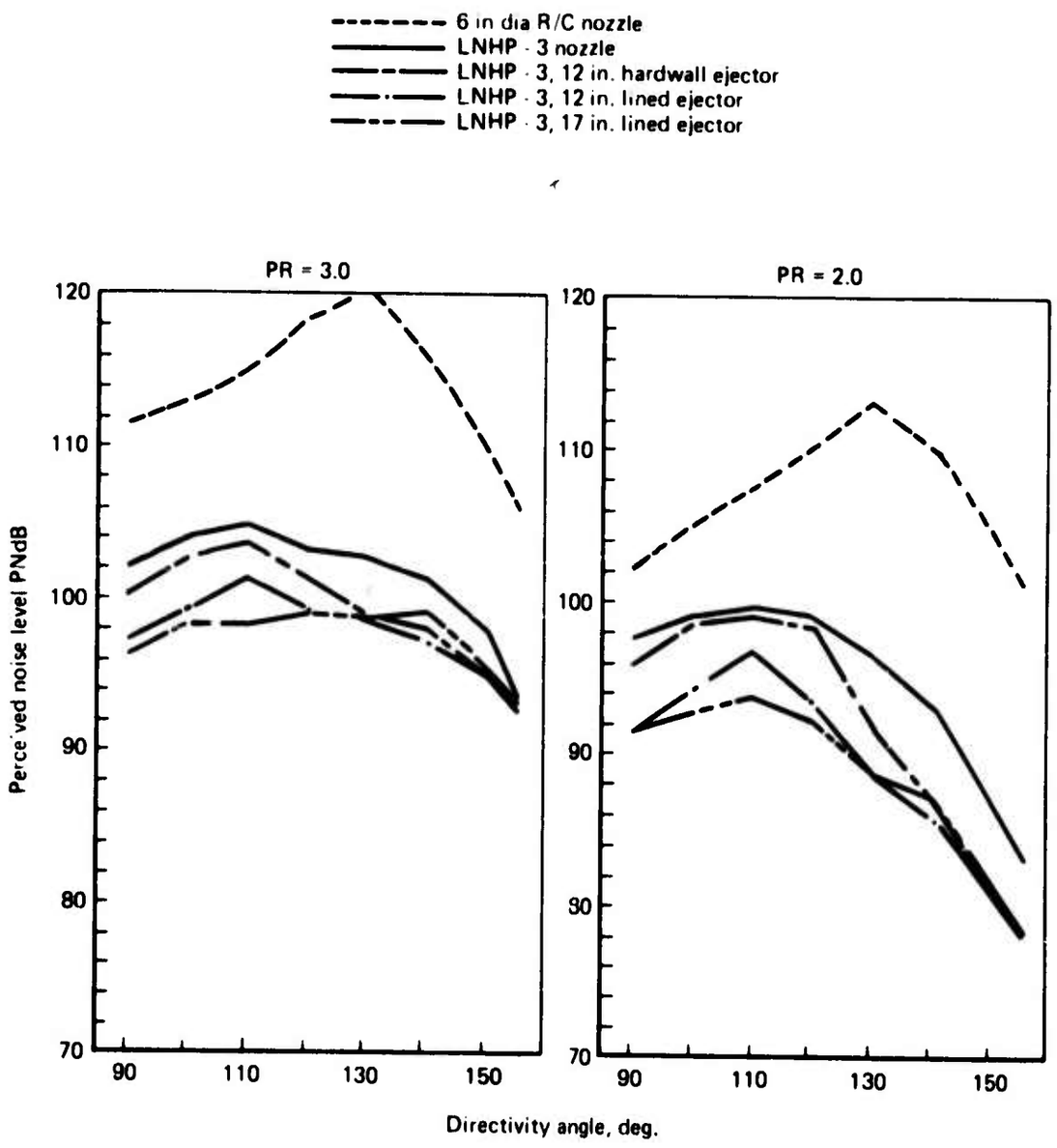

Figure 48. – LNHP – 3 Suppressor, 2128-ft. Sideline PNL Directivity, T_T = 1500° F

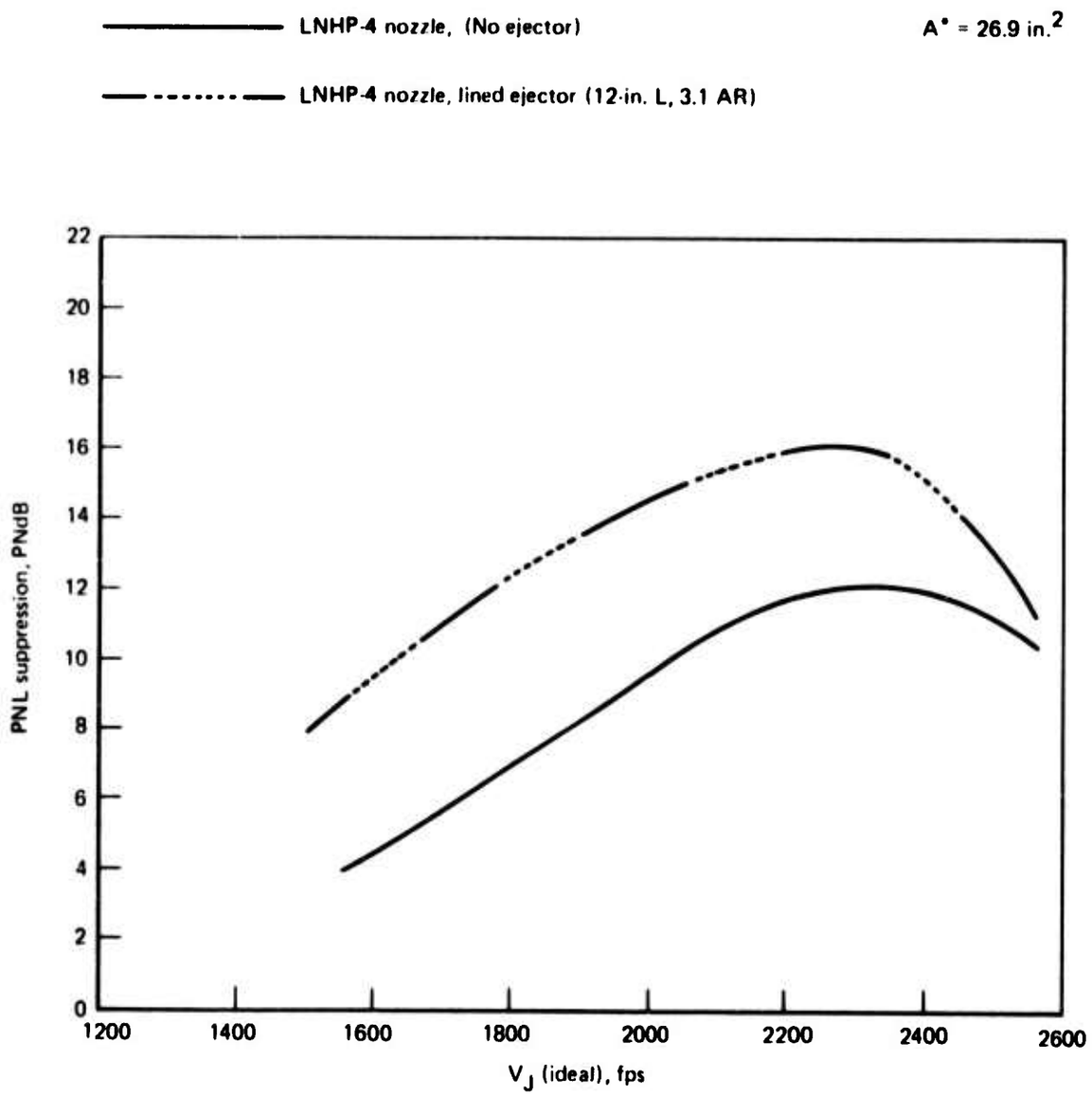

Figure 49.—LNHP-4 Suppressor, 2128-ft SL PNL Suppression, T_T = 1150°F

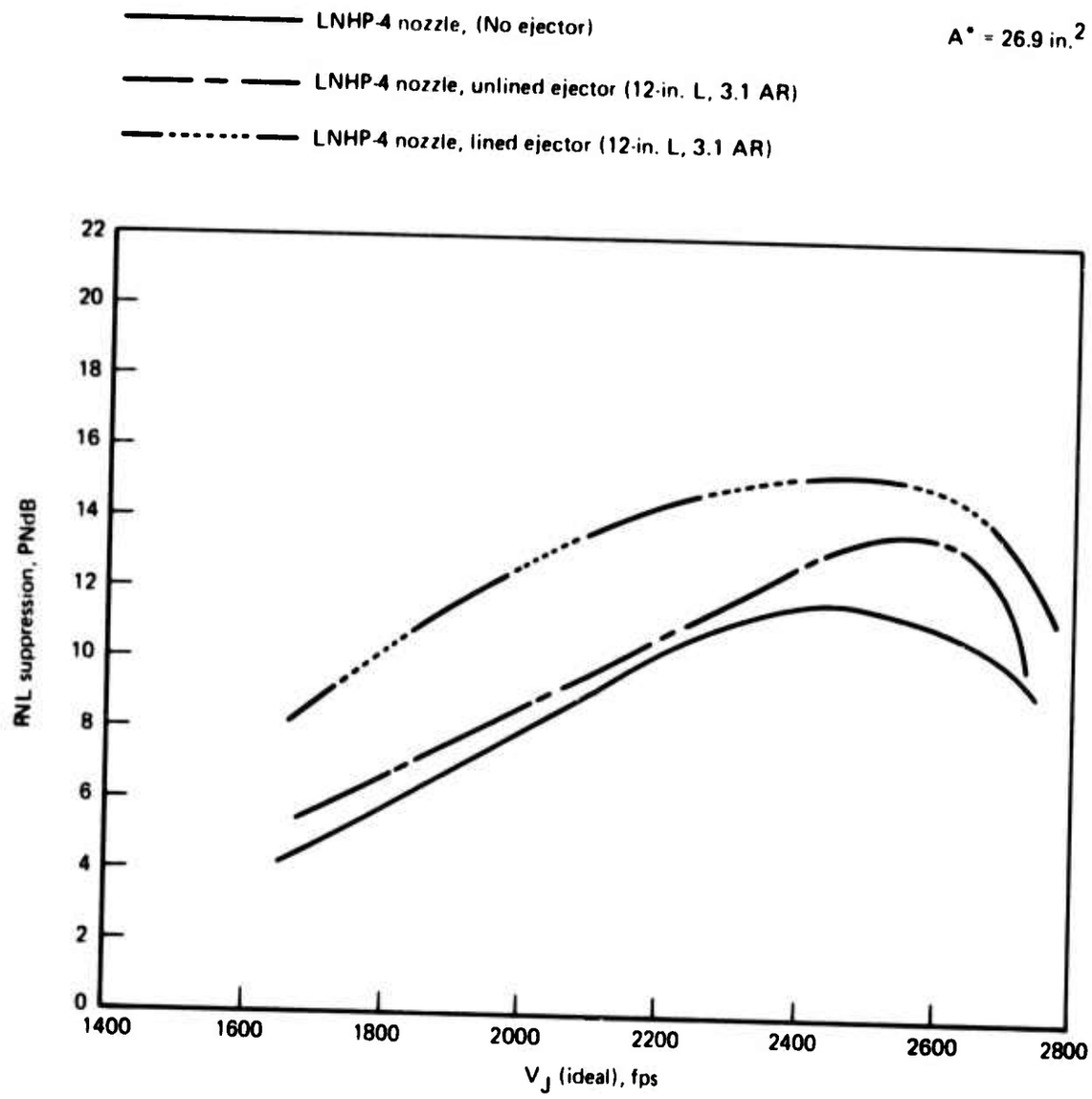

Figure 50.—LNHP-4 Suppressor, 2128-ft SL PNL Suppression T_T = 1500°F

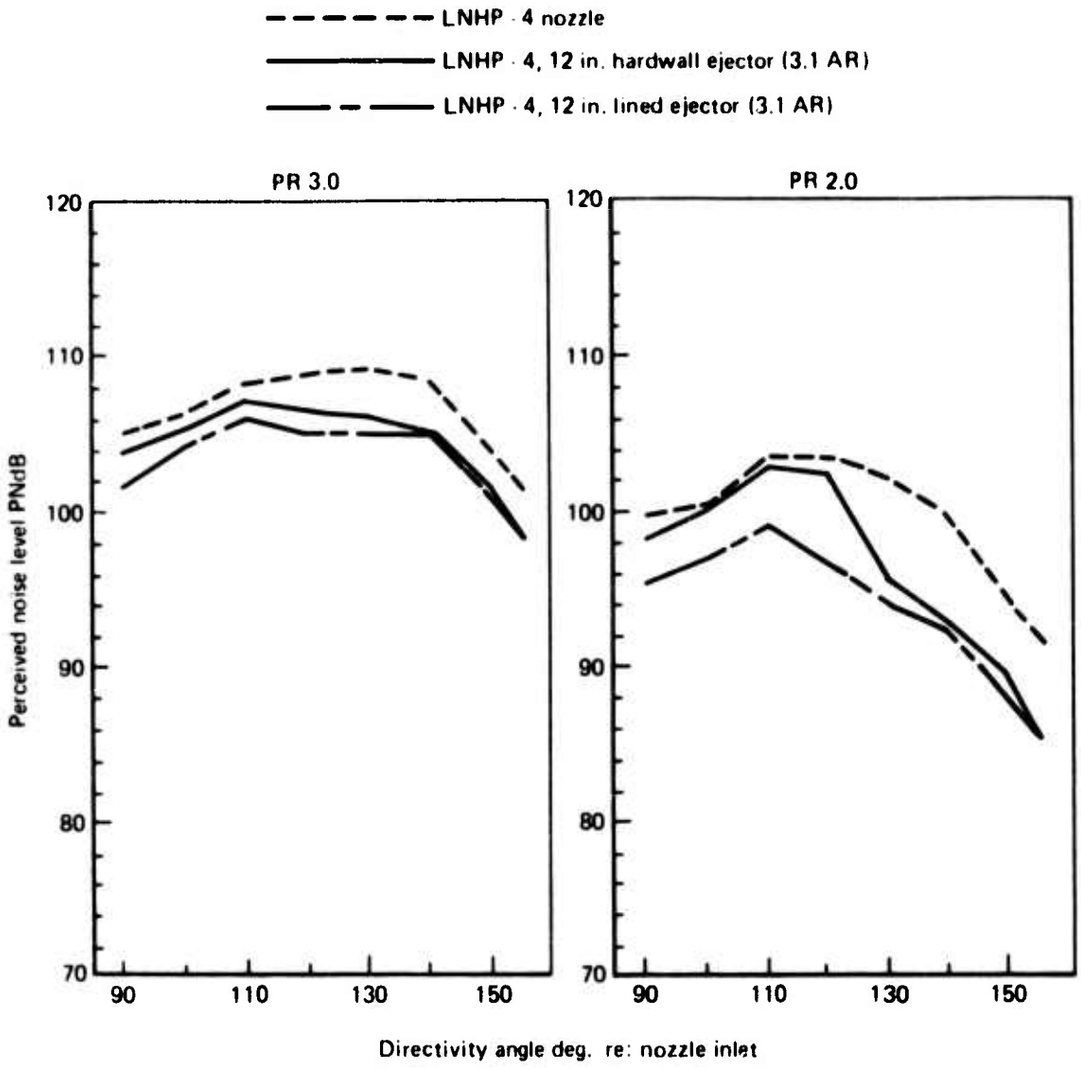

Figure 51. – LNHP – 4 Suppressor, 2128-ft. Sideline PNL Directivity T_T = 1500° F

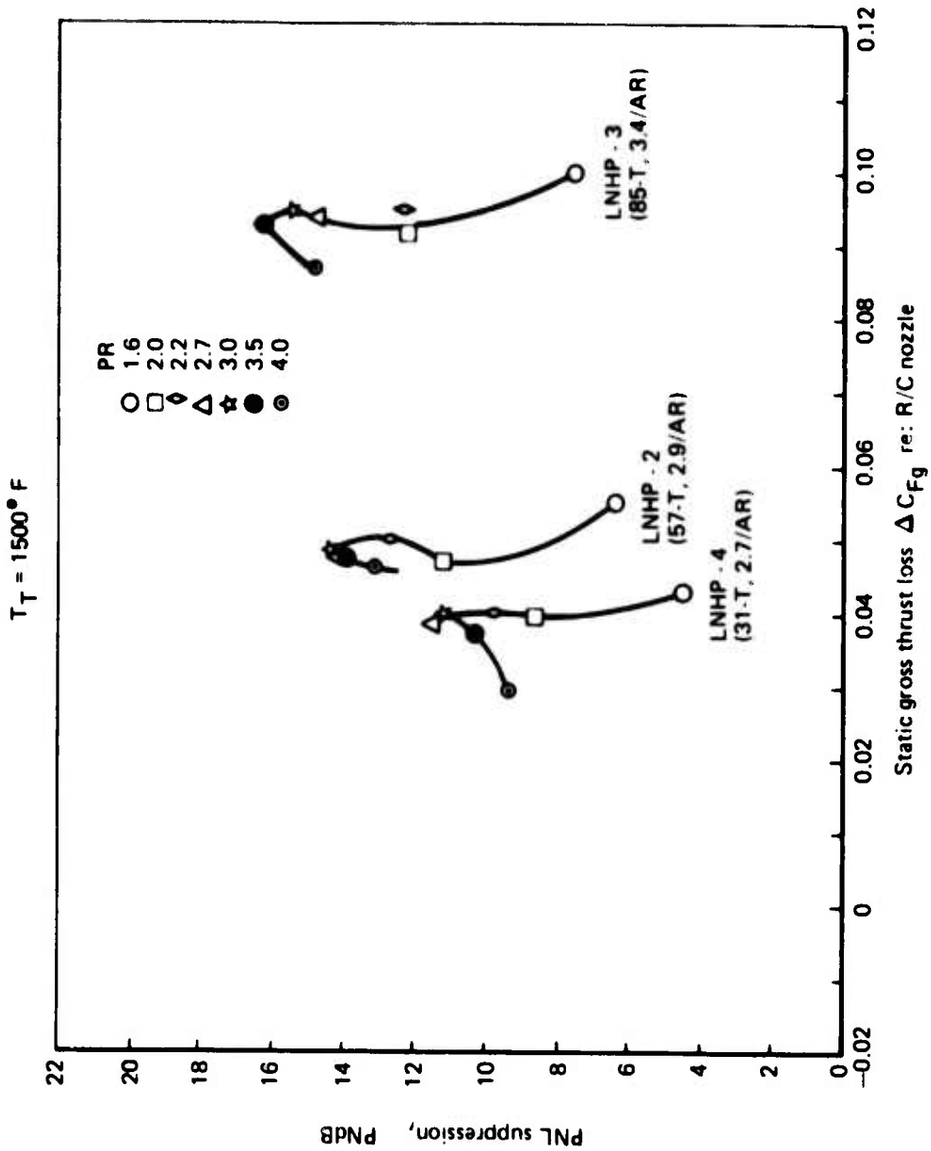

Figure 52. – Multitube Nozzle 2128-ft. Sideline Δ PNdB versus Δ C_{Fg}

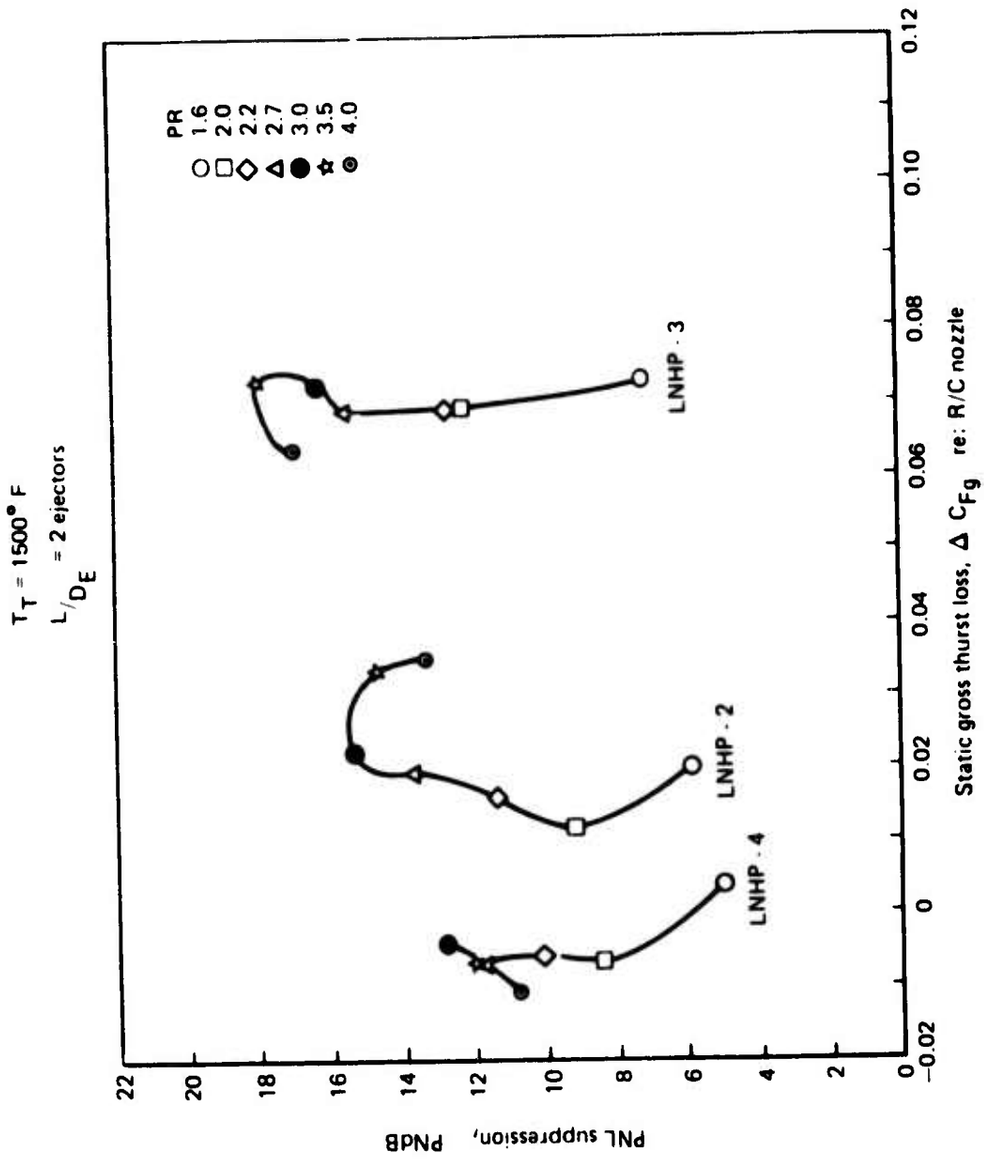

Figure 53. – Multitube Suppressor, 2128-ft. Sideline Δ PNdB Versus Δ C_{Fg} With Hardwall Ejectors

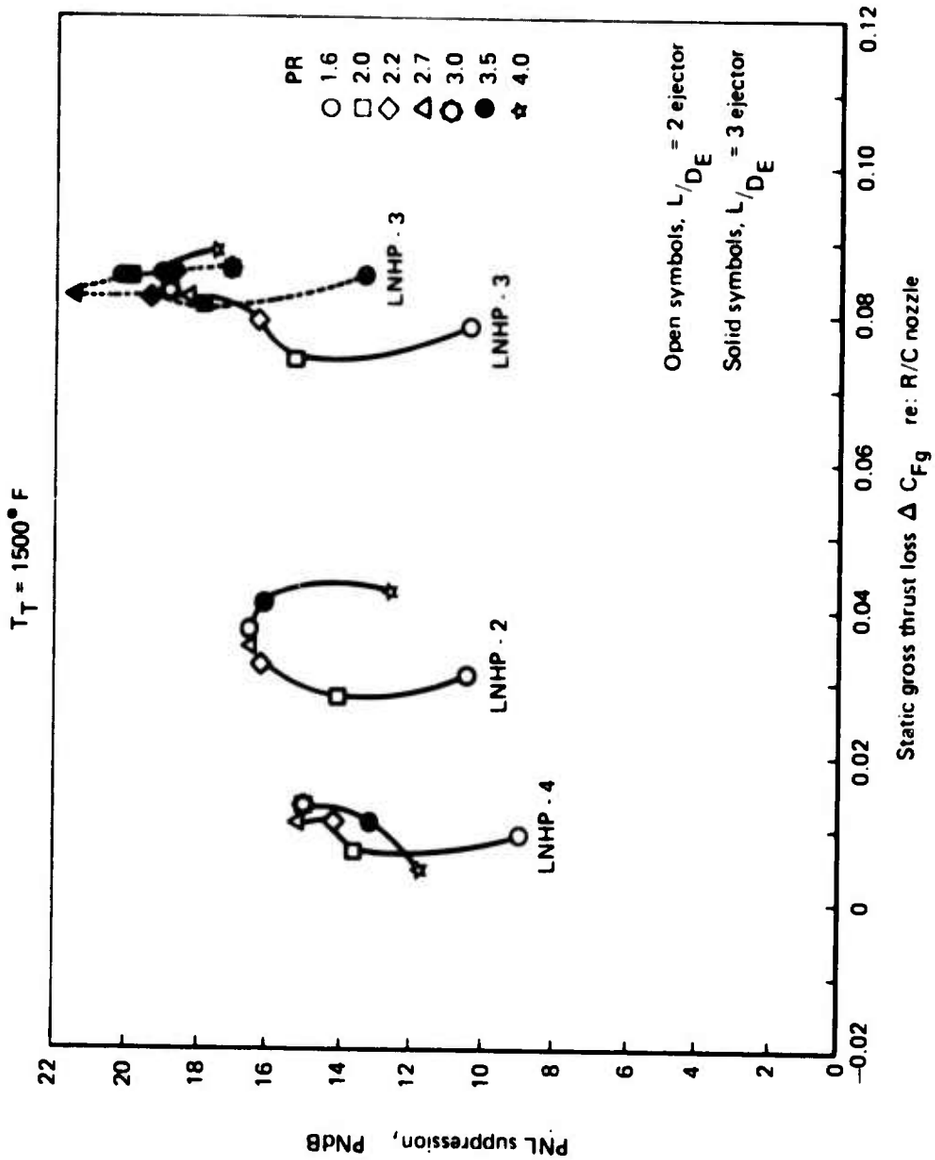

Figure 54. – Multitube Suppressor, 2128-ft. Sideline Δ PNdB versus Δ C_{Fg}, With Lined Ejectors

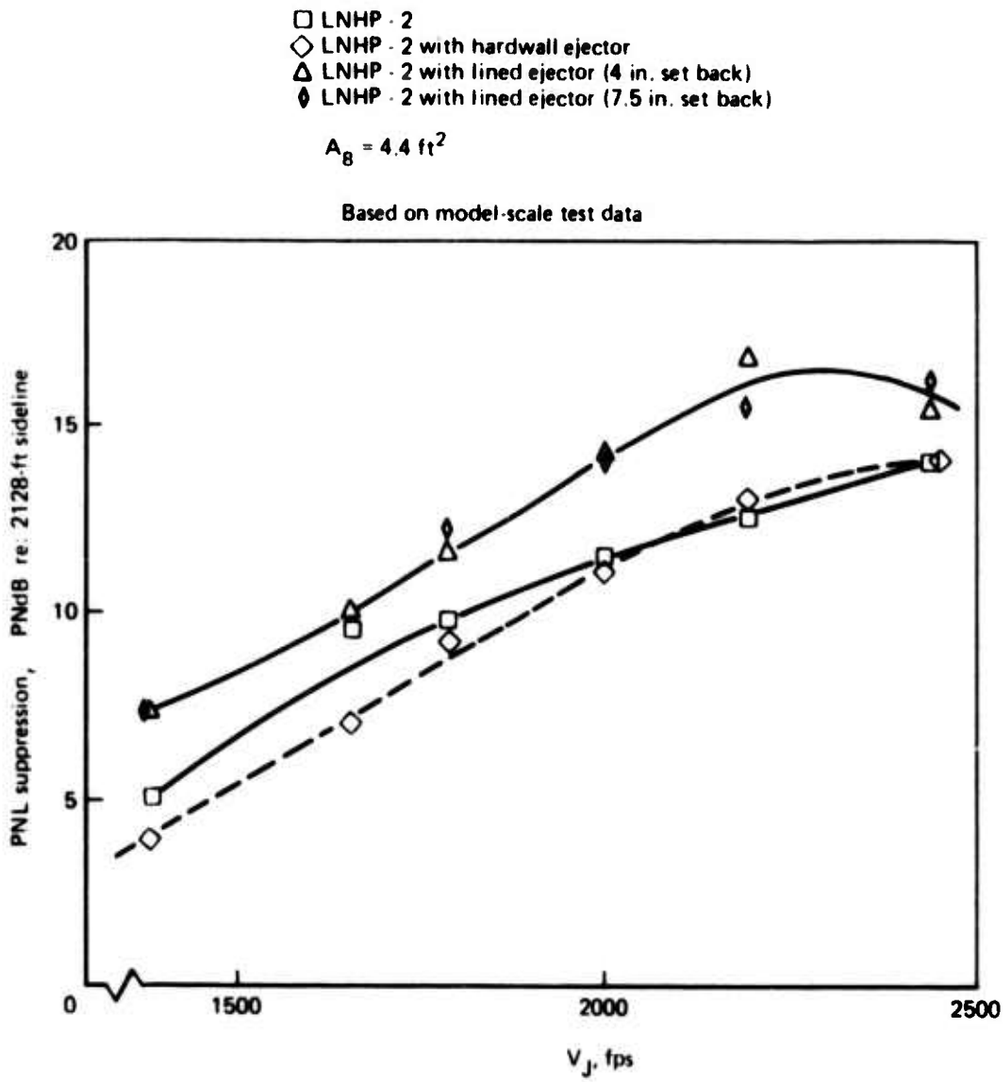

Figure 55. – Predicted LNHP–2 Suppressor Characteristics for the J-58 Engine Operating Conditions

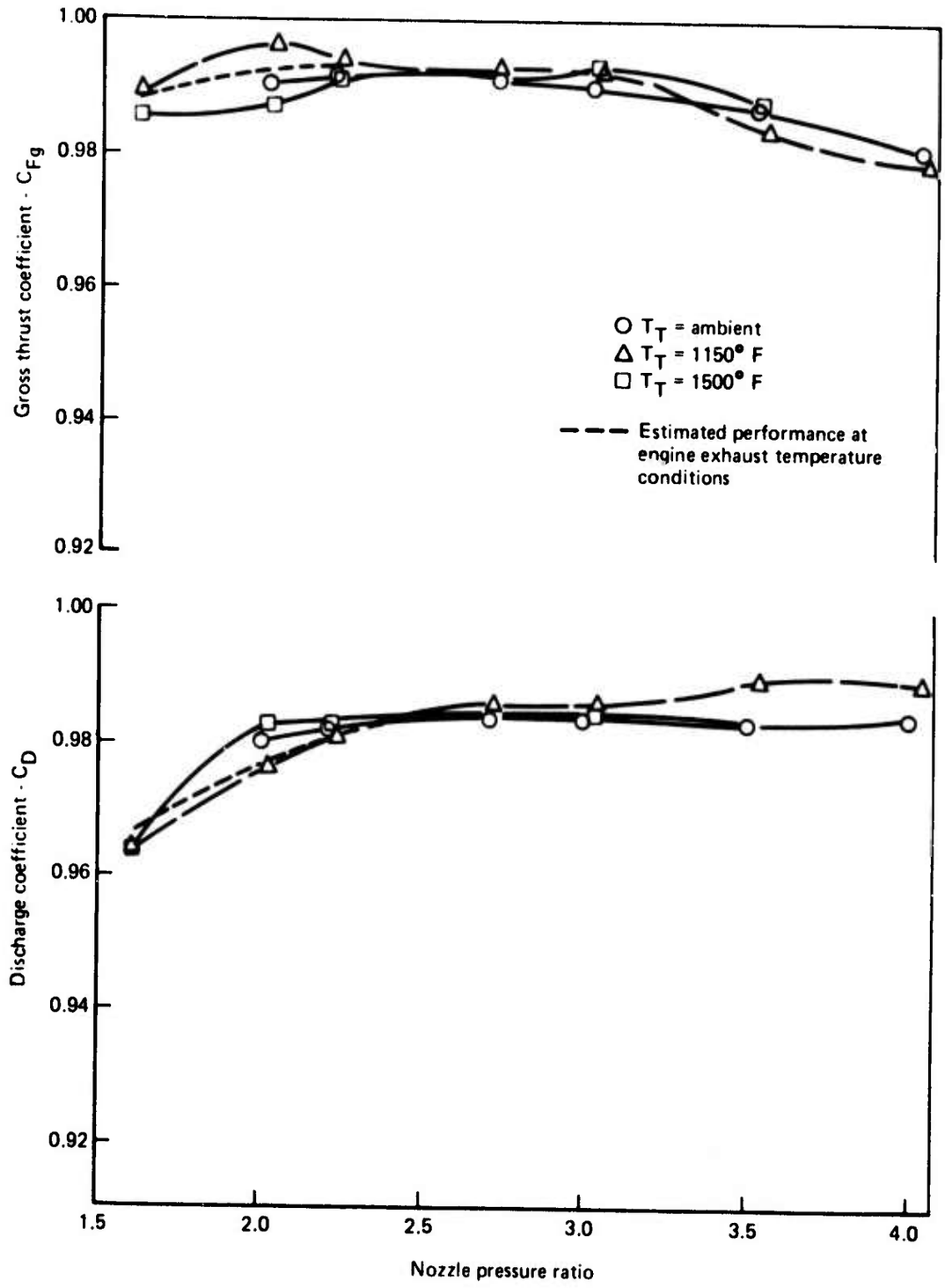

Figure 56. – Performance of 6 in. R/C Nozzle

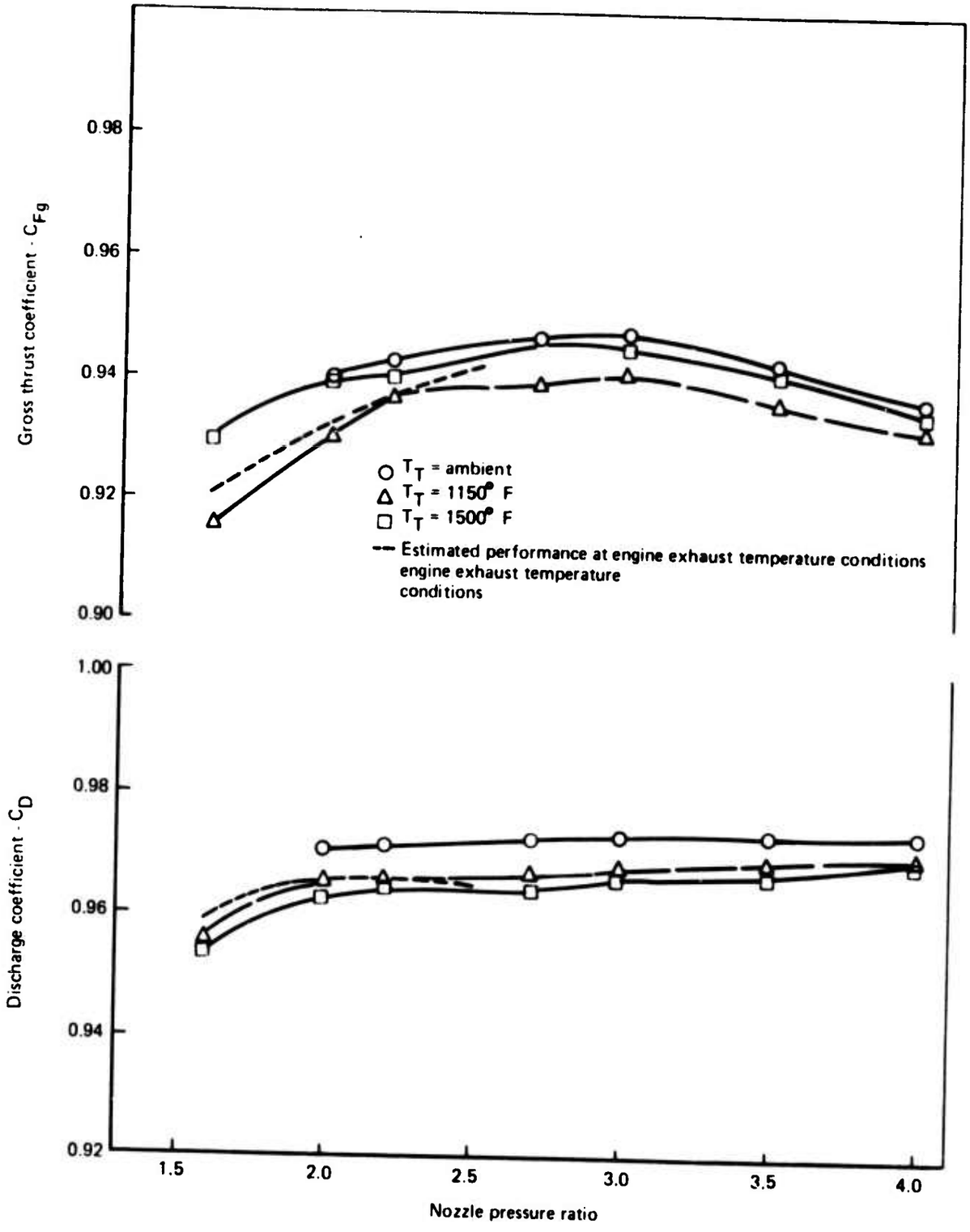

Figure 57. — Performance of LNHP – 2 Primary Nozzle Alone

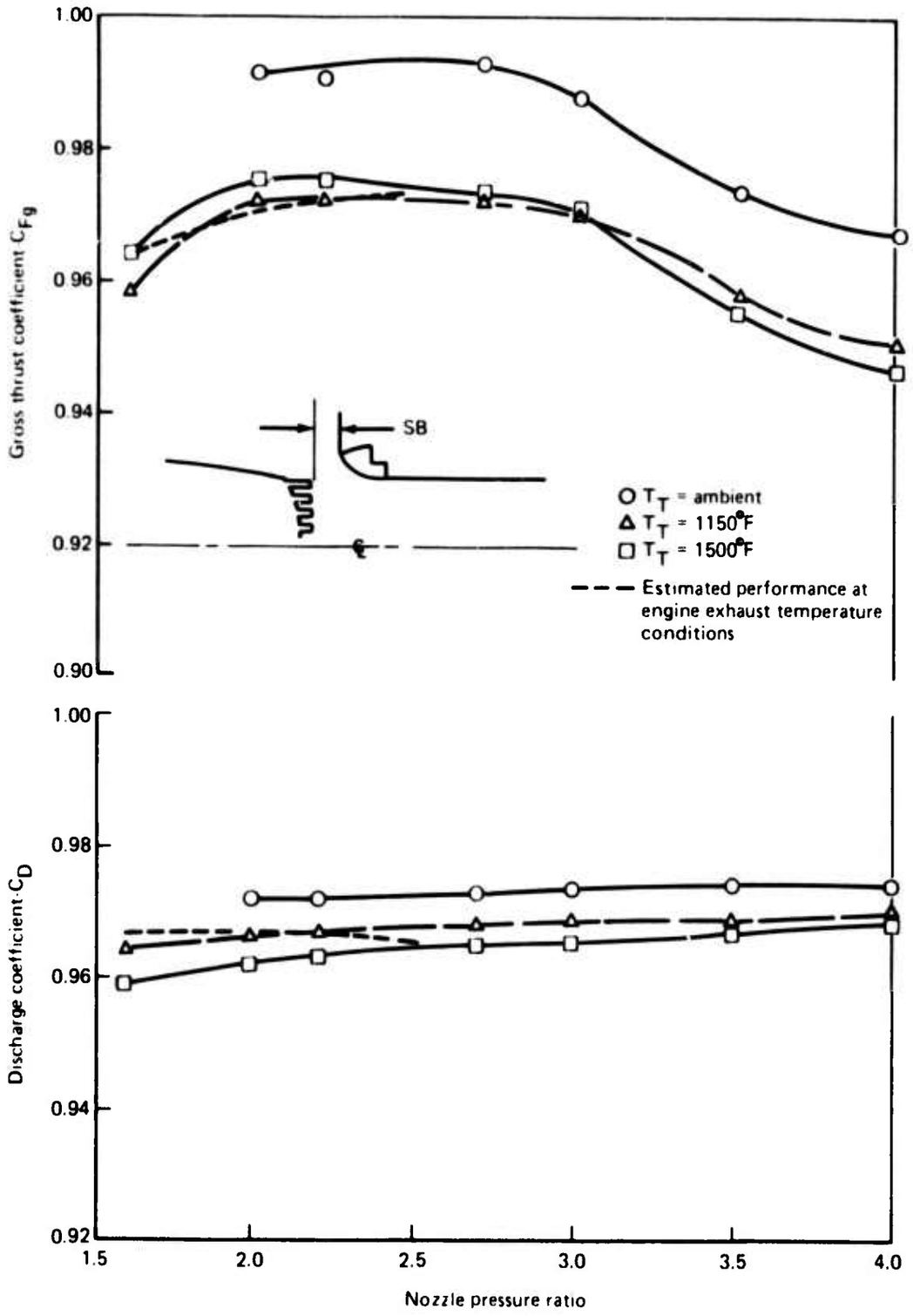

Figure 58.–Performance of LNHP-2/Hardwall Ejector at SB=0.8 in.

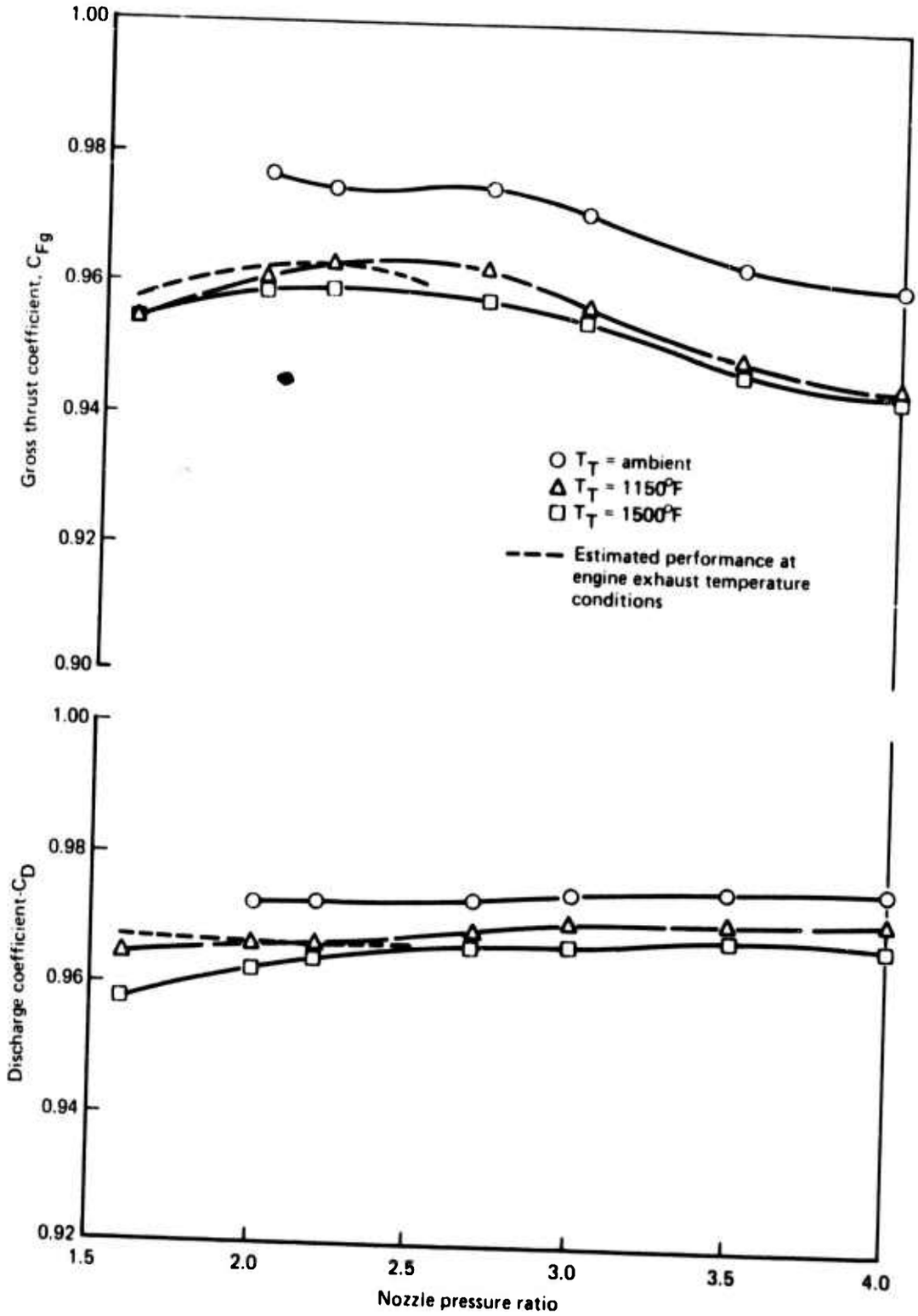

Figure 59.—Performance of LNHP-2/Lined Ejector at SB=0.8 in.

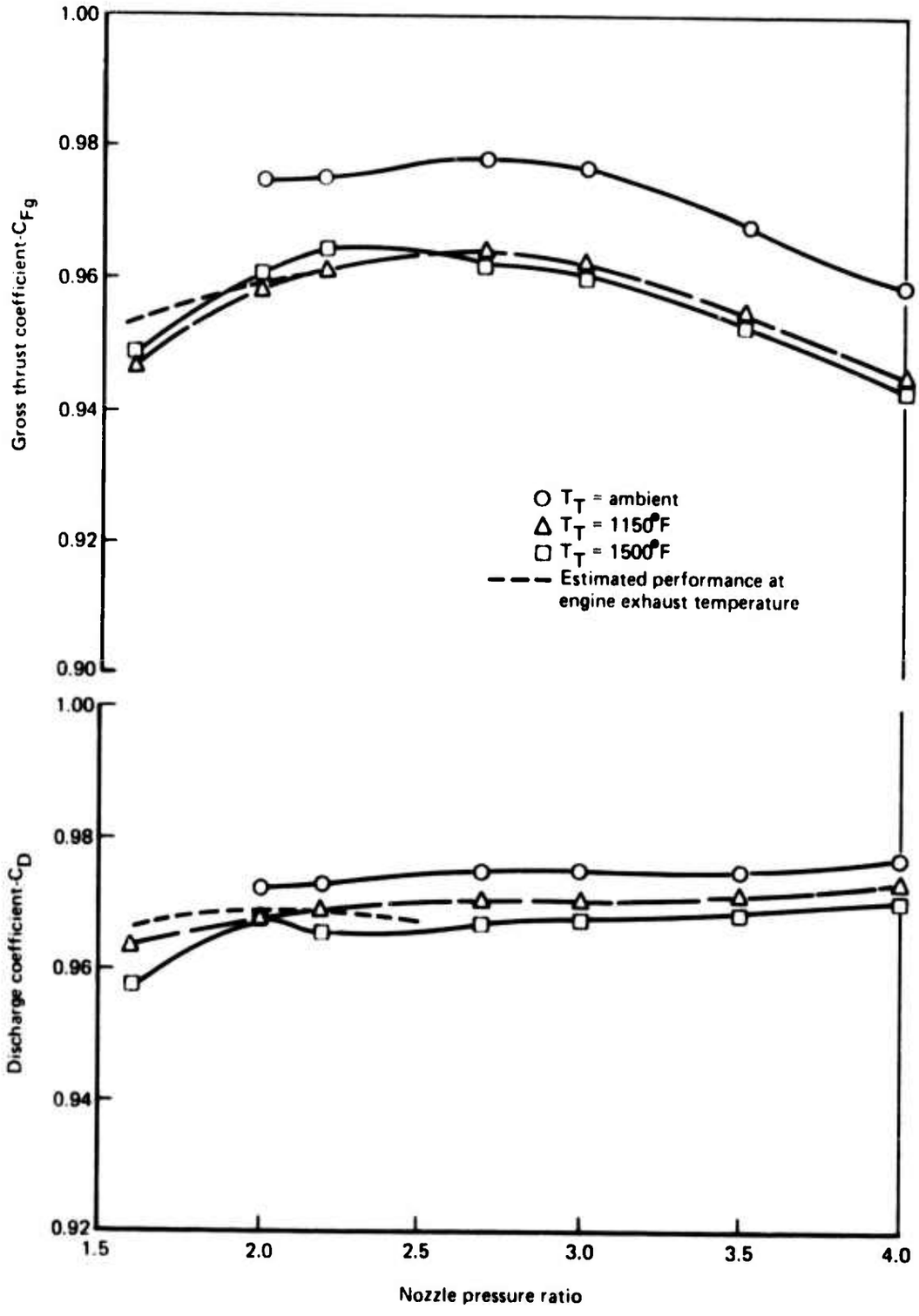

Figure 60.–Performance of LNHP-2/Lined Ejector at SB=1.5 in.

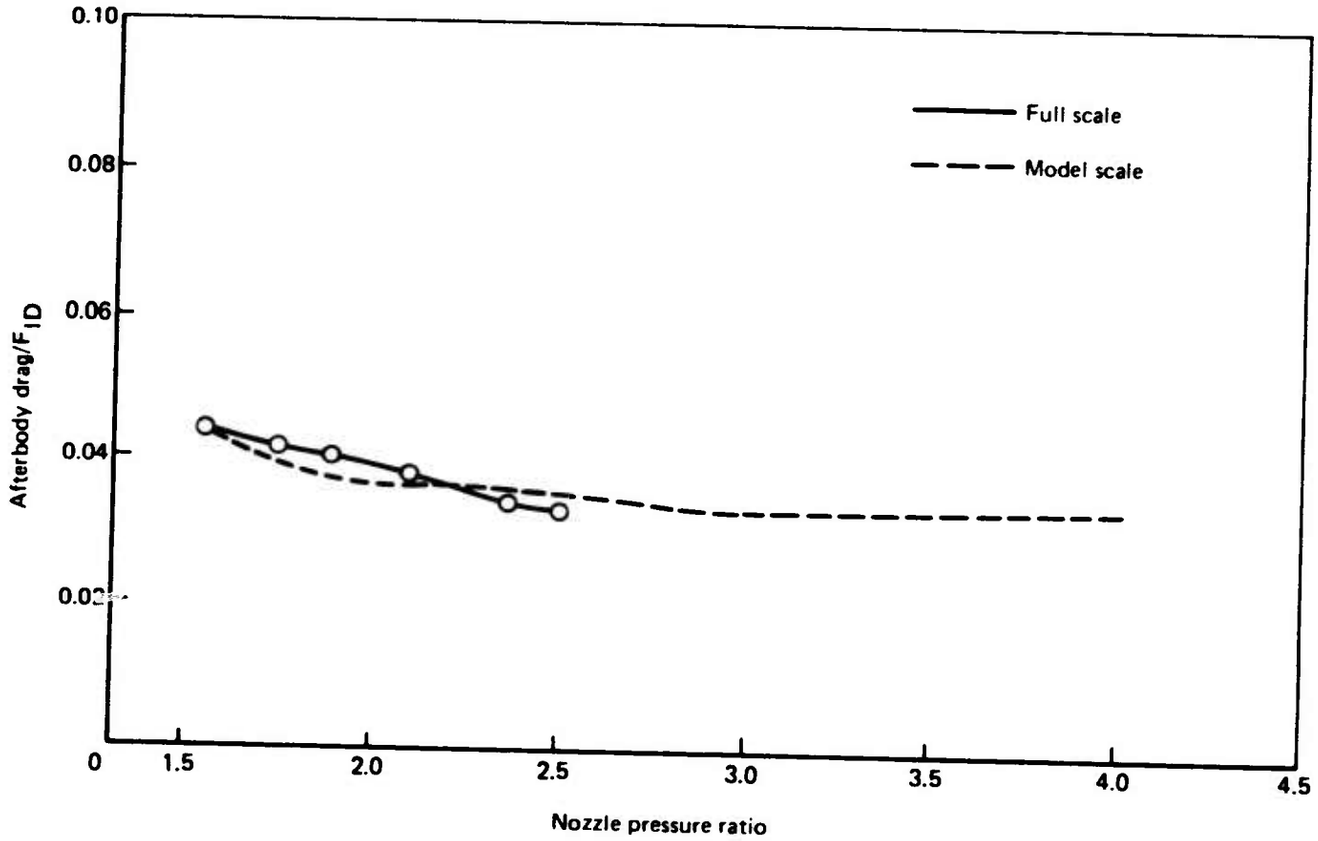

Figure 61.—Model- and Full-Scale Suppressor, Nozzle-only, Afterbody Drag

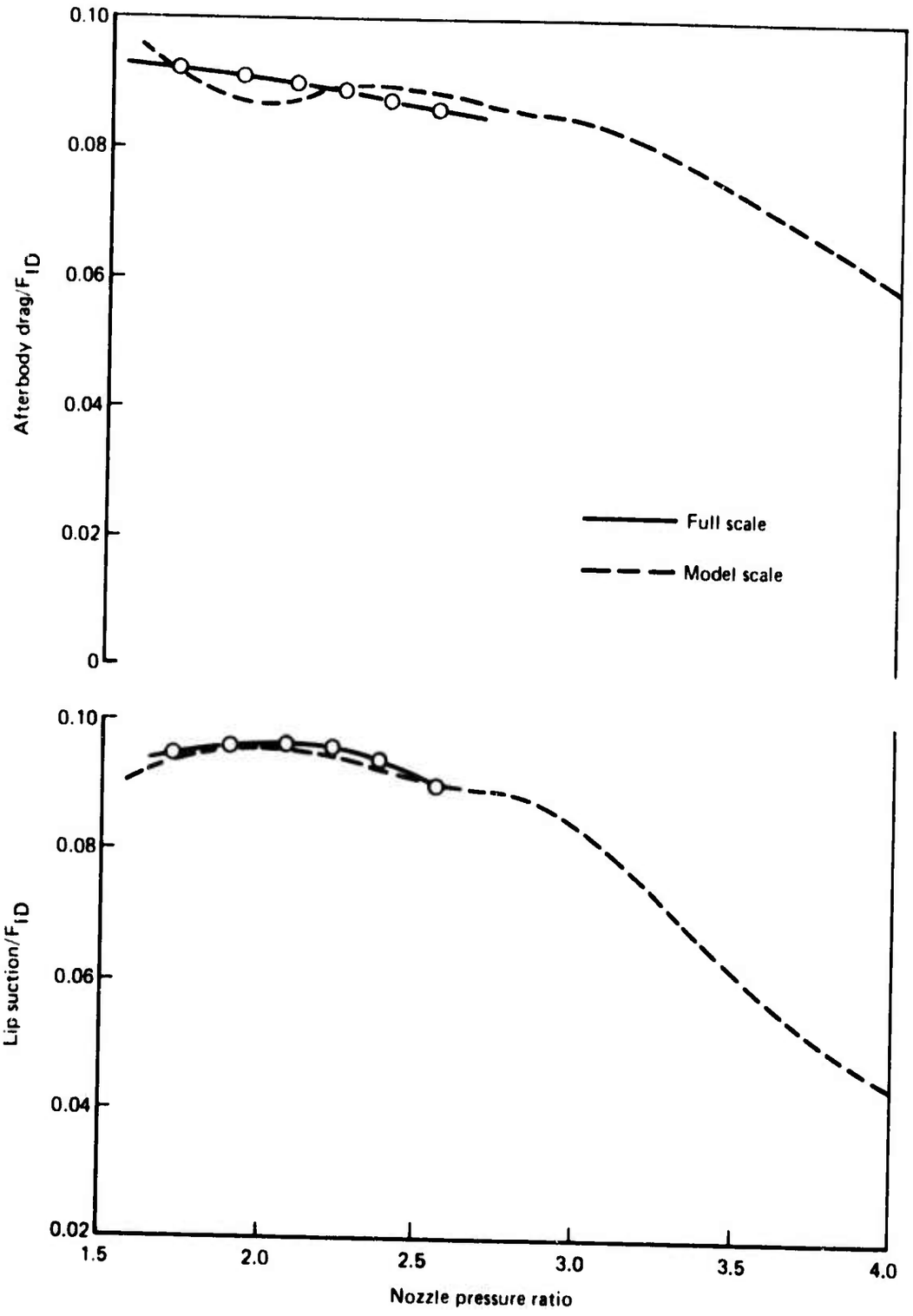

Figure 62.—Model- and Full-Scale Body Forces Hardwall Ejector Installed

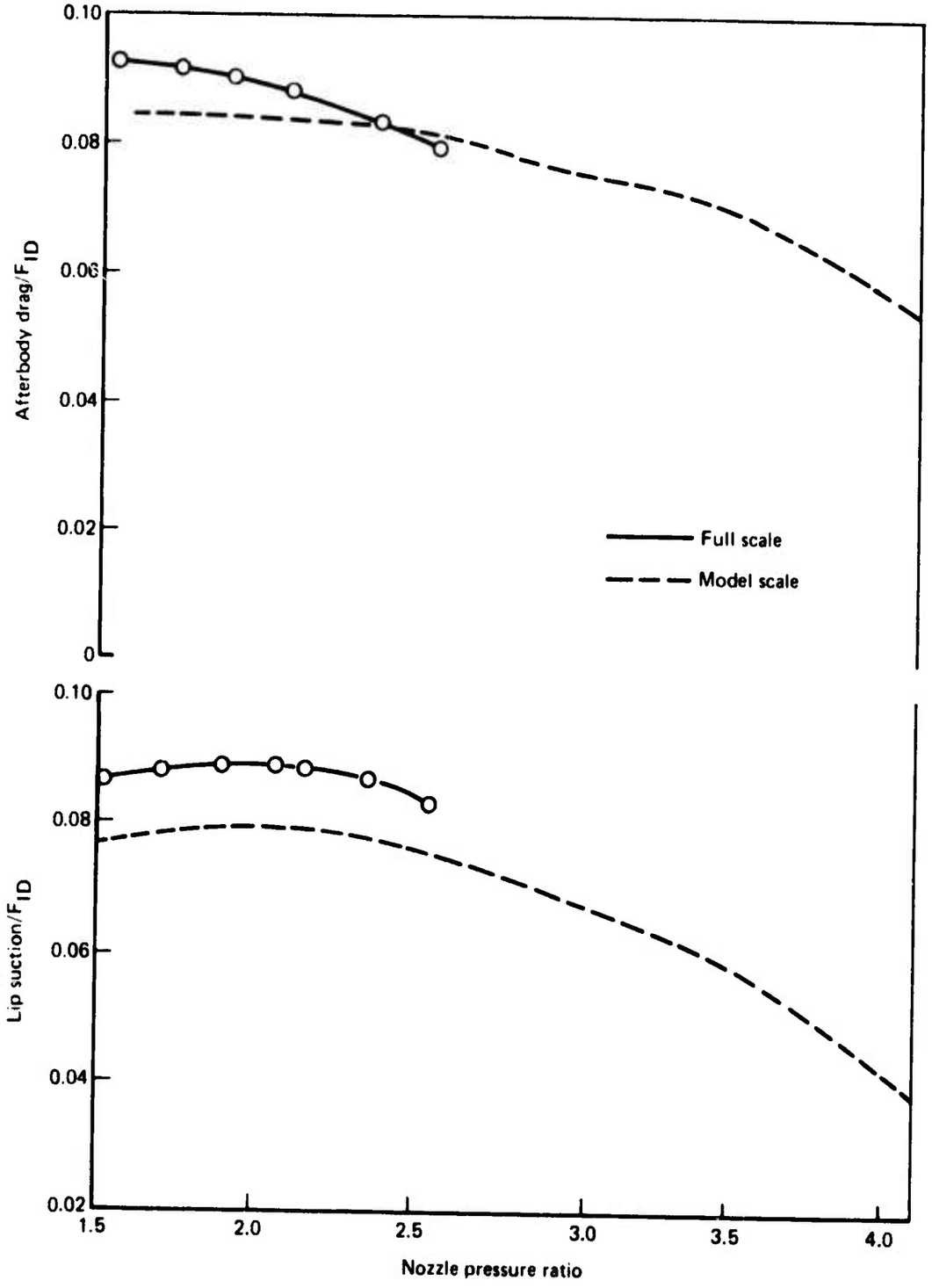

Figure 63.—Model- and Full-Scale Body Forces With Lined Ejector Installed

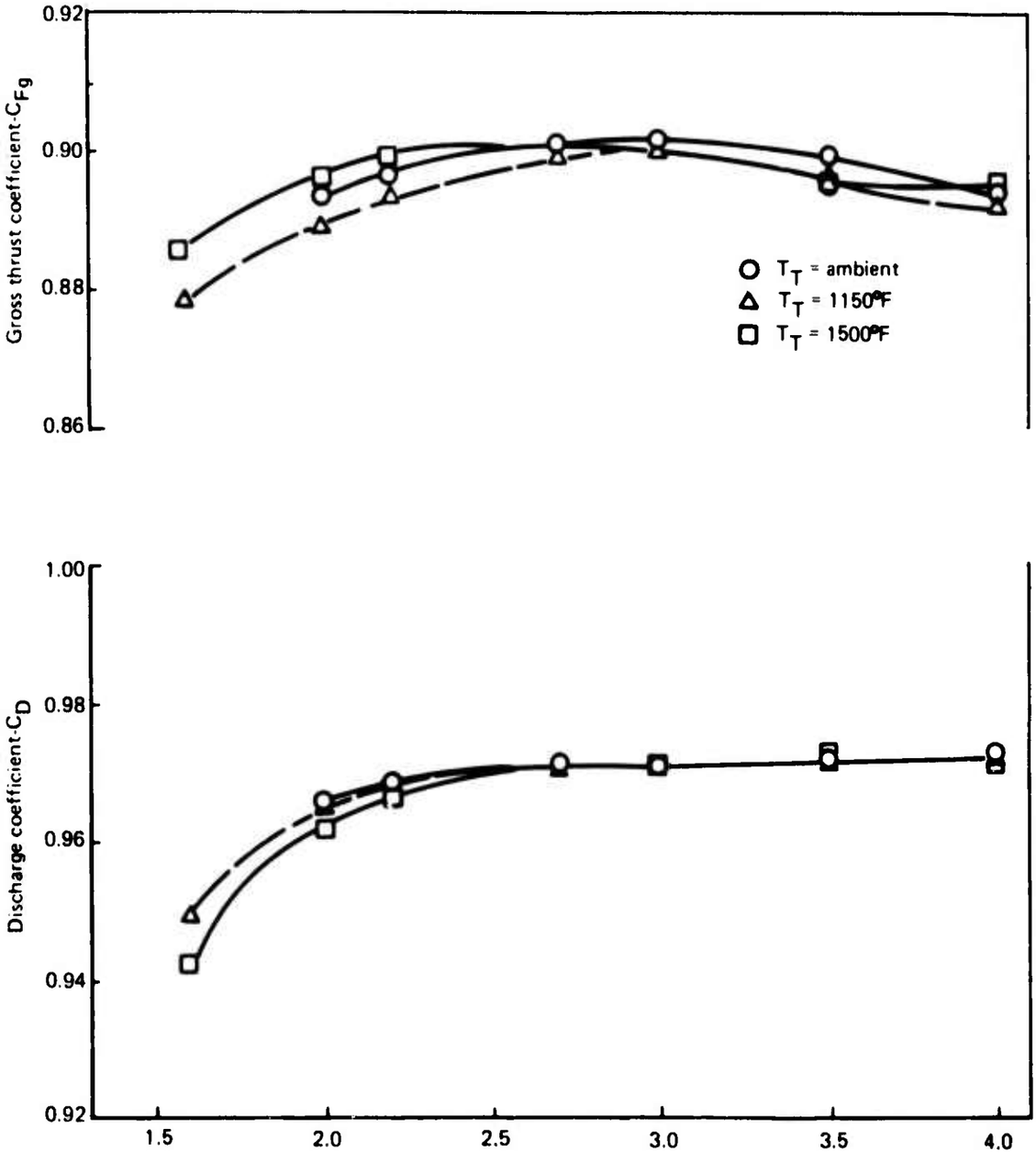

Figure 64.—Performance of LNHP-3 Primary Nozzle Alone

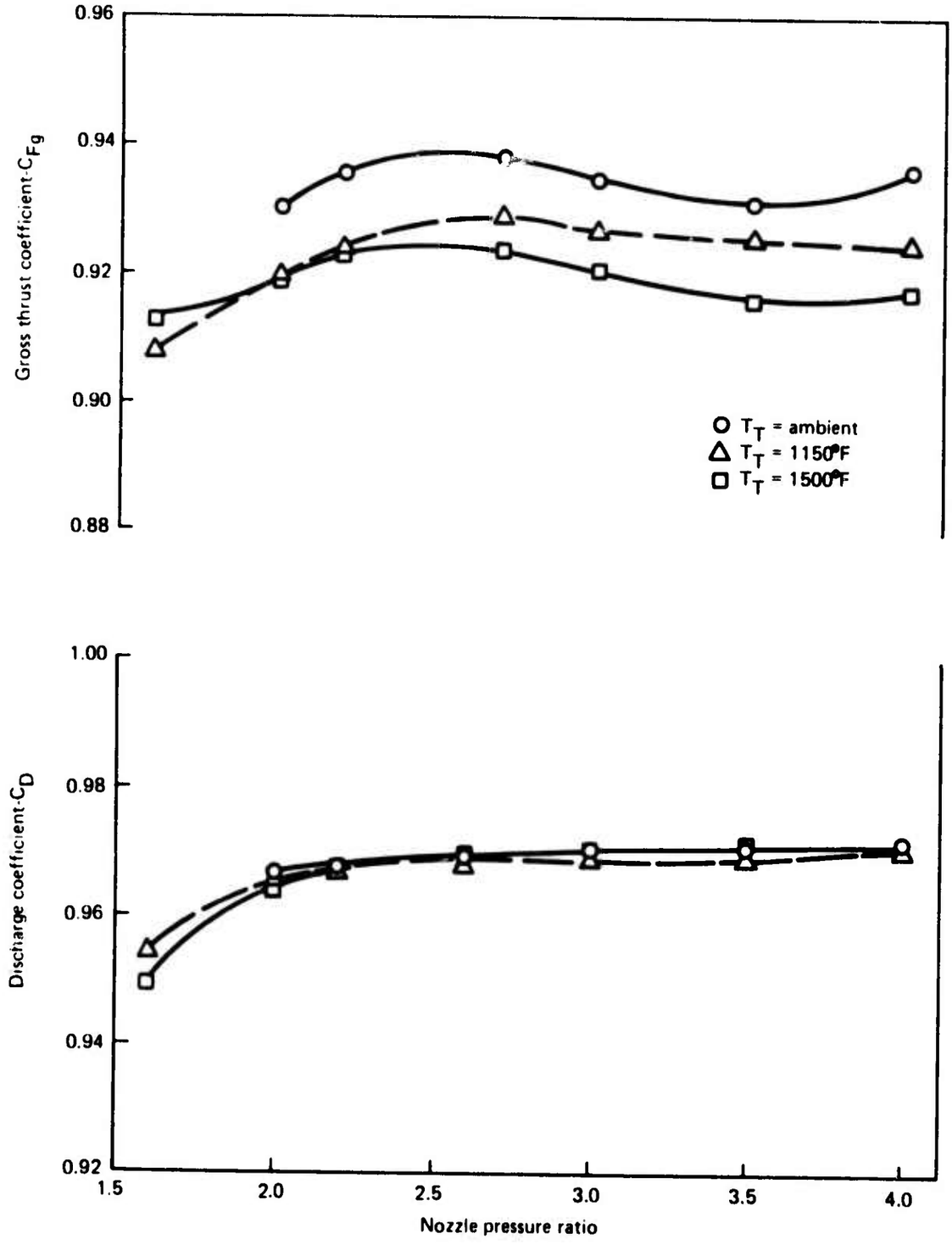

Figure 65.–Performance of LNHP-3/Hardwall Ejector at SB=0.74 in.

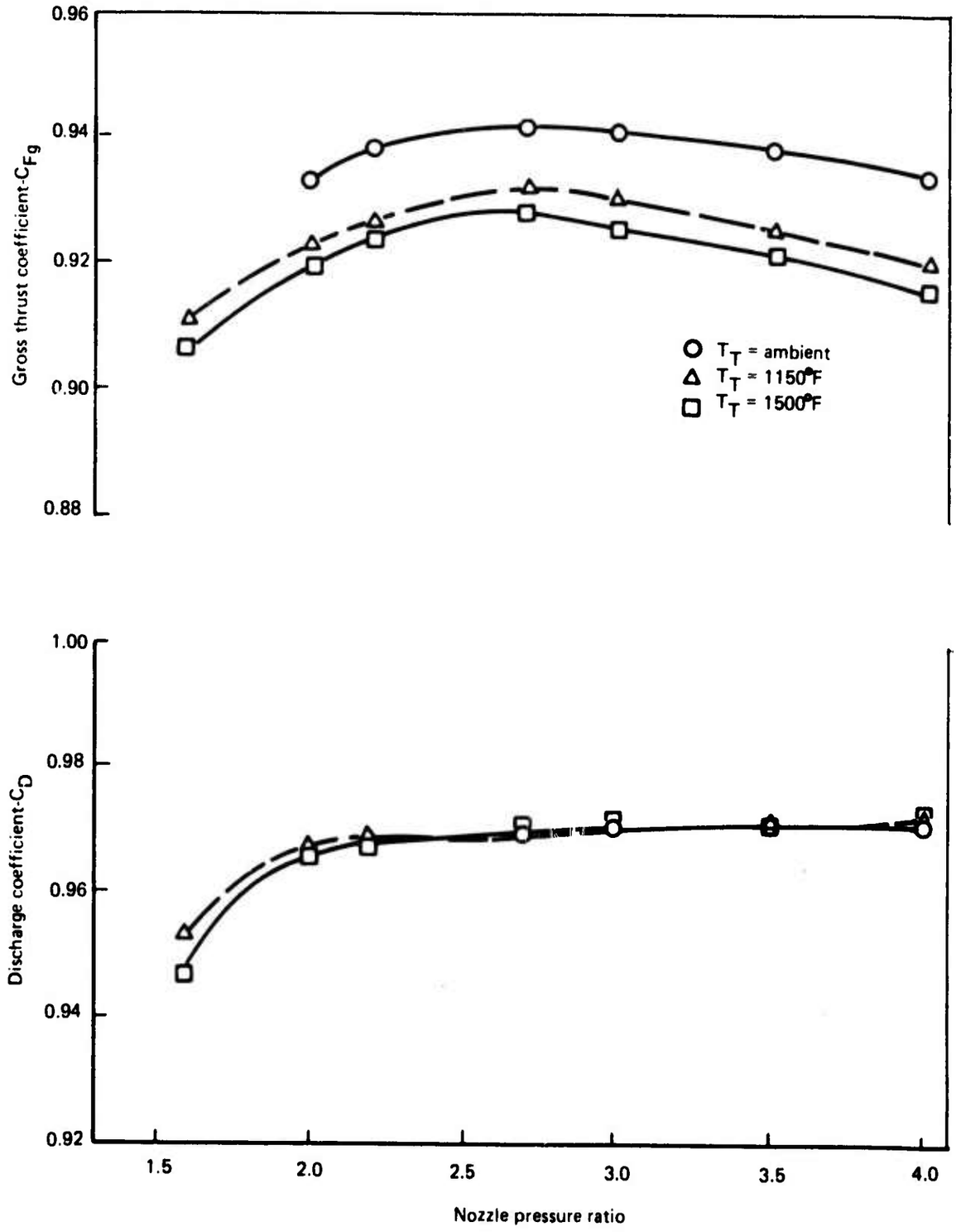

Figure 66.–Performance of LNHP-3/Hardwall Ejector at SB=1.44 in.

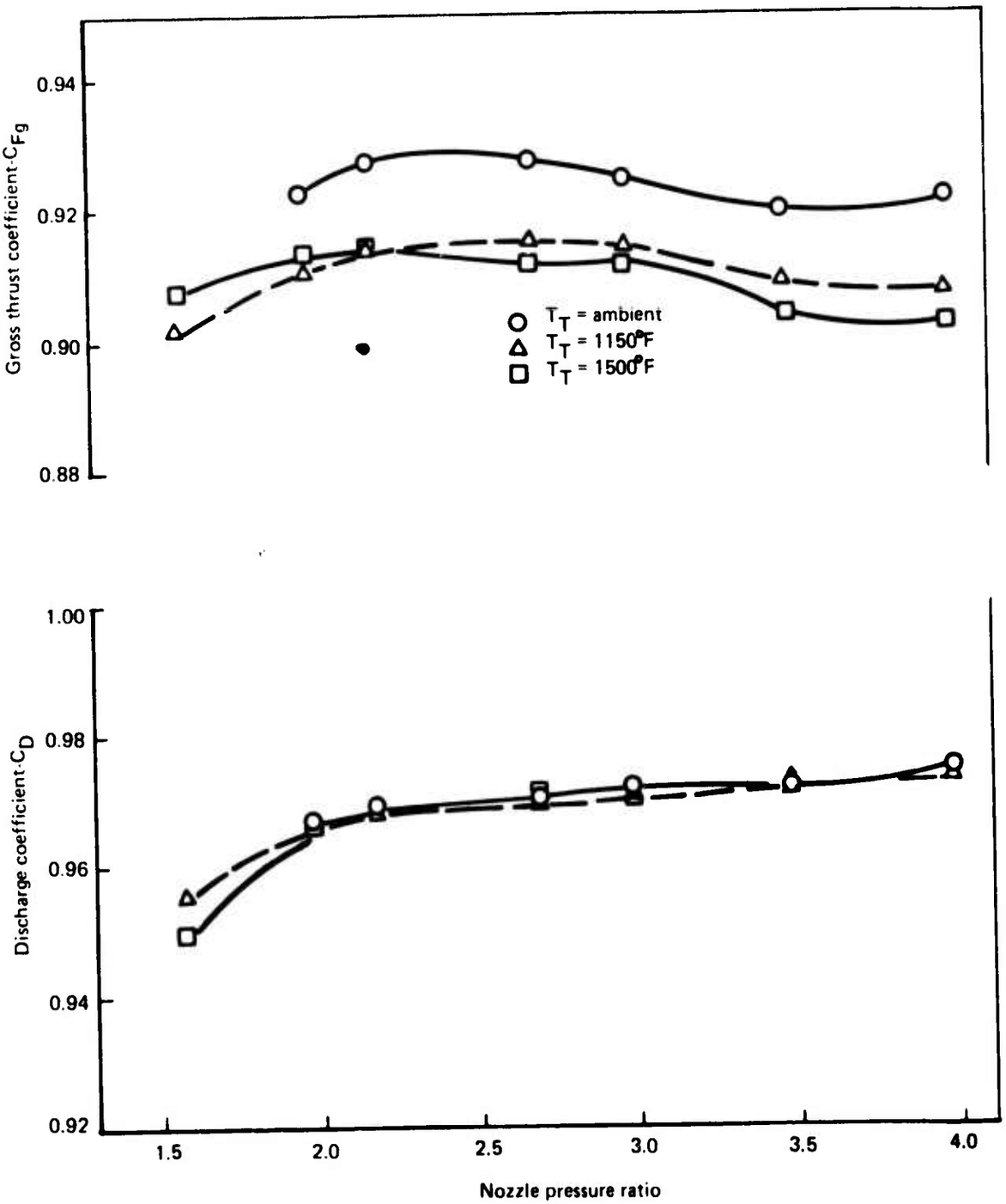

Figure 67.–Performance of LNHP-3/12-in. Lined Ejector at SB=0.74-in.

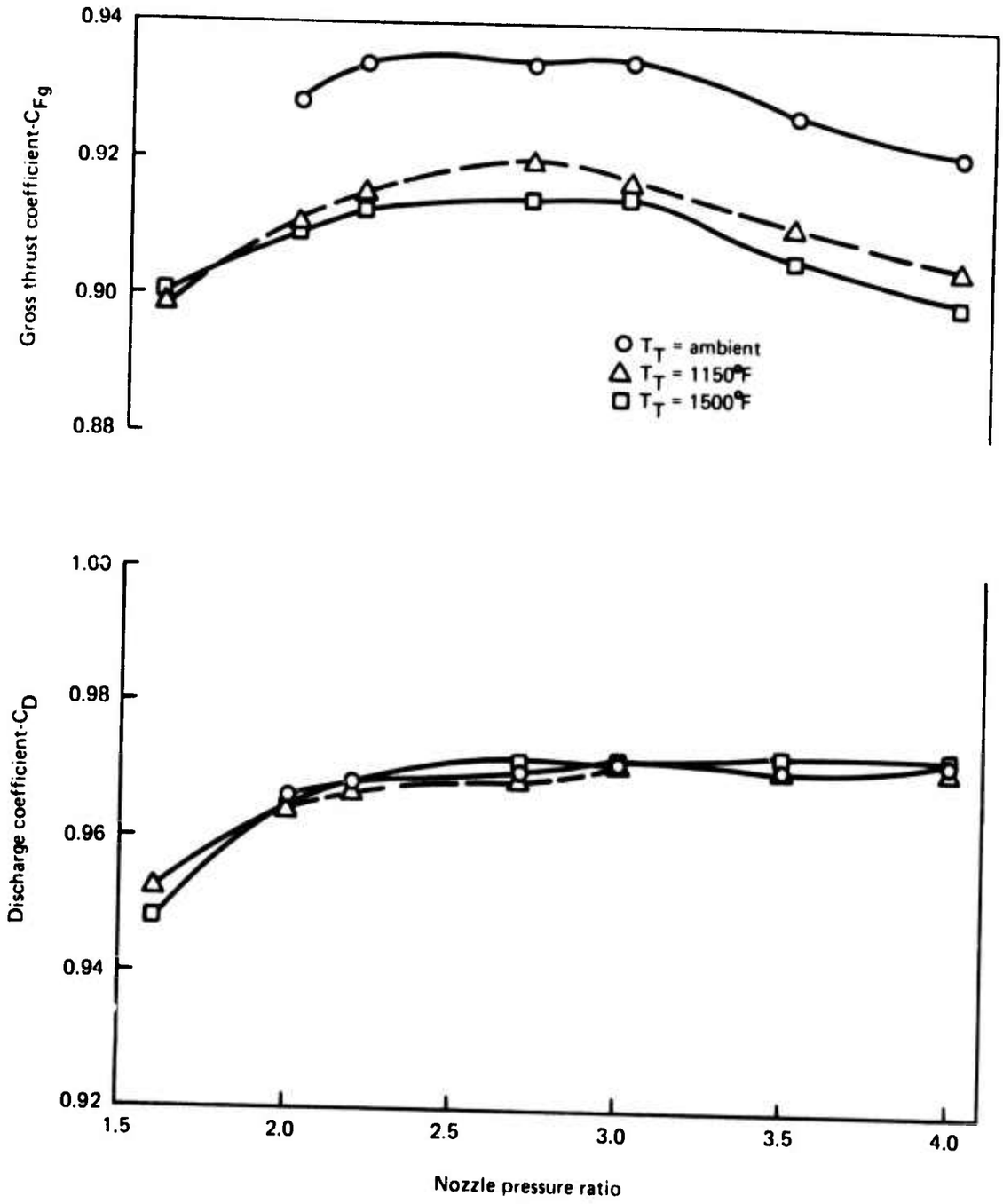

Figure 68.--Performance of LNHP-3/12-in. Lined Ejector at SB=1.44-in.

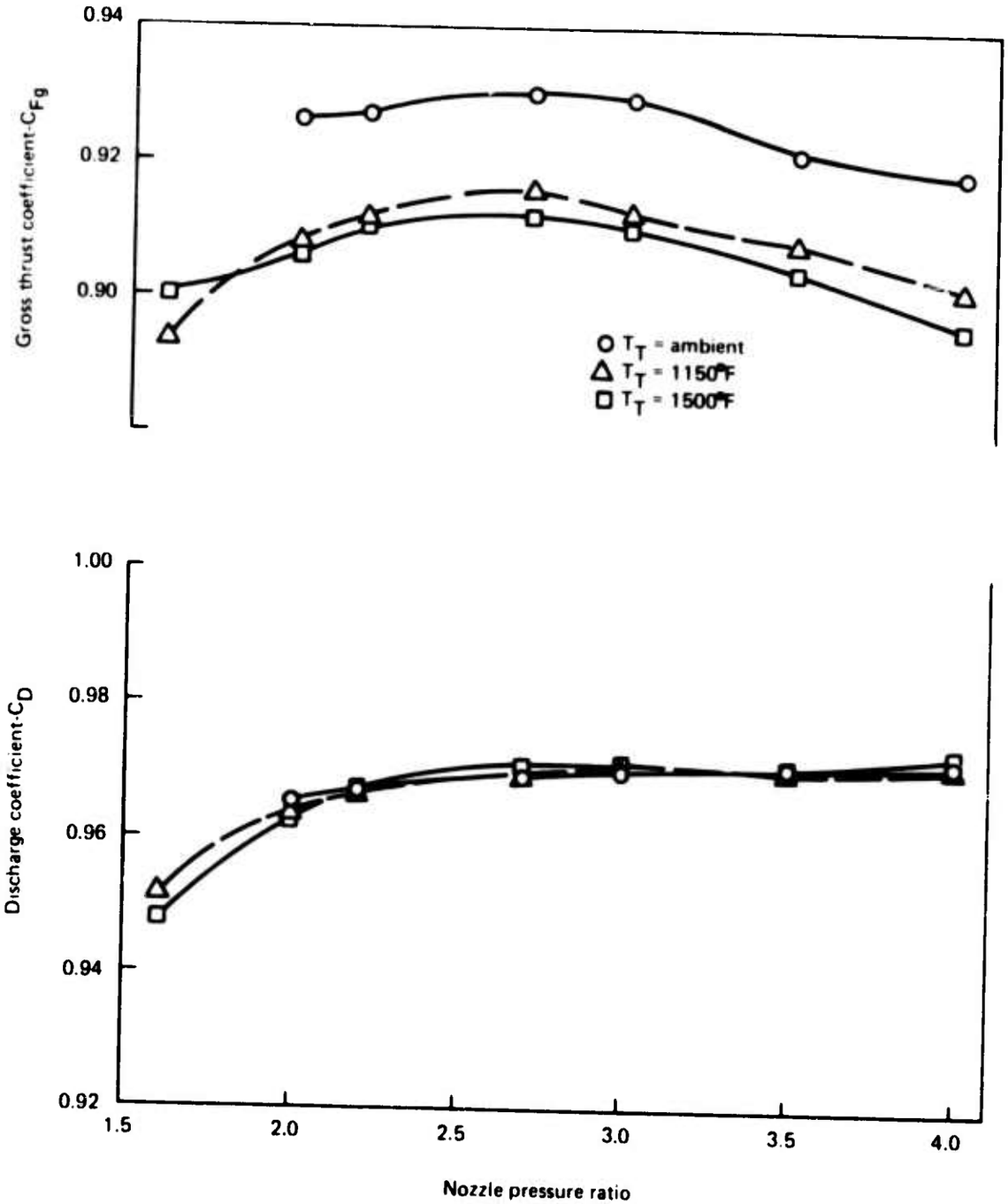

Figure 69.–Performance of LNHP-3/17-in. Lined Ejector at SB=1.44-in.

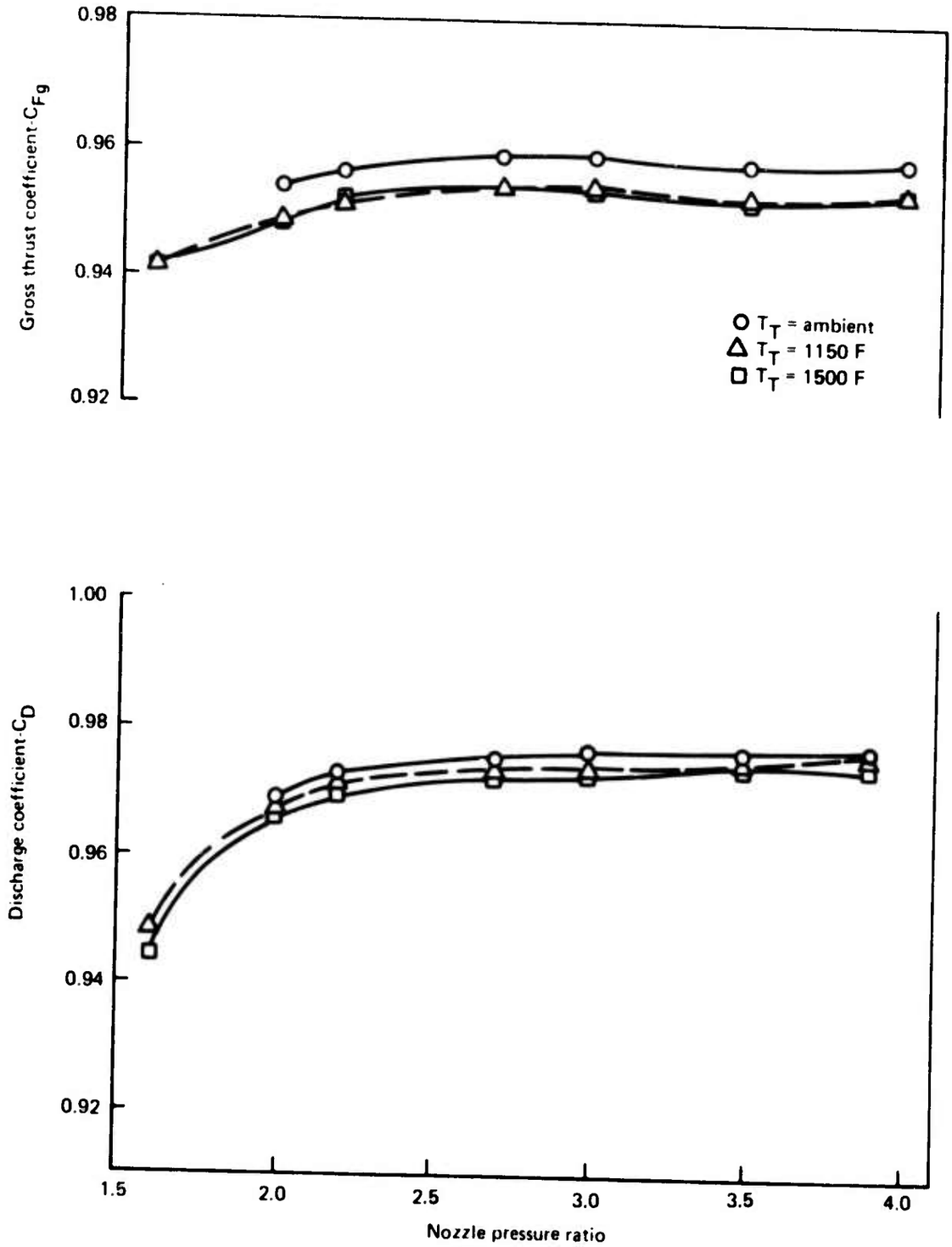

Figure 70.--Performance of LNHP-4 Primary Nozzle Alone

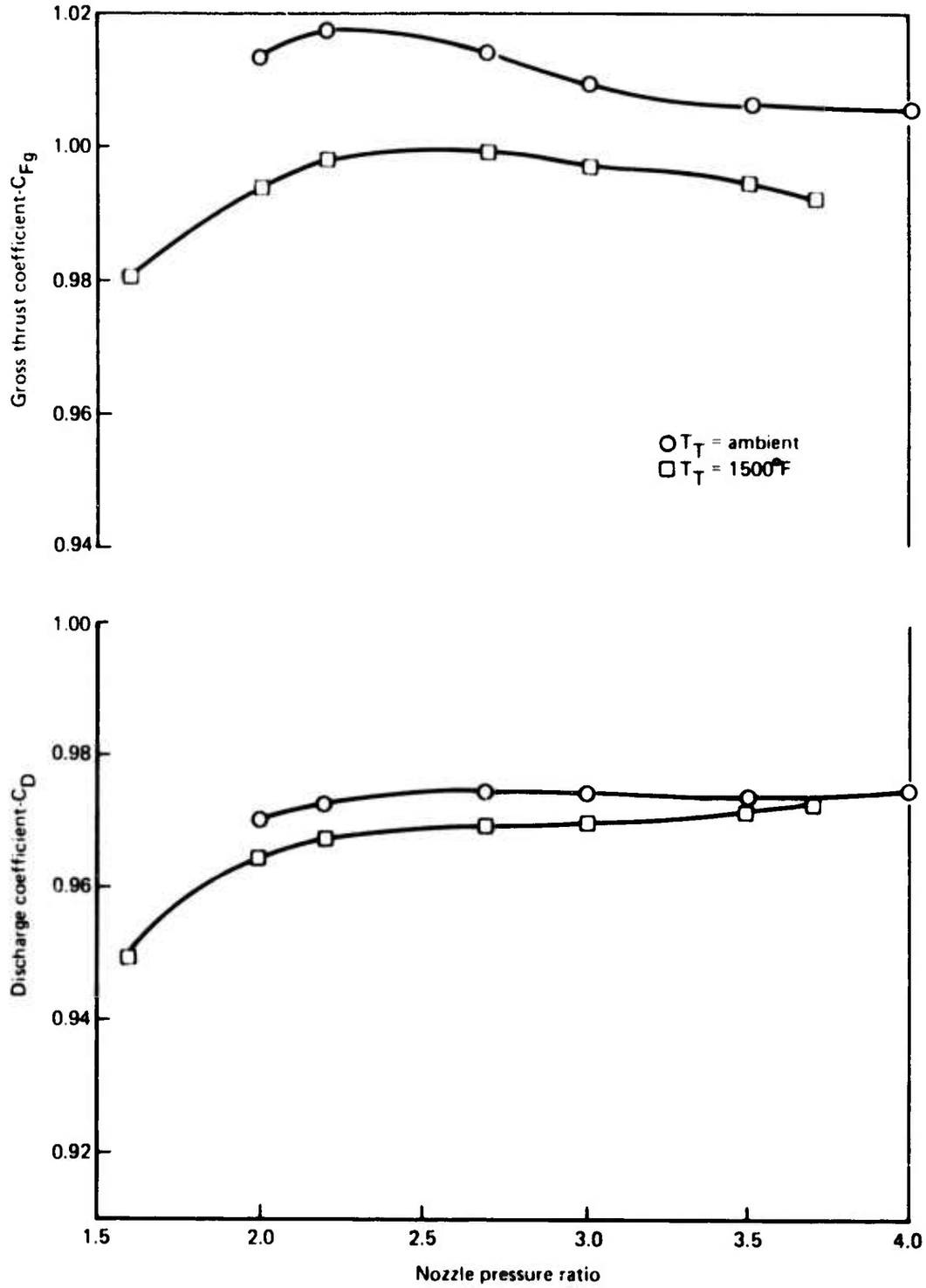

Figure 71.--Performance of LNHP-4/Hardwall Ejector at SB= 0.74 in.

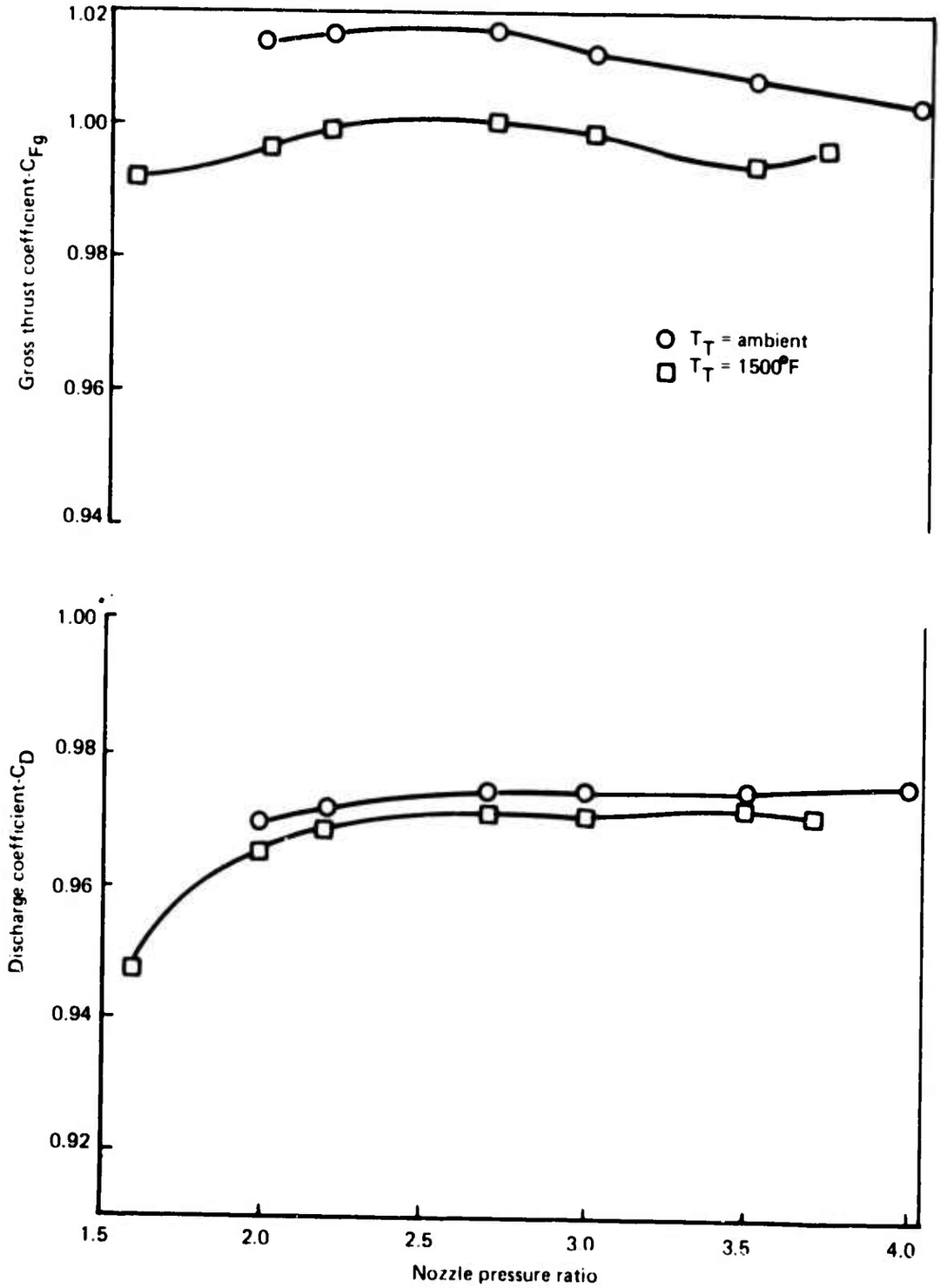

Figure 72.—Performance of LNHP-4/Hardwall Eiector at SB=1.44 in.

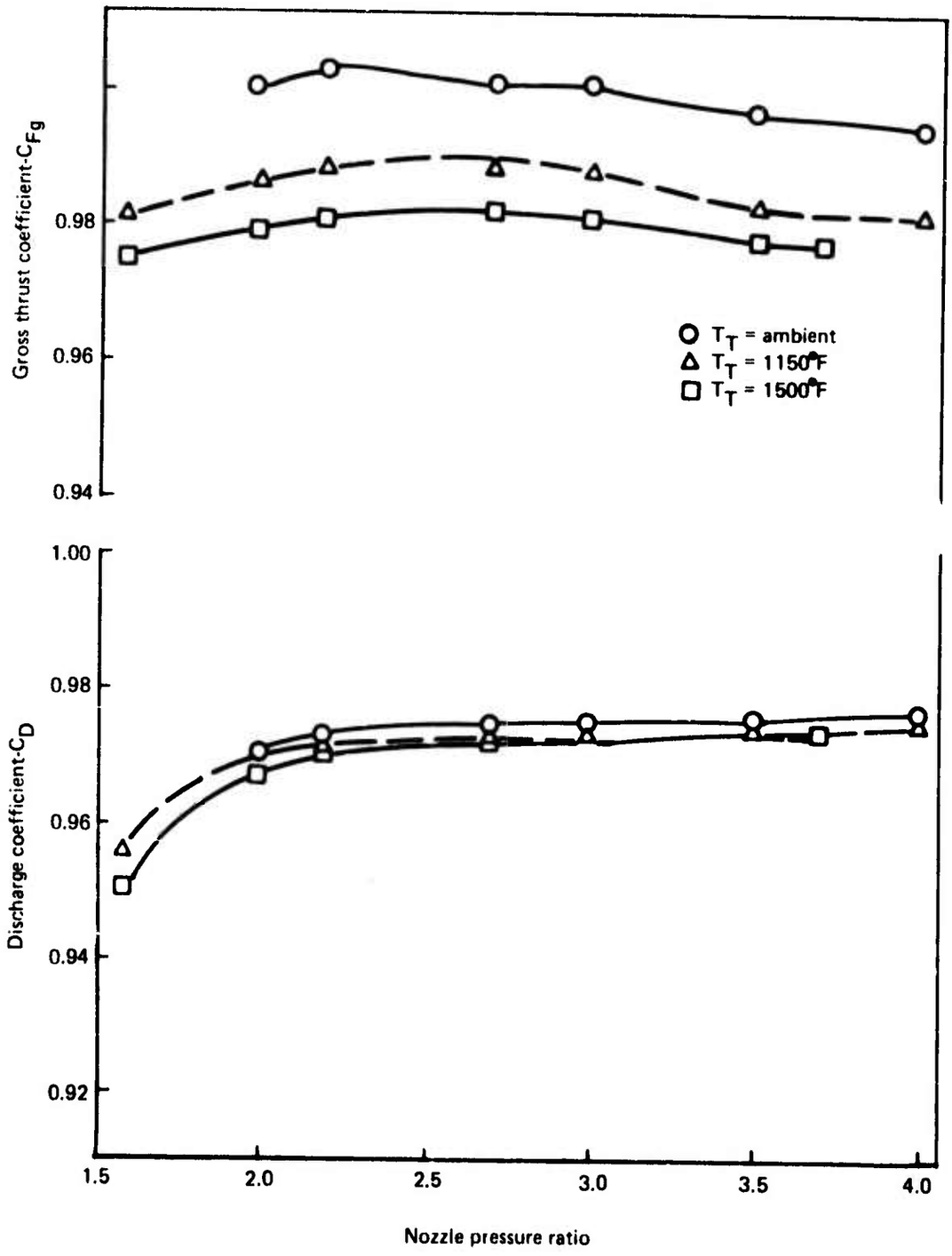

Figure 73.—Performance of LNHP-4/Lined Ejector at SB=0.74 in.

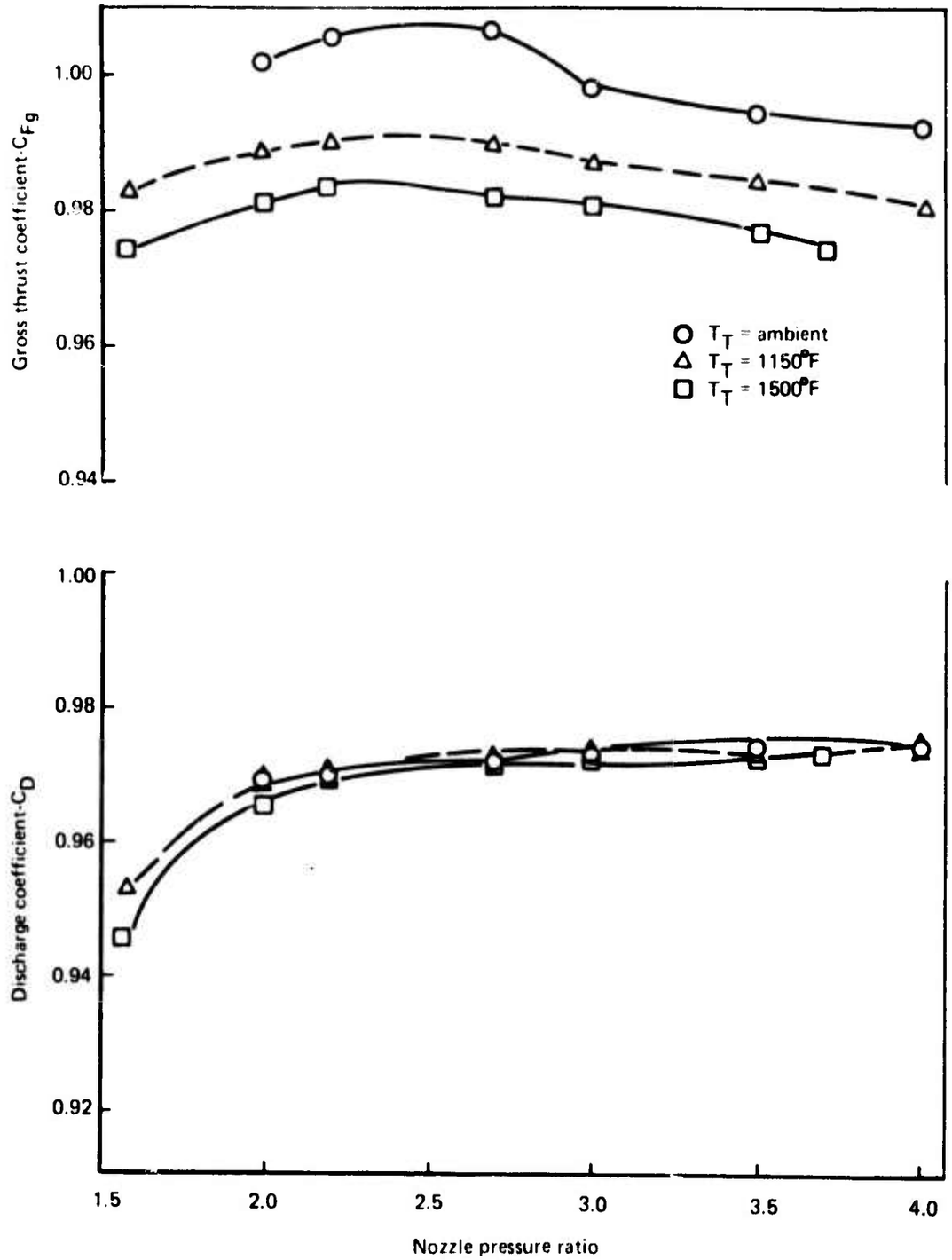

Figure 74.–Performance of LNHP-4/Lined Ejector at SB=1.44 in.

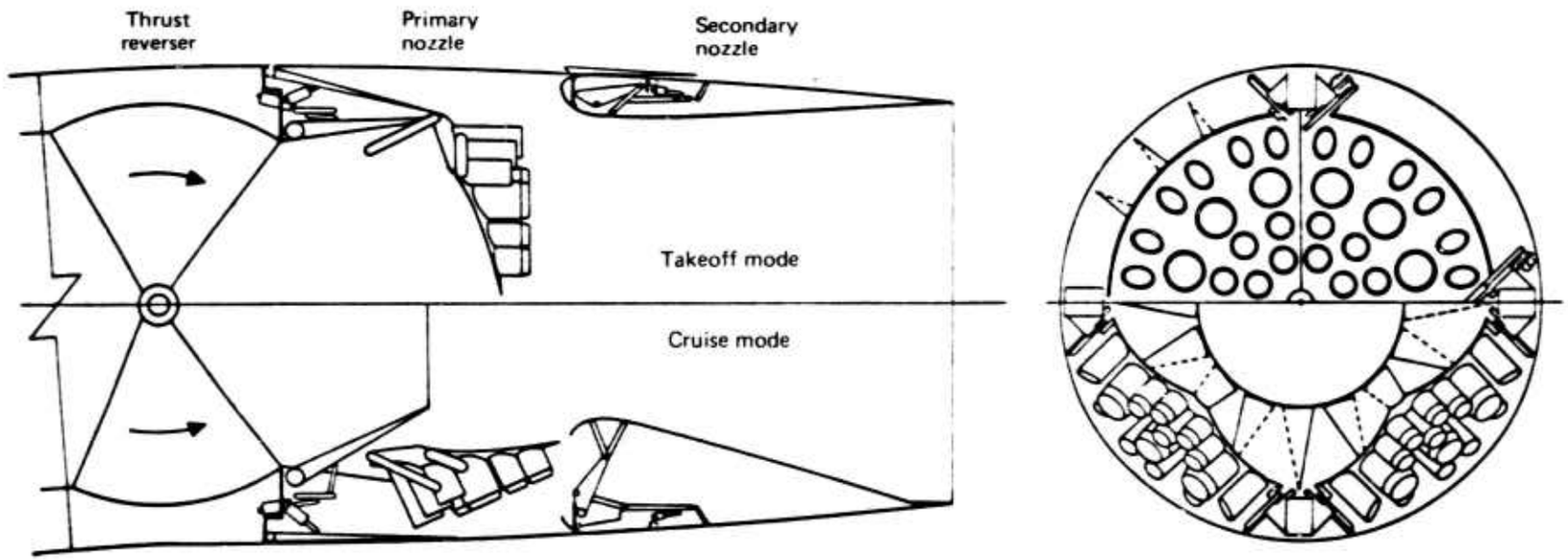

Figure 75.—Application of the LNHP-2 Suppressor to an Advanced SST Exhaust System

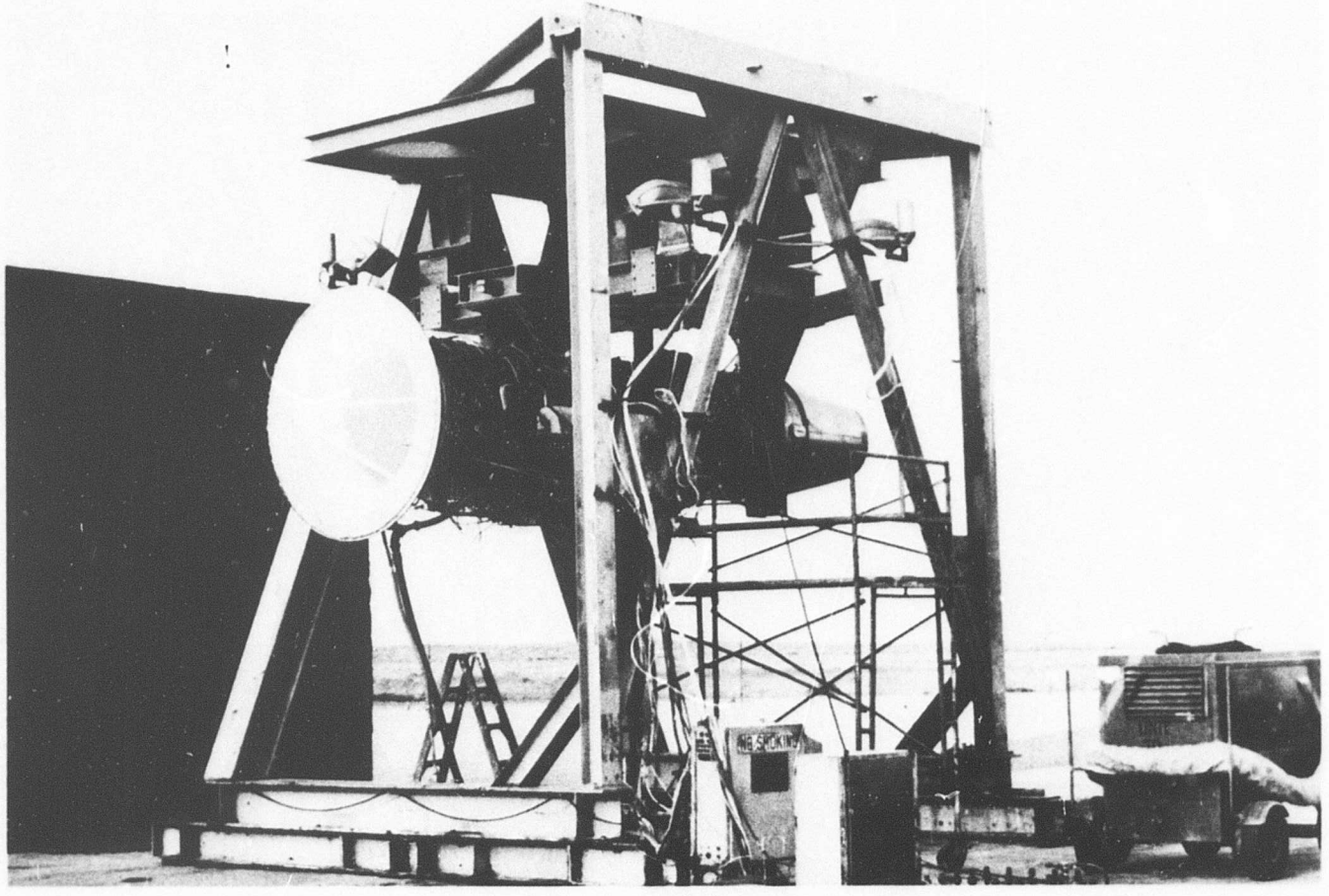

Figure 76.—J-58 Engine Installation at Boardman Test Facility

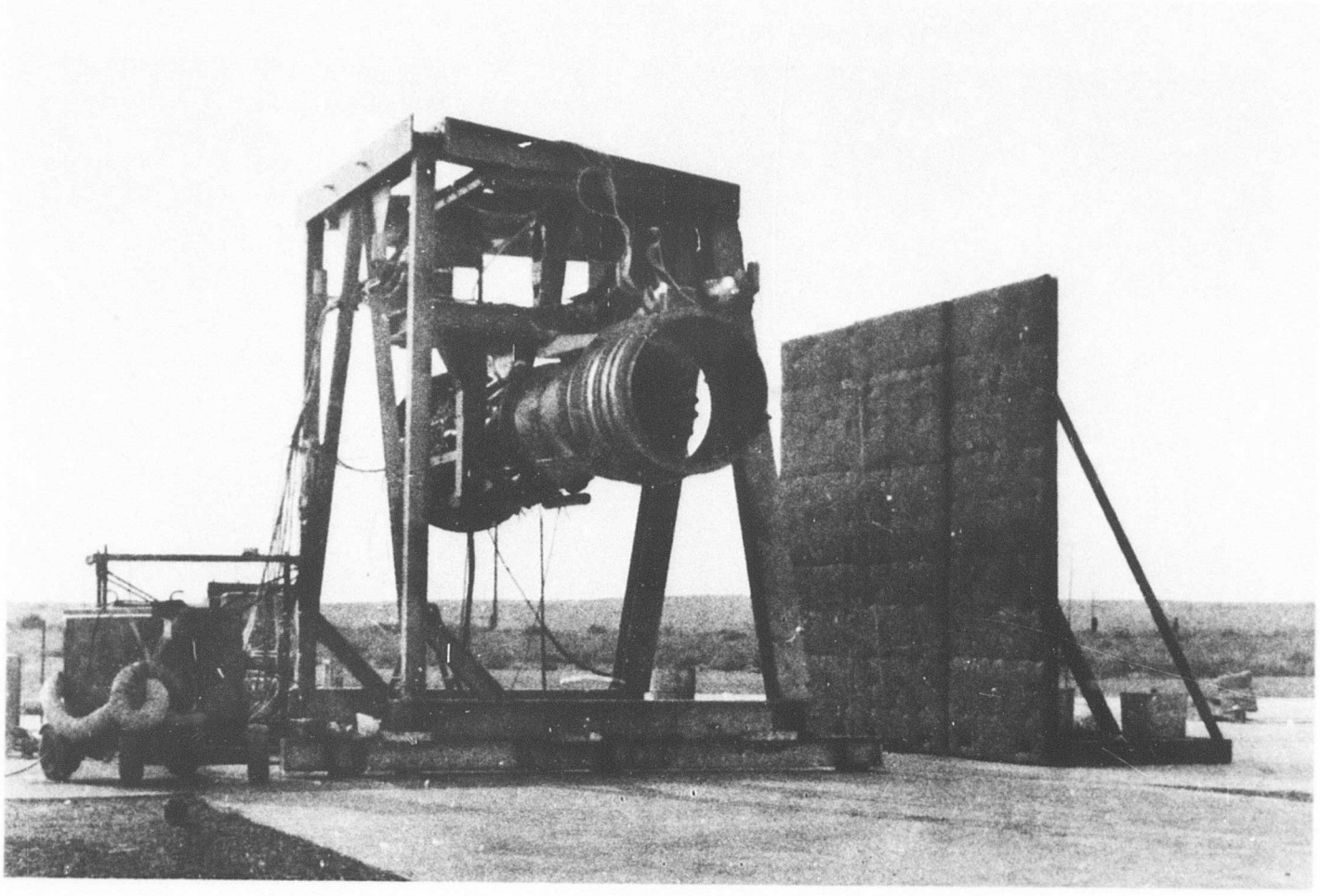

Figure 77.—LNHP-2 Suppressor Installed on the J-58 Engine at Boardman

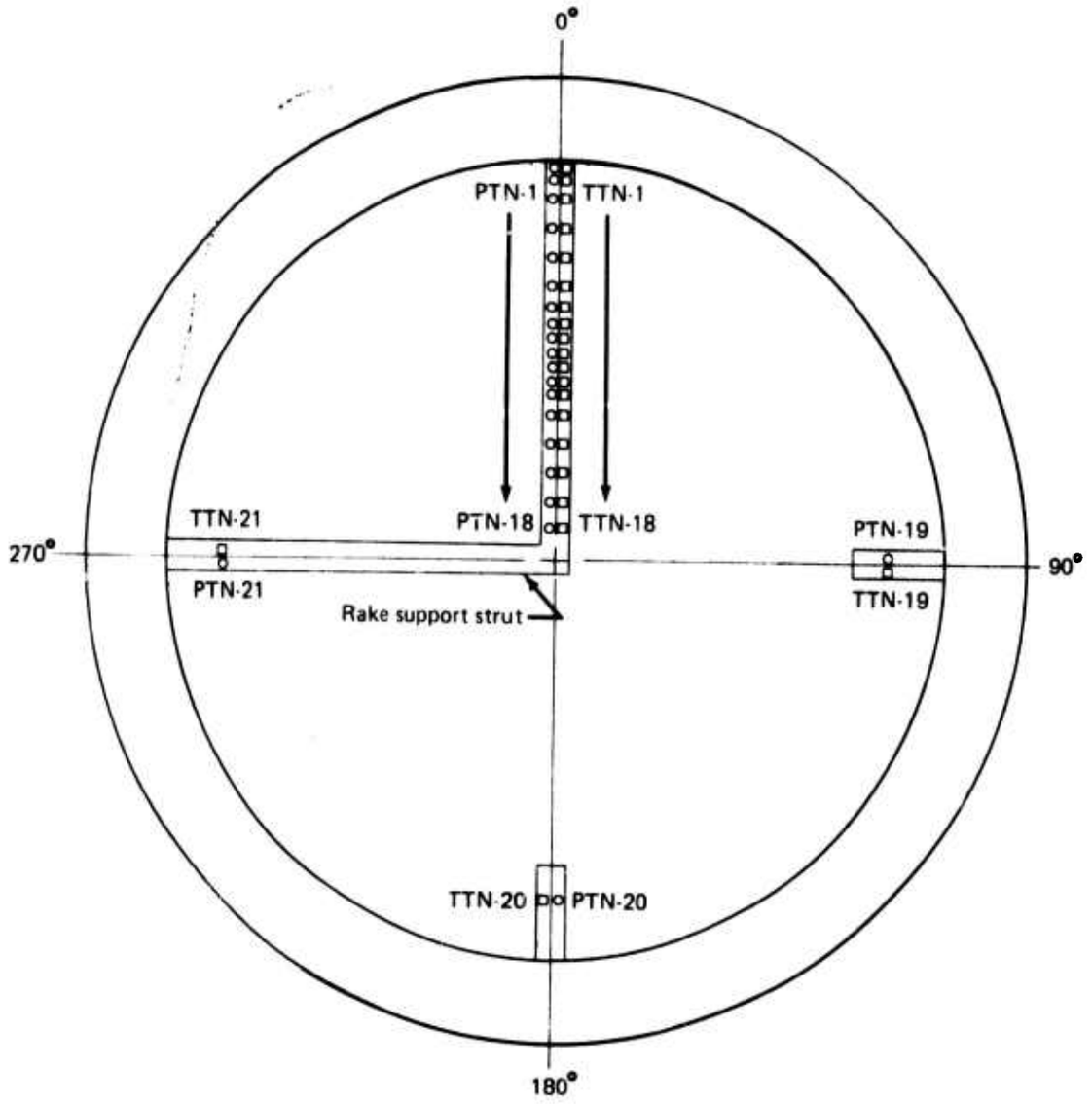

Figure 78.—Schematic of Total Pressure-Total Temperature Charging Station Instrumentation, Full-Scale Test

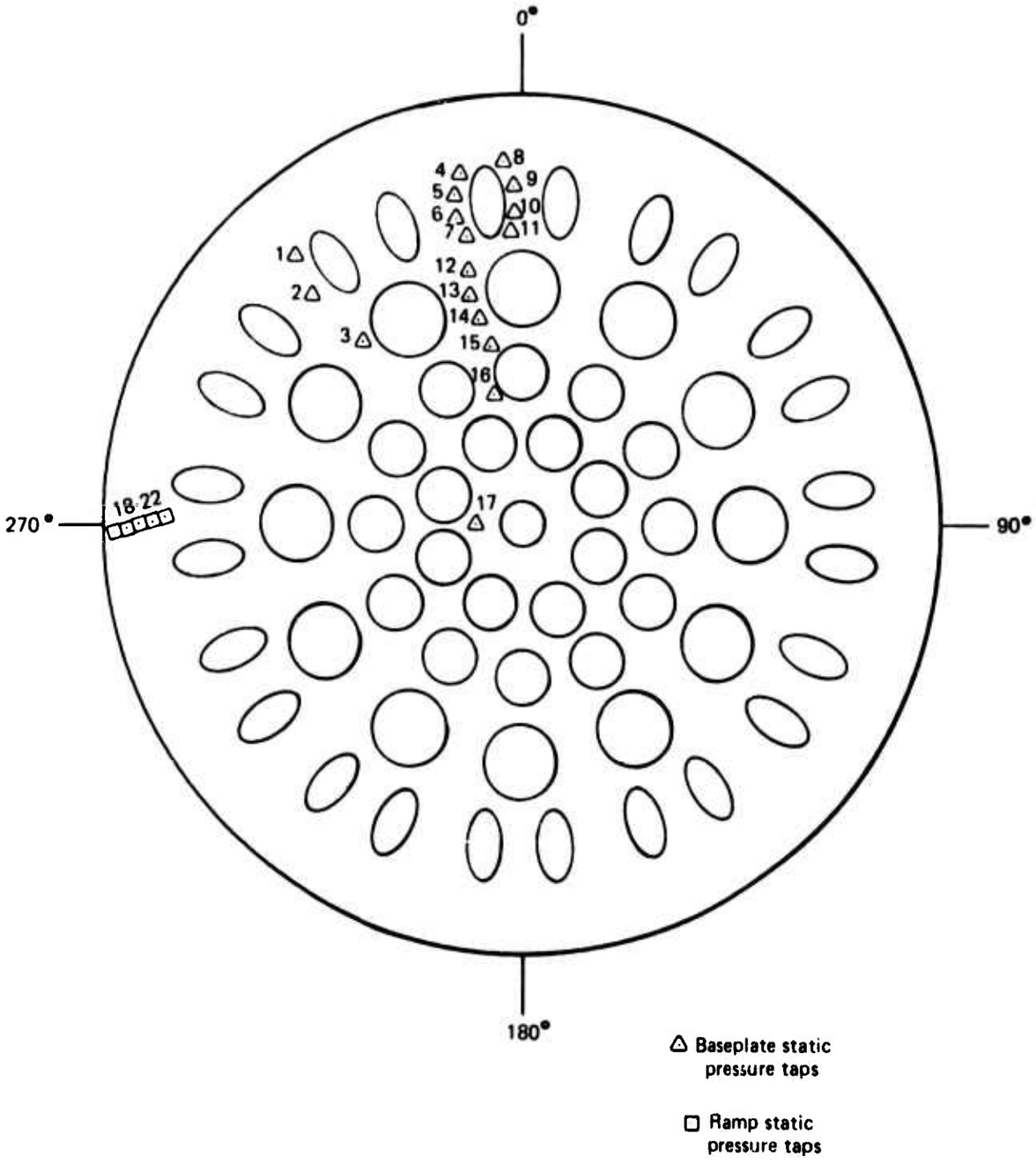

Figure 79.–57-Tube Suppressor, Static Pressure Tap Location

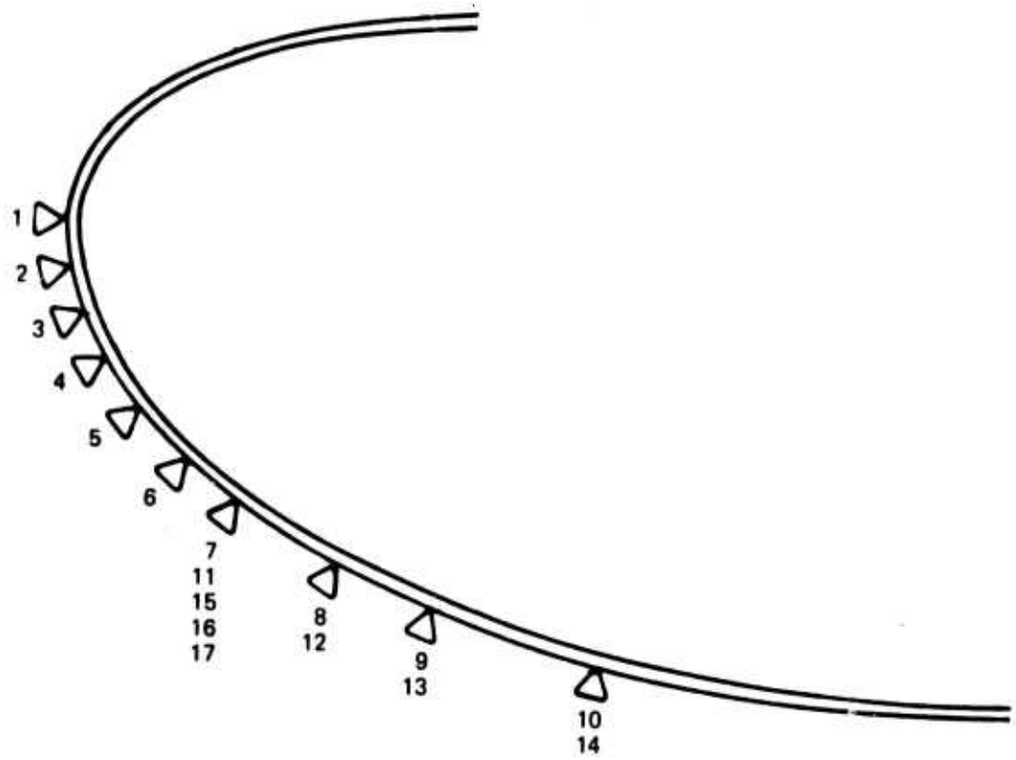

Taps 1-10 at 0°
Taps 11-14 at 45°
Taps 15 at 90°
Taps 16 at 180°
Taps 17 at 270°

Figure 80.—Full-Scale Ejector Lip, Static Pressure Tap Location

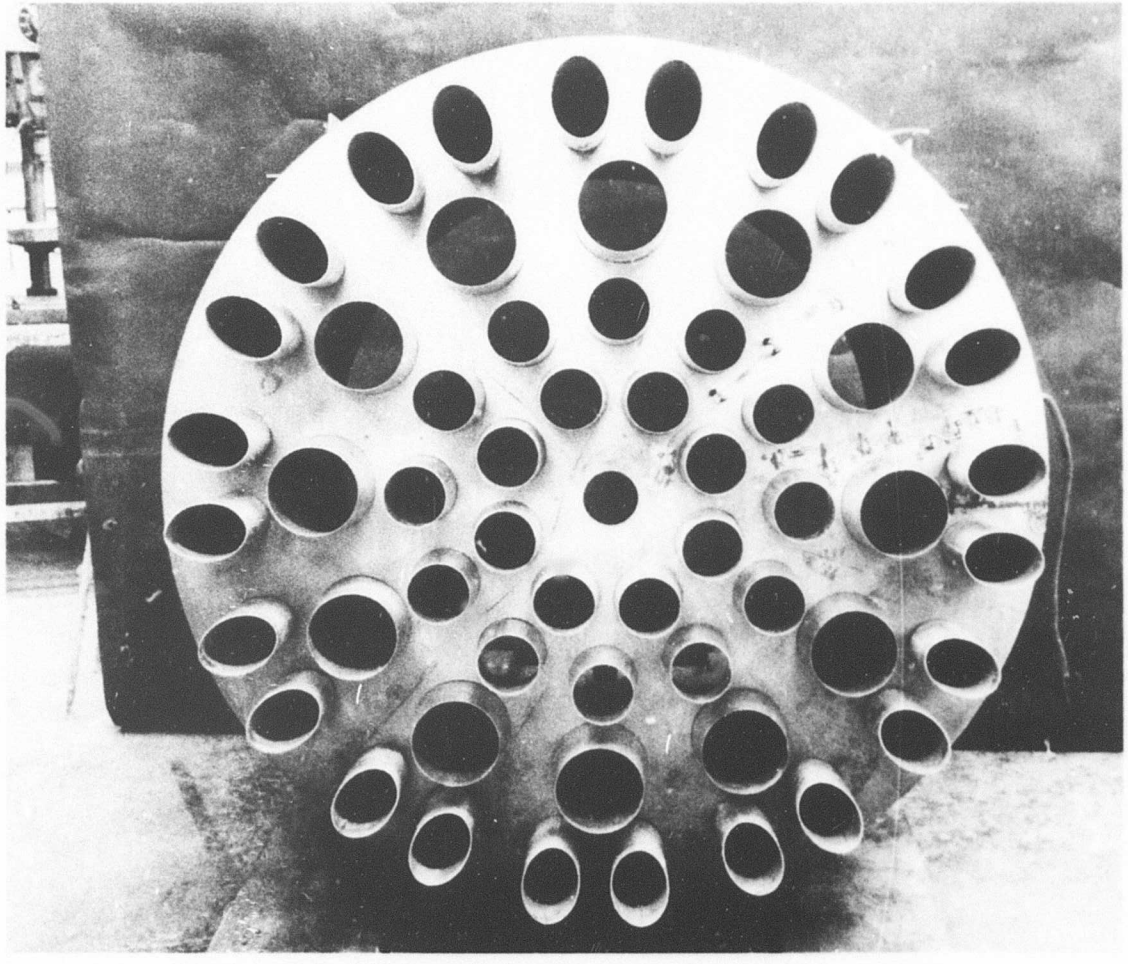

Figure 81.—Full-Scale LiNHP-2 Suppressor Nozzle

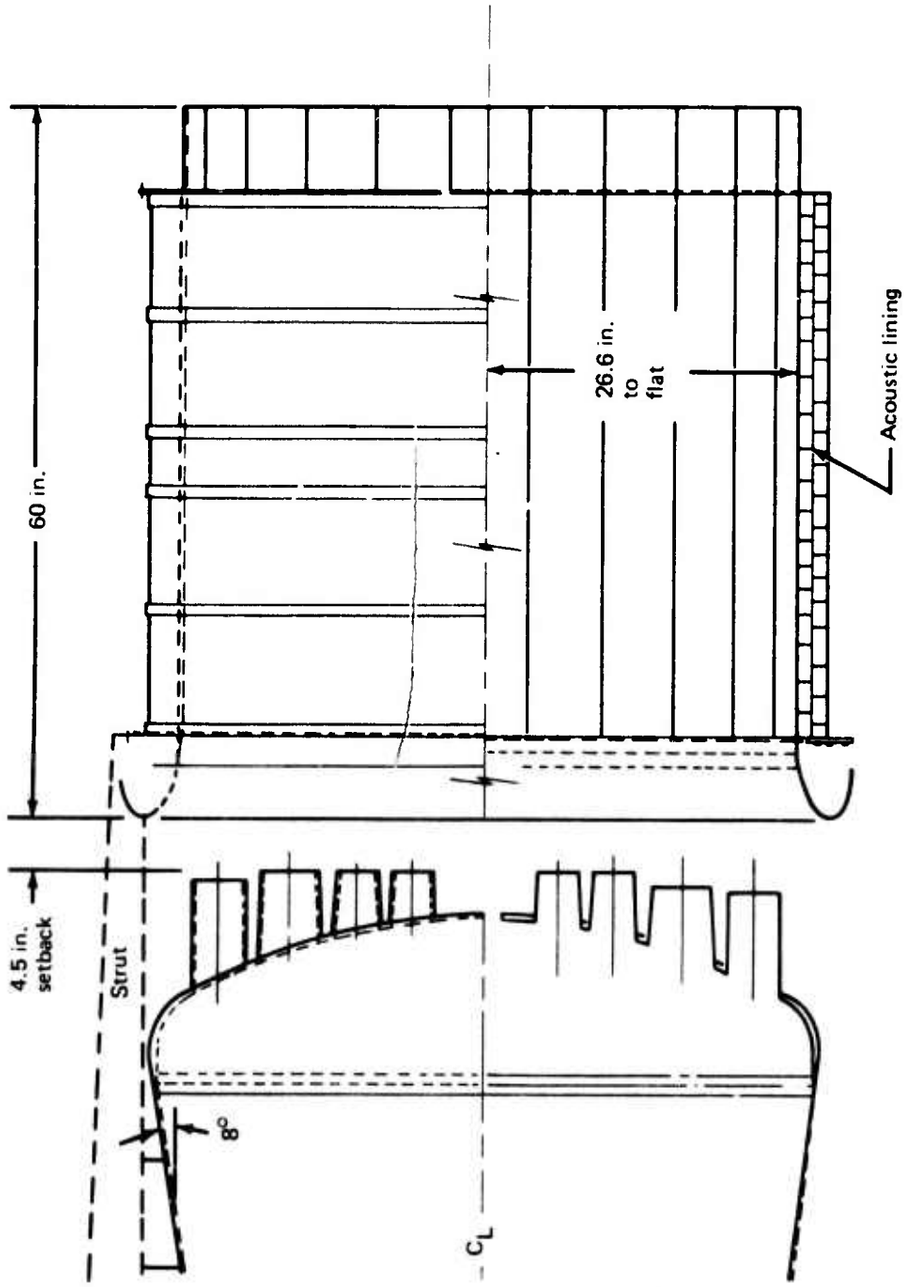

Figure 82.–Full-Scale LNHP-2 Suppressor/Ejector Installation

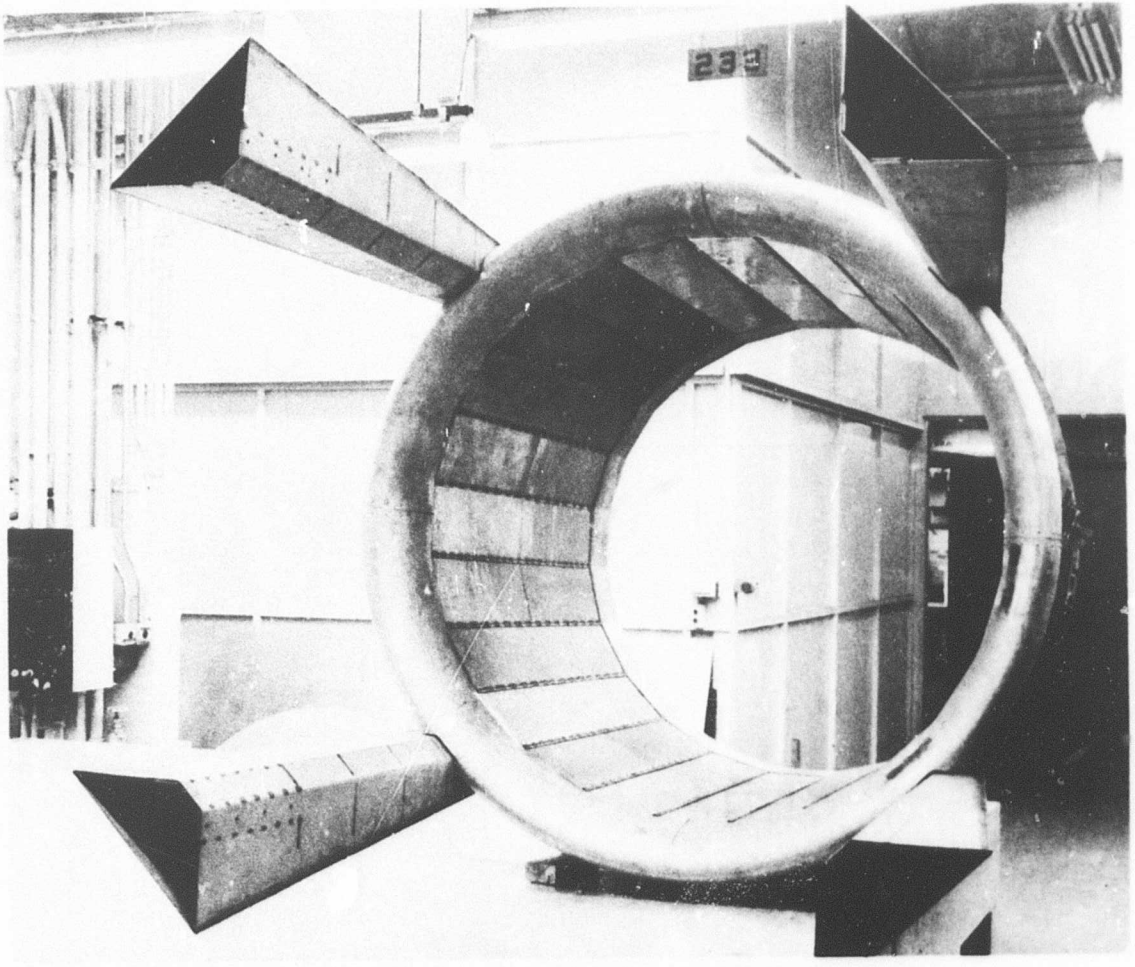

Figure 83.—Full-Scale Ejector Hardware

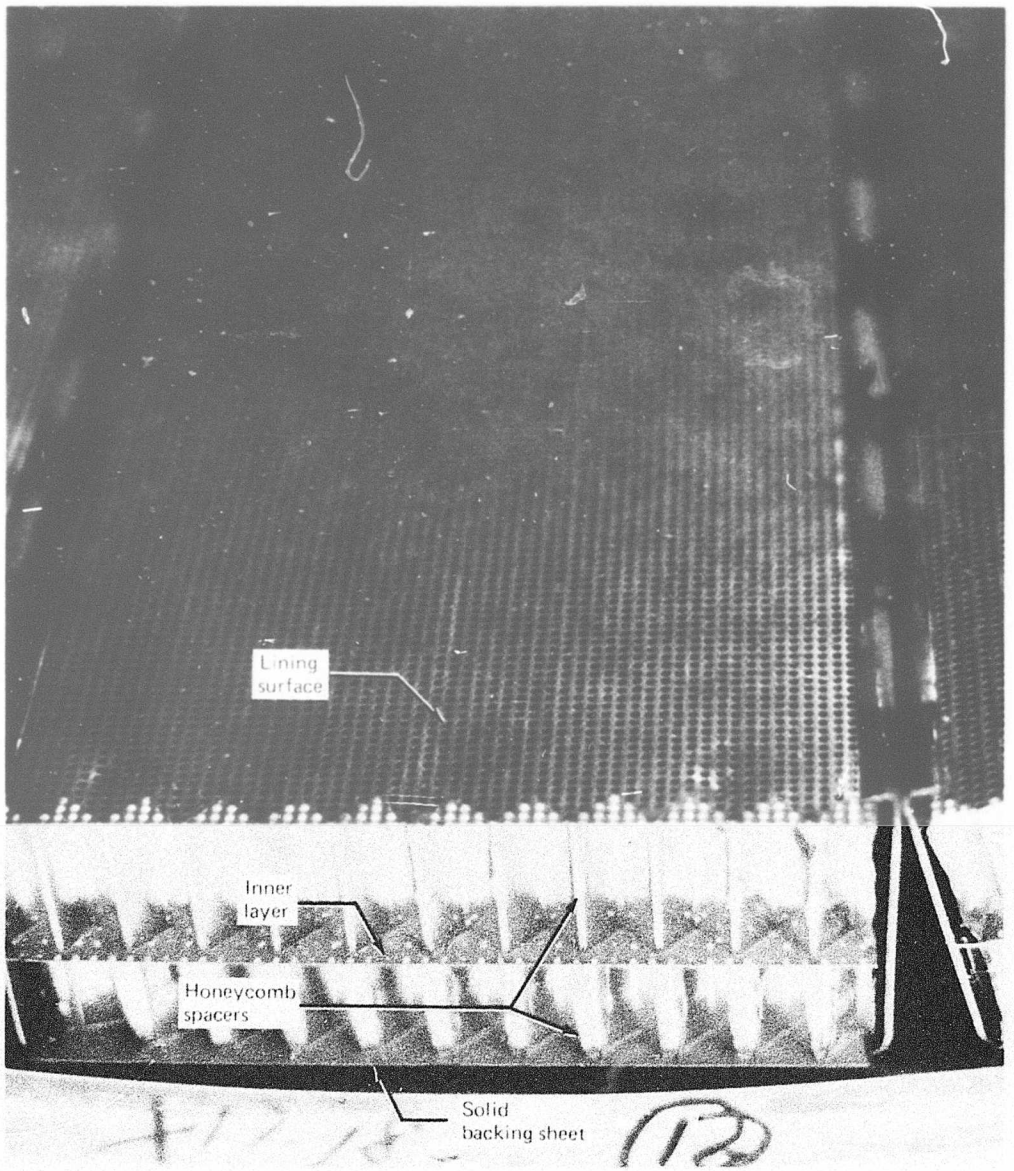

Figure 84.—Full-Scale, Double-Layer Acoustic Lining

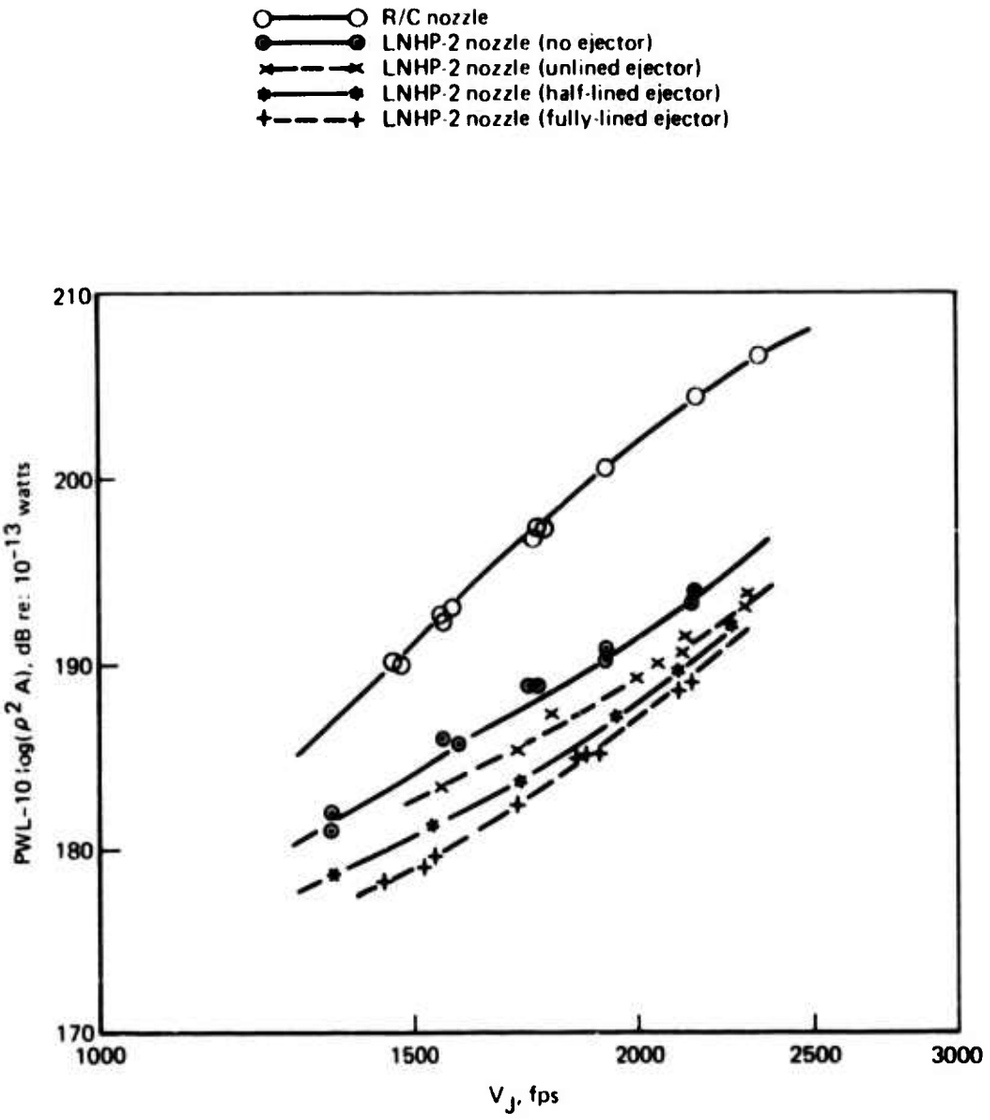

Figure 85.—Normalized PWL for LNHP-2 Suppressor

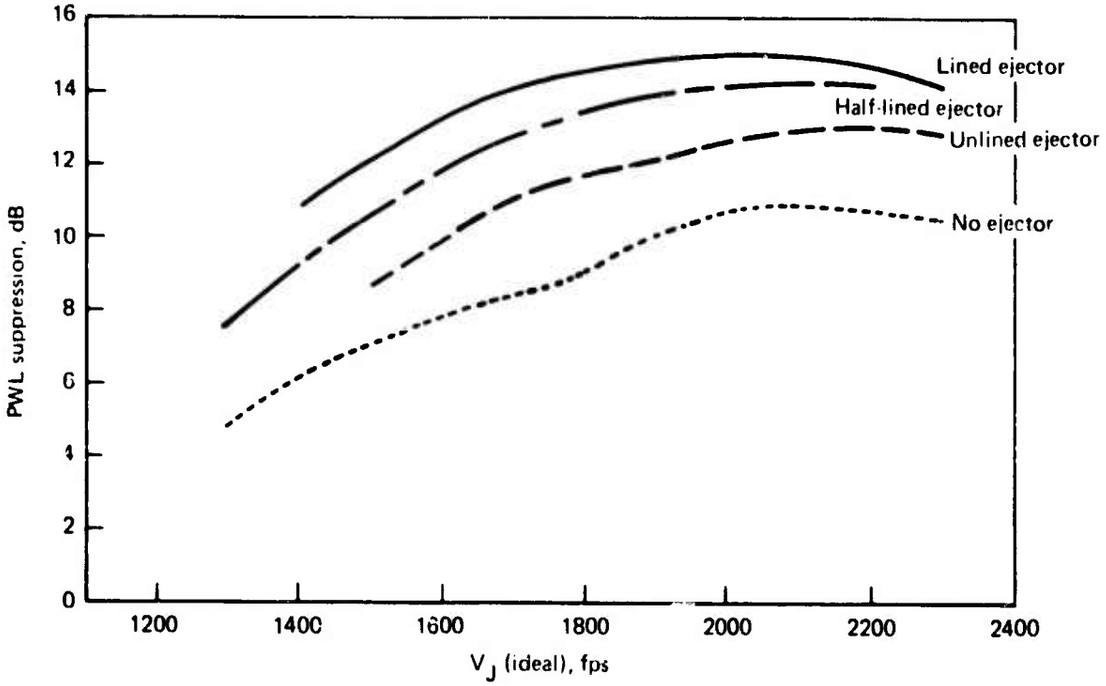

Figure 86.—Full-Scale LNHP-2 Suppressor, Sound Power Suppression

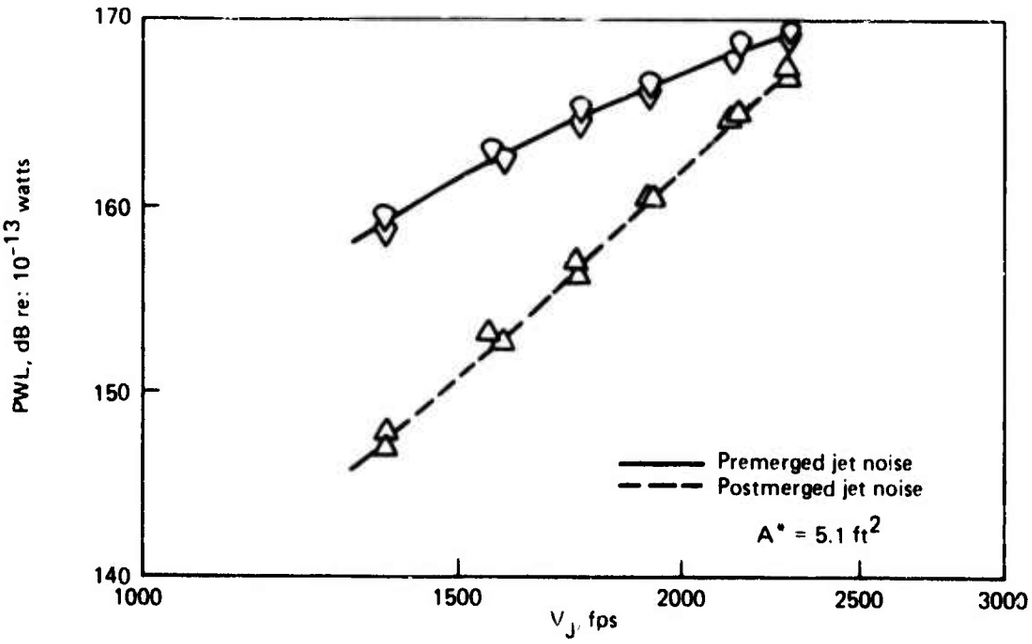

Figure 87.—LNHP-2 Suppressor, Sound Power Levels Without Ejector

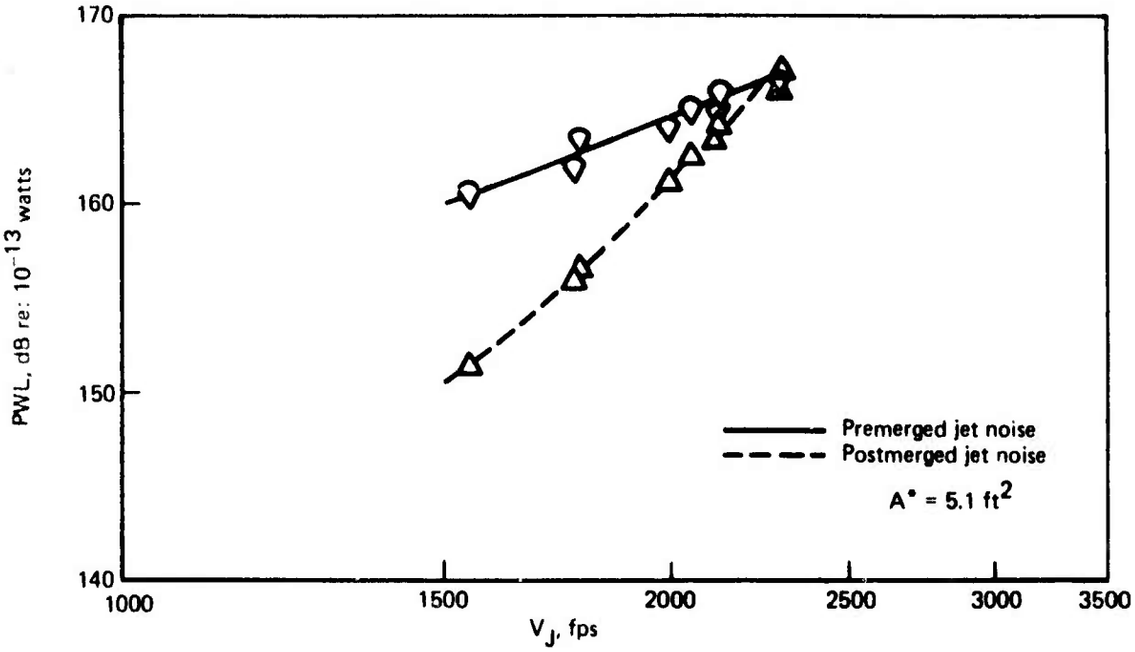

Figure 88.—LNHP-2 Suppressor Sound Power Levels With Hardwall Ejector

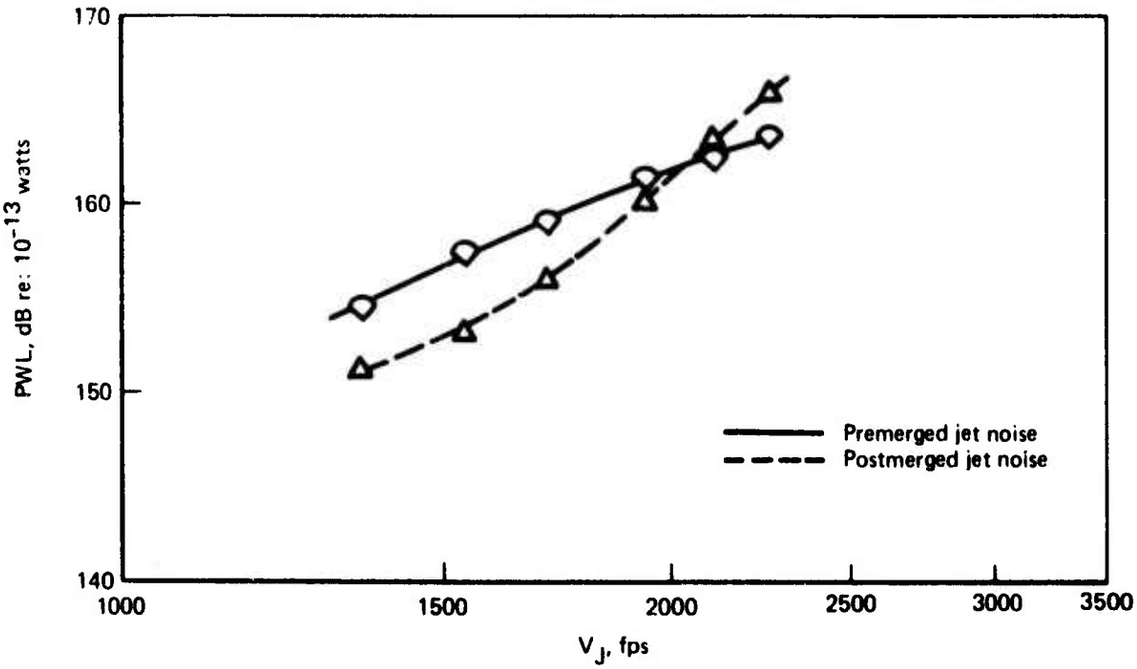

Figure 89.—LNHP-2 Suppressor, Sound Power Levels With 50% Lined Ejector

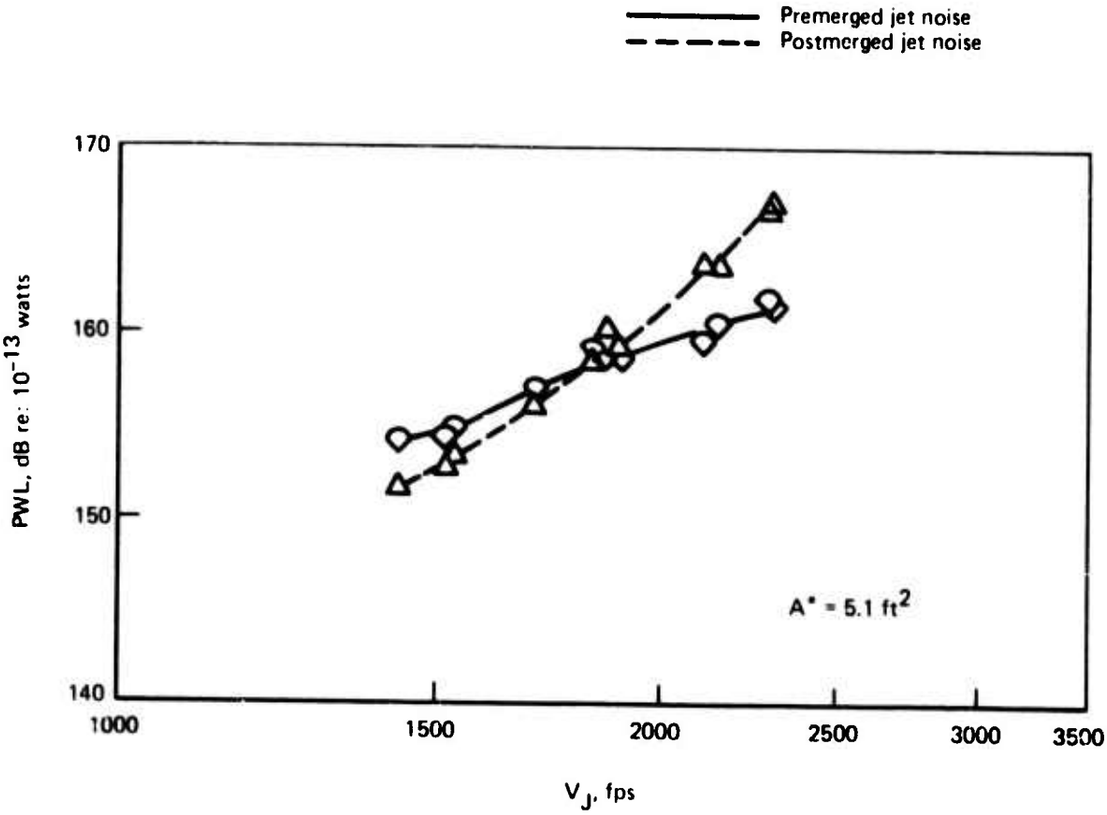

Figure 90.—LNHP-2 Suppressor Sound Power Levels With Fully-Lined Ejector

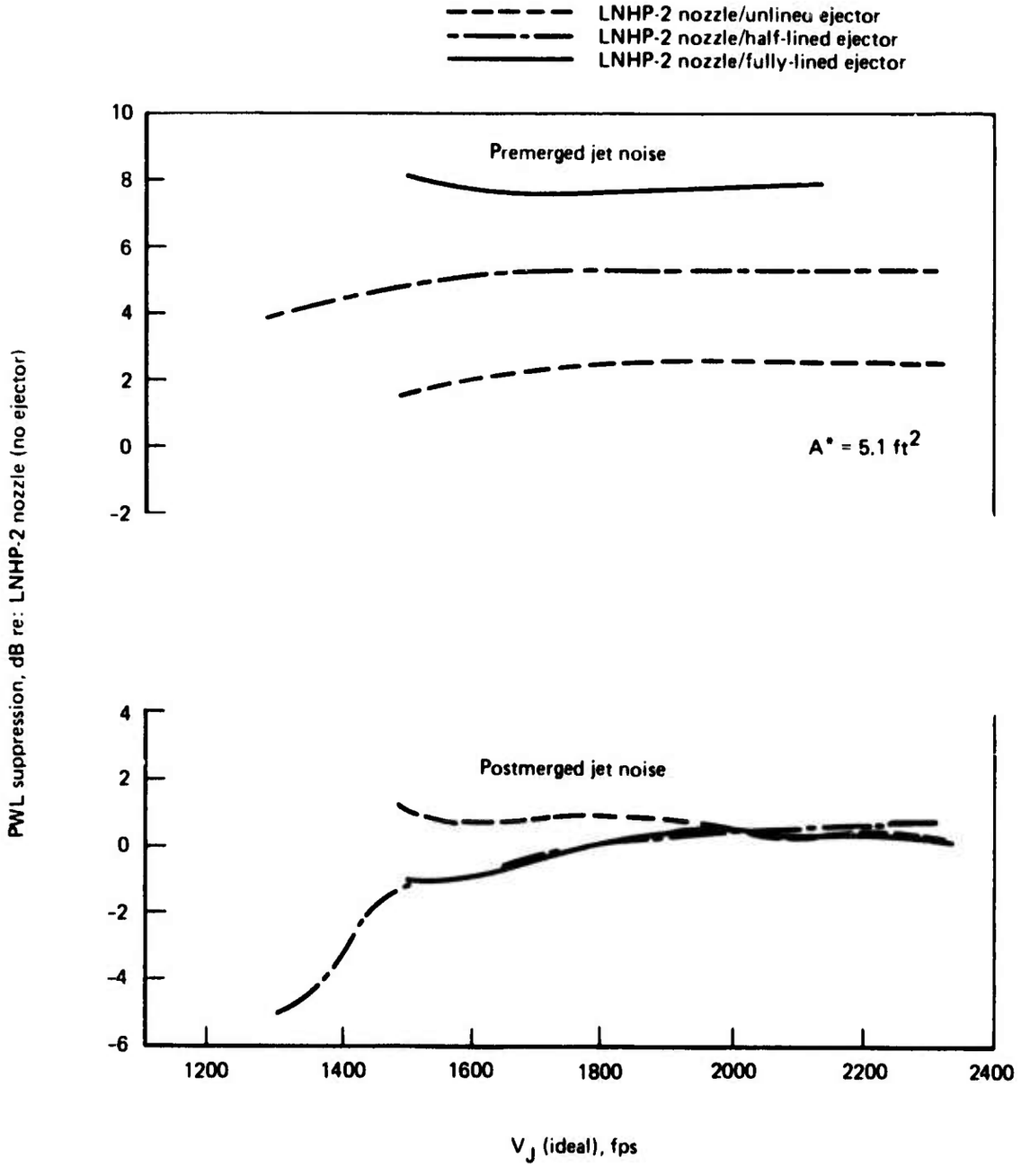

Figure 91.—Ejector Suppression of Premerged and Postmerged Jet Noise Power

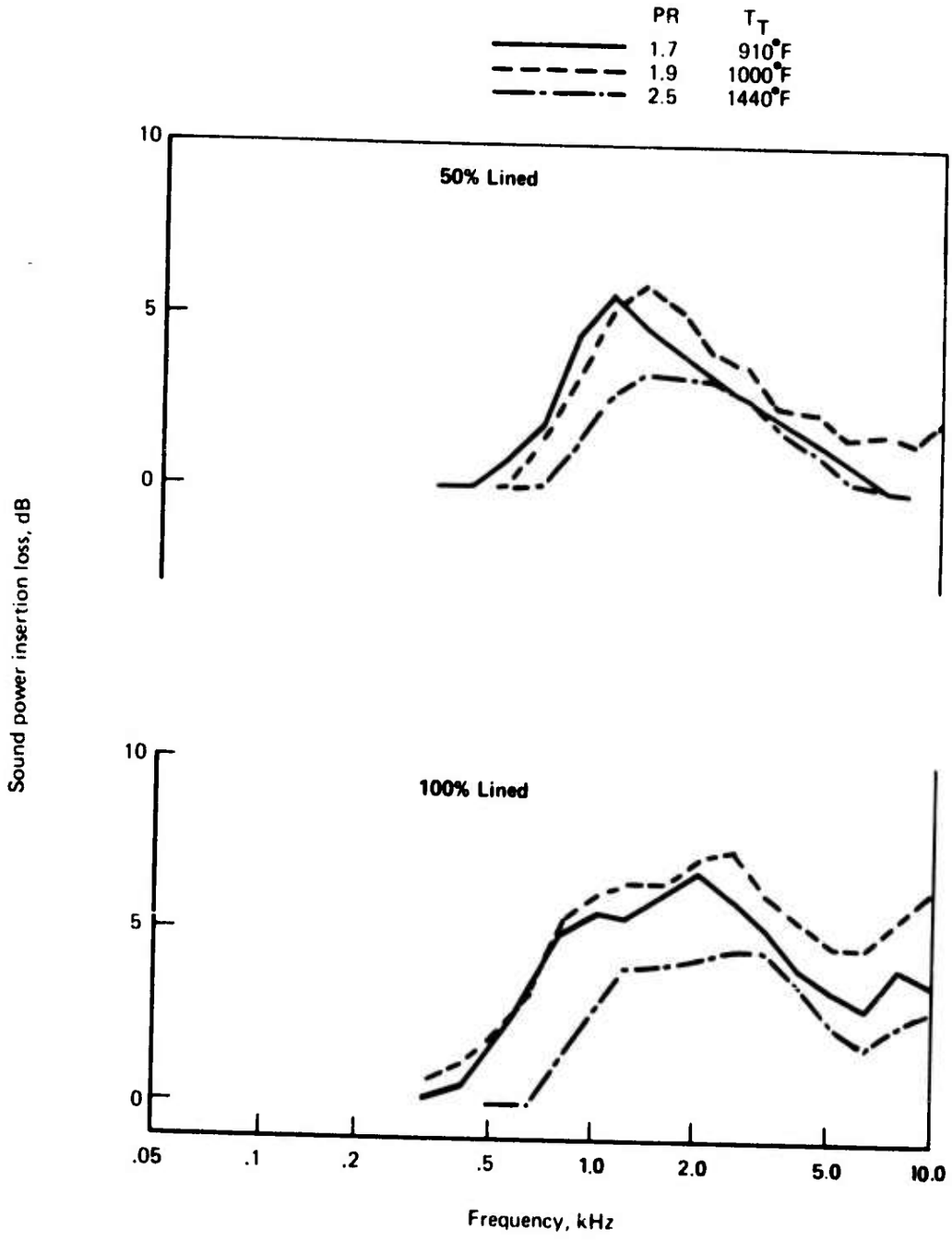

Figure 92.—Full-Scale (J-58) Lined Ejector Results

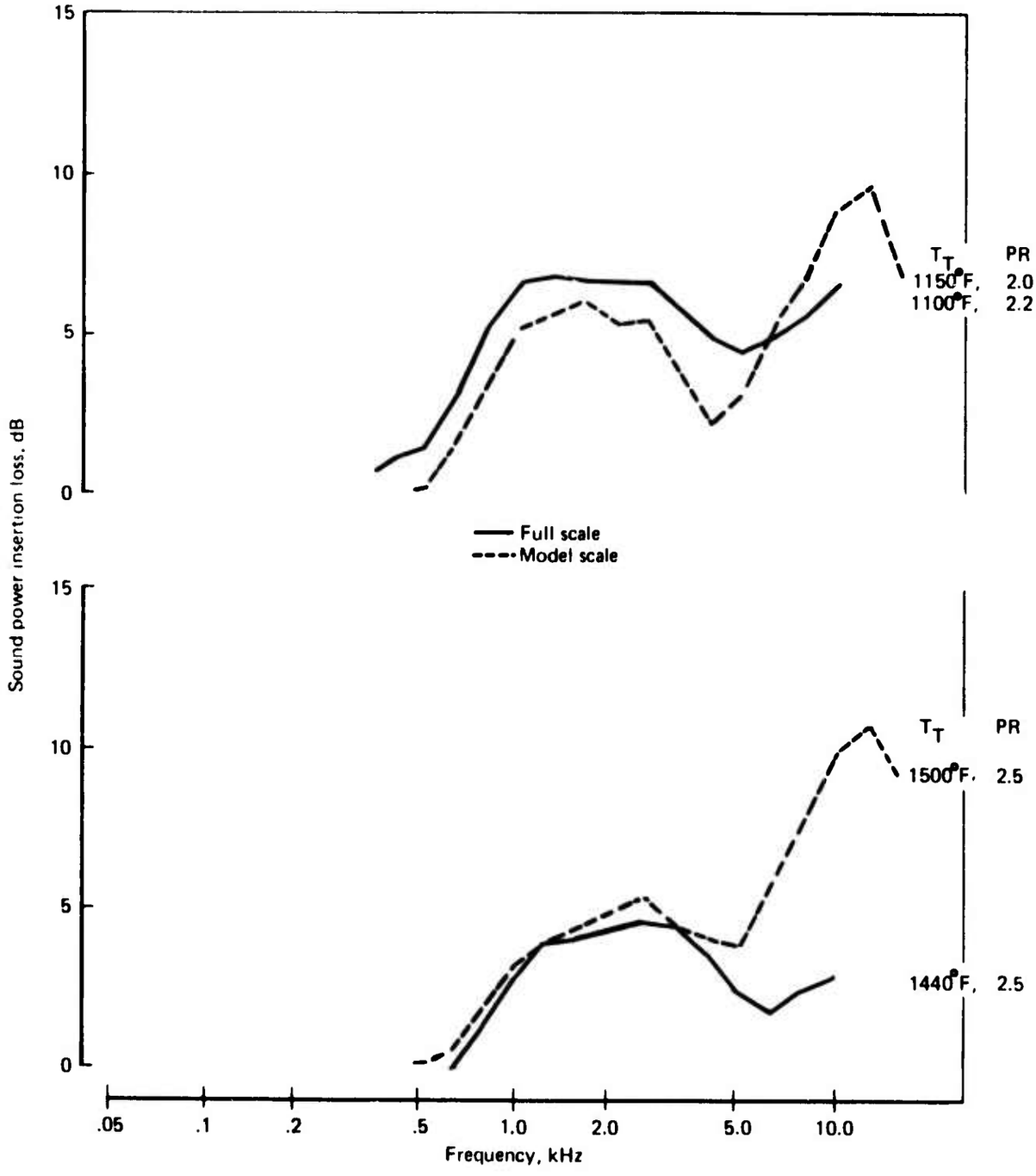

Figure 93.—Lined-Ejector Scaling Comparison

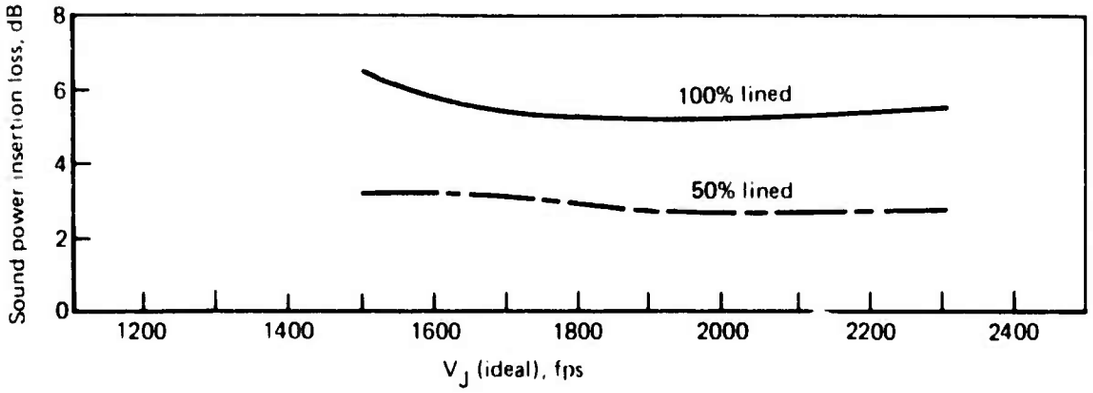

Figure 94.–Full-Scale Lined Ejector Premerged Jet Noise Power Insertion Loss

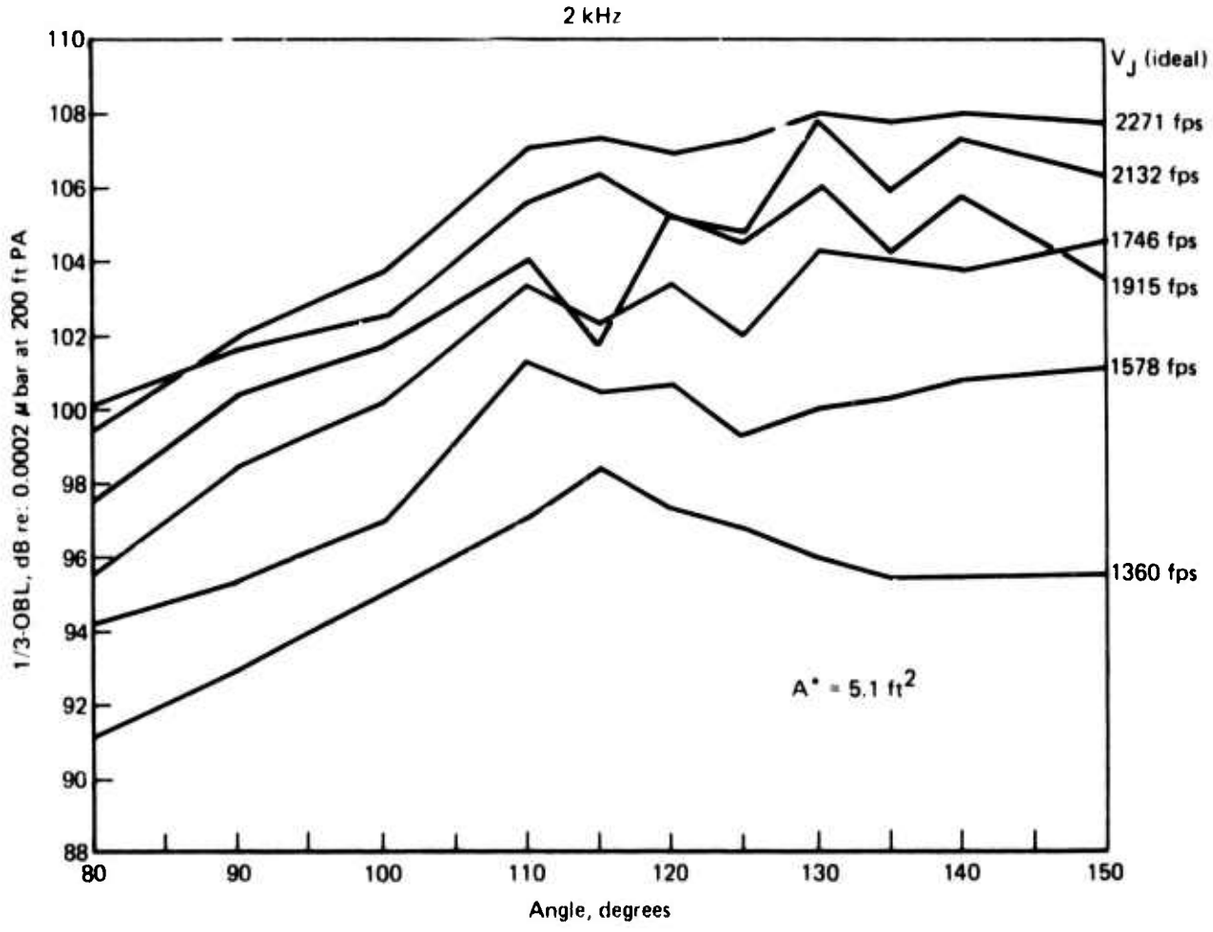

Figure 95.–LNHP-2 Suppressor Peak Premerged Jet Noise Beam Patterns, No Ejector

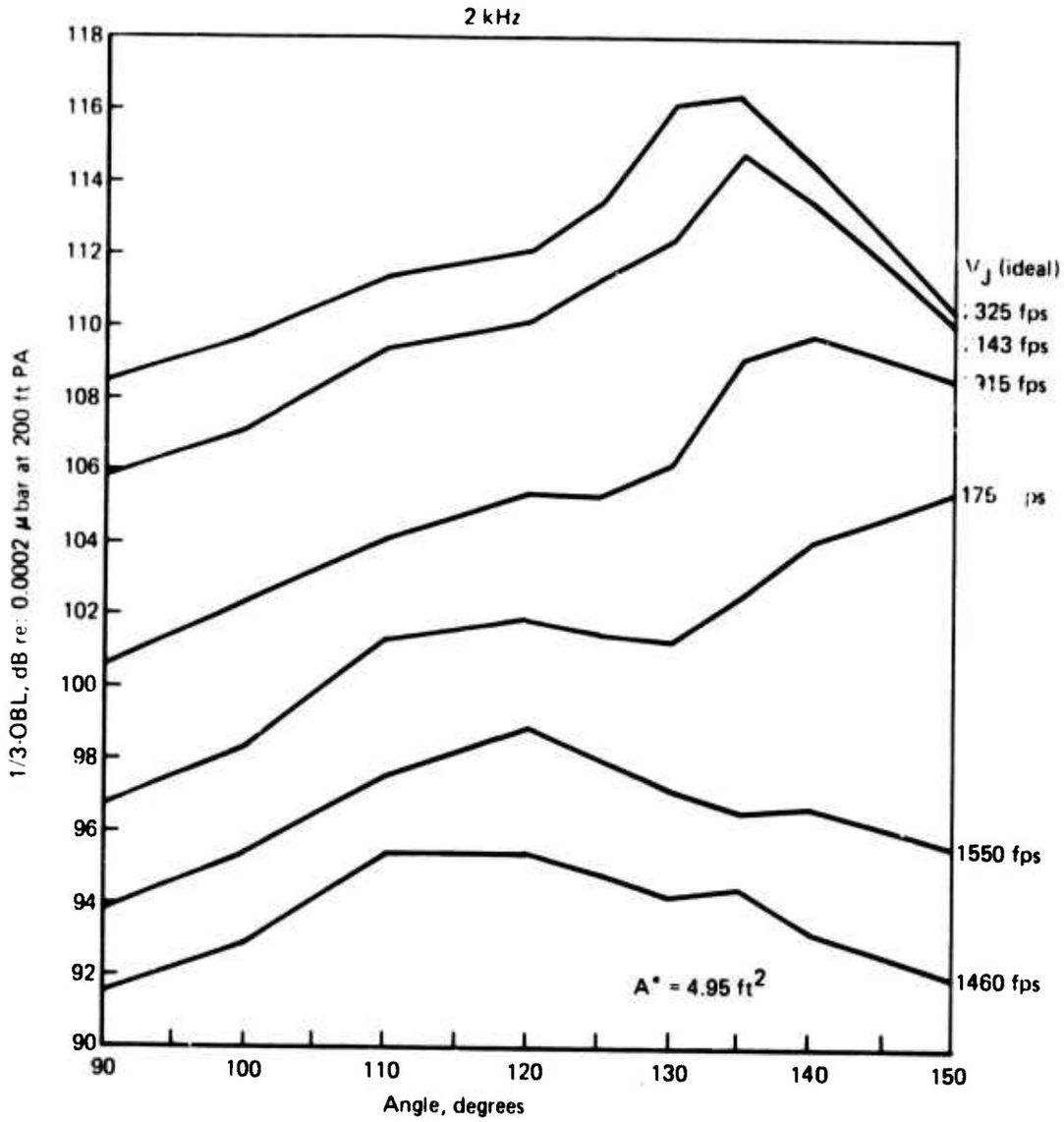

Figure 96.—Round/Convergent Nozzle Jet Noise Beam Patterns

2 kHz

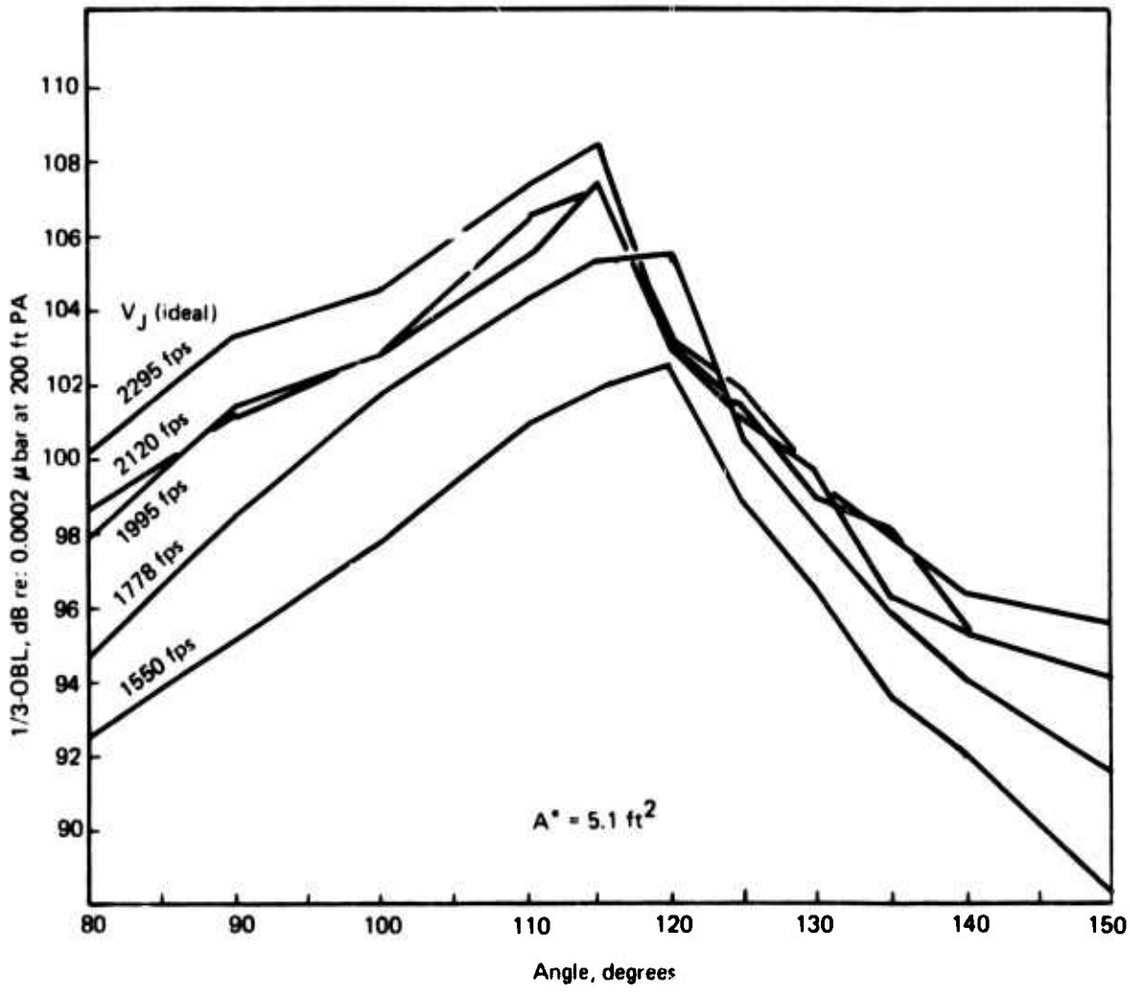

Figure 97.—LNHP-2 Suppressor Peak Premerged Jet Noise Beam Patterns, Unlined Ejector

2 kHz

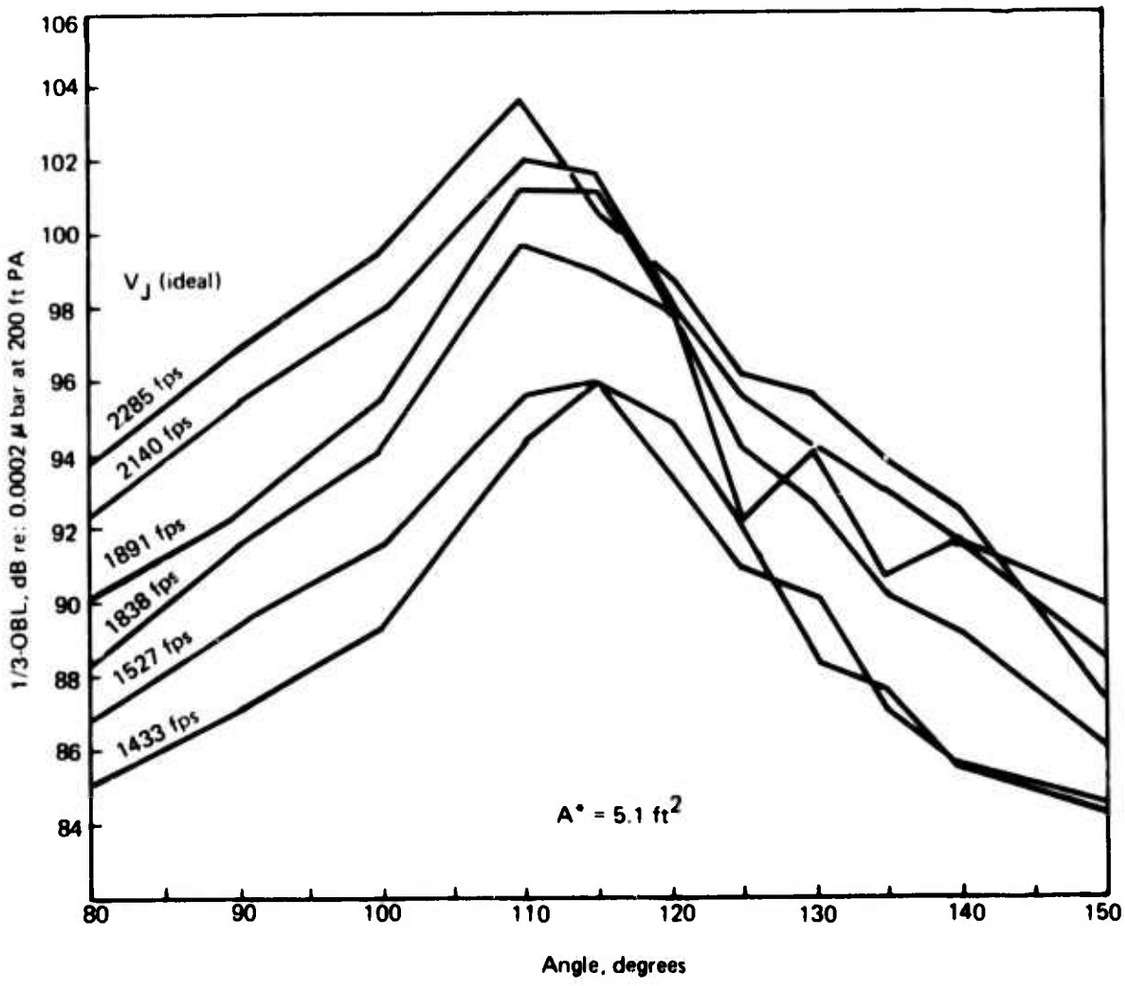

Figure 98.—LNHP-2 Suppressor Peak Premerged Jet Noise Beam Patterns, Fully-Lined Ejector

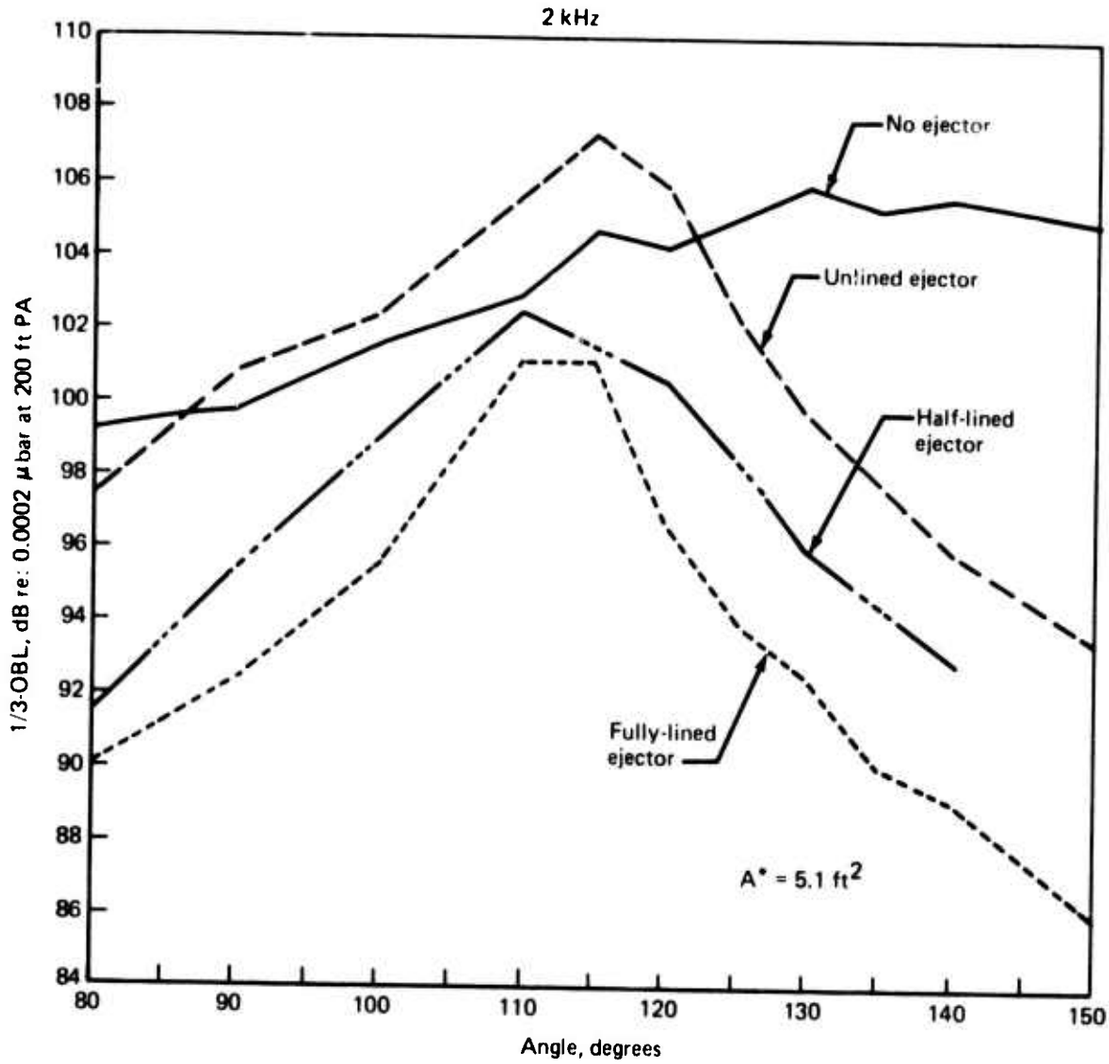

Figure 99.—LNHP-2 Peak Premerged Jet Noise Beam Patterns, at V_J = 1910 fps

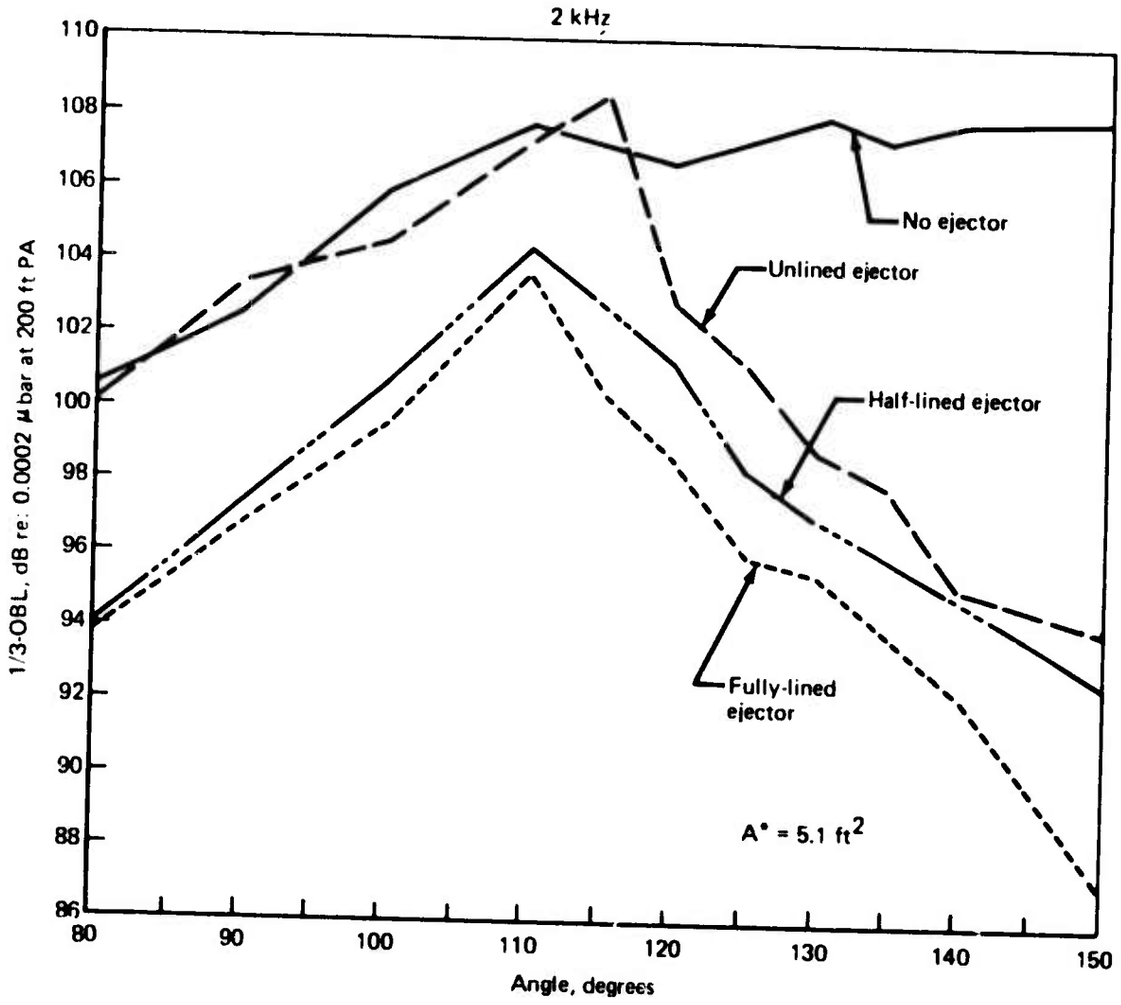

Figure 100.—LNHP-2 Suppressor Peak Premerged Jet Noise Beam Patterns, at V_J = 2250 fps

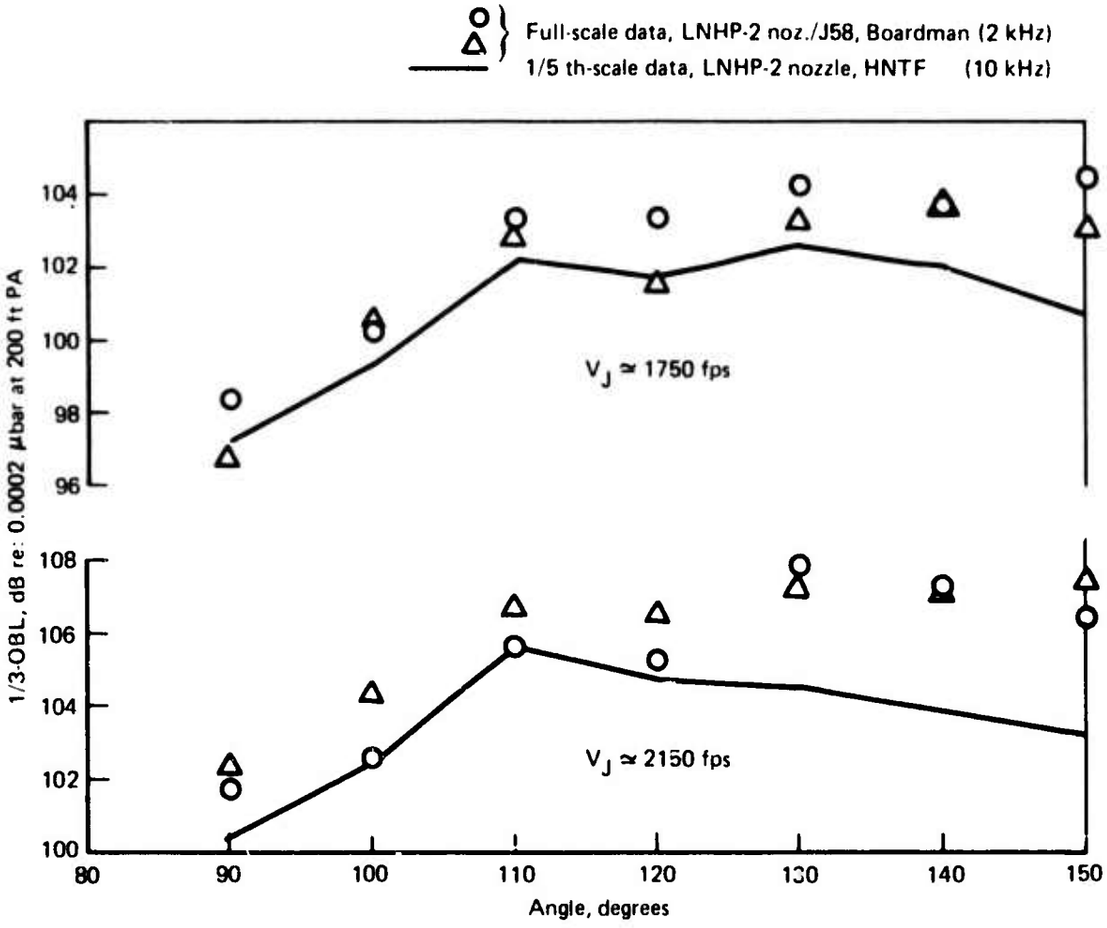

Figure 101.—LNHP-2 Nozzle Peak Premerged Jet Noise Beam Patterns, 1/5 th-Scale Data Versus Full-Scale

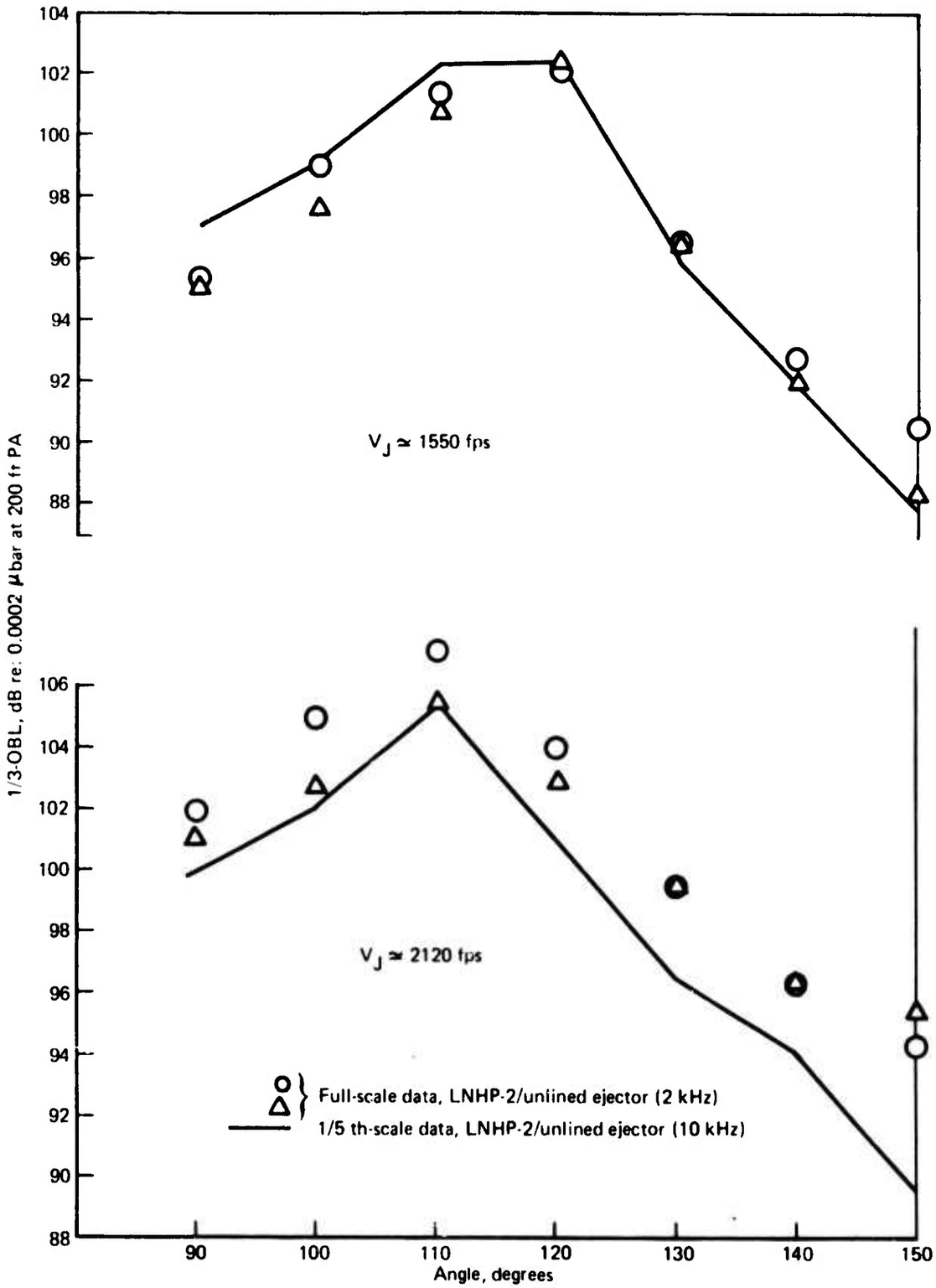

Figure 102.—LNHP-2/Unlined Ejector Peak Premerged Jet Noise Beam Patterns 1/5 th-Scale Data Versus Full-Scale

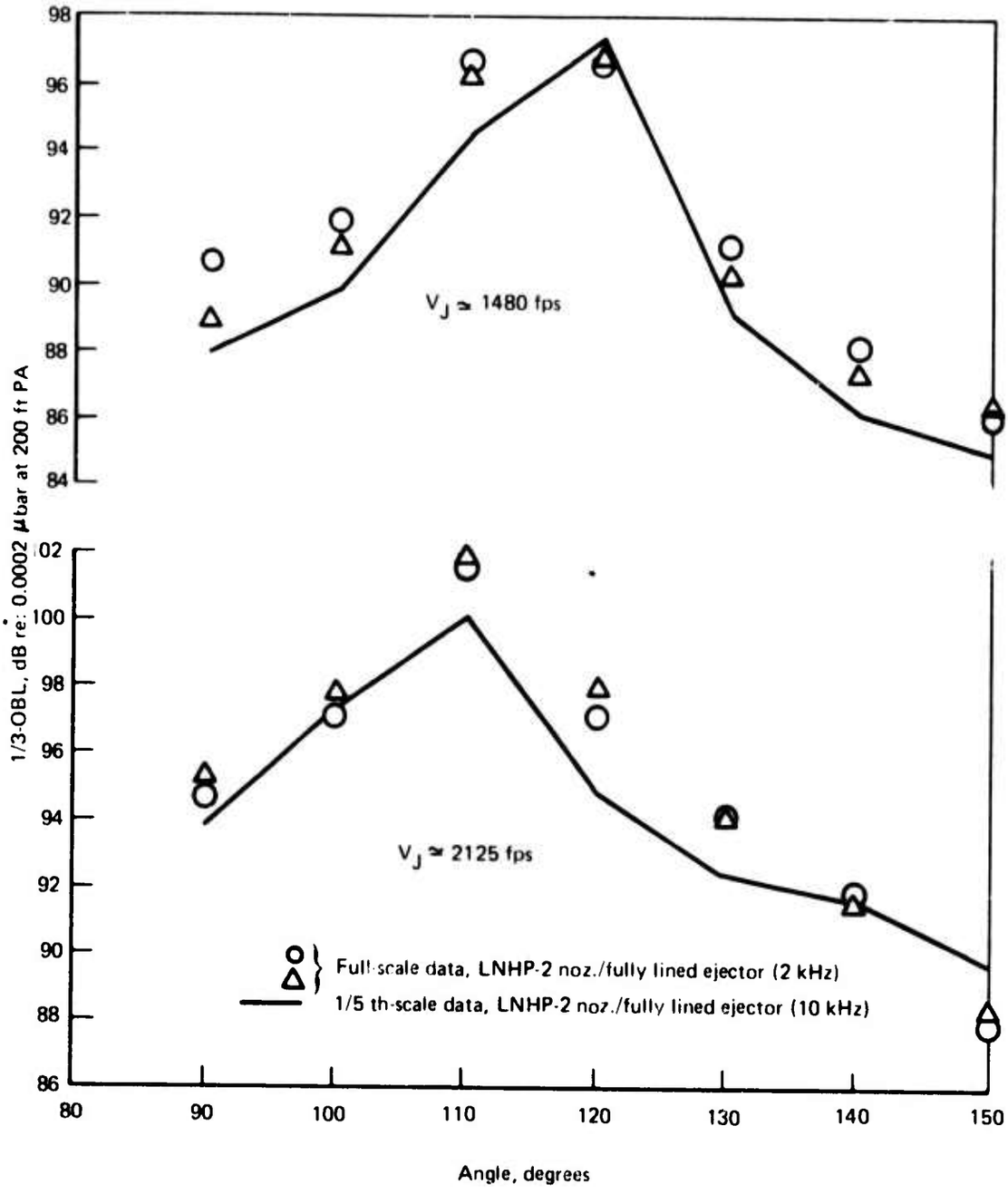

Figure 103.—LNHP-2/Lined Ejector Peak Premerged Jet Noise Beam Patterns 1/5 th-Scale Data Versus Full-Scale

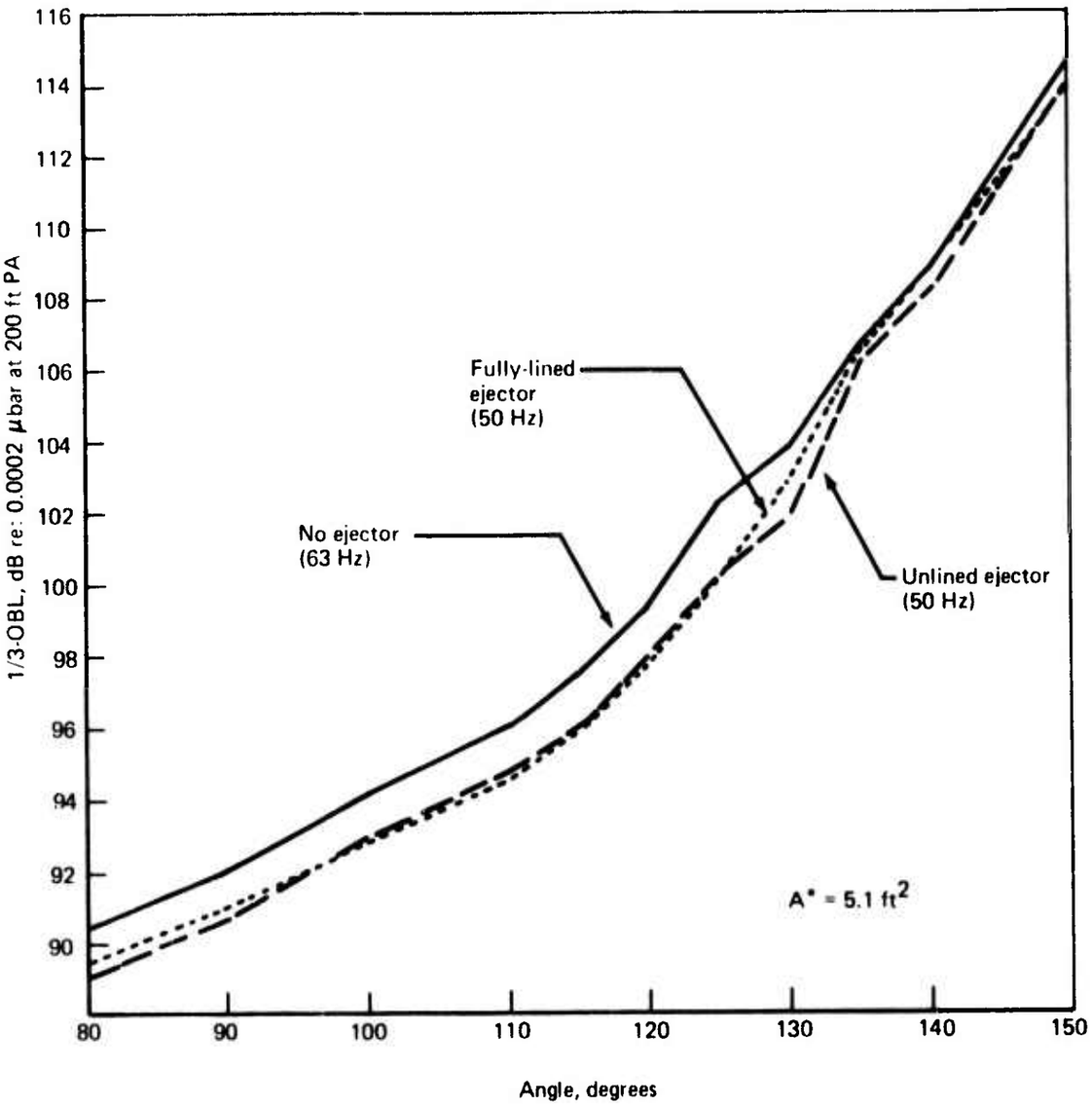

Figure 104.—LNHP-2 Suppressor Peak Postmerged Jet Noise Beam Patterns, at $V_J \simeq 2250$ fps

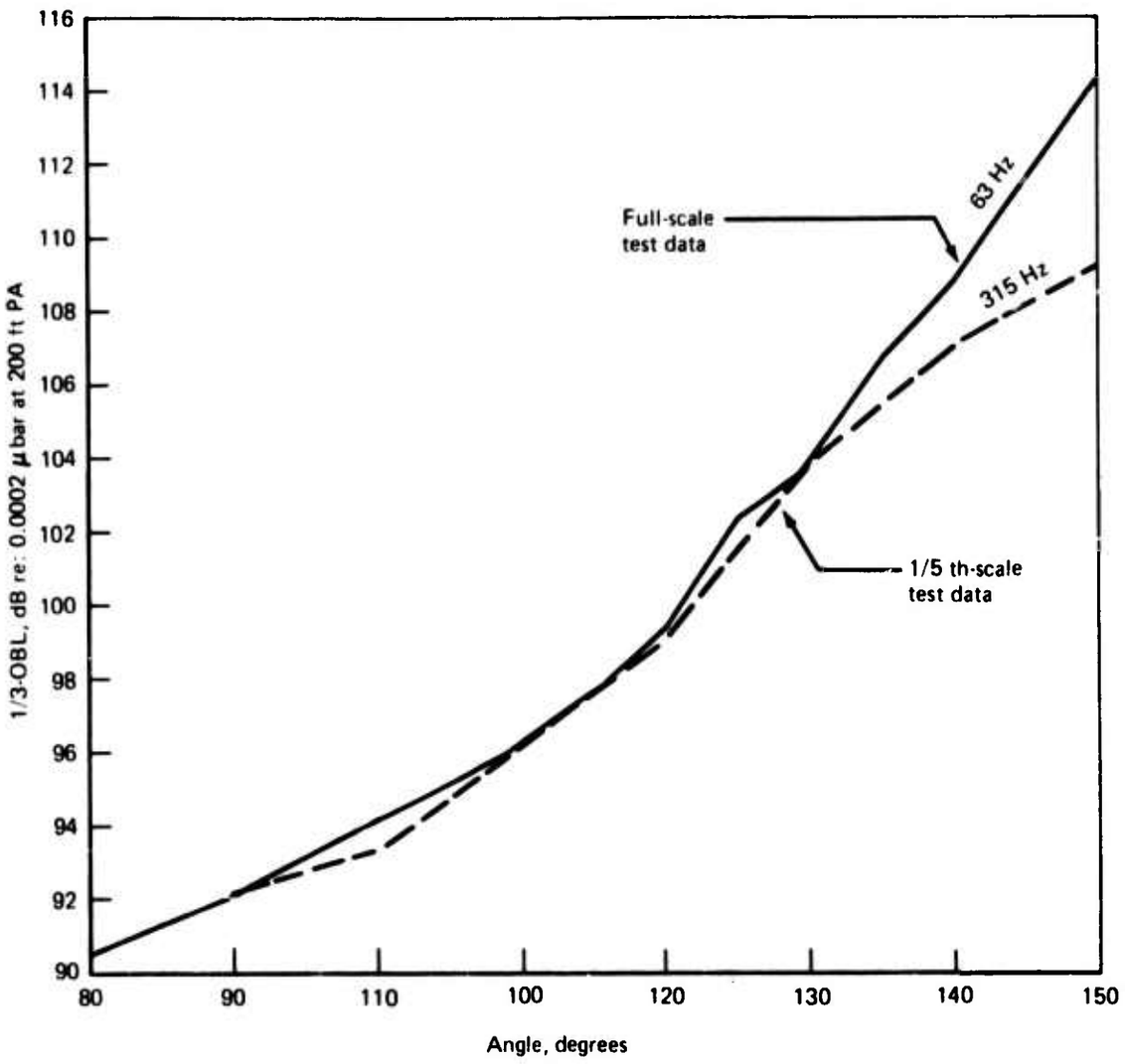

Figure 105.–LNHP-2 Nozzle Peak Postmerged Jet Noise Beam Patterns, 1/5 th-Scale Versus Full-Scale at $V_j \approx 2250$ fps

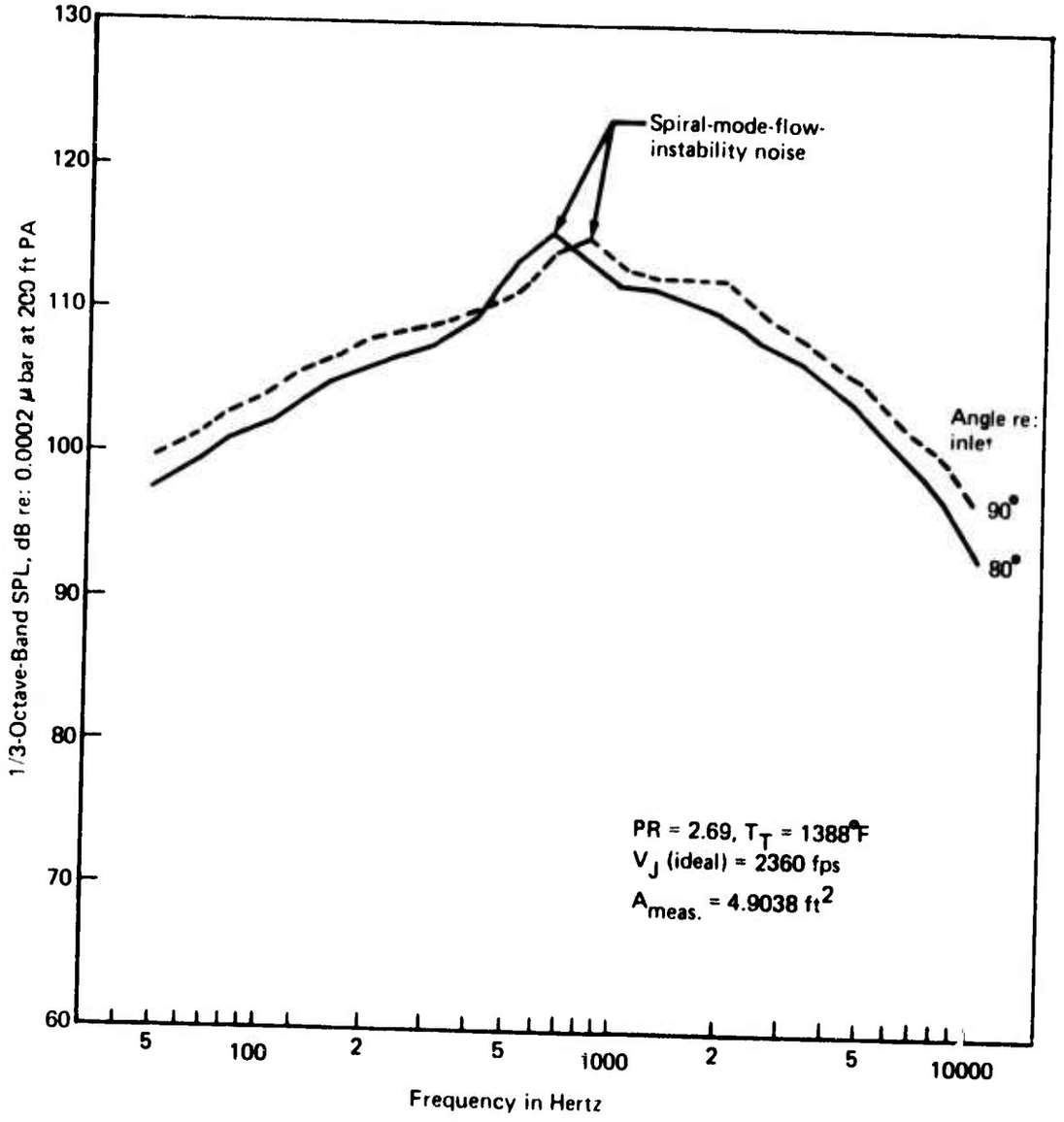

Figure 106.—J-58 Engine-R/C Nozzle Jet Noise Spectra

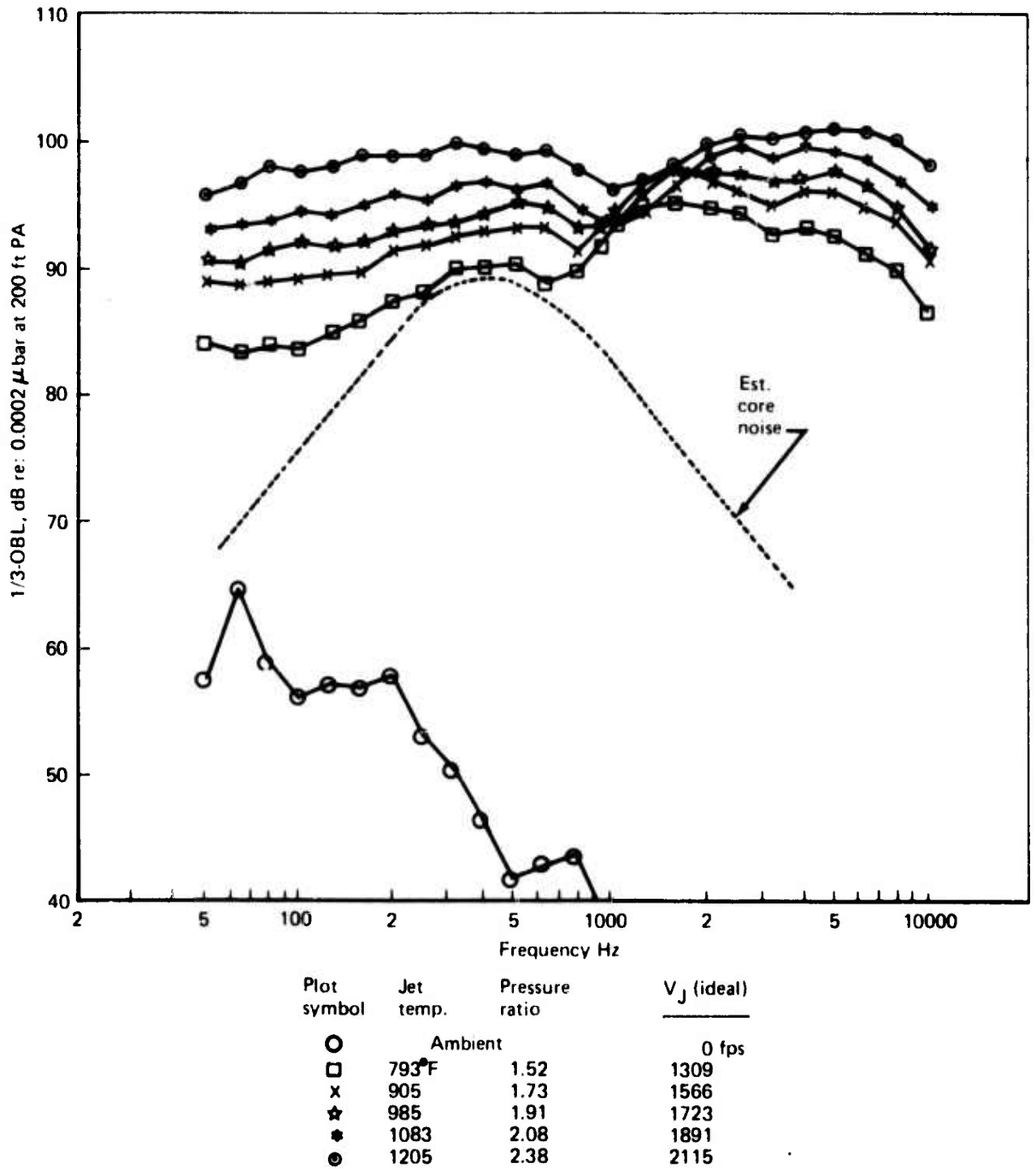

Figure 107.—LNHP-2 Nozzle/Lined Ejector (J-58 Engine) Noise Spectra at 120°

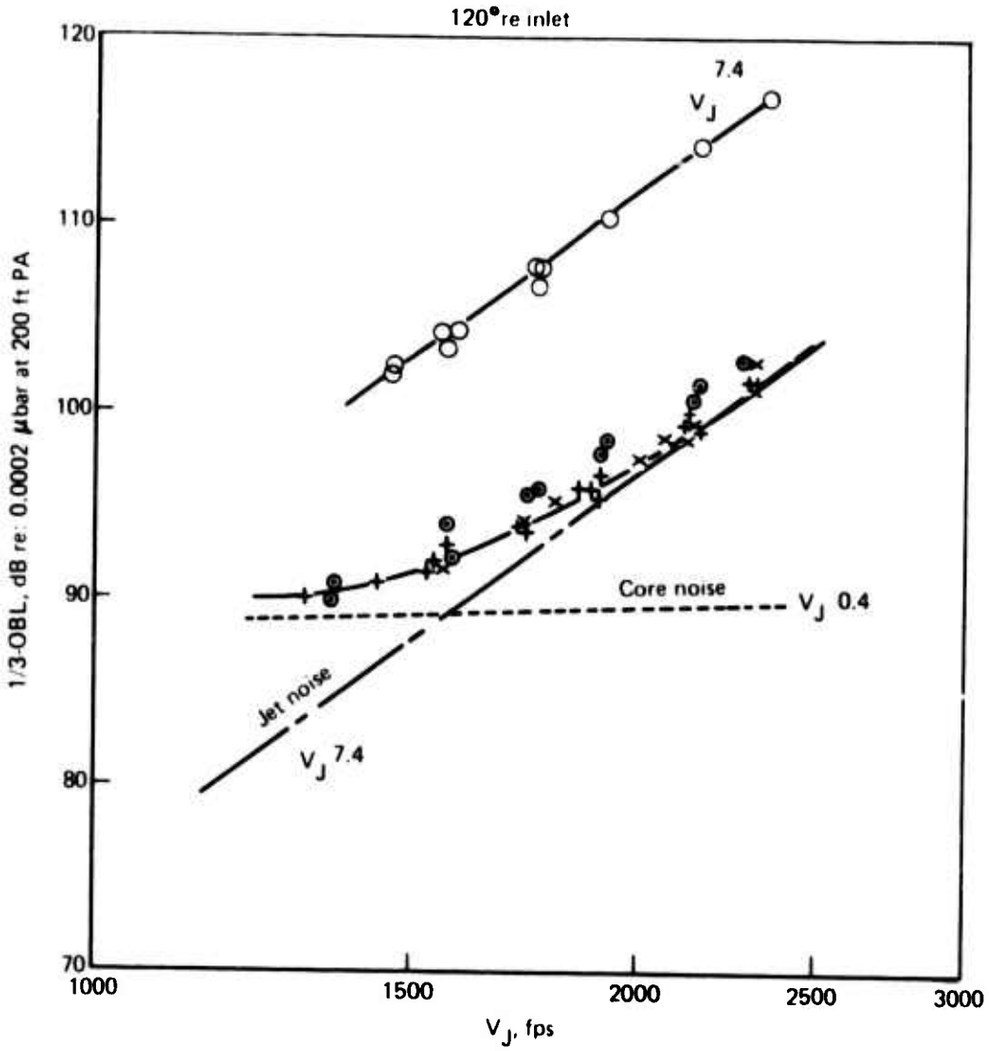

Figure 108.—R/C and LNHP-2 Suppressor/J-58 Engine Radiated Noise at 250 Hz

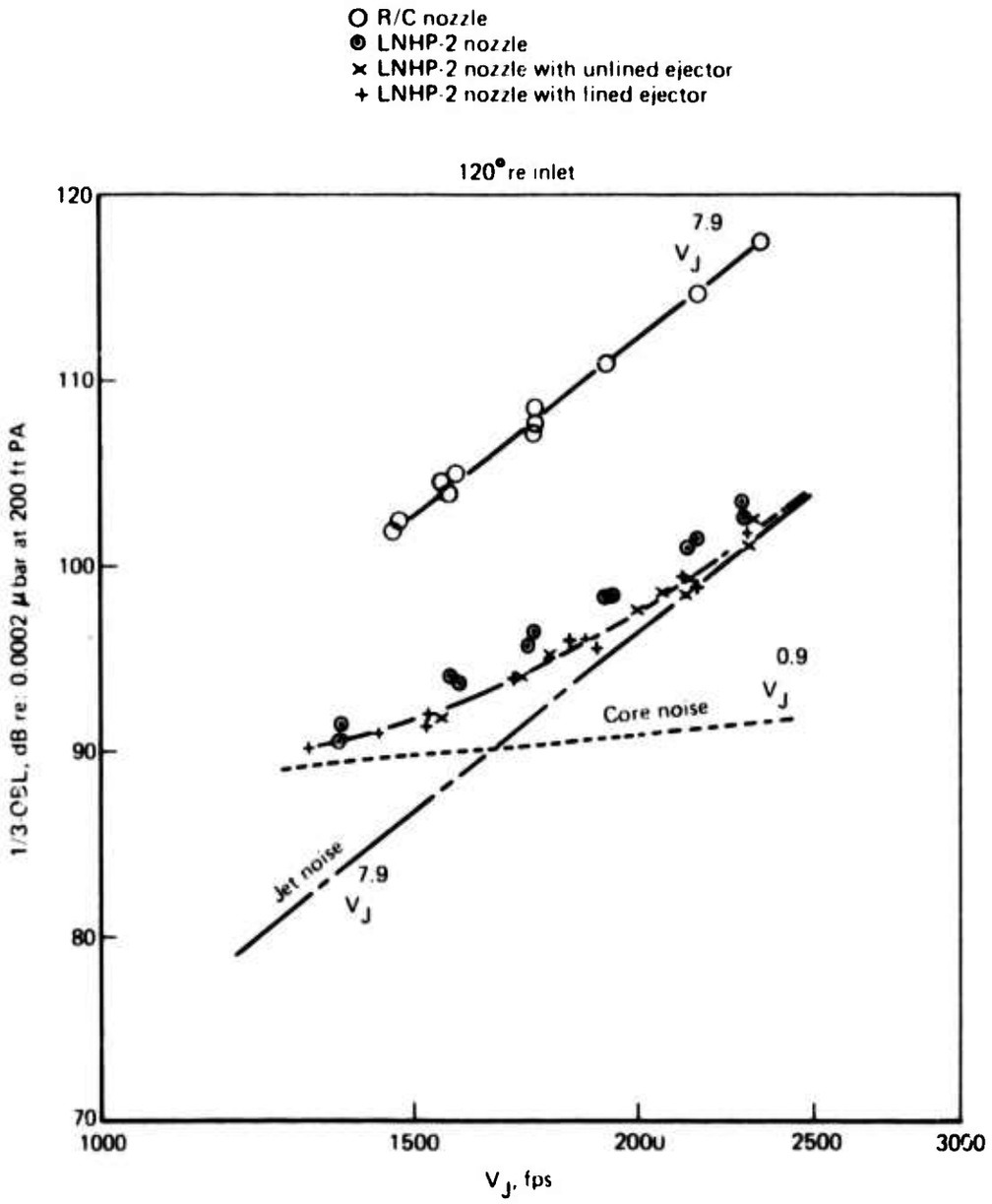

Figure 109.—R/C and LNHP-2 Suppressor/J-58 Engine Radiated Noise 315 Hz

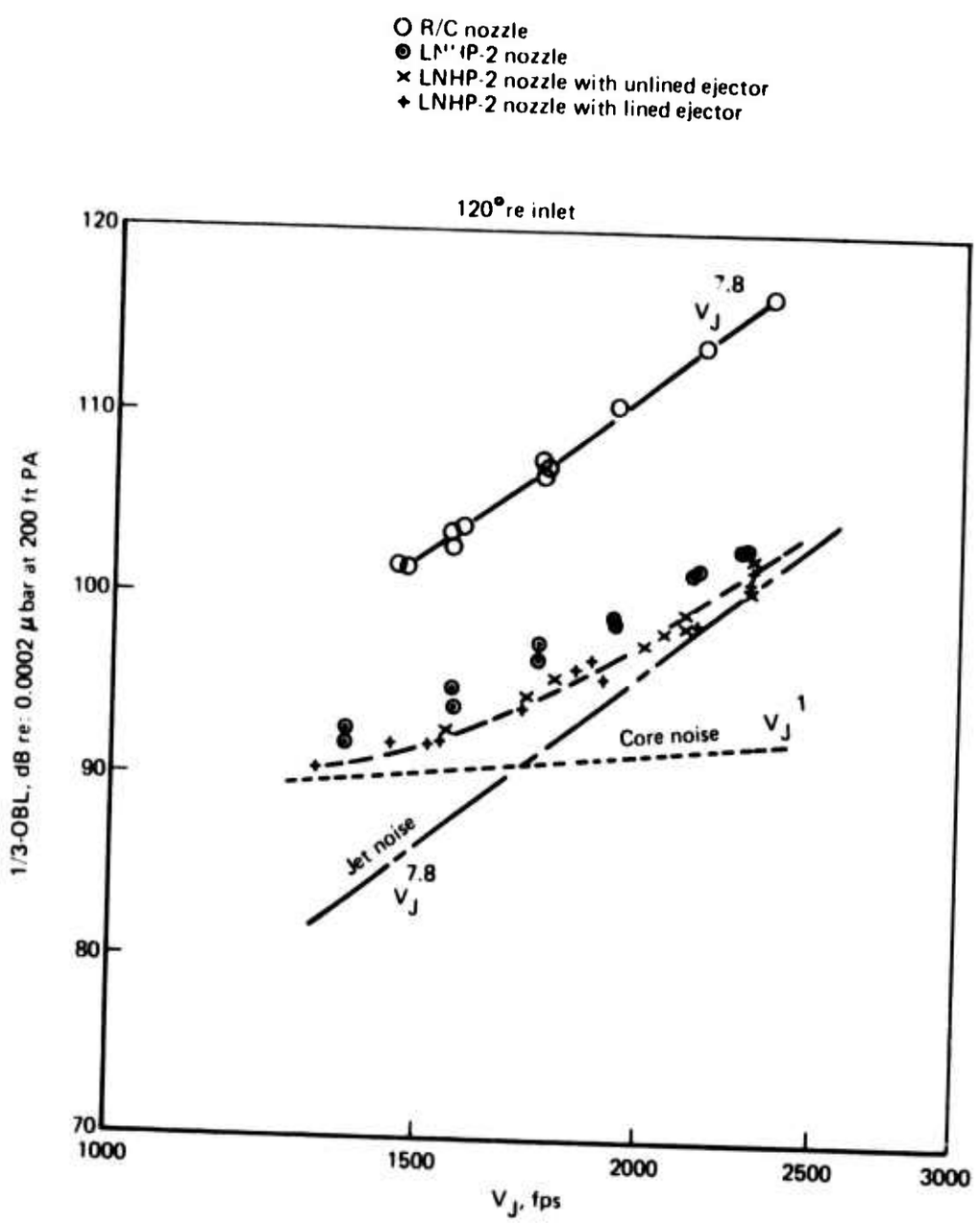

Figure 110.–R/C and LNHP-2 Suppressor/J-58 Engine Radiated Noise at 400 Hz

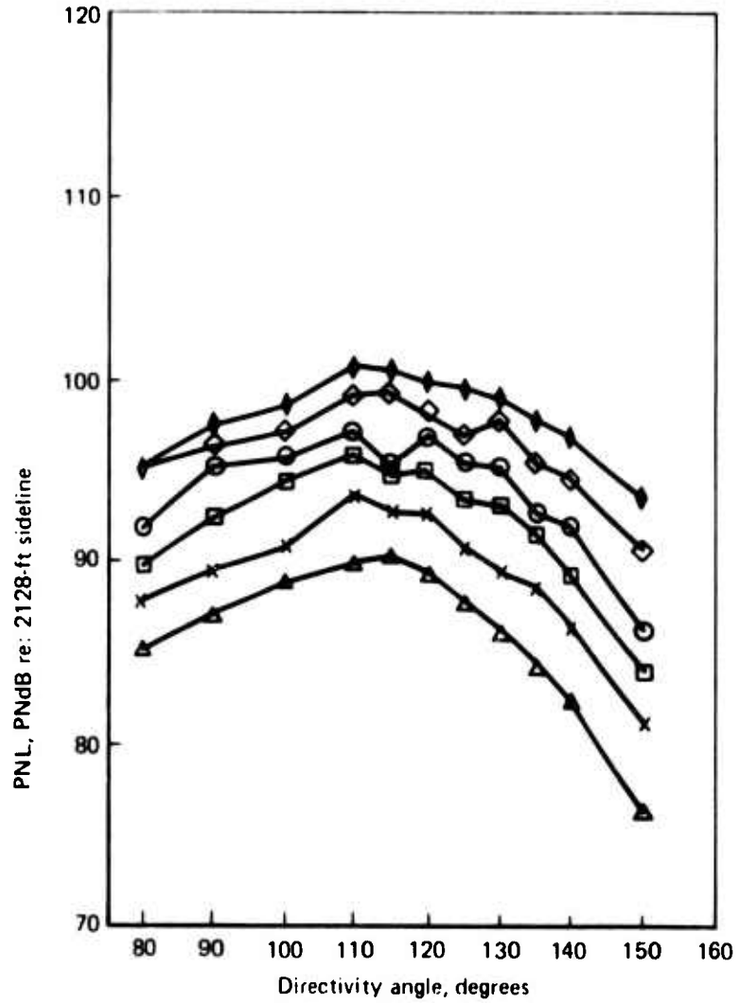

Figure 111.–Full-Scale LNHP-2 Nozzle, Sideline PNL Beam Patterns

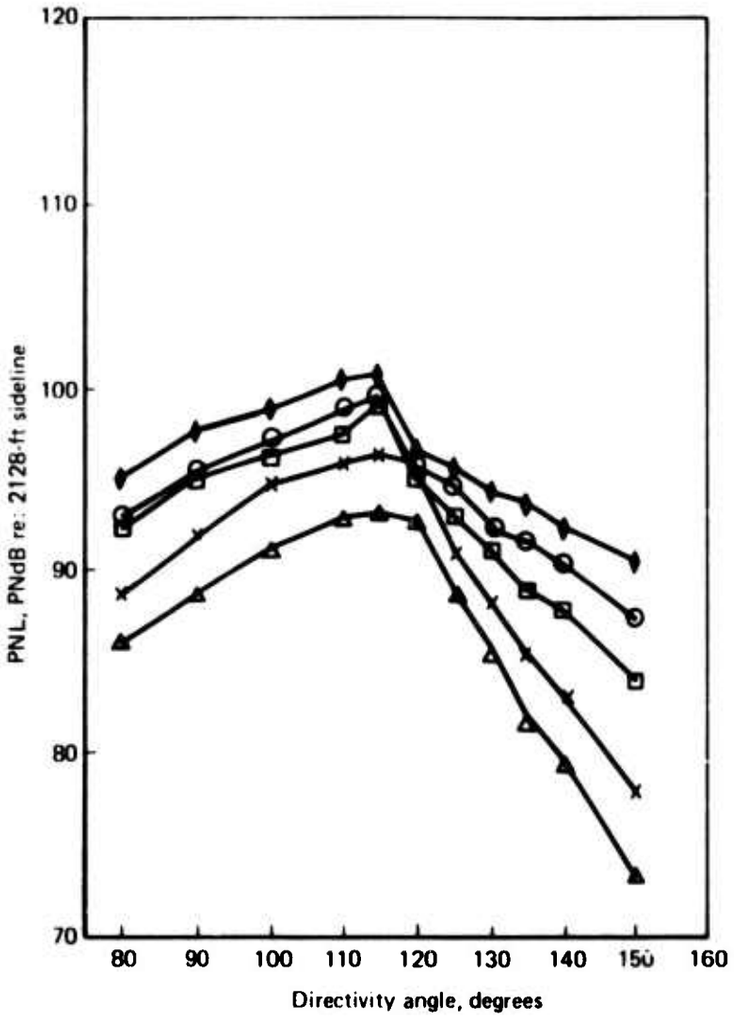

	Pressure ratio	Jet temp	V_J (ideal)
△	1.72	916°F	1550 fps
x	1.95	1039	1778
□	2.22	1150	1995
○	2.36	1238	2120
◊	2.53	1386	2295

Figure 112.—Full-Scale, LNHP-2 Suppressor With Hardwall Ejector Sideline PNL Beam Patterns

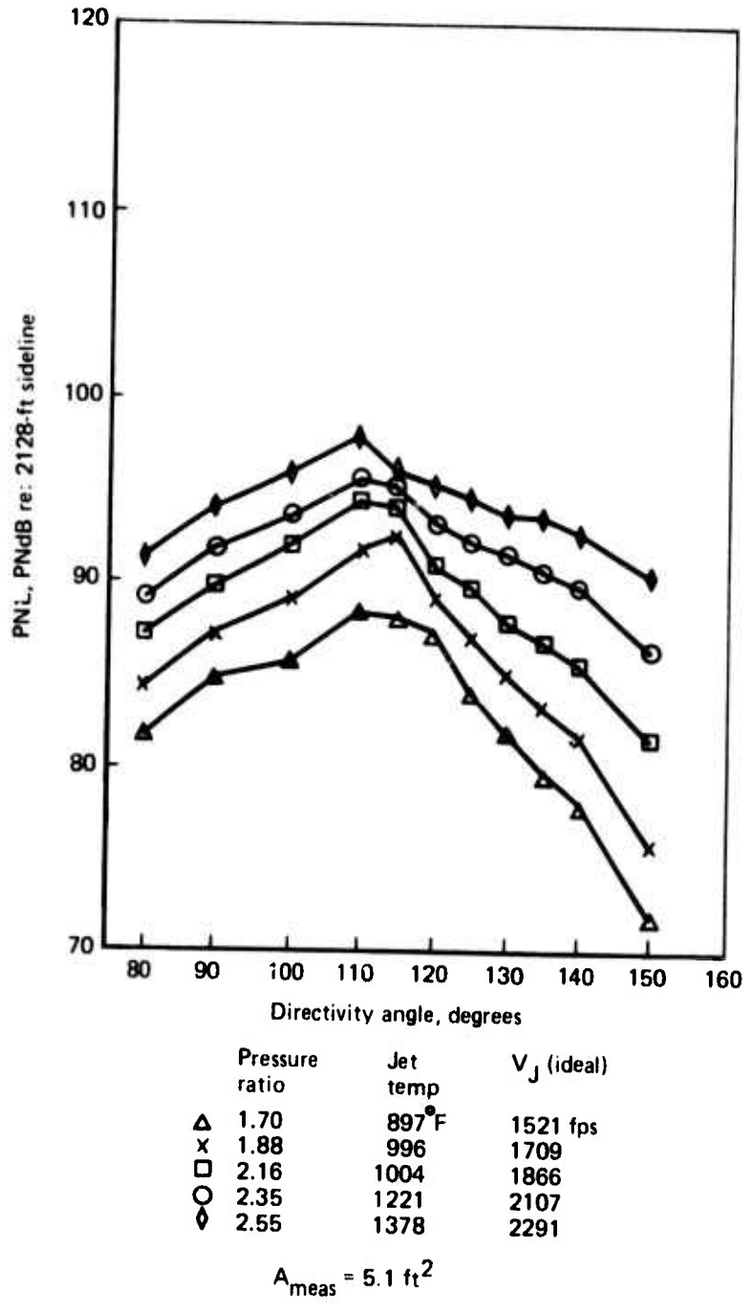

Figure 113.—Full-Scale, LNHP-2 Suppressor With Lined Ejector Sideline PNL Beam Patterns

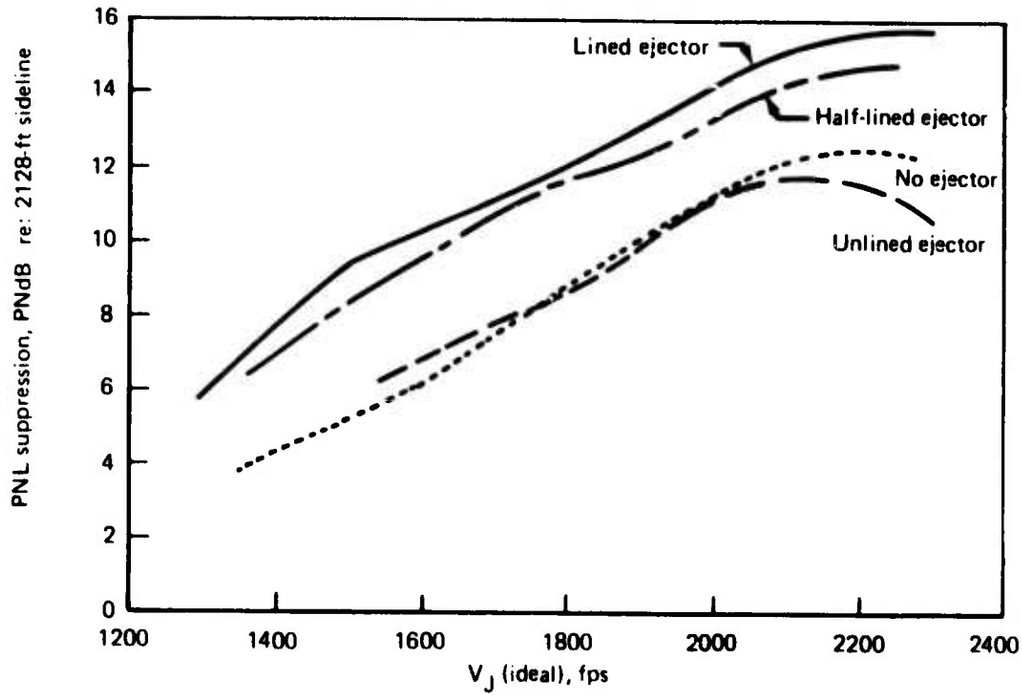

Figure 114.—Full-Scale LNHP-2, 2128-ft SL PNL Suppression

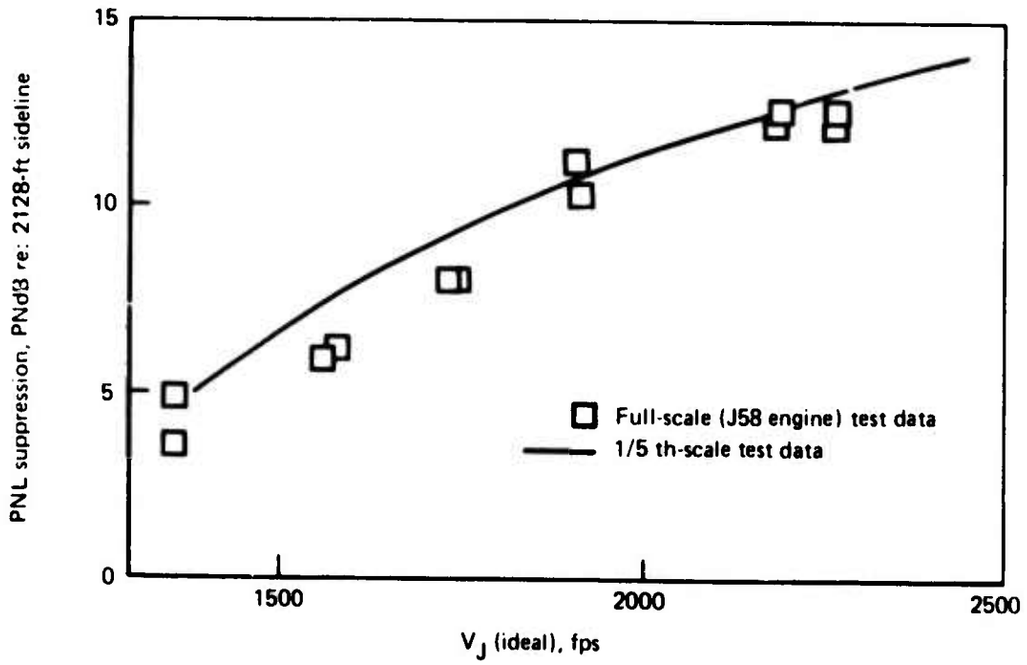

Figure 115.—LNHP-2 Nozzle Without Ejector Suppression Scaling Comparison

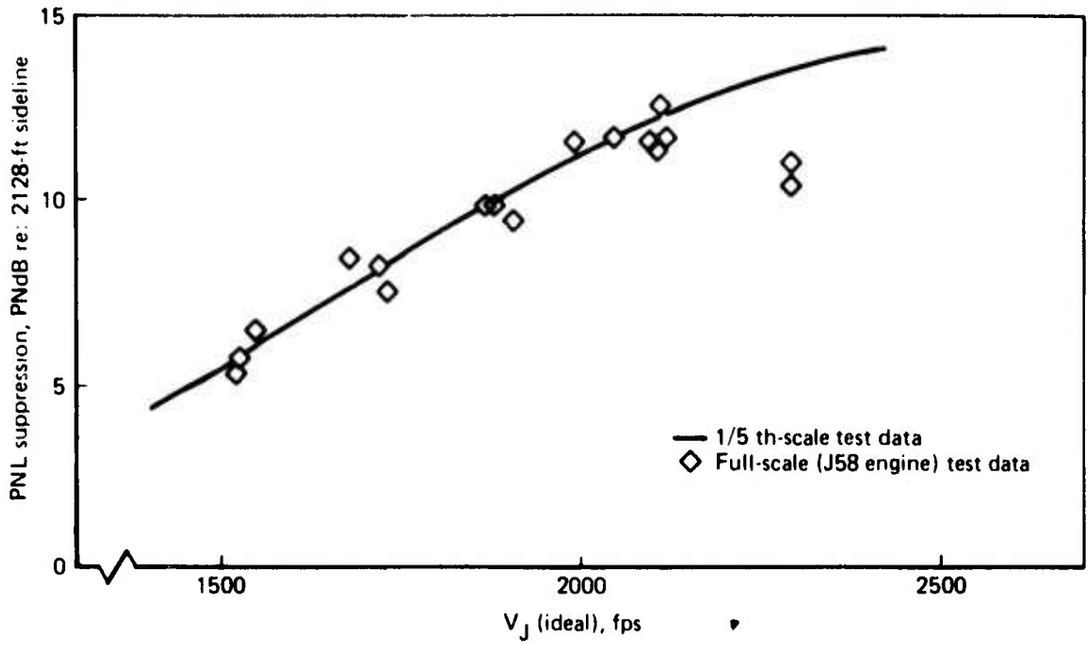

Figure 116.–LNHP-2 Suppressor With Hardwall Ejector Suppression Scaling Comparisons

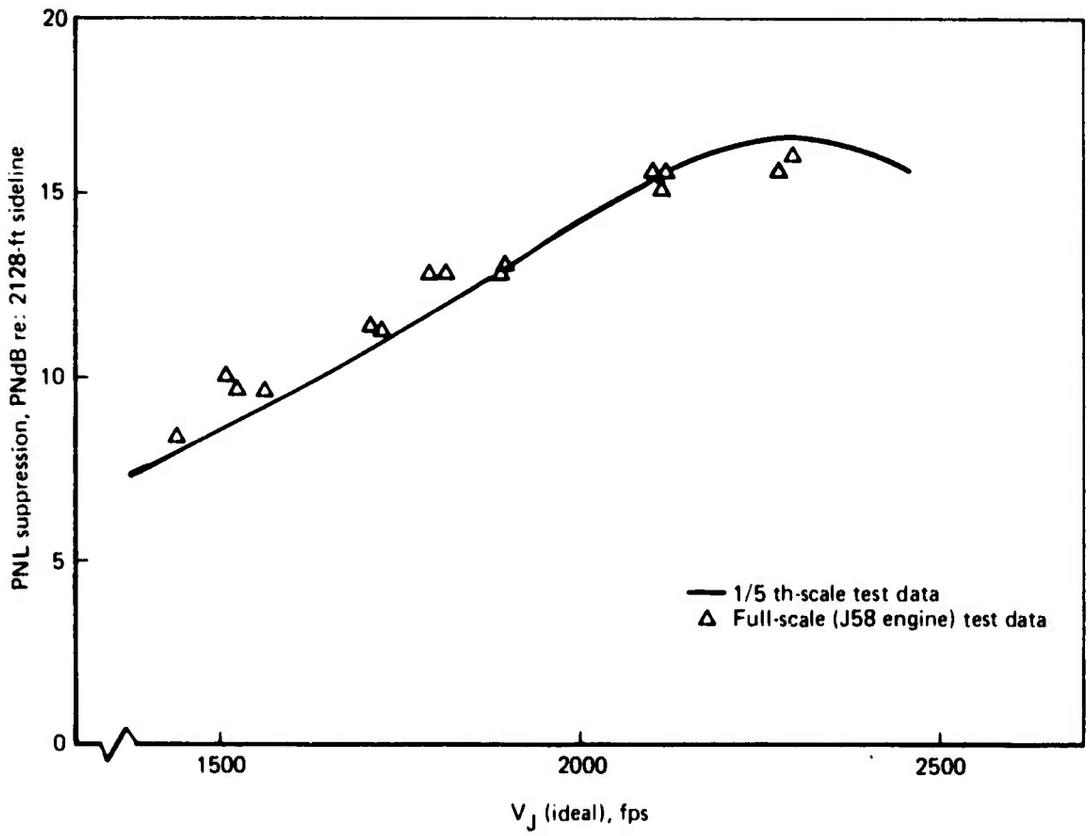

Figure 117.–LNHP-2 Suppressor With Lined Ejector Suppression Scaling Comparisons

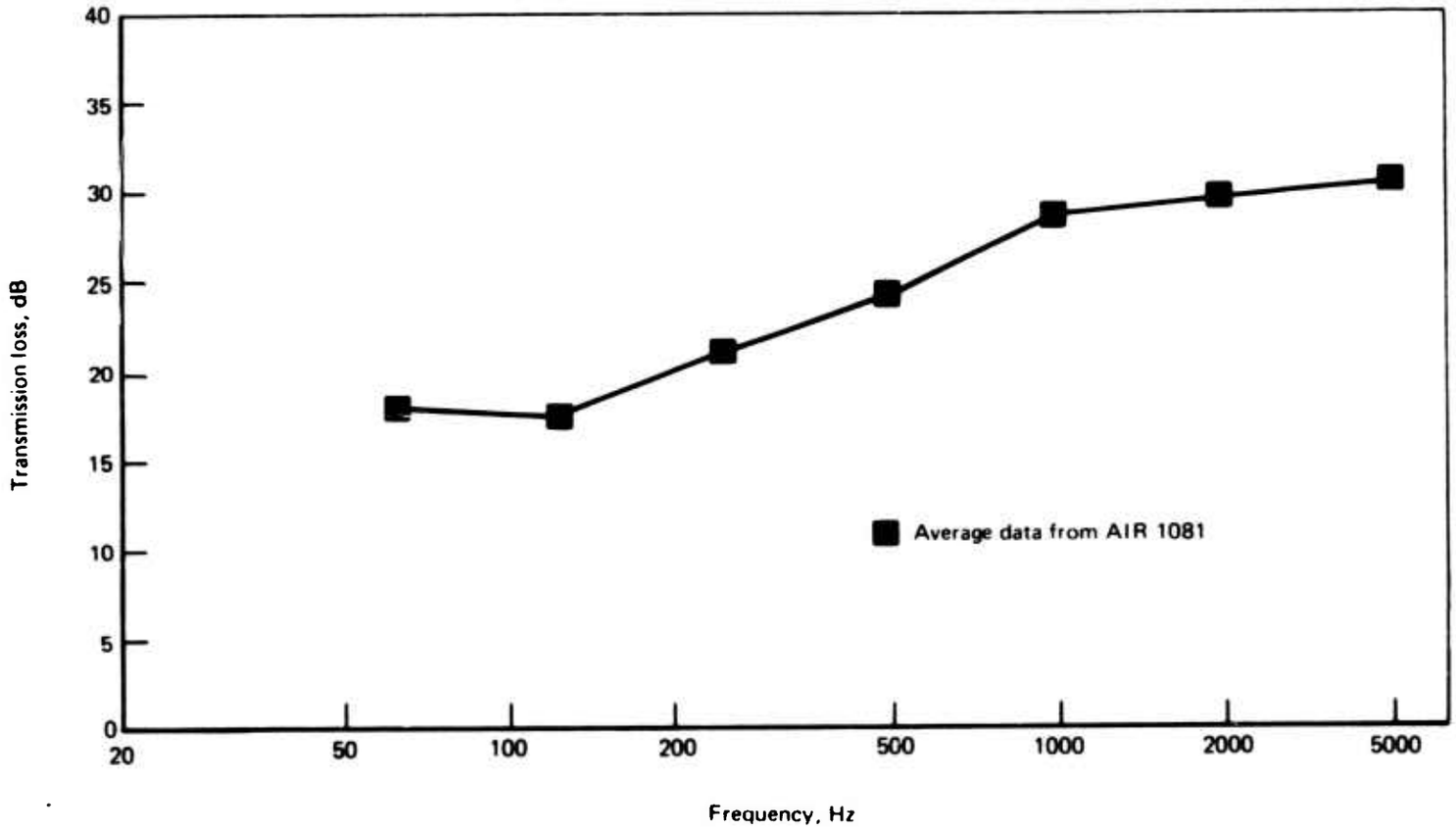

Figure 118.—Typical Noise Reduction Values For Family Dwellings (Windows Closed)

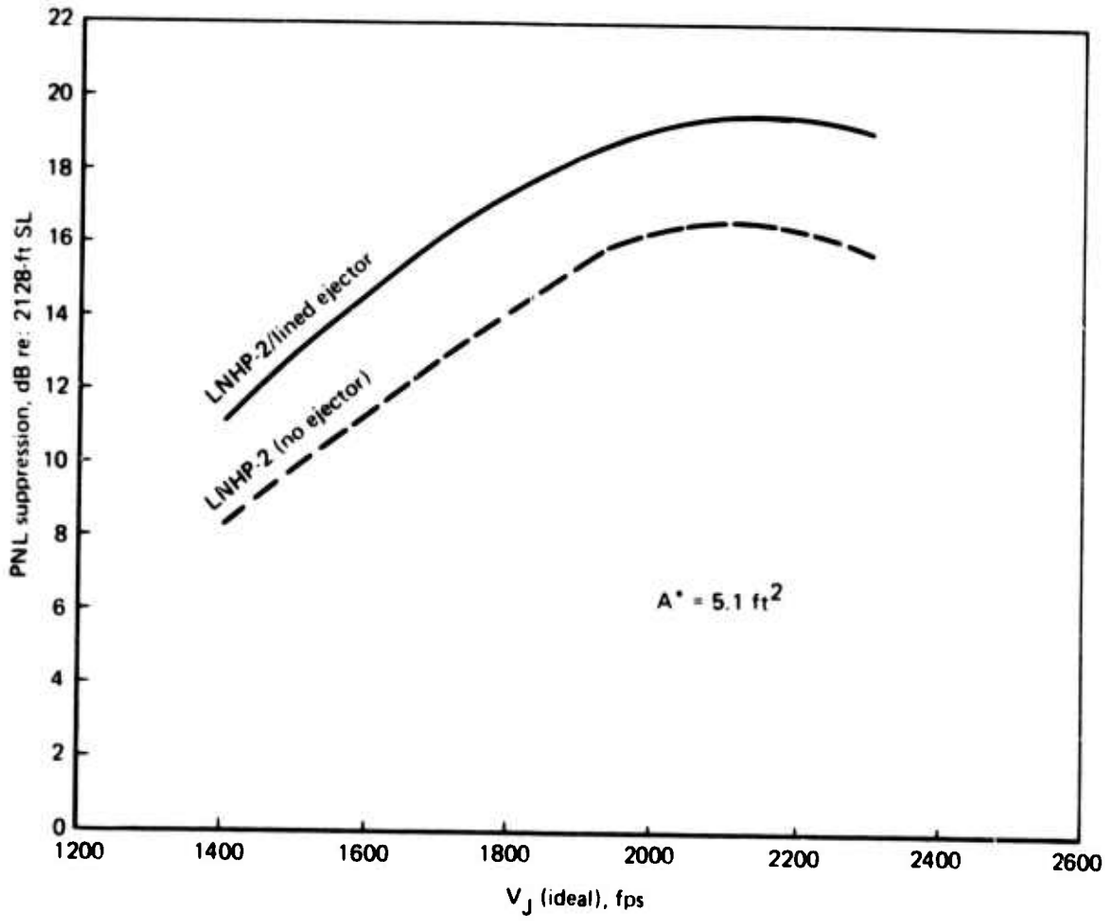

(AIR 1081 dwelling transmission loss values used)

Figure 119.—LNHP-2 Suppressor Indoor (Dwelling) PNL Suppression Values

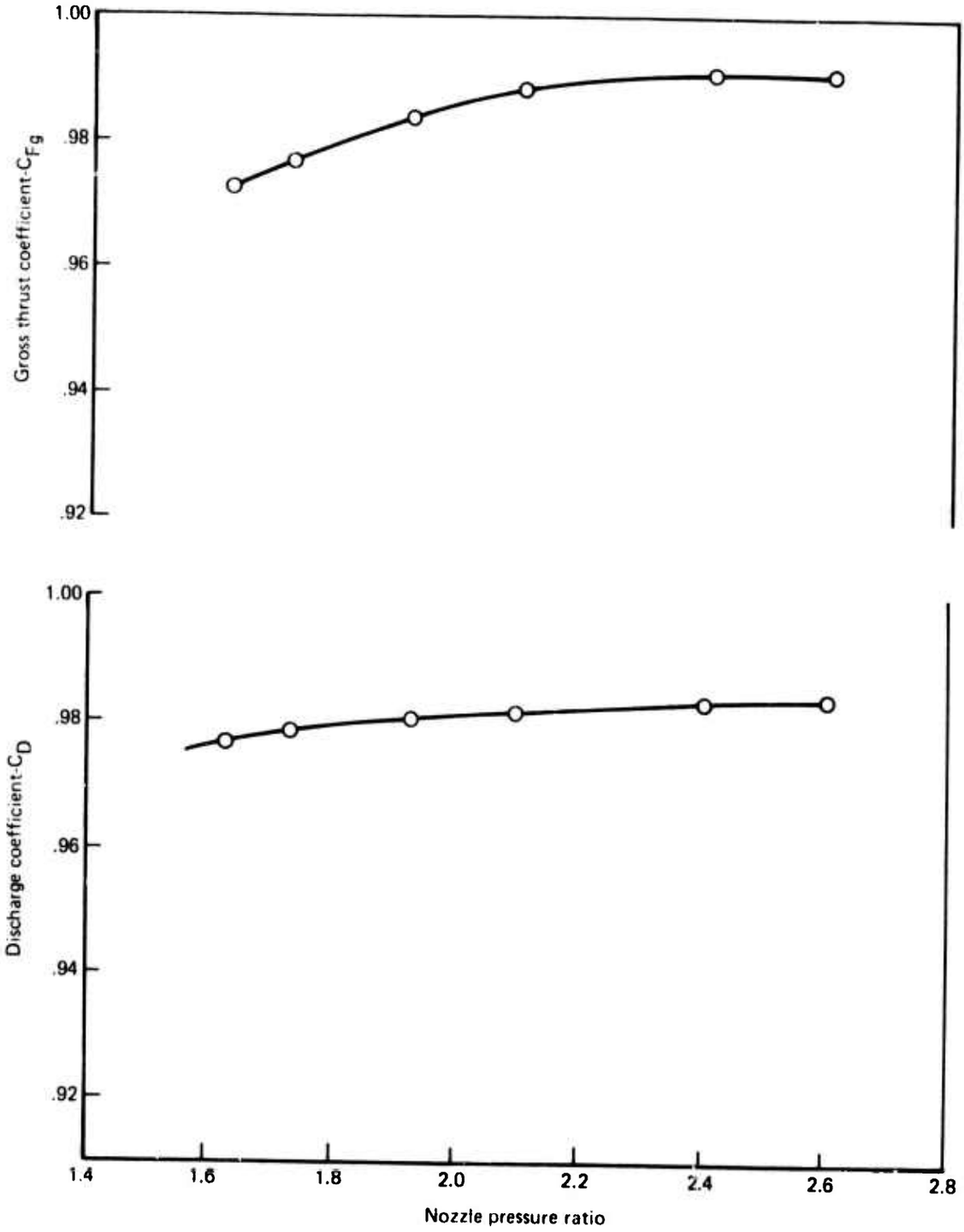

Figure 120.—Performance of Full-Scale R/C Nozzle

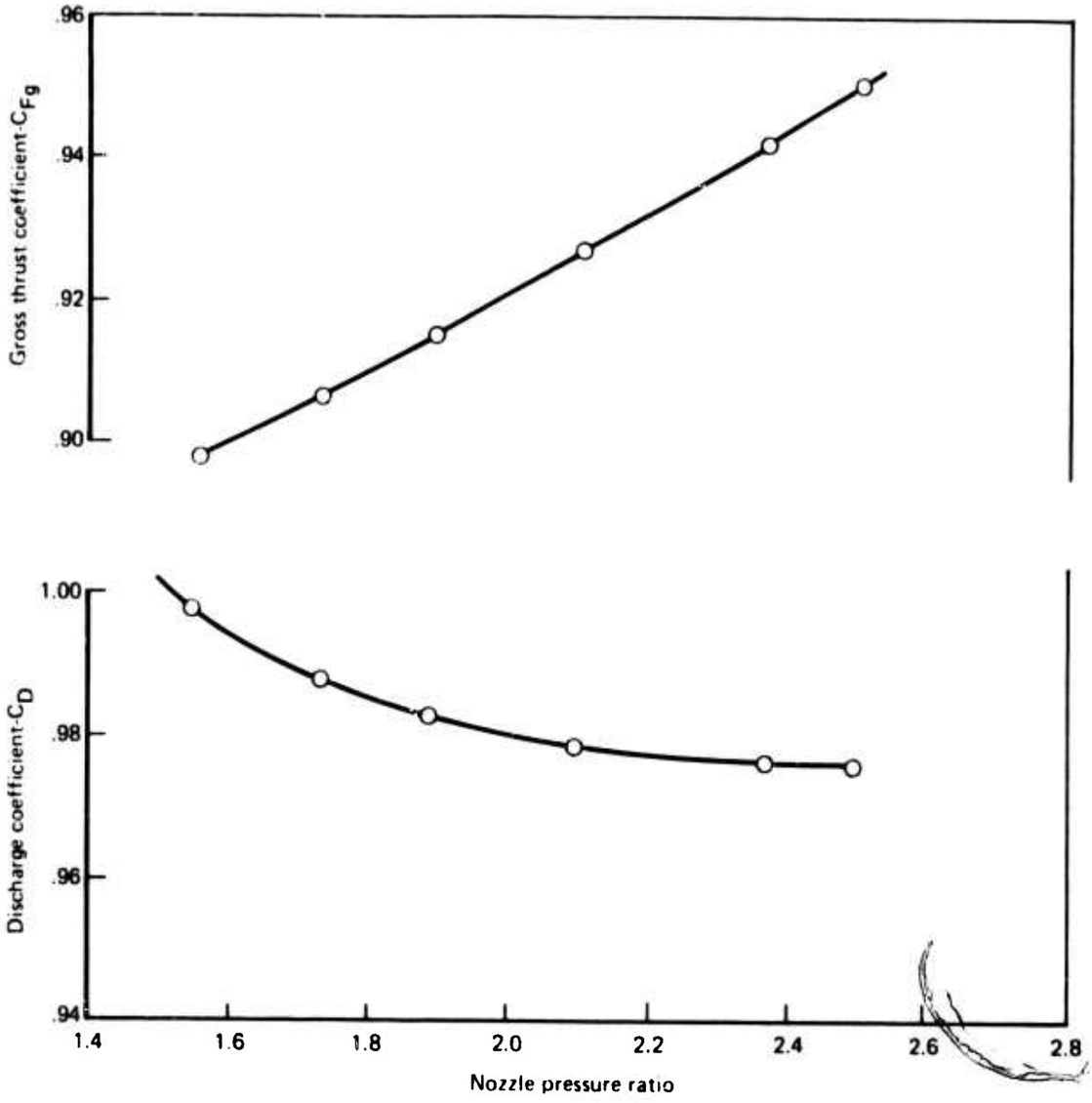

Figure 121.–Performance of Full-Scale Suppressor, Nozzle Only

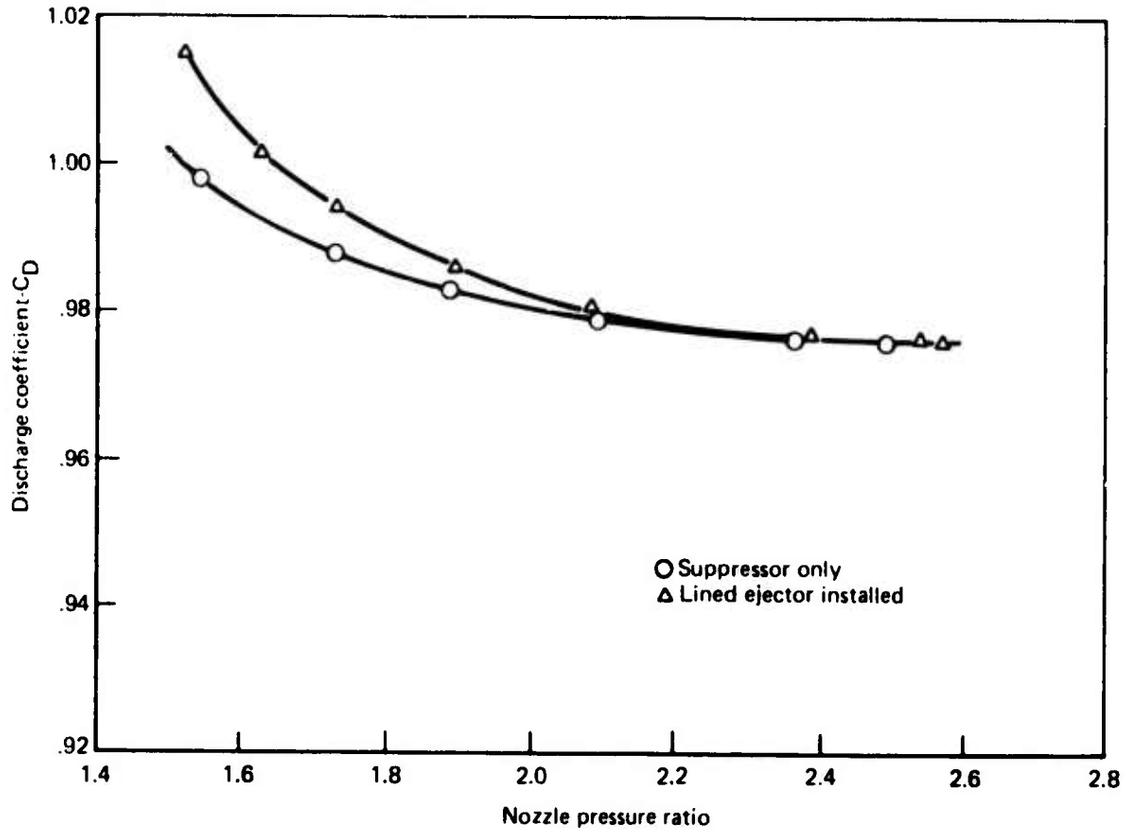

Figure 122.—Full-Scale Suppressor Nozzle Discharge Coefficient With and Without Ejector Installed

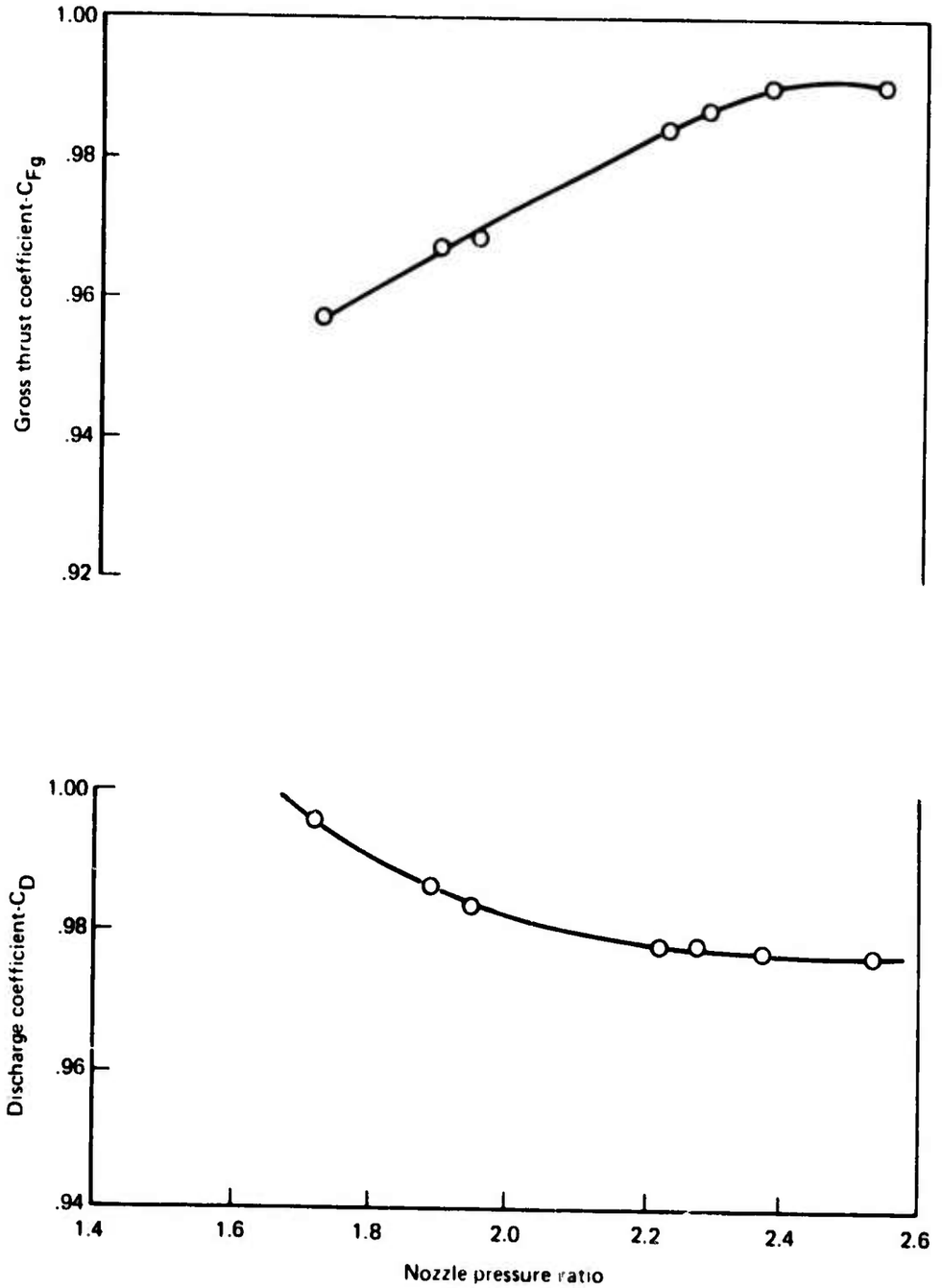

Figure 123.—Performance of Full-Scale Nozzle With Hardwall Ejector Installed at Setback of 4.5 Inches

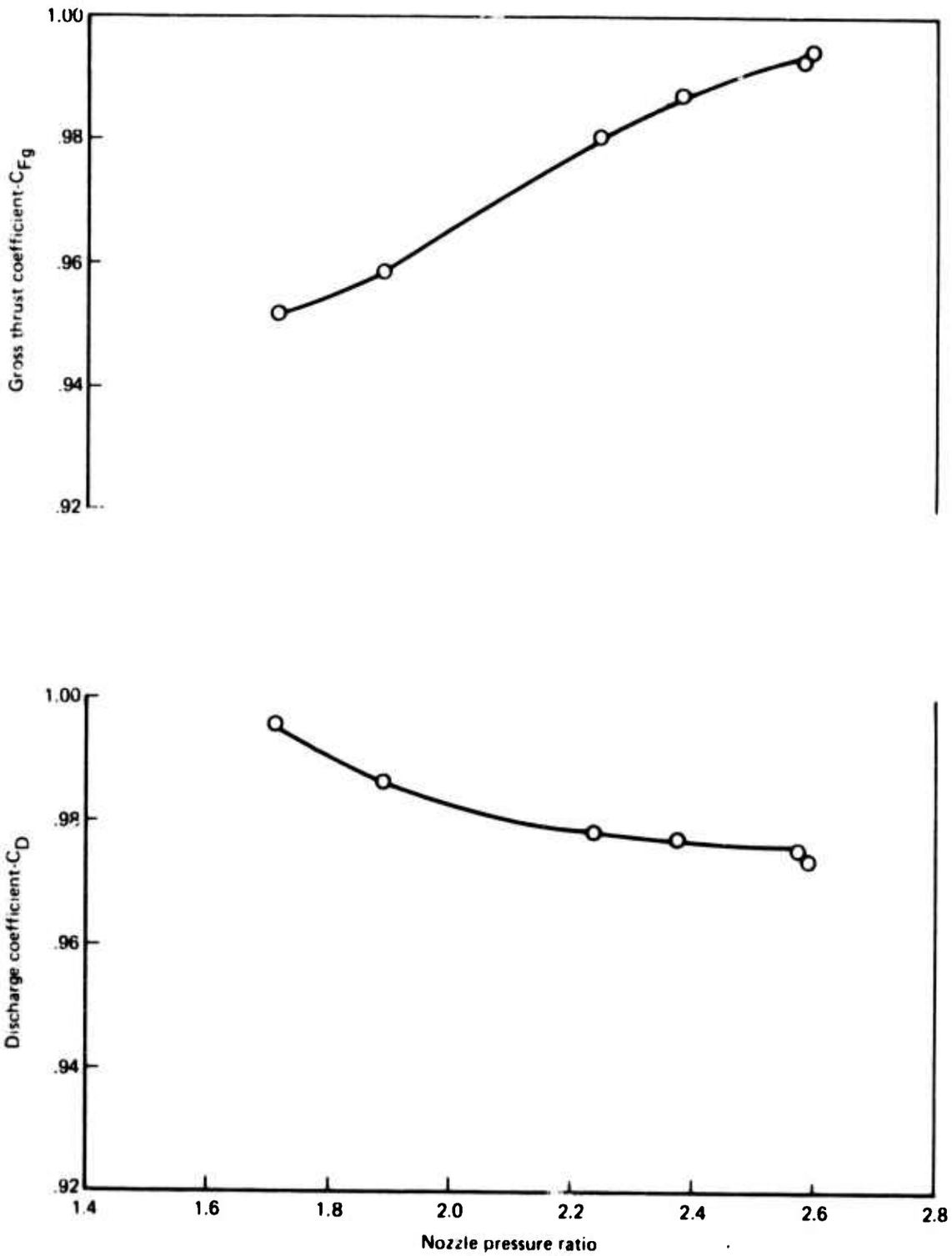

Figure 124.–Performance of Full-Scale Nozzle With Hardwall Ejector Installed at Setback of 8.25 Inches

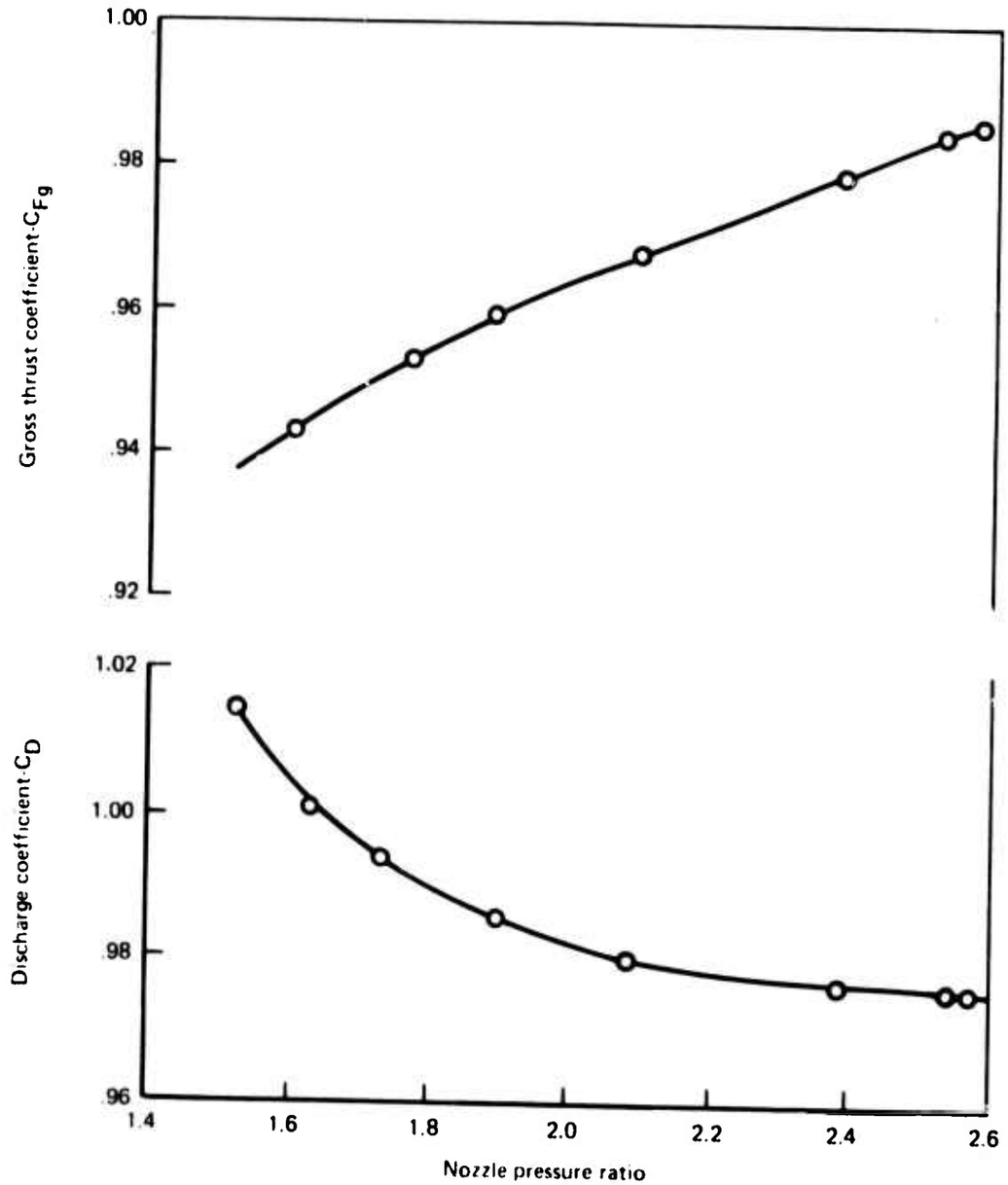

Figure 125.—Performance of Full-Scale Nozzle With Lined Ejector Installed at Setback of 4.5 Inches

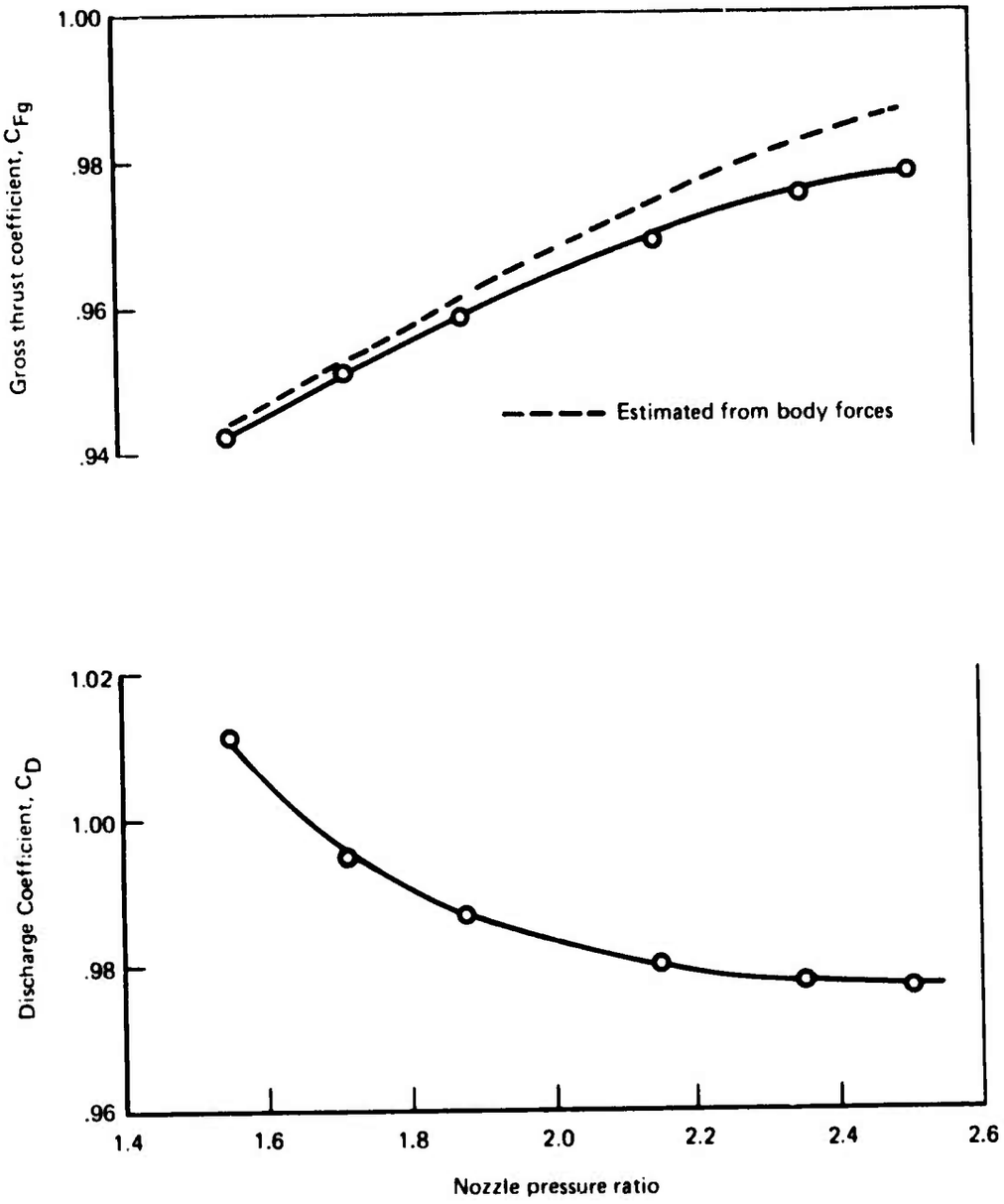

Figure 126.–Performance of Full-Scale Nozzle With Half-Lined Ejector Installed at Setback of 4.5 Inches

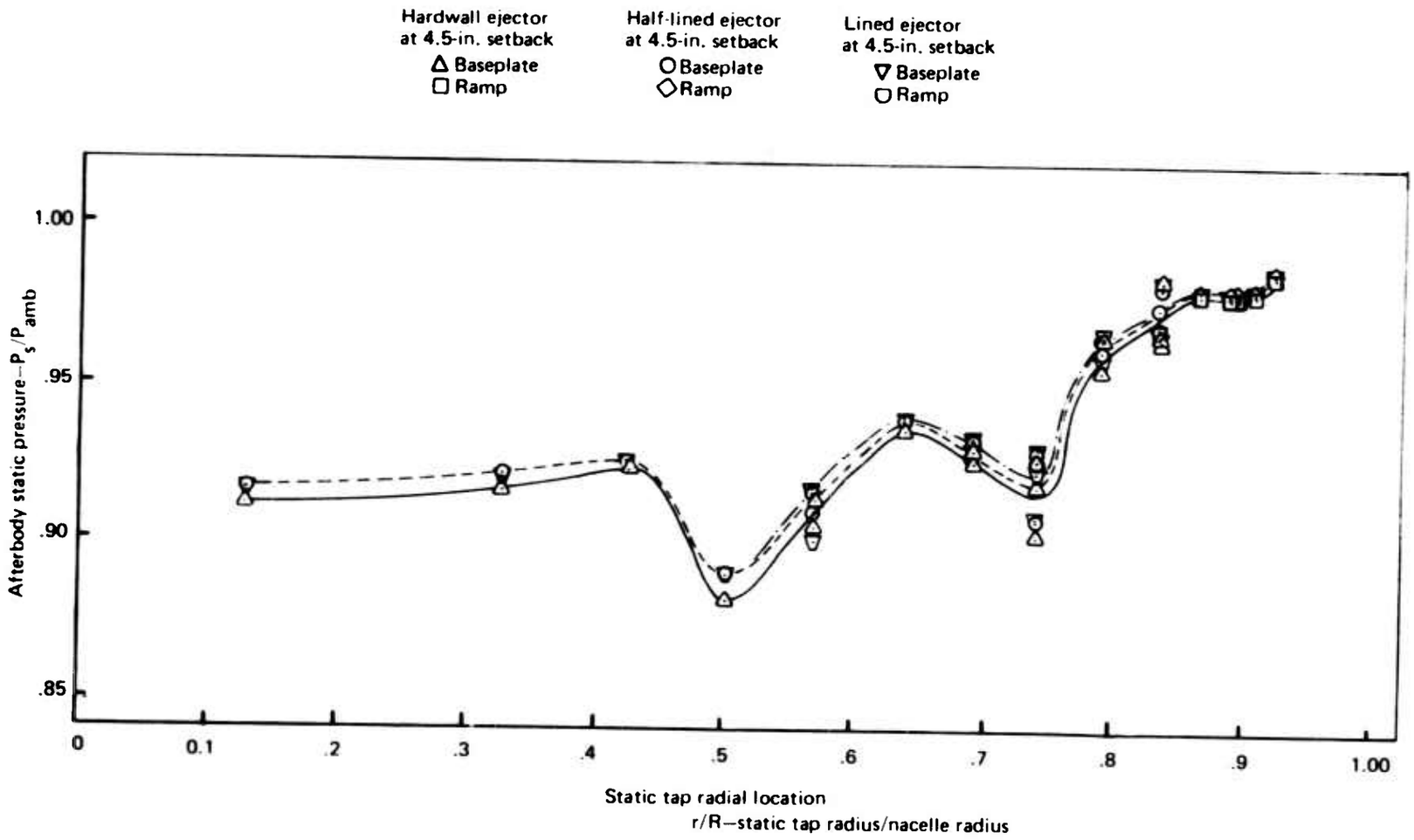

Figure 127.—Full-Scale Suppressor Baseplate and Ramp Radial Static Pressure Profiles

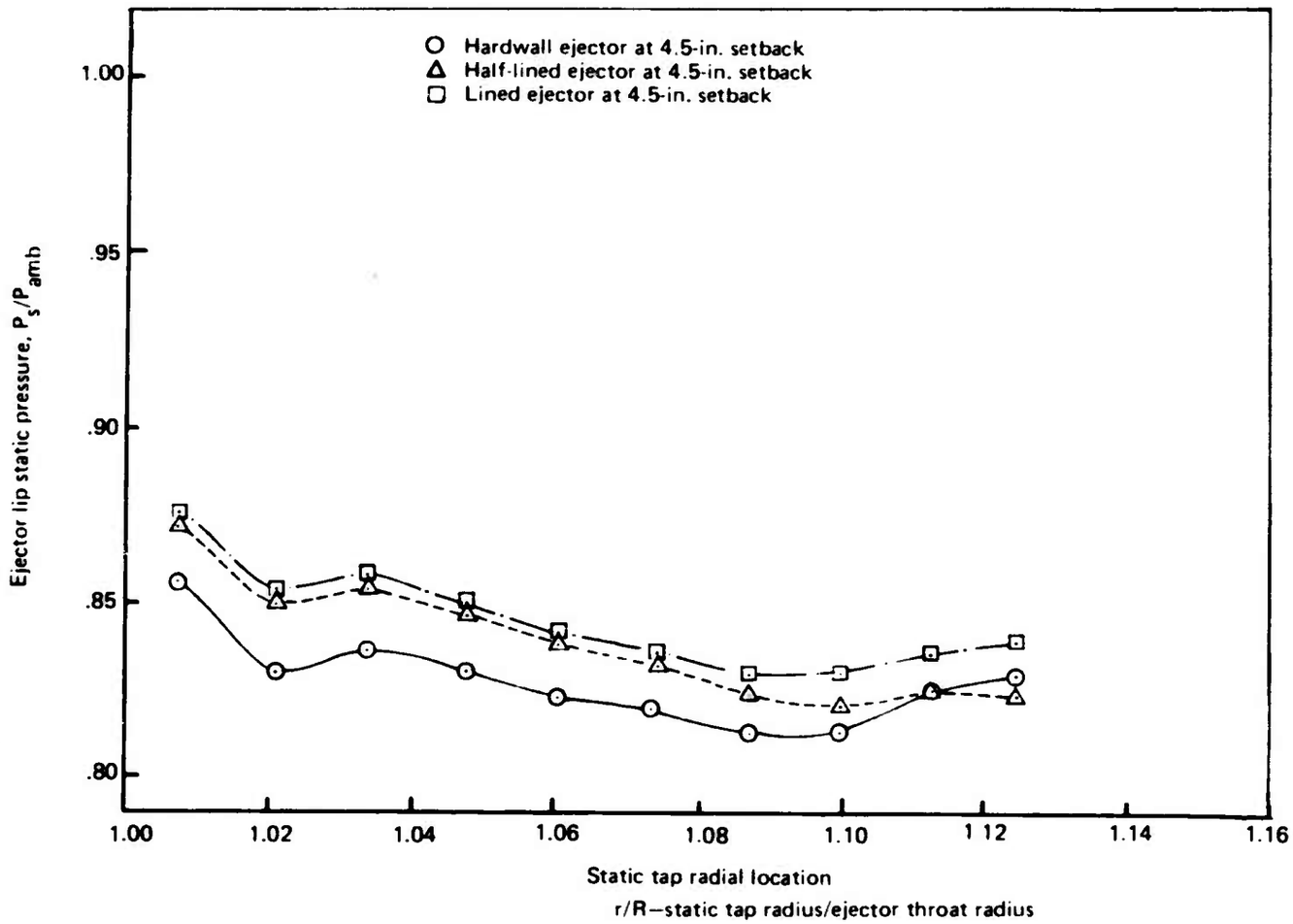

Figure 128.—Full-Scale Ejector Lip Radial Static Pressure Profiles

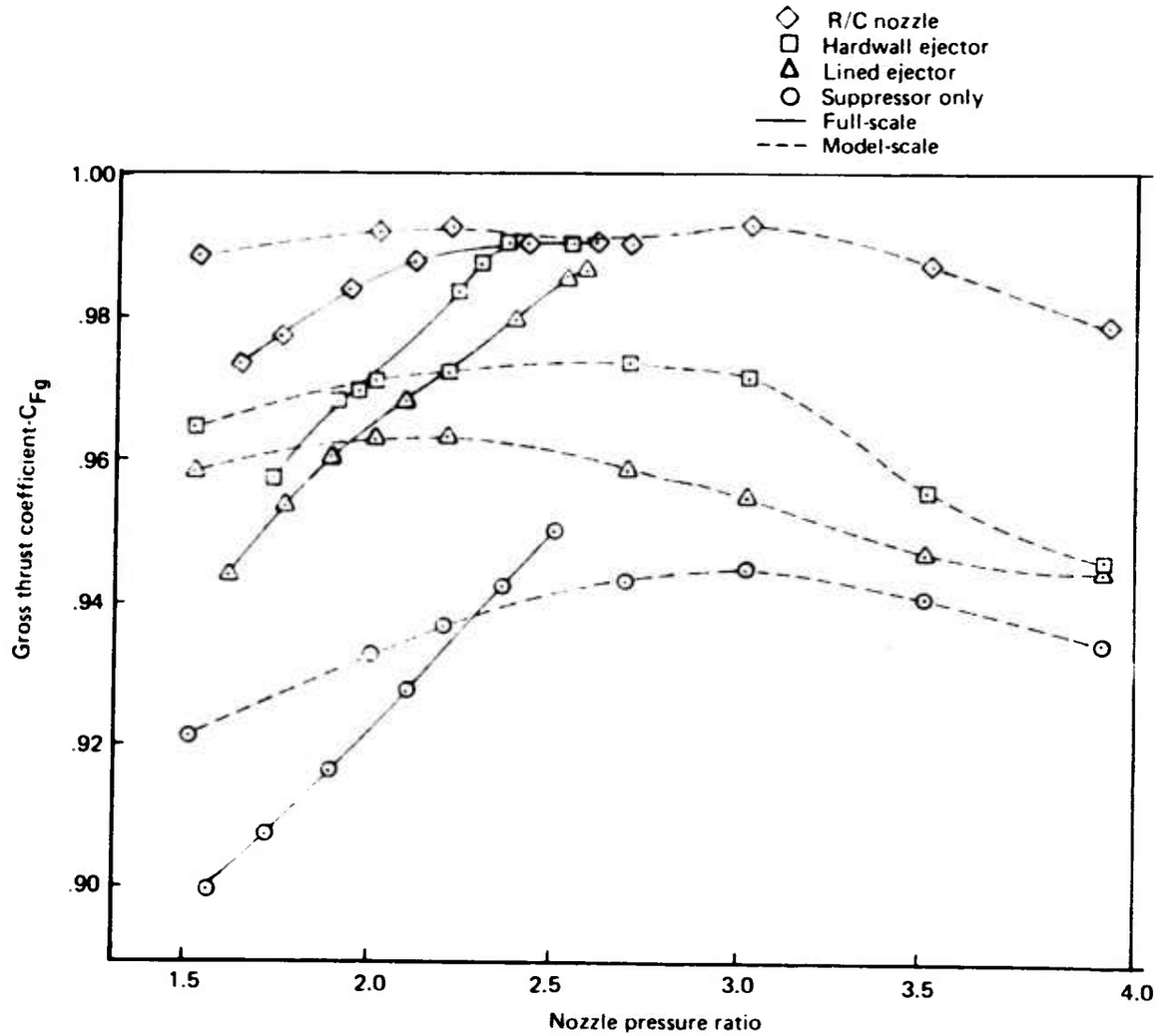

Figure 129.—Summary of Model- and Full-Scale Gross Thrust Coefficients

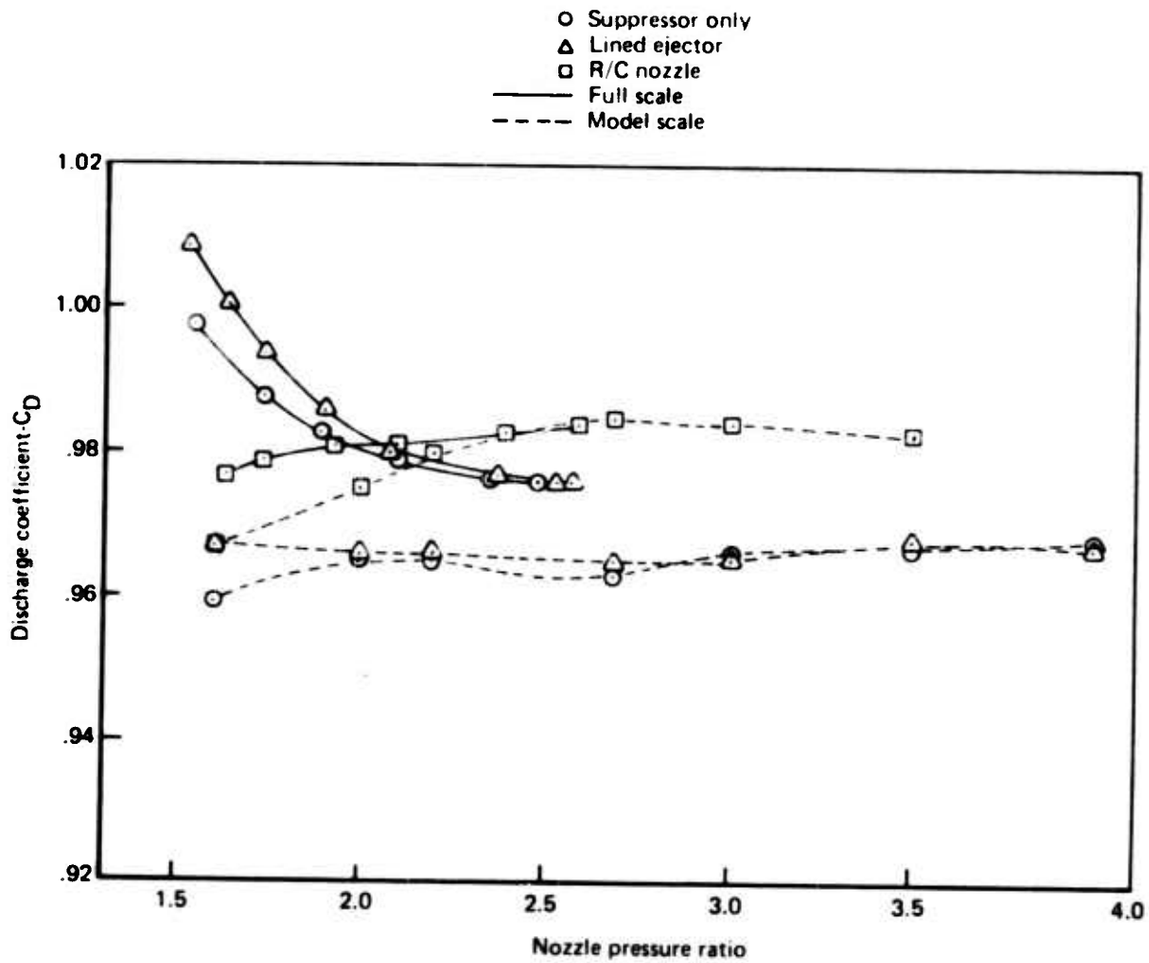

Figure 130.–Summary of Model and Full-Scale Discharge Coefficients

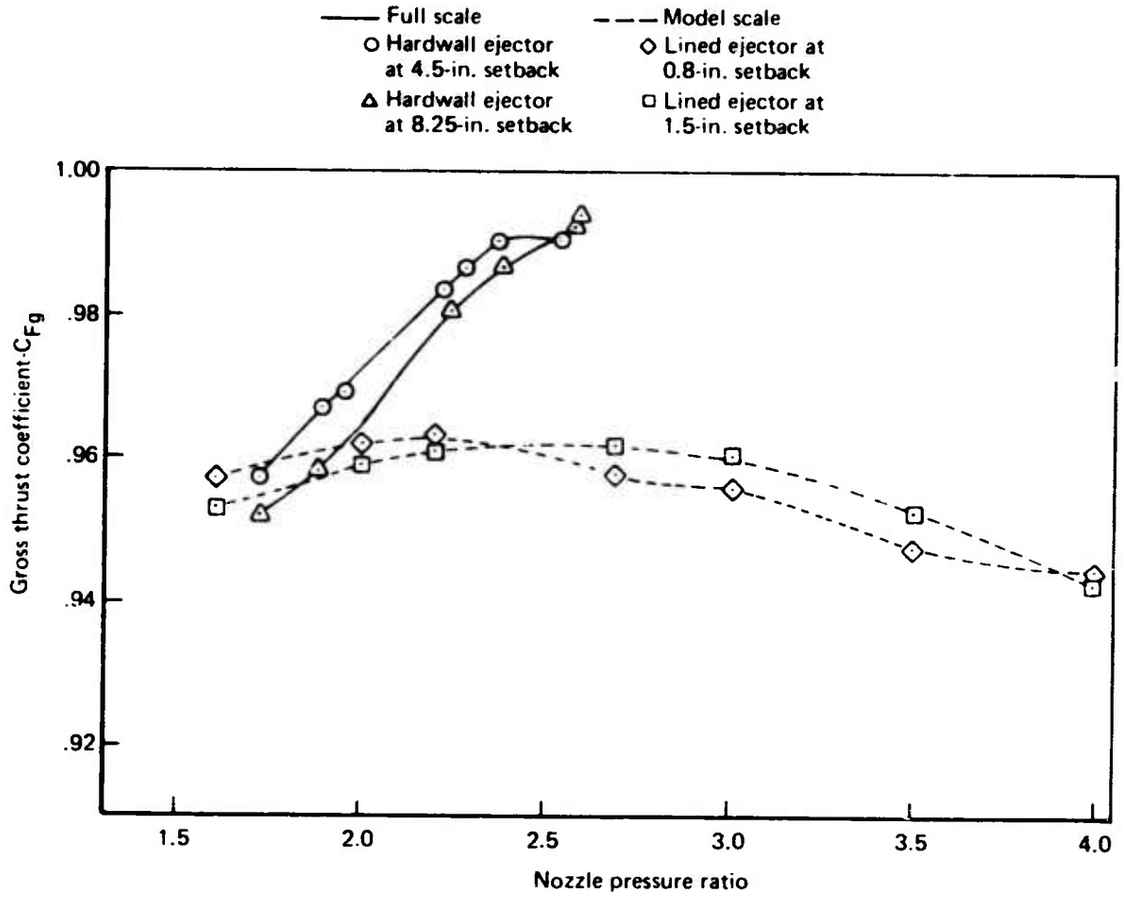

Figure 131.—Effects of Alternate Ejector Setback on Model Full-Scale Gross Thrust Coefficient

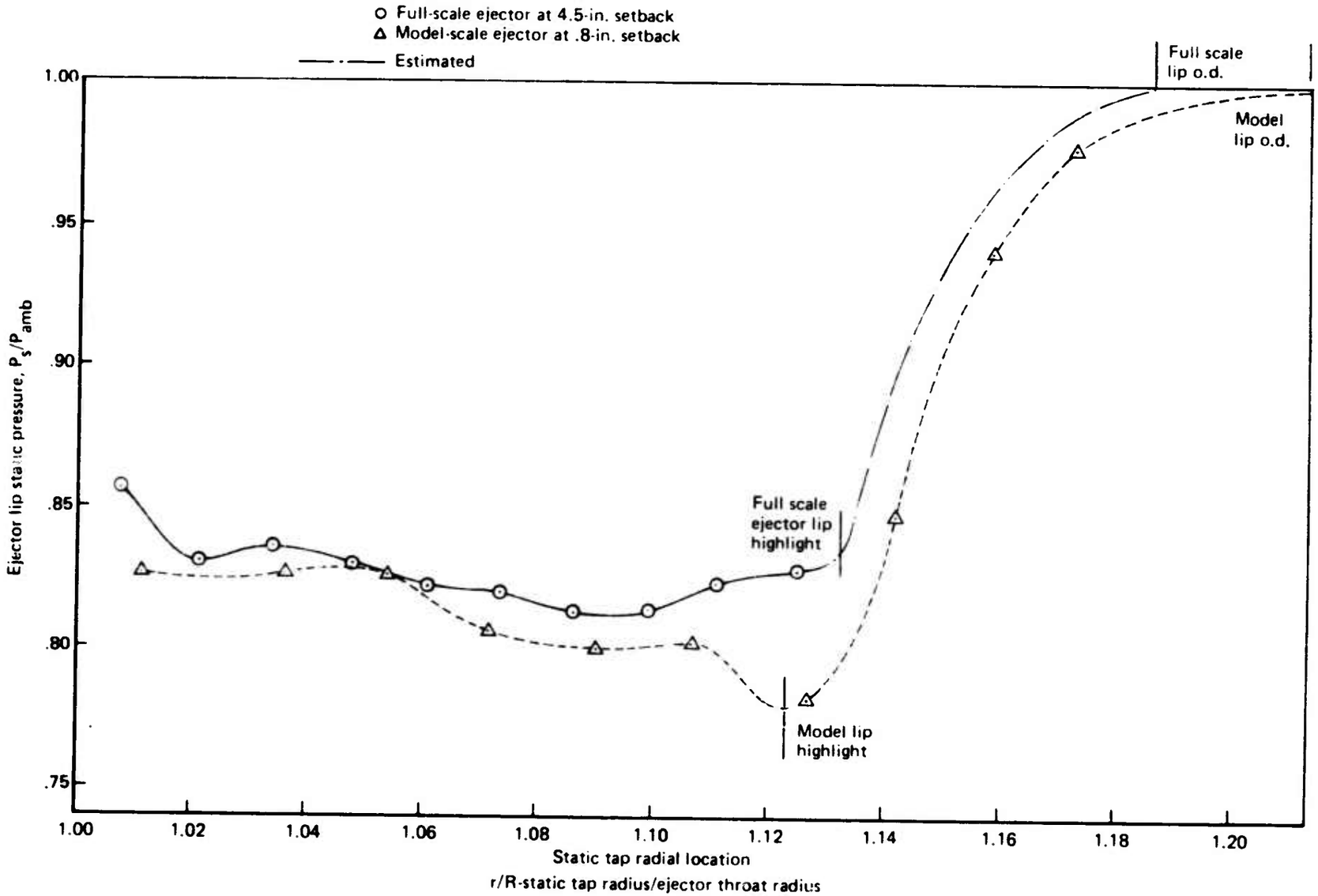

Figure 132.—Model- and Full-Scale Hardwall Ejector-Lip Radial Static Pressure Profiles

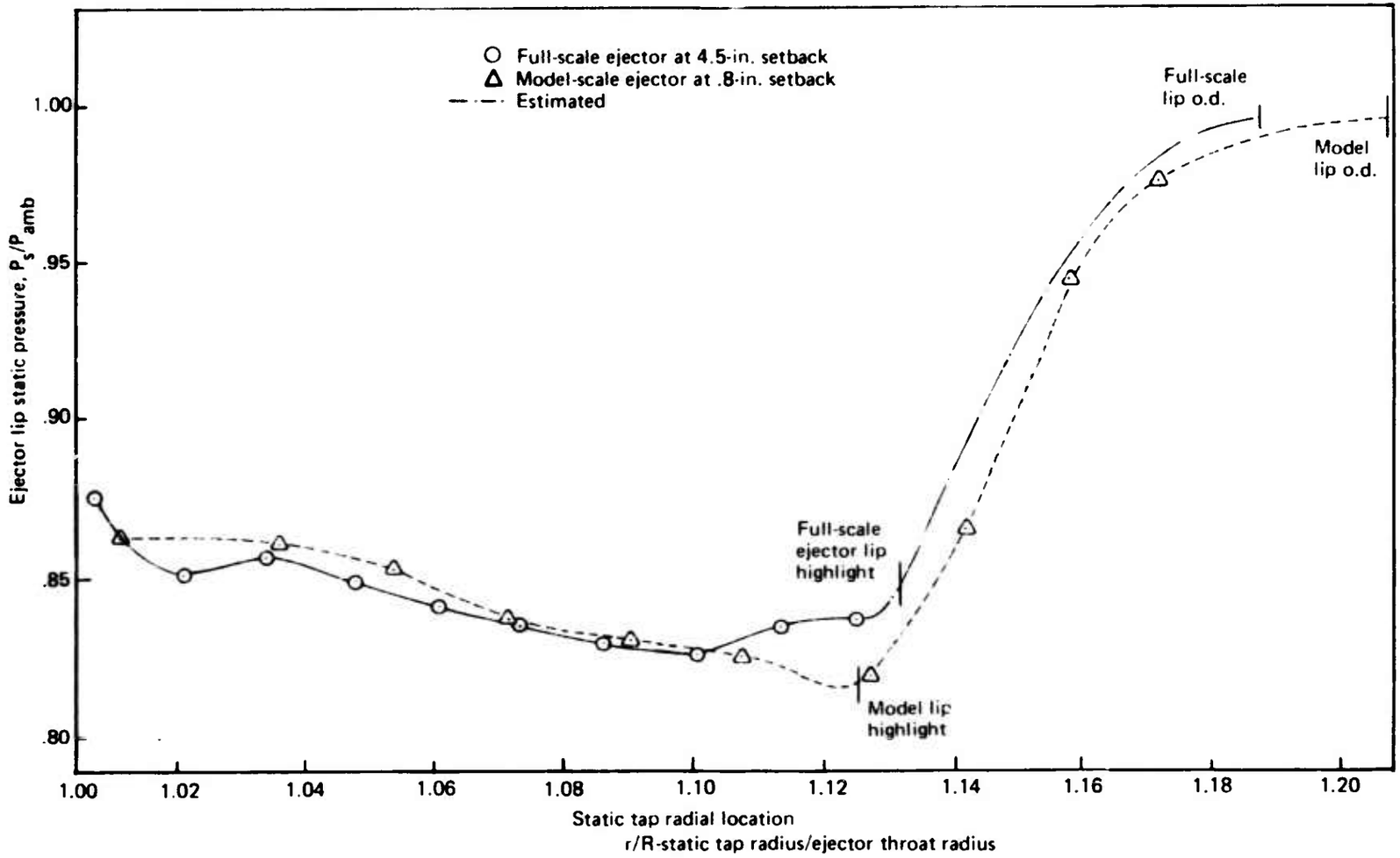

Figure 133.—Model- and Full-Scale Lined Ejector Lip Radial Static Pressure Profiles

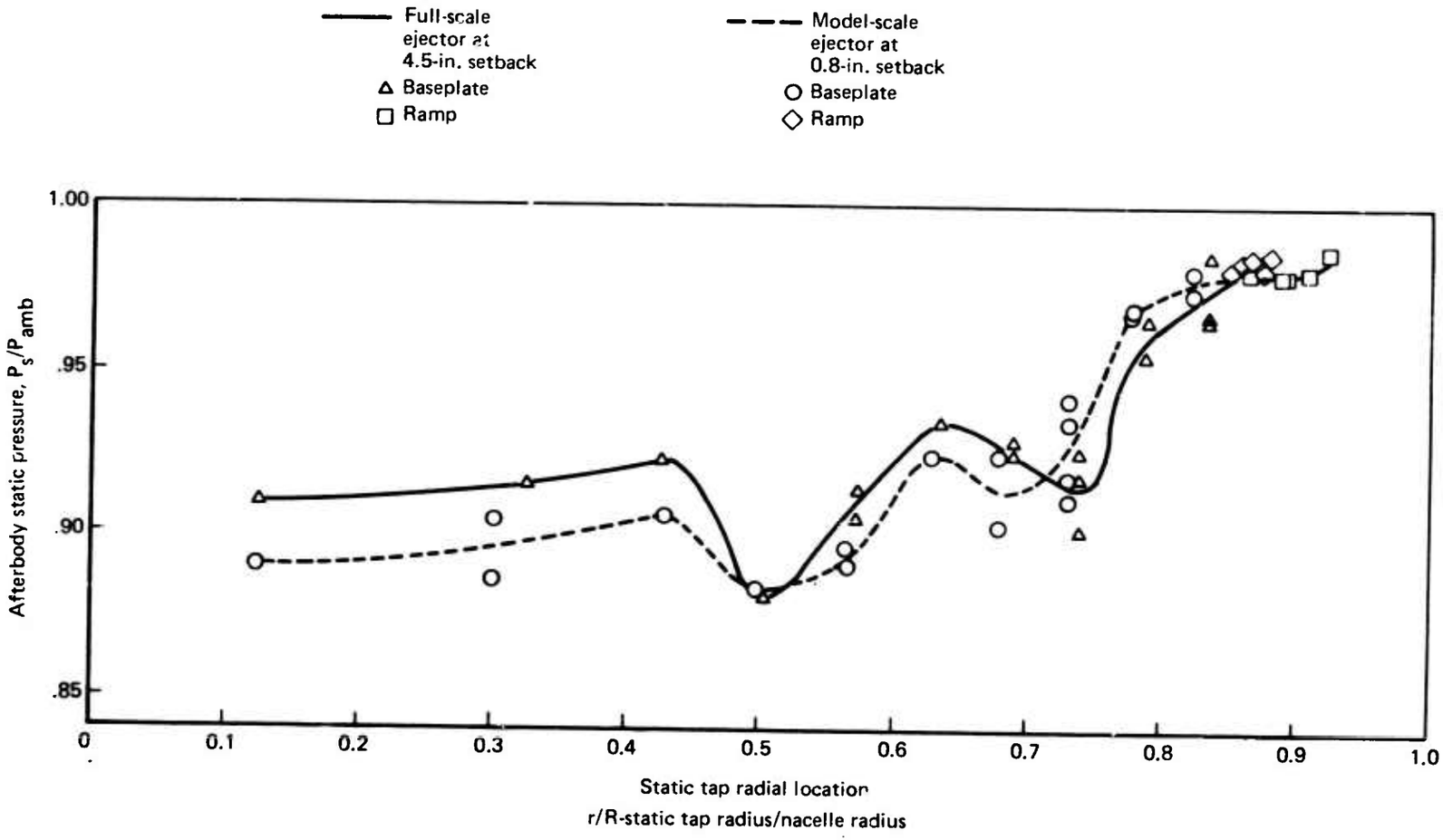

Figure 134.—Model- and Full-Scale Baseplate and Ramp Radial Static Pressure Profiles With Hardwall Ejector Installed

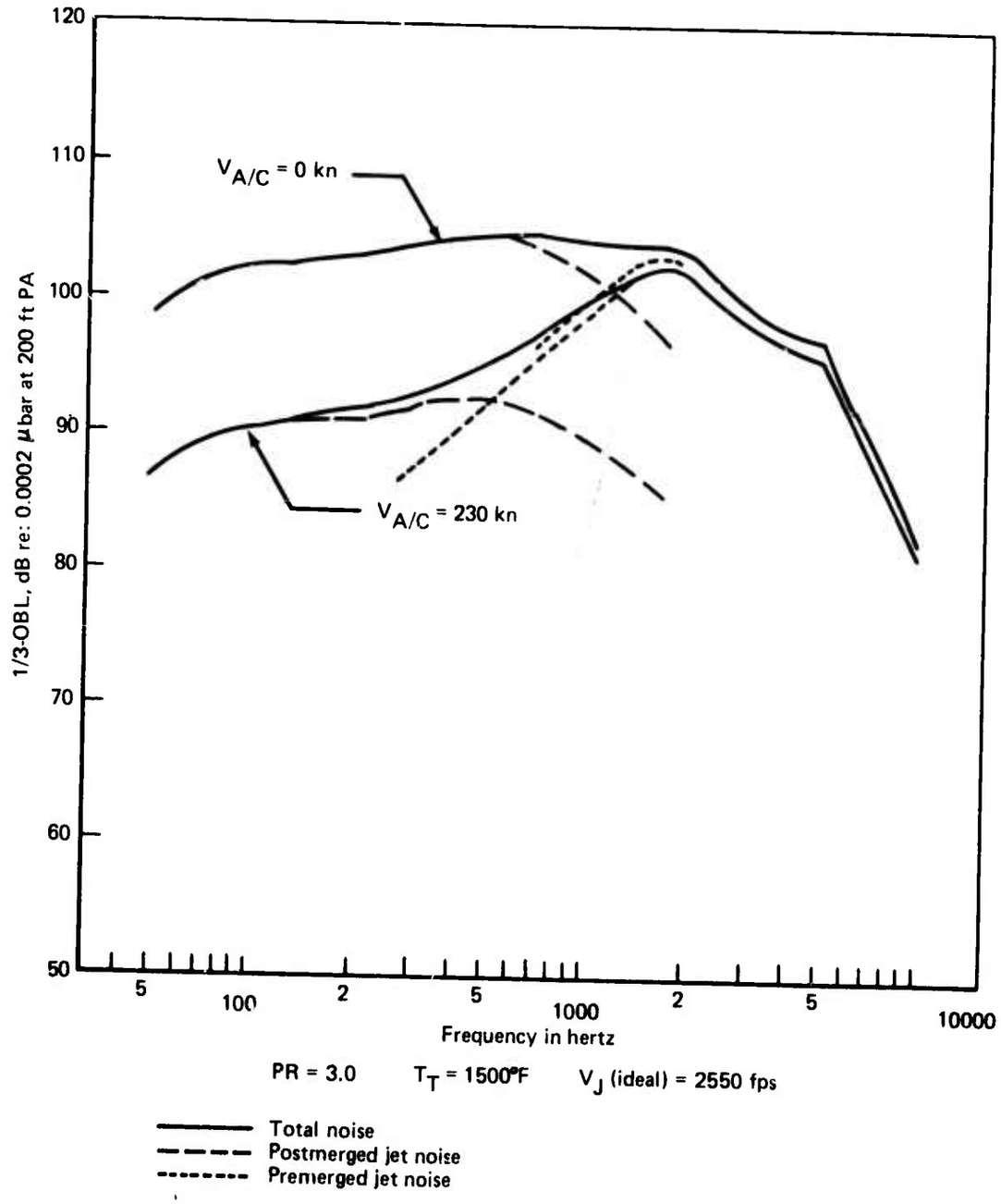

Figure 135.—Estimated Takeoff V_R Effect on LNHP-2 Suppressor, Noise Spectrum at 110° RE: Inlet axis

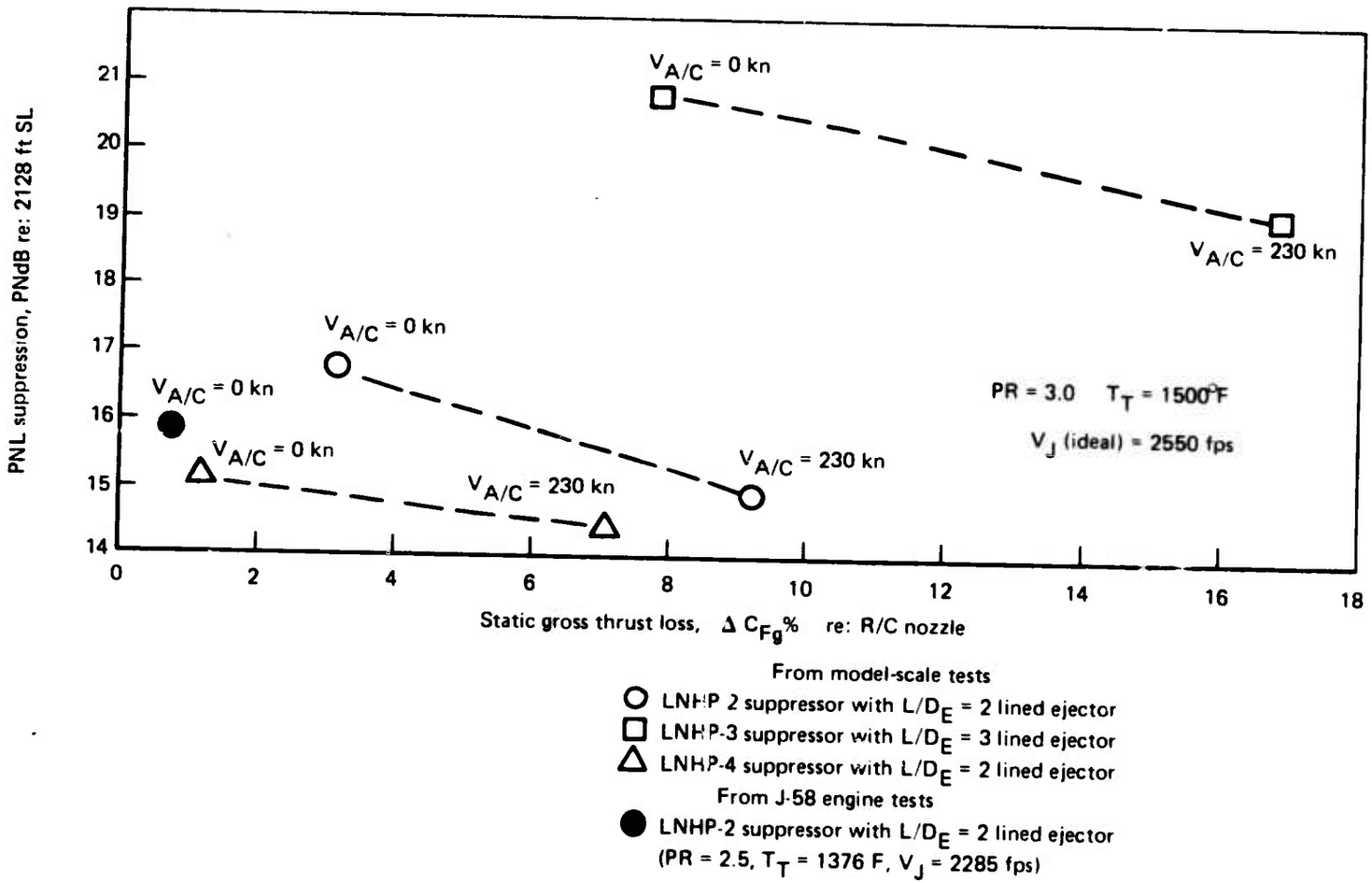

Figure 136.—Estimated Noise Suppression and Thrust Loss Values For 230 Knot Takeoff Velocity

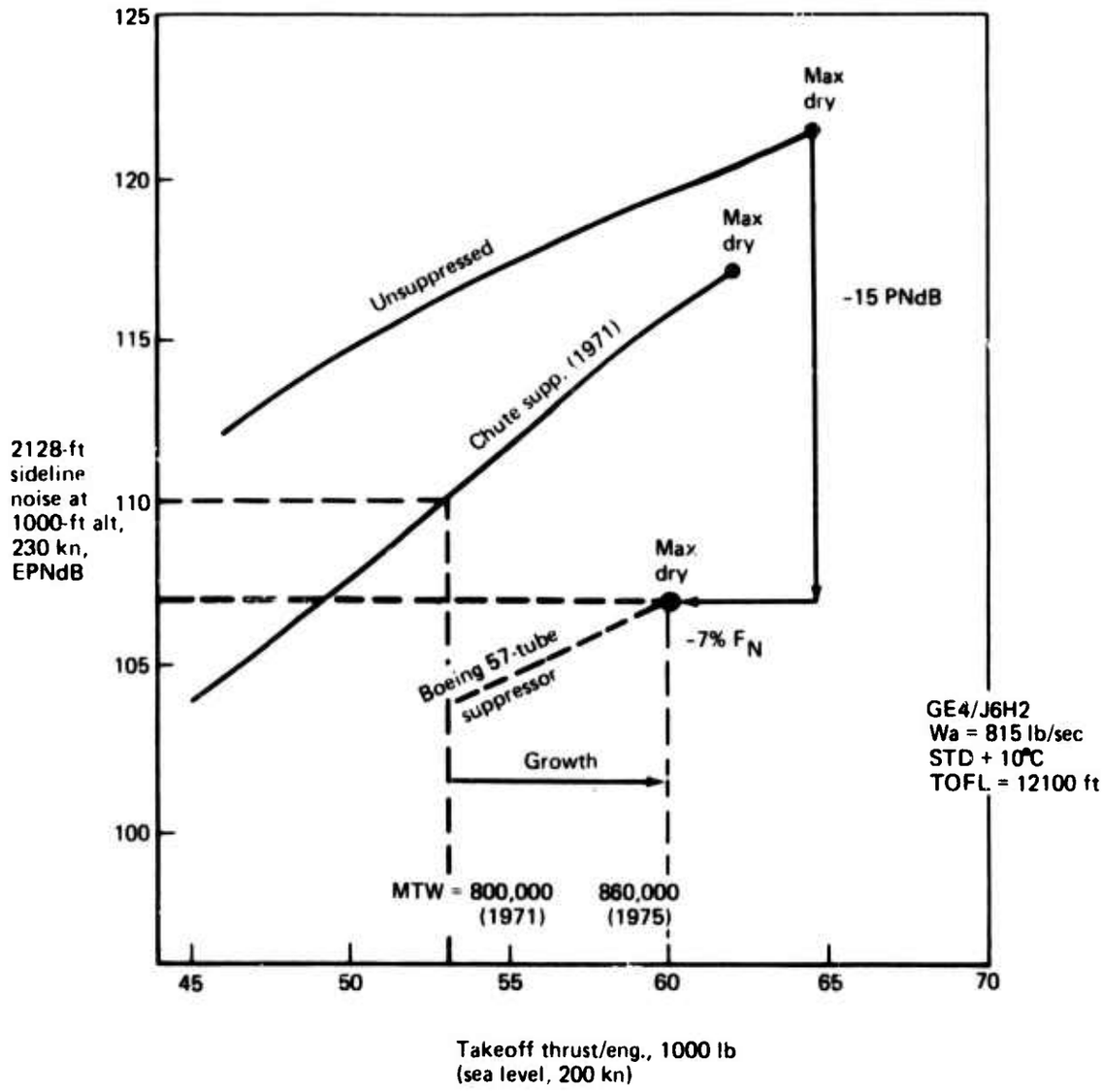

Figure 137.--Application of Multitube Suppressor System to SST Sideline Noise Reduction

REFERENCES

1. H. Y. Lu, "Acoustic Far-Field of a Point Source in Cylindrical and Planar Parallel Flowing Fluid Layers," AIAA paper 75-500, 1975.

2. Christopher K. W. Tam, "On the Noise of a Nearly Ideally Expanded Supersonic Jet," Journal of Fluid Mechanics, 1972. Vol. 51, pt 1, p 69

3. S. B. Kazin, and Emmerling, J. J., "Low Frequency Core Engine Noise," ASME, 74-WA/Aero-2. November 1974.

4. R. E. Smith, Jr., R. J. Matz, "A Theoretical Method for Determining Discharge Coefficients for Venturis Operating at Critical Flow Conditions," ASME Trans., Journal Basic Engineering, December 1962.

5. R. E. Smith, Jr., R. J. Matz, "Verification of a Theoretical Method of Determining Discharge Coefficients for Venturis Operating at Critical Flow Conditions," AEDC-TR-61-8, September 1961.